



Abdul Shakoor  
Kerry Cato *Editors*

# IAEG/AEG Annual Meeting Proceedings, San Francisco, California, 2018— Volume 3

Mining, Aggregates, Karst



 Springer

---

IAEG/AEG Annual Meeting Proceedings,  
San Francisco, California, 2018—Volume 3

---

Abdul Shakoor • Kerry Cato  
Editors

# IAEG/AEG Annual Meeting Proceedings, San Francisco, California, 2018—Volume 3

Mining, Aggregates, Karst



 Springer

*Editors*

Abdul Shakoor  
Department of Geology  
Kent State University  
Kent, OH, USA

Kerry Cato  
Department of Geological Sciences  
California State University  
San Bernardino, CA, USA

ISBN 978-3-319-93129-6      ISBN 978-3-319-93130-2 (eBook)  
<https://doi.org/10.1007/978-3-319-93130-2>

Library of Congress Control Number: 2018947486

© Springer Nature Switzerland AG 2019

This work is subject to copyright. All rights are reserved by the Publisher, whether the whole or part of the material is concerned, specifically the rights of translation, reprinting, reuse of illustrations, recitation, broadcasting, reproduction on microfilms or in any other physical way, and transmission or information storage and retrieval, electronic adaptation, computer software, or by similar or dissimilar methodology now known or hereafter developed.

The use of general descriptive names, registered names, trademarks, service marks, etc. in this publication does not imply, even in the absence of a specific statement, that such names are exempt from the relevant protective laws and regulations and therefore free for general use.

The publisher, the authors and the editors are safe to assume that the advice and information in this book are believed to be true and accurate at the date of publication. Neither the publisher nor the authors or the editors give a warranty, express or implied, with respect to the material contained herein or for any errors or omissions that may have been made. The publisher remains neutral with regard to jurisdictional claims in published maps and institutional affiliations.

Cover illustration: Golden Gate Bridge at night. Frederic Prochasson © 123rf.com

This Springer imprint is published by the registered company Springer Nature Switzerland AG  
The registered company address is: Gewerbestrasse 11, 6330 Cham, Switzerland



---

## Preface

The XIII IAEG Congress and 61st AEG Annual Meeting, San Francisco, USA, chose *Engineering Geology for a Sustainable World* as the theme for 2018. Based on the topical symposia and technical sessions, the proceedings are organized into six volumes and sub-categories as follows:

Volume 1: Slope Stability: Case Histories, Landslide Mapping, Emerging Technologies

Volume 2: Geotechnical and Environmental Site Characterization

Volume 3: Mining, Aggregates, Karst

Volume 4: Dams, Tunnels, Groundwater Resources, Climate Change

Volume 5: Geologic Hazards: Earthquakes, Land Subsidence, Coastal Hazards, and  
Emergency Response

Volume 6: Advances in Engineering Geology: Education, Soil and Rock Properties, Modeling

Participants of this joint meeting had the option to submit either a full paper or only an abstract. The editors would like to thank the authors for their valuable contributions. One hundred eighty-six full papers were submitted for review, and 153 papers successfully completed the process. Each paper submitted for the proceedings was peer-reviewed by two reviewers. Authors revised their papers in accordance with reviewers' comments. The reviewers, from across the globe, included professional experts as well as authors of other papers. The editors greatly appreciate the help provided by reviewers. A list of reviewers follows.

The editors are also very grateful to Karen Smith and Paisley Cato for their assistance throughout the review process.

Kent, OH, USA  
San Bernardino, CA, USA  
2018

Abdul Shakoor  
Kerry Cato

---

# Organization

## **General Meeting Chairs**

Sarah Kalika, Cornerstone Earth Group  
Gary Luce, Resource Concepts, Inc.  
Coralie Wilhite, United States Army Corps of Engineers

## **Field Course Chairs**

Chase White, California Geological Survey  
Drew Kennedy, Sage Engineers

## **IAEG Planning Committee Heads**

Scott Burns, Portland State University  
Jeffrey R. Keaton, Wood

## **Proceedings Editors**

Abdul Shakoor, Kent State University  
Kerry Cato, Cato Geoscience, Inc./California State University, San Bernardino

## **Editorial Assistants**

Karen Smith, Kent State University  
Paisley Cato, Cato Geoscience, Inc.

## **Short Course Chairs**

E. Morley Beckman, Kleinfelder  
Byron Anderson, Kleinfelder  
Chrissey Villeneuve, Shannon & Wilson, Inc.

## **Technical Program Committee**

Abdul Shakoor, Kent State University  
Kerry Cato, Cato Geoscience, Inc./California State University, San Bernardino  
William Godwin, Consulting Geologist  
Sarah Kalika, Cornerstone Earth Group

## **Symposium Chairs**

Robert E. Tepel, Retired Professional Geologist and Certified Engineering Geologist  
Brian H. Greene, United States Army Corps of Engineers  
Donald Bruce, Geosystems, L.P.  
Holly Nichols, California Department of Water Resources  
Keith Turner, Colorado School of Mines  
Fred Baynes, Consulting Engineering Geologist  
Kevin McCoy, Colorado Geological Survey

Hilary Whitney, Environmental Resources Management  
Michelle Sneed, United States Geological Survey  
Thomas Oommen, Michigan Technological University  
Julien Waeber, AECOM  
Ed Medley, Consulting Geological Engineer  
Mark Bailey, Asbestos TEM Labs  
Atiye Tugrul, Istanbul University, Avcilar Campus, Turkey  
Lindsay Swain, Dudek  
Ike Isaacson, Brierley Associates  
Mike Piepenburg, Aldea Services, LLC  
Bruce Hilton, Kleinfelder  
Anne Rosinski, California Geological Survey  
Steve Parry, Parry Engineering Geological Services  
Jan Novotny, Ceska Geologicka Sluzba, Czech Republic  
Xiaolei Liu, Shandong Provincial Key Laboratory of Marine Environment and Geological Engineering (Ocean University of China), China

### **Field Course Leaders and Contributors**

William Godwin, Consulting Geologist  
William McCormick, Kleinfelder  
Bradley Erskine, Kleinfelder  
Marina Mascorro, Langan  
Frank Rollo, Rollo & Ridley  
John Egan, Sage Engineers  
Ken Johnson, WSP  
John Wallace, Cotton, Shires and Associates, Inc.  
Ryan Seelbach, Geosyntec  
Tom Barry, California Department of Conservation, Division of Oil, Gas and Geothermal Resources  
John Wakabayashi, Fresno State University  
Greg Stock, Yosemite National Park  
Janet Sowers, Fugro  
Jim Lienkaemper, United States Geological Survey  
Keith Kelson, United States Army Corps of Engineers  
Carol Prentice, United States Geological Survey  
Gordon Seitz, California Department of Conservation  
Chris Madugo, Pacific Gas & Electric Company  
Mike Jewett, Miller Pacific Engineers  
Ray Sullivan, San Francisco State University  
George Ford, Geosyntec  
Wayne Akiyama, APTIM  
Ryan Coe, Terracon  
Kate Zeiger, AECOM  
John Murphy, California State Water Resources Control Board  
Jennifer Gomez, Syar Industries  
Mike George, BGC Engineering  
Nick Sitar, University of California, Berkeley  
Peter Holland, California Geological Survey  
Chris Hundemer, C2earth  
Jake Hudson, Holdrege & Kull/NV5  
Shane Cummings, Holdrege & Kull/NV5  
Chris Hitchcock, InfraTerra  
Roxanne Renedo, BSK Associates  
Tim Dawson, California Department of Conservation

Margaret Doolittle, Kleinfelder  
Kevin Clahan, Lettis Consultants  
Donald Wells, AMEC/Foster Wheeler  
Jennifer Dean, California State Water Resources Control Board  
Felix Desperrier, Lettis Consultants  
Karen Grove, San Francisco State University

**Guest Tour Chairs**

Alice Tepel  
Linda Upp

**Publicity Committee**

Nathan Saraceno, DiGioia Gray & Associates  
Courtney Johnson, Sage Engineers  
Maggie Parks, ENGEO

**Sponsorship Chair**

Courtney Johnson, Sage Engineers

**Technical Session Editing**

Bill Yu, Case Western Reserve University

**Guidebook App**

Clayton Johnson, Golder Associates  
Nathan Saraceno, DiGioia Gray & Associates

**Fed IGS**

Jean-Louis Briaud, Texas A&M University

**K-12 Teacher Workshop**

Cynthia Pridmore, California Geological Survey

**Special Event**

E. Morley Beckman, Kleinfelder

**AEG Meeting Manager**

Heather Clark, Association of Environmental & Engineering Geologists

**AEG Headquarters**

AMR Management

---

## List of Reviewers

David Abbott, USA  
Biljana Abolmasov, Serbia  
Okechukwu Aghamelu, Nigeria  
M. Farooq Ahmed, Pakistan  
Paolo Allasia, Italy  
Priyanthi Amarasinghe, USA  
Sofia Anagnostopoulou, Greece  
Pedro Andrade, Portugal  
Luis Bacellar, Brazil  
Marco Baldo, Italy  
Elizabeth Beckman, USA  
Zbigniew Bednarczyk, Poland  
Eduardo Bergillos Navarro, Spain  
David Bieber, USA  
Candan BiLen, Turkey  
Andrée Blais-Stevens, Canada  
Peter Bobrowsky, Canada  
Nana Bolashvili, Georgia  
James Borchers, USA  
Anika Braun, Germany  
Stephanie Briggs, USA  
Luke Brouwers, United Arab Emirates  
Brian Bruckno, USA  
Matthias Brugger, Germany  
Fintan Buggy, Ireland  
Domenico Calcaterra, Italy  
Michael Carpenter, USA  
Kerry Cato, USA  
Andrea Cevasco, Italy  
Hannah Chapella, USA  
Xiaoli Chen, China  
Sibonakaliso Chiliza, South Africa  
Jeff Coe, USA  
Mike Collins, USA  
Brian Conway, USA  
Jasper Cook, UK  
Isabela Coutinho, Brazil  
John Cripps, UK  
Balázs Czinder, Hungary  
Ranjan Kumar Dahal, Nepal  
Jerome De Graff, USA  
Rachael Delaney, USA  
Artem Demenev, Russia

---

Diego Di Martire, Italy  
Matthys Dippenaar, South Africa  
Angelo Doglioni, Italy  
Anastasia Dorozhko, Russia  
Peter Ellecosta, Germany  
Selman Er, Turkey  
Olga Eremina, Russia  
Georg Erharter, Austria  
Moises Failache, Brazil  
Andrew Farrant, UK  
Zhen Feng, China  
Clark Fenton, New Zealand  
Maria Ferentinou, South Africa  
Kenneth Ferguson, USA  
Isabel Fernandes, Portugal  
Paz Fernandez, Spain  
Mohammad Feruj Alam, Bangladesh  
Phil Flentje, Australia  
Yannis Fourniadis, UK  
Edwin Friend, USA  
Irina Galitskaya, Russia  
George Gaprindashvili, Georgia  
George Gardner, USA  
Jesus Garrido Manrique, Spain  
Eldon Gath, USA  
Ben Gilson, UK  
Daniele Giordan, Italy  
William Godwin, USA  
Robert Goldsmith, Australia  
Dick Gray, USA  
Brian Greene, USA  
James Hamel, USA  
Hans-Balder-Havenith, Belgium  
Greg Hempen, USA  
Egerton Hingston, South Africa  
Peter Hudec, Canada  
Matthew Huebner, USA  
Maria Ingunza, Brazil  
Upali De Silva Jayawardena, Sri Lanka  
Filipe Jeremias, Portugal  
Brendon Jones, South Africa  
Frank Jordan, USA  
Kumud Raj Kafle, Nepal  
Sarah Kalika, USA  
Efstratios Karantanellis, Greece  
Ekaterina Karfidova, Russia  
Hamza Karrad, Algeria  
Heiko Käsling, Germany  
Brian Katz, USA  
Katerina Kavoura, Greece  
Andrey Kazeev, Russia  
Jeffrey Keaton, USA  
Klaus-Peterkeilig, Germany  
Alexey Kindler, Russia  
Matheus Klein Flach, Brazil

Aliko Kokkala, Greece  
Goh Thian Lai, Malaysia  
Hana Lee, Austria  
Nkopane Lefu, South Africa  
Leticia Lescano, Argentina  
Cheng Li, China  
Wenping Li, China  
Qian Liu, Austria  
José Lollo, Brazil  
Silvina Marfil, Argentina  
Vassilis Marinos, Greece  
Milos Marjanovic, Serbia  
Kristofer Marsch, Germany  
Pedro Martins, New Zealand  
Flora Menezes, Germany  
Amira Merchichi, Algeria  
Olga Meshcheriakova, Russia  
Stuart Millis, Hong Kong  
Omar Mimouni, Algeria  
Oleg Mironov, Russia  
Matthew Morris, USA  
Tim Mote, Australia  
Elena Mraz, Germany  
Marcos Musso, Uruguay  
Masashi Nakaya, Japan  
Arpita Nandi, USA  
Marivaldo Dos Nascimento, Brazil  
Monique Neves, Brazil  
Holly Nichols, USA  
Vanessa Noveletto, Brazil  
Takehiro Ohta, Japan  
Kazuhiro Onuma, Japan  
Thomas Oommen, USA  
Rolando Orense, New Zealand  
Ibrahim Oyediran, Nigeria  
George Papathanasiou, Greece  
Steve Parry, UK  
Darren Paul, Australia  
Osni Jose Pejon, Brazil  
Giacomo Pepe, Italy  
Regina Pläskén, Germany  
Lindsay Poluga, USA  
Joaquim Pombo, Portugal  
Martin Potten, Germany  
Constantin Prins, Germany  
Mário Quinta-Ferreira, Portugal  
Rute Ramos, Portugal  
Emanuele Raso, Italy  
Liana Rocha, Brazil  
Valéria Rodrigues, Brazil  
Michael Rucker, USA  
Nicholas Sabatakakis, Greece  
Rosanna Saindon, USA  
Mahin Salimi, Iran  
Ligia Sampaio, Brazil

---

Paul Santi, USA  
Regiane Sbroglia, Brazil  
David Scarpato, USA  
Malcolm Schaeffer, USA  
William Schulz, USA  
Jorge Sfragulla, Argentina  
Sachin Shah, USA  
Abdul Shakoor, USA  
Timothy Shevlin, USA  
Anna Shidlovskaya, Russia  
Roy Shlemon, USA  
Zachary Simpson, South Africa  
Alessandra Siqueira, Brazil  
Young-Suk Song, South Korea  
Georg Stockinger, Germany  
Alexander Strom, Russia  
Wanghua Sui, China  
Valentina Svalova, Russia  
Debora Targa, Brazil  
Ashley Tizzano, USA  
Ákos Török, Hungary  
Emil Tsereteli, Georgia  
Ryosuke Tsuruta, Japan  
Atiye Tugrul, Turkey  
Alan Keith Turner, USA  
Anatilius Tushev, Ukraine  
Resat Ulusay, Turkey  
Isabella Magalhães Valadares, Brazil  
Lazaro Valezuquette, Brazil  
J. Louis Van Rooy, South Africa  
Ioannis Vazaios, Canada  
Marlene Villeneuve, New Zealand  
Nicholas Vlachopoulos, Canada  
Yasuhiko Wakizaka, Japan  
Chester (Skip) Watts, USA  
Luke Weidner, USA  
Baoping Wen, China  
Charles Wilk, USA  
Stephen Wilkinson, UK  
John Williams, USA  
Louis Wong, Hong Kong  
Martin Woodard, USA  
Richard Wooten, USA  
Yang Yang, China  
Katherine Yates, New Zealand  
Julia Yeakley, USA  
Murat Yilmaz, Turkey  
Zelin Zhang, China



---

# Contents

## Part I Mining

- Geotechnical Investigations of Mine-Induced Ground Movements in Polish Opencast Mines** . . . . . 3  
Zbigniew Bednarczyk
- Regularities in the Development of Geological Processes upon Collapses at the Undermined Territories of the Potassium Salt Deposit in the Perm Region, Russia** . . . . . 13  
Yuri Mamaev, Victor Osipov, Alexey Yastrebov, Andrey Kazeev, Ksenia Fedotova, and Olga Eremina
- The Petrographic and Geotechnical Properties of a Dolerite Intrusion in the Assessment of Its Blasting Performance at the Magdalena Colliery, Dundee, South Africa** . . . . . 19  
Quinton Nankua, Egerton Daniel Christian Hingston, Sihle Mtshali, and Cebolenkosi Khumalo
- Preliminary Study of the Adsorption Capacity of Pb, Zn and Cd Through Zeolite and Organic Compost** . . . . . 27  
Jacqueline Zanin Lima, Isabela Monici Raimondi, and Valéria Guimarães Silvestre Rodrigues
- A Comparison of Two Methods of Sequential Extraction in a Former Mining Waste Deposit of Pb—Adrianópolis (Brazil)** . . . . . 35  
Mariana Consiglio Kasemodel and Valéria Guimarães Silvestre Rodrigues
- Stability Evaluation and Grouting of Abandoned Coal Mines Used for Building Constructions** . . . . . 43  
Wanghua Sui, Jiawei Liu, and Guangtao Cai
- Detection of Subsidence by Radar Interferometric Data in the Seruci-Nuraxi Figus Coal Mine Area (Sardinia, Italy)** . . . . . 51  
Serena Tessitore, Diego Di Martire, Nicola Mondillo, Lorenzo Ammirati, Maria Boni, and Domenico Calcaterra
- Field Observation of the Unsaturated Characteristics in a Mine Waste Dump During Rainfall** . . . . . 59  
Young-Suk Song and Yong-Chan Cho

## Part II Aggregates

- Petrographic Characterization of Waste Rocks: Applicability as Concrete Aggregates** . . . . . 67  
Maria del Pilar Durante Ingunza, Antonio Carlos Galindo, and Ana Beatriz Azevedo de Medeiros


<b>The Search for New Aggregate Sources in Hong Kong</b> . . . . .	73
Kitty Chan and Stuart Millis	
<b>Abrasiveness Properties at Different Temperatures of Basalt, Marble and Limestone in Turkey</b> . . . . .	79
Candan Alptekin Bilen, Selman Er, Murat Yılmaz, Erdi Avcı, and Atiye Tugrul	
<b>Aggregate Mining in Megacities and Existing Problems: An Example from İstanbul, Turkey</b> . . . . .	85
Atiye Tugrul and Murat Yılmaz	
<b>Study of Hungarian Rocks Regarding Potential Reactivity to Alkalis</b> . . . . .	91
Isabel Fernandes, Maria dos Anjos Ribeiro, and Ákos Török	
<b>Long-Term Wear of Aggregates Assessed by Micro-Deval Tests</b> . . . . .	95
Balázs Czinder and Ákos Török	
 <b>Part III Karst</b>	
<b>Bacterial Processes in Oil-Polluted Karst Environments in Perm Region (Russian Federation)</b> . . . . .	103
Nikolay Maksimovich, Olga Meshcheriakova, and Vadim Khmurchik	
<b>The Influence of Technogenic Factors on the Intensification of Karst on the Eastern Slope of the Urals in Russia</b> . . . . .	109
S. N. Elokhina and S. V. Gorbova	
<b>The Effectiveness of an Inverse Wenner-Schlumberger Array for Geoelectrical Karst Reconnaissance, on the Swabian Alb High Plain, New Line Wendlingen–Ulm, Southwestern Germany</b> . . . . .	115
Constantin Prins, Kurosch Thuro, and Michael Krautblatter	
<b>Experimental Study on Coupled Stress-Dissolution of Carbonate Rocks in Rocky Desertification Area of Karst Plateau, Guizhou, China</b> . . . . .	123
Qi Liu, You'en Bai, Yaoru Lu, and Zhuping Sheng	
<b>Author Index</b> . . . . .	133

---

**Part I**  
**Mining**



# Geotechnical Investigations of Mine-Induced Ground Movements in Polish Opencast Mines

Zbigniew Bednarczyk 

## Abstract

Mine-induced landslide hazard in Polish opencast mines and spoil dumps are a common phenomena. It is caused by a high depth of exploitation, low strength parameters of clayey soils on the slopes and geological or groundwater triggers. In this paper chosen examples of landslides occurring in the largest Polish lignite opencast mines together with implemented investigation and remedial measures are presented. These included the latest monitoring results obtained inside EU Euracoal SLOPES project “Smarter Lignite Open Pit Engineering Solutions” conducted by six European partners. The Polish part of the investigation in this project was performed in the largest lignite opencast excavation in Europe, with a length of 13 km and a width of 3 km. Belchatow mine with a depth of 310 m is affected by numerous landslides with volumes of few thousand to 3.5 million m<sup>3</sup>. Geotechnical investigations carried out for the SLOPES project on the western slope of the mine included 100 m depth on-line shape accelerated inclinometer and pore pressure transducer at 30 m depth. The obtained data should allow for better risk management and were implemented in numerical modeling of instability associated with the pit slope.

## Keywords

Slope stability • Opencast mining • Geotechnical engineering

## 1 Introduction

Lignite opencast mining makes an important contribution to electricity production in a number of European countries. In Poland, Germany, Bulgaria, Romania, Czech Republic and Greece 433.8 million tones is mined every year. This constitutes, approximately 96% of lignite mining in the EU. Brown coal mining is often associated with a number of risks due to the size and depth of the open-pit excavations. This makes it necessary to exploit deeper and deeper deposits and store very large masses of overburden at spoil heaps. Landslide processes are the most important threats to safety and efficiency of exploitation and stability of spoil dumps. Their elimination is often difficult or even impossible. The extent of this serious risk is influenced by the geological structure, low strength parameters, land use, rainfall, changes in groundwater levels, the use of explosives, seismicity, karsts, seepage and suffusion processes. Landslide prevention is all the more important in the mines because the scale of potential failures can be large. Potential losses could cause risk for human life, exploitation efficiency and may adversely affect the environment. To gain a better understanding of the genesis of these processes, their scope, further activity and effective counteraction, the application of complementary research methods is of particular importance.

In order to determine the threats it is necessary to have detailed knowledge of geological structure and engineering geology conditions. These data must be identified and qualitatively characterized. The aim of using innovative monitoring technologies is to obtain reliable data that can be used for risk assessment, validation, and numerical simulation. Individually dedicated strategies for counteracting risks in selected areas could be prepared this way. In each opencast mine, there are three types of slopes: (1) fixed slopes, delimiting the operating limits designed to obtain the license and after the slope is formed by exploitation it remains, unchanged for years, (2) time slopes, which are created in

Z. Bednarczyk (✉)  
Poltegor-Institute, Institute of Opencast Mining, Parkowa 25,  
51-616 Wrocław, Poland  
e-mail: zbyszbed@gmail.com

the mining process, determining the current limit of exploitation, and (3) spoil dump slopes for stored of overburden material.

Loss of slope stability could pose a number of risks to adjacent areas. In order to improve the reliability of geotechnical surveillance methods adapted to each configuration, it is necessary to select appropriate testing and monitoring methods. Monitoring methods could check the size of the recorded displacements in relation to those predicted earlier at the design stage. Very important, good-quality core drilling, combined with geophysics, laboratory tests, and numerical modeling could provide results that are as close to the actual conditions in the mines. The surface displacements in large open pits can be identified by modern surveying methods as laser scanning (terrestrial or airborne UAV), ground-based SAR radar scanning or high-resolution satellite interferometry radar scanning (PSI). However, precise inclinometer measurements could deliver more detailed information about subsurface displacements, their depth range and directions before significant surface displacements could be observed.

Three important factors, influencing the stability of slopes of opencast mines are (1) pore pressure increase in soil and (2) unfavourable soil strength parameters and (3) the dipping of layers. Sand, silt, clay, claystone and others low strength soils or rocks are common in slopes and have a significant influence on the slope inclination design. Geological structure, groundwater conditions and mine drainage system are influencing partial saturation of soils and causing significant changes in their strength parameters. A more reliable interpretation of these conditions could help to optimize safer slope inclination. Exploitation of lignite layers also requires relocation and storage of large masses of overburden on external or internal spoil dump sites. A number of studies on this issue have been carried out in Great Britain (Bishop 1973) and more recently elsewhere (Nguyen and Chowdhury 1984; Steiakakis and Kavouridis 2009).

Landslide activation depends mainly on local geotechnical conditions. Trigger mechanisms are usually very complex and time-dependent. This typically includes a range of complex geological factors such as weathering, variations in stresses, seepage, moisture content variations and shear strength reduction. The effect of the destruction of soil structure and weathering processes over time are important factors to be taken into account especially in clayey soils and rocks subjected to repeated cycles of increasing moisture content and drying (Chowdhury and Nguyen 1986; Ulusay et al. 1995). Opencast mine slopes contain a large number of silts and shale's, which can be disintegrated during wetting and therefore they have an increased amount of the fine-grained clay material. This may reduce their shear strength and make them more prone to high pore pressure

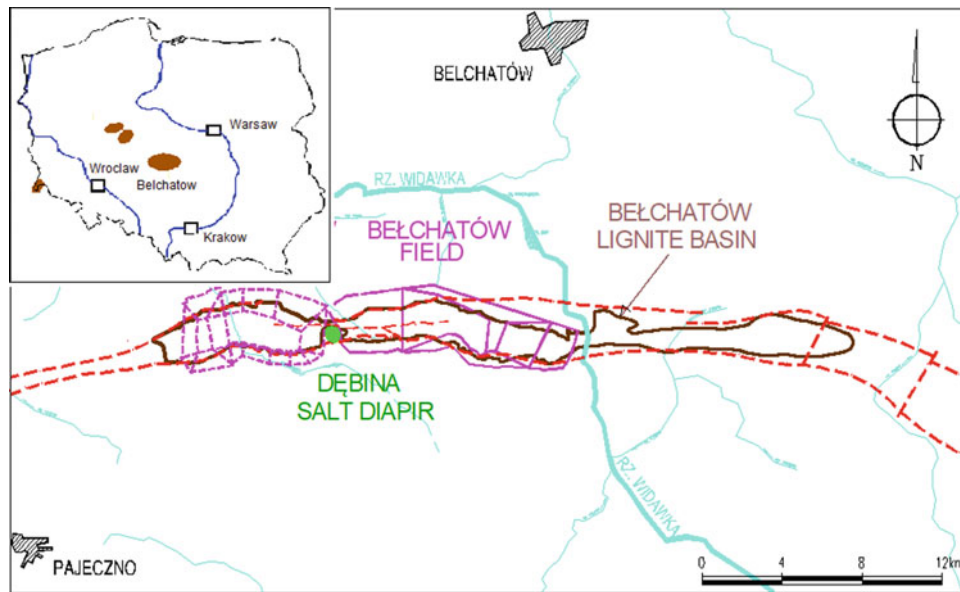
variations which are one of the activating factors (Ulusay et al. 1995; Bednarczyk 2017).

As a part of the Euracoal "Smarter Lignite Open Pit Engineering Solutions" SLOPES project, a laboratory testing, numerical modeling and risk assessment programme are planned. This will include the characterization of soil and spoil dump samples obtained from various European mines using modern research equipment. Special models will be used for this purpose. This paper presents some preliminary results of geotechnical investigations in Polish lignite open-pit mine in Belchatow performed by the author inside the SLOPES project. The project conducted by an international consortium of six European countries. The coordinator of the project is University of Nottingham (UK). Project participants are also University of Exeter (UK), Geocontrol (Spain), Subterra (Spain), VUHU Institute (Czech Republic), Certh Institute (Greece), Ineris Institute (France) and Poltegor-Institute (Poland). The project aims at the practical implementation of a new monitoring methods in lignite opencast mining. The project is conducted in selected opencast mines in Poland (Belchatow), Czech Republic (Most), Spain (Aragón) and Greece (Megalopoli). For a better risk prediction and understanding of its genesis effective implementation of complementary research and counteraction methods have a special role. The paper also includes a general description of project objectives and obtained results.

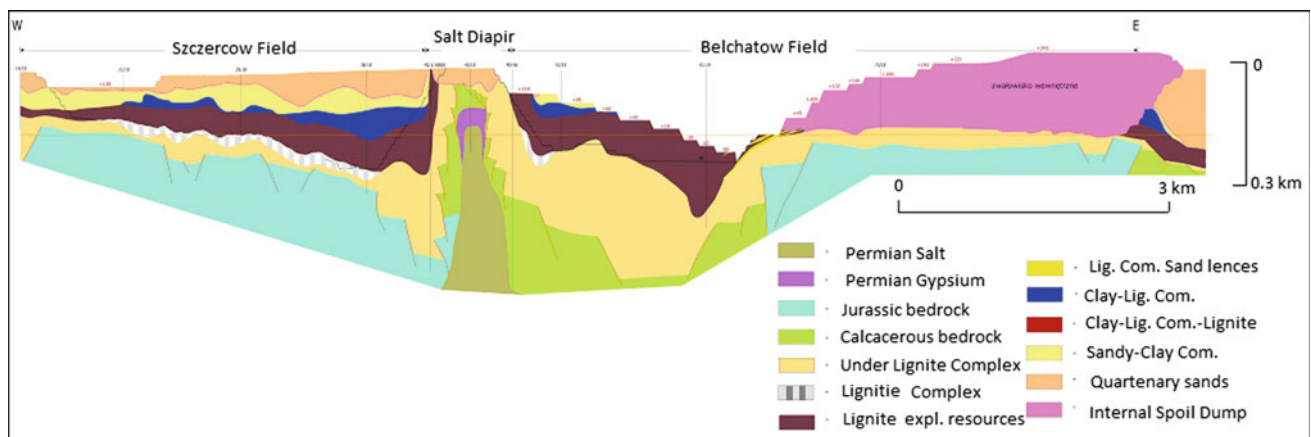
---

## 2 Mine Geology and Location of Ground Movements

Belchatow mine is situated in central Poland, 30 km SW from the city of Lodz (Fig. 1). The mine is located in tectonic rift, formed in Mesozoic limestones and marls and filled by Neogene deposits. Mesozoic blocks are separated along faults and dislocations. The thickness of the deposits within the rift is over 300 m, approximately 5–15 times higher than outside it. The main lignite seam is 20–60 m thick. The mine leads the lignite exploitation on two operational fields, separated by a salt dome. Exploitation of Belchatow field will end in 2018, and at Szczercow field in 2038. The largest volume of lignite is situated in deep secondary graben near the south slope of the Belchatow field. The main landslide-prone structural surfaces are contacts of Quarterly and Neogene deposits, contact of Neogene clays and main lignite deposit. Others landslide-prone surfaces are faults, cracks, tectonic and glaciectonic surfaces, low strength soils and varved Neogene clays (Rybicki 1996). The northern slope of this mine built of Quaternary low-strength varved clays posed numerous risks for conveyor belts transportation lines. In recent years, due to high depth of exploitation and neighboring salt dome structure, eight slope failure risk zones with active or expected



**Fig. 1** Location of the Belchatow Mine



**Fig. 2** Belchatow Mine, W-E geological cross-section

landslides were reported on the west slope at the contact zone of the salt dome and the pit. This slope was selected by the mine personnel for the investigations inside the SLOPES project. New 100 m depth in situ inclinometer and pore pressure instrumentation were installed on the level +42 m a. s.l., 158–258 m below the natural terrain level (Fig. 2).

### 3 Methods of Research

The main objective of the SLOPES project is to respond to geotechnical problems in many fields related to lignite opencast mining. Advanced research methods tested in

selected mines can contribute to its better understanding and risk reduction. The project included four research tasks: (i) development and implementation of modern monitoring techniques in opencast mines, (ii) advanced numerical modeling and risk analysis, (iii) long-term stability of spoil dump slopes. New ground and surface displacement monitoring systems were installed and used for data collection and processing (WP-1). Risk-based methods of prevention are included in project tasks (WP-2). The aim of these studies is to provide new information for the safe design of mine slopes and spoil dump sites in chosen location (WP-3). The fourth task (WP-4) is dedicated to the project coordination.

Complementary monitoring, laboratory tests, modeling and risk analyses are in progress. These include advanced in situ monitoring methods, Persistent Scattered Interferometry (PSI), ground-based laser scanning, different types of laboratory tests from mines and spoil dumps: index test of basic physical parameters of soils (soil type, grain size, moisture content, unit weight, dry unit weight, content of organic material, Attenberg limits), compressibility, direct shear and CID, CIU triaxial tests. Additional centrifuge test for spoil dump soils from Bechatow Mine (Poland) and Most Mine (Czech Republic) are performed at the Centre of Geomechanics University of Nottingham at exceeded gravitational acceleration values using a 50 t centrifuge apparatus with a radius of 2 m. It will allow collection of data from laboratory experiments on a small scale with known soil parameters and individually defined boundary conditions, which can be related to the conditions on dump sites, reflecting real gravity loads (Matziaris et al. 2015).

The results of monitoring will be compared with the numerical modeling. These could provide data for risk assessments, early warning and help optimize and support mining efficiency. In situ monitoring nearly real-time systems allow comprehensive detection of movement depth, range, direction and rate of displacement. Automatic, continuous recording of ground displacement and pore pressure in the ground may facilitate in better prediction of possible threats (Bednarczyk 2012, 2017). The SLOPES project uses unmanned drones to produce Lidar monitoring data. This is a new application of this technology in the opencast mining and RFCS projects. The application of on-line monitoring, data management, and modern monitoring systems should also be a beneficial element of the project.

The suitability of these new methods is tested, among others in the Belchatow Mine in Poland. Shape Accelerated Array monitoring system was installed there for the SLOPES project in 2016. Others implemented in Belchatow monitoring methods includes PSI interferometry, terrestrial laser scanning, UAV Lidar scanning, laboratory tests and numerical modeling. The obtained measurements will provide 3D images and allow for mass movements volume calculation using the special point cloud processing software. It is also planned to use high-resolution PSI radar satellite interferometry, which compares the phases of many surface radar images.

The new methods of monitoring and laboratory tests should allow for the detection of ground movements and pore pressure together with testing of soil strength parameters in conditions similar to those prevailing in the rock

mass, which is subjected to high stress, overburden pressure and occurs in conditions of partial saturation. Precipitation, changes in groundwater table level, partial saturation caused by the mine drainage system can have a significant impact on slope stability conditions.

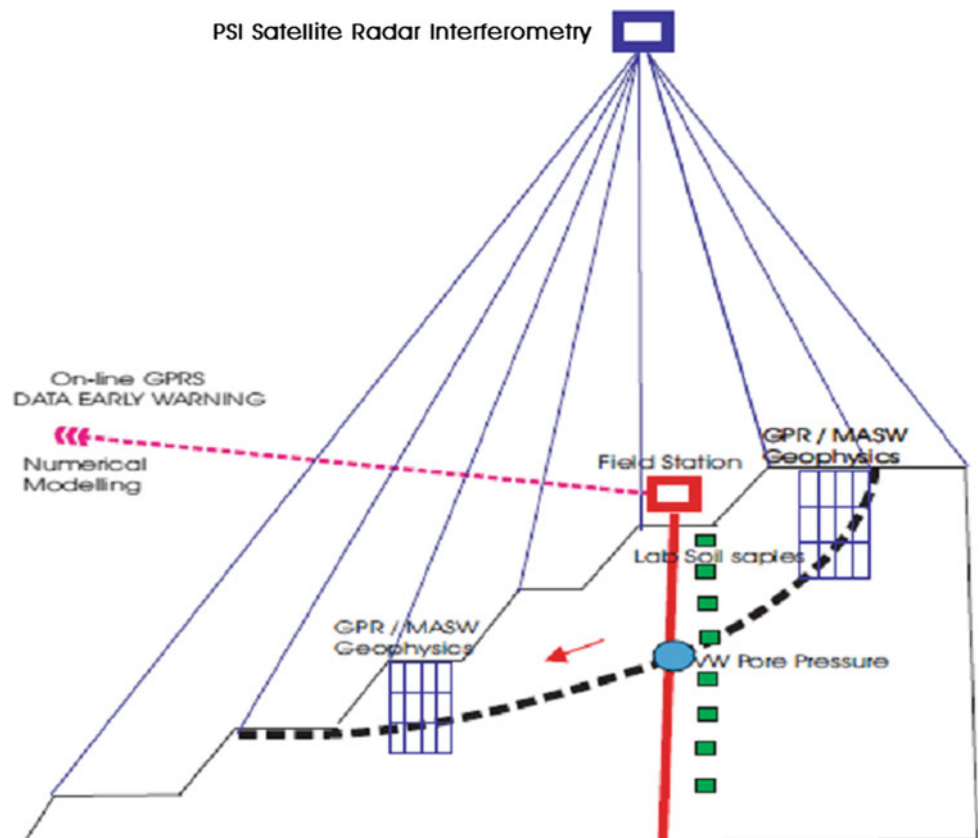
#### 4 Investigations in Belchatow Mine

Investigations for the Slope project were performed in northern part of west slope of Belchatow field. Borehole instrumentation in bentonite-cement grout was performed in December 2016. The scheme of the research is presented on Fig. 3. The investigations include drilling, sampling, monitoring instrumentation and geophysical scanning. A borehole of 132 mm diameter was drilled up to the depth of 100 m at northern part of west slope at level +42 m a.s.l.. The borehole was located in contact zone of the salt dome. The description of the core included soil type, moisture content, consistency and field tests of the soil strength parameters. For laboratory tests, 31 NNS undisturbed samples 90 mm in diameter and 500–700 mm in length were collected. The results of field strength penetrometer tests indicated that soil cohesion ( $C_u$ ) varied 24–44.7 kPa. Undrained shear strength in vane test  $\tau_f$  varied 23.9–47.8 kPa. The lowest values of these test were recognized for silty clays at 54 m depth. Instrumentation included innovative field station with Shape Accelerated Arrays System contains 200 ground displacement sensors every 0.5 m (Fig. 4). The installation is 100 m depth, built from rigid segments and includes 3 magnetometers for rotation control. One segment includes 3 tilt sensors with measuring range of  $\pm 45^\circ$ , accuracy of 0.02 mm/m, an admissible error of joints of  $\pm 0.25^\circ$ . Every octet (8 segments) is equipped with a ground temperature sensor. It was additionally equipped with VW pore pressure sensor located at depth of 30 m. Instrumentation included recorder, GPRS data transmission devices powered by a solar panel. Data registered every 360 min are available online from 19 December 2016. The results of cumulated displacements obtained in 280 days time till 4 October 2017 are presented on Fig. 5. Cumulated displacements in slope inclination direction X reached 110 mm. In the perpendicular Y direction it was 70 mm (Fig. 6).

The largest shear strains in the direction of slope inclination X were recorded at the depths of 0–45 m. In Y direction the largest shear strains were recorded at 15 m depth (Fig. 5). The largest displacement rates were observed in the first 40 days of measurements (Jan–Feb 2017) when



**Fig. 3** The scheme of performed by Poltegor-Institute research



**Fig. 4** Nearly real-time monitoring station installed in Belchatow Mine



they reached 70 mm and in 210–255 days (Aug–Sept 2017) when they increased next 40 mm. The directions of movement were generally parallel with the slope inclination in E and NE directions (Fig. 7a). The total magnitude of observed displacements reached 110 mm.

The values of initially observed pore pressures of 258 kPa at 30 m depth dropped significantly to 120 kPa (Fig. 7b). The largest movements were observed after the pore pressure significant drop. The displacements in deeper layers were probably caused by complex factors including



uplift of the coal seams by the salt dome. The alarm setting was defined using previous alarm setting from the mine as 30 mm a day. However, this was not observed until August 2017.

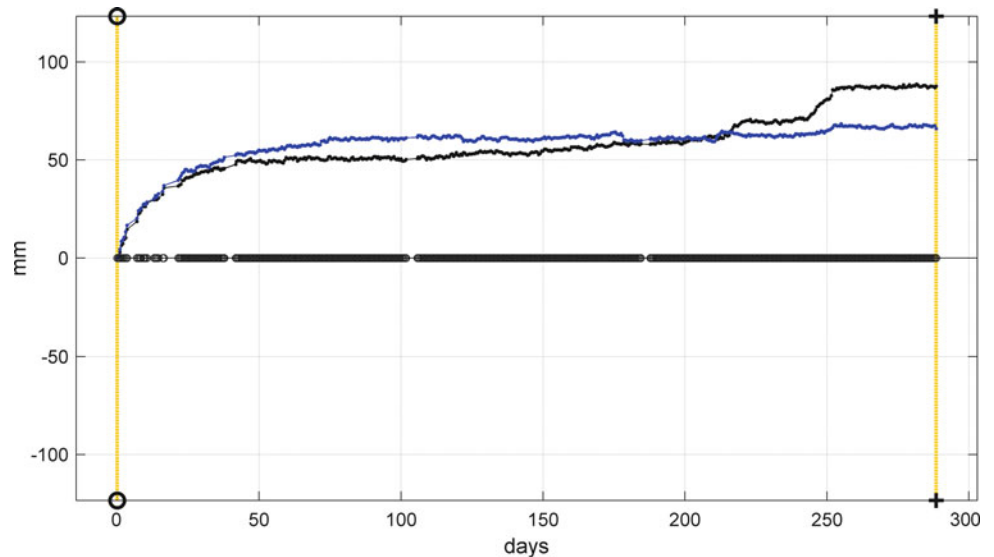
## 5 Numerical Modeling

Numerical modeling using Flac 8.0 and Shear Strength Reduction Method (SSR) was performed in two cross-sections in lines with the highest slope inclination. It allowed identification of factors of safety ( $F_{os}$ ) for the selected slope. The SSR Method tends to reflect the actual condition on the slopes leading to the reduction of shear strength of soil till to stage of losing stability. The implemented Mohr-Coulomb elastoplastic strength model required specification of bulk density, effective cohesion and effective angle of internal friction. The principles of soil and rock classification recommended by the Eurocode 7 (CEN 1994) introduced general concepts in geotechnical design. It includes derived characteristic and design values of effective strength parameters from so-called comparable experience (Kulhawy 1992; Phoon and Kulhawy 1999). The strength parameters used for the calculations were assumed

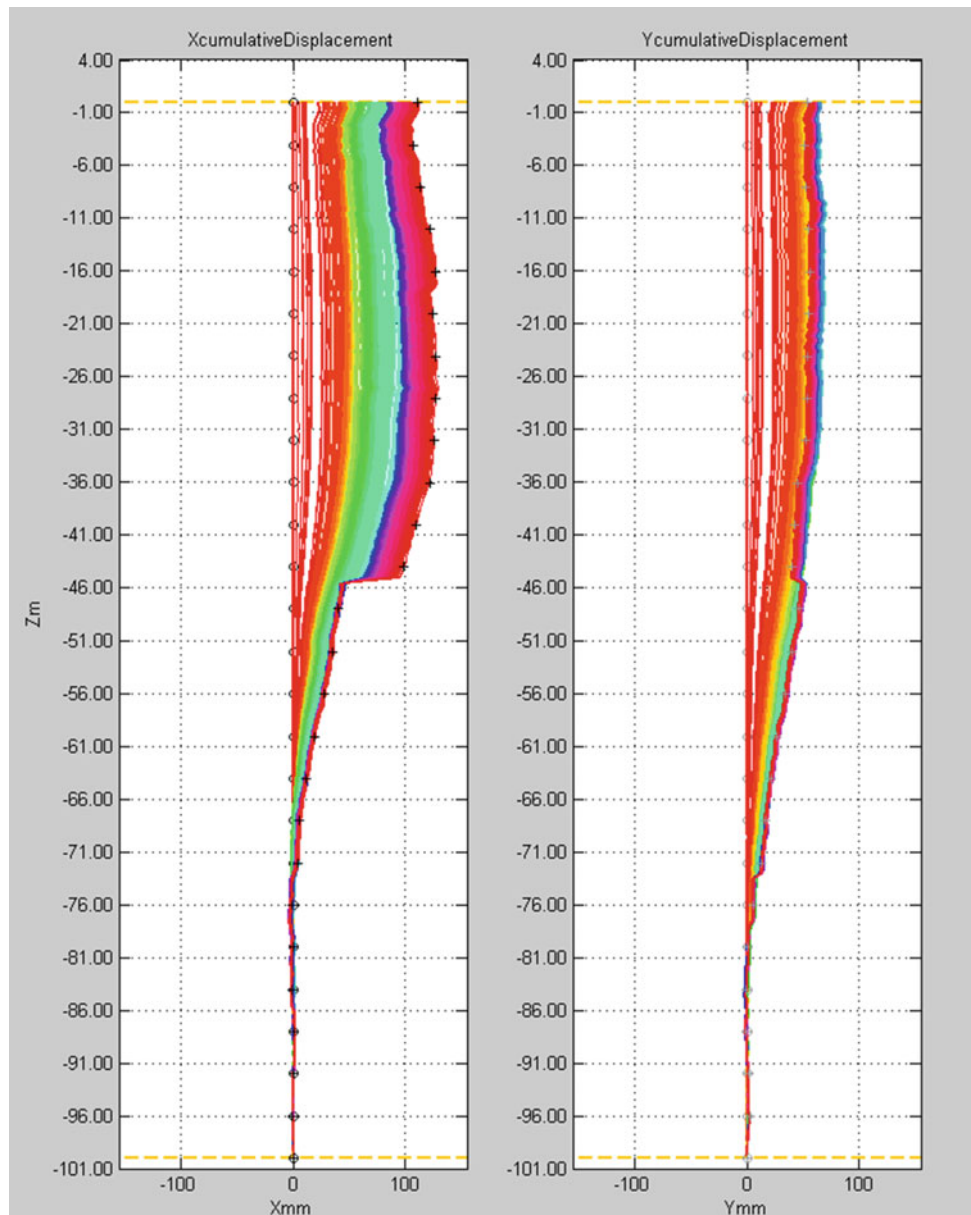
on the basis of corrected values from previous investigations and modeling (Bednarczyk 2017). For Mesozoic rocks, parameters were specified using GSI classification (Marinos and Hoek 2005). The complex geological structure of the slope required generalization of selected layers characterized by similar strength parameters. An example of the geometry of layers in analyzed cross-section is presented in Fig. 8.

The obtained factors of safety values were low ranging from 0.85 in section 20 WE to 1.14 in section 18WE (Fig. 9). The result indicates that it is a high risk affecting the entire west slope. These results were confirmed by the field inspection and monitoring which detected activation of mass movements close to this area (Fig. 10). The ground movements were caused by multiple factors as mining, low strength parameters, slope height and salt dome influence. The investigated slope is subjected to a very complex state of stresses in the rift. The changes in the stress conditions cause the reactivation of faults, tectonic surfaces and cracks, uplift of coal seams at the west slope and opening of natural cracks prone to water infiltration. The presented results are preliminary and will require confirmation in more representative studies taking into account results of the laboratory tests and monitoring results.

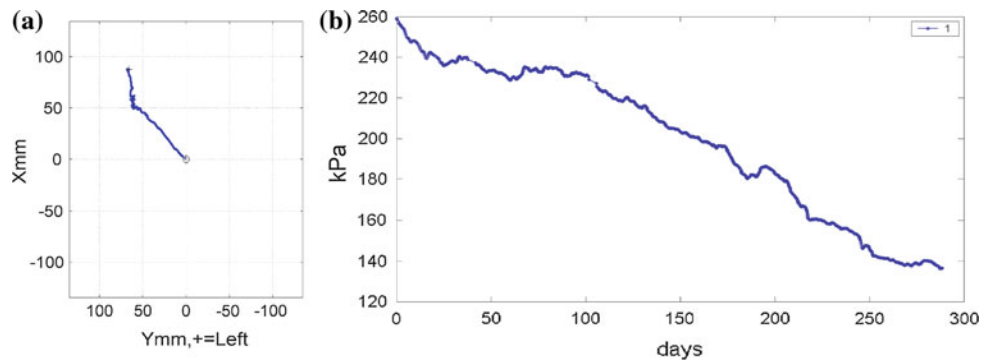
**Fig. 5** Monitoring results, X, Y displacements magnitude with time, Belchatow Mine

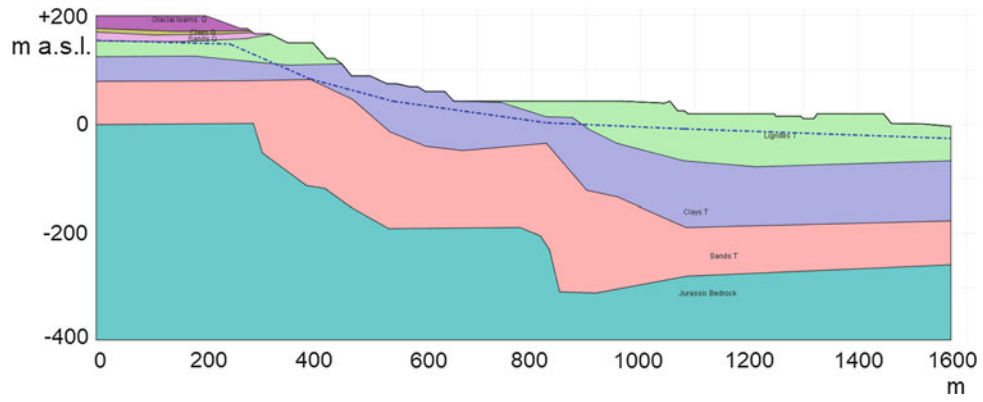


**Fig. 6** Monitoring results, X, Y cumulated displacements, Belchatow Mine

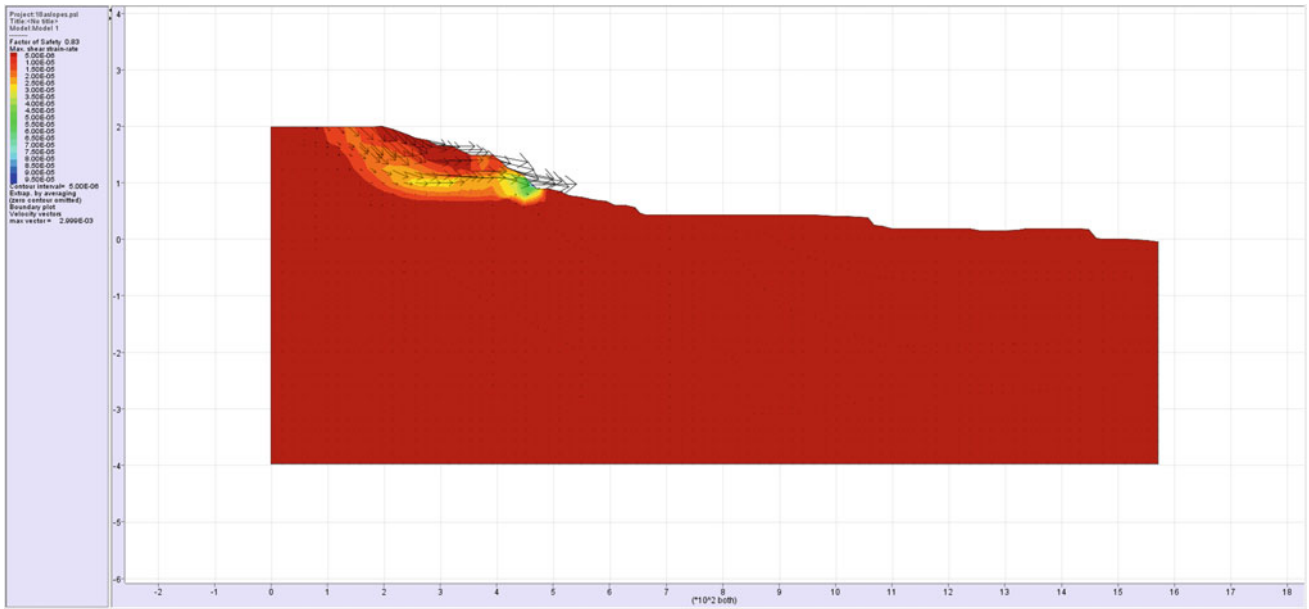


**Fig. 7** Monitoring results, **a** total displ. directions [mm], **b** pore pressure [kPa]





**Fig. 8** Simplified mesh for the stability analyses, cross-section 18WE, Belchatow Mine



**Fig. 9** Slope stability analysis result, cross-section 18WE,  $F_{os} = 0.83$ , Belchatow Mine

**Fig. 10** Landslide near the cross-section 18WE, west slope of Belchatow Mine



## 6 Summary and Conclusions

This paper presents the methods of investigations in open-cast mines and the preliminary results from the research performed by the author for the SLOPES project. It includes an experimental field programme and slope stability analyses in the selected areas of open-cast mines. Modern monitoring methods provided new geotechnical data for hazard warning and risk analysis. The results of the field on-line monitoring on the west slope of Belchatow Mine detected displacement magnitude of 110 mm and excess of pore pressure of 120 kPa in one year time. The slope is characterized by low factor of safety  $F_{os} = 0.83\text{--}1.10$ . These data will be compared and validated by the results obtained from laboratory tests and numerical modeling.

**Acknowledgements** The author would like to acknowledge the EU Euracoal Agency and the Polish Ministry of Science and Higher Education for the financing of the SLOPES RFCR-CT-2015-00001 project. I would like to thank the PGE GIEKSA Company for involvement and help in presented research.

## References

- Bednarczyk, Z.: Landslide investigation and monitoring methods. In: Surface Mining Surface Mining, Wrocław, 213 p (2012)
- Bednarczyk, Z.: Landslide monitoring and counteraction technologies in polish lignite opencast mines. In: Advancing Culture of Living with Landslides, vol. 5, pp. 33–43. Springer, Berlin (2017)
- Bishop, A.W.: The stability of tips and spoil heaps. *Q. J. Eng. Geol.* **6**, 335–376 (1973)
- CEN. Eurocode 7: geotechnical design. Part 1: General rules, ENV 1997-1. European Commission for Standardization, Brussels. (1994)
- Chowdhury, R.N., Nguyen, V.U.: Spoil stability considering progressive failure. *Min. Sci. Technol.* **3**, 127–139 (1986)
- Kulhawy, F.H.: On the evaluation of static soil properties. In: Geotechnical Special Publication 31 ASCE. pp. 95–115 (1992)
- Marinos, V.P., Hoek, E.: The geological strength index: applications and limitations. *Bull. Eng. Geol. Environ.* **2005(64)**, 55–65 (2005)
- Matziaris, V., Marshall A.M., Yu, H.S.: Centrifuge model tests of rainfall-induced landslides. In: Springer Series in Geomechanics and Geoengineering, vol. 1, pp. 73–83, (2015)
- Nguyen, V.U., Chowdhury, R.N.: Probabilistic study of spoil pile stability in strip coal mines—two techniques compared. *Int. J. Rock Mech. Min. Sci. Geomech. Abstr.* **21**, 303–312 (1984)
- Phoon, K., Kulhawy, F.H.: Characterization of geotechnical variability. *Can. Geot. J.* **36(4)**, 612–624 (1999)
- Rybicki S.: Zjawiska osuwiskowe w krajowych kopalniach węgla brunatnego, ich skala, charakter i uwarunkowania. „Problemy Geotechniczne. Wydawnictwo Politechniki Krakowskiej: 157–164 (in Polish) (1996)
- Steiakakis, E., Kavouridis, K.: Large scale failure of the external waste dump at the “South Field” lignite mine, Northern Greece. *Eng. Geol.* **104**, 269–279 (2009)
- Ulusay, R., Arıkan, F., Yöleri, M.F.: Engineering geological characterization of coal mine waste material and an evaluation in the context of back-analysis of spoil pile instabilities in a strip mine, SW Turkey. *Eng. Geol.* **40**, 77–101 (1995)

# Regularities in the Development of Geological Processes upon Collapses at the Undermined Territories of the Potassium Salt Deposit in the Perm Region, Russia

Yuri Mamaev, Victor Osipov, Alexey Yastrebov, Andrey Kazeev, Ksenia Fedotova, and Olga Eremina

## Abstract

The studies performed at the Sergeev Institute of Environmental Geoscience RAS (IEG RAS) in the territory of VerkhneKamskoe potassium salt deposits in the Perm region of the Russian Federation are aimed at the assessment of geological conditions and the forecast of geohazard occurrence within the undermined areas of potassium mines in Solikmask-Berezniki urban and industrial agglomeration (SBUIA). The work mainly involves engineering geological interpretation of the available data on geological and engineering survey, complex monitoring, as well as numerical simulation of geoenvironment for investigating groundwater filtration and the data on the transformation of the stress-strain state of rock massifs. The results obtained are important for minimizing risks of accidents at the operating mining facilities.

## Keywords

Deposit of potash salts • Mine workings • Dips in the earth's surface • Regularities of changes in geological conditions

## 1 Engineering Geological Conditions

According to the tectonic scheme of the East-European platform, the studied SBUIA territory is located within the CisUrals tectonic foredeep. In terms of tectonics, this area belongs to the zone of faulty-blocky structures of different level with numerous disjunctions of different age renewed in

the period of neotectonic activation. Major tectonic sublatitudinal faults intersect the potassium salt deposit (which stretches from north to south for about 140 km) to divide it into 7 large subregional blocks, each of them being cut into smaller blocks by minor tectonic disruptions of different stretch. Neighbor blocks may be displaced along the tectonic faults for tens of meters in amplitude.

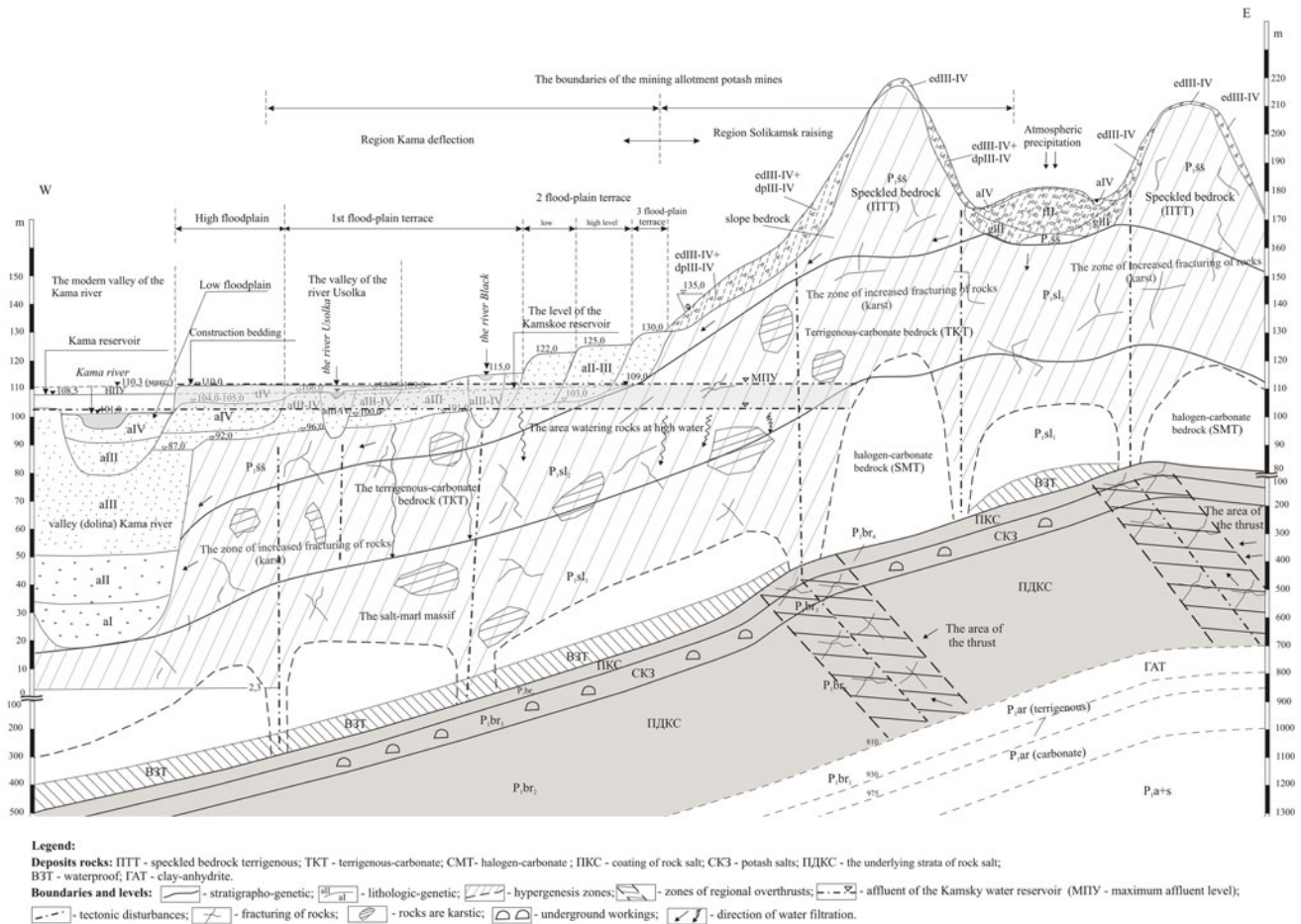
The terrigenous-carbonate and halogen-carbonate bedrock of Lower Permian crop out at the surface (Fig. 1). Prevailing are the terrigenous-carbonate deposits of Solikamskaya suite ( $P_{1usl_2}$ ) composed of interbedding marl, clayey gypsiferous limestone, sandstone, aulerolite and limestone clay, all the deposits being of low and moderate strength, fractured, weathered, and water saturated. The massif thickness reaches 150 m. Locally, the salt-marl massif of Solikamskaya suite ( $P_{1usl_1}$ ) occurs close to the surface, which is represented by marl with interlayers of limestone, calcareous clay, gypsum and rock salt. These rocks manifest low strength, poor deformability, high solubility and high karstification degree. They are underlain by a thick (>400 m) rock salt bed containing the potassium salt deposit. Mantle deposits are represented by alluvial (aIII, aIII-IV, aIV), proluvial (pIV), deluvial (dIII-IV), eluvial-deluvial (edII-IV), fluvio-glacial (fIII-IV) and other lithological genetic Quaternary complexes. The thickness of Quaternary mantle varies from 1–2 to 10 m, more rarely to 20 m. Two main aquifer complexes are distinguished in the regarded area. The alluvial Quaternary groundwater aquifer complex is widespread within alluvial terraces of different level and age. This groundwater complex consists mainly of unconfined stratal-porous aquifers with infiltration recharge, which is closely hydraulically connected with the Kama water reservoir level.

The Permian aquifer complex consists of groundwater differing in filtration conditions, i.e., of fracture-ground, stratal-fracture, fracture-karst, etc. types. Mineralization and the soluble salt composition of groundwater vary widely from freshwater to brine with mineralization up to 300 g/dm<sup>3</sup>. This aquifer recharges from precipitation

Y. Mamaev · V. Osipov · A. Yastrebov · A. Kazeev (✉)  
K. Fedotova · O. Eremina  
Sergeev Institute of Environmental Geoscience RAS, Ulanskiy  
lane 13/2, Moscow, 101000, Russia  
e-mail: kazeev@yandex.ru

Y. Mamaev  
e-mail: mamaev47ya@mail.ru





**Fig. 1** Schematic engineering-geological section of the site of work

infiltration and from the interflow from the Quaternary aquifers to the weathered highly fractured zones. This groundwater complex discharges to the overdeepened Kama River valley, and partially, to the surface waterflows and water reservoirs.

Hazardous geological processes are widespread and very active in the area, being inspired, above all, by technogenic activity. Flooding and waterlogging of territories, surface subsidence due to the mined subsurface in the zone occupied by industrial facilities and residential houses, as well as karst and suffusion processes inducing sinkholes and collapses are registered there. High seismicity in the area (up to 6 points of magnitude) is caused by both natural tectonic block movements and mine works in oil, gas, and mineral deposit extraction. The induced seismicity upon the rock bumps, failure of mine workings roofs, surface collapses, and technological explosions. Hypergenic transformation of Permian deposits appears to be the long-developing process in the studied area. It leads to the transformation of composition,

state and properties of rocks due to their decompaction, fracturing, physical and chemical weathering, and leaching. Geophysically, the depth of hypergenesis zone is bounded to 90 m from the surface, and it may spread down to hundreds meters along highly fractured zones of major tectonic disjunctions. Karst and suffusion are considered to be the most hazardous processes in the given territory. All types of karst, i.e., carbonate, sulfate, and halogen karst are registered in the geological cross-section of the region. The present-day karst process develops most intensely in the zone of yearly cyclic fluctuations of river and groundwater tables. It is intensified by the economic activity, namely, huge water intake. The intensity of karst-suffusion processes has increased considerably in the regarded area since 2006 as a result of the accident at one of the potassium mine, where an active downward seepage through the above-salt strata went for a long time as a result of enormous water ingress (up to 7000 m<sup>3</sup>/h) to the subsurface mine workings. Simultaneously, all surface water bodies (minor rivers and streams, ponds and wells) were drained.

## 2 Research Methods

In order to study, predict and prevent the geohazard development and to minimize related losses, complex real-time monitoring observations over the geoenvironment state, dynamics of geological processes and deformations of engineering structures are carried out in the territory of SBUIA mine fields. Long-term monitoring observations are arranged in the mining zone using a vast complex of aerospace, geodetic, underground surveying, geomechanic, geophysical, seismological, geochemical, hydrogeological, gas geochemical, geomorphological and other methods. The studies in groundwater filtration assessment, contaminant migration, and the transformation of stress-strain state of rock massifs are performed using 3D mathematical models of the geoenvironment. These studies permit researchers to reveal regularities in the development of geological processes and to predict them. Suggestions and recommendations are elaborated on ensuring the safe operation of rock salt deposits and on minimizing losses for industrial and civil engineering structures.

## 3 The Established Regularities of Geological Processes

### 3.1 Geomechanical

The results of long-term geodetic observation performed at different sites of the SBUIA mine fields permitted us to derive some regularities in the development of surface deformations and collapses. The undisturbed areas located within the uplifted territory show the background values of the possible surface deformations equal to 0–3 mm/year due to ground swelling, shrinkage, frost heaving and thawing of frozen clay soils. In the undisturbed areas by mining within the Kama River basin and the waterlogged zone as affected by the Kama reservoir, the day surface deformations may reach 12–15 mm/year. As a rule, they show annual cycles, being explained by weighing of fine particles of Quaternary deposits upon floods in the high water season and the subsequent compaction in the low water season.

In the areas disturbed by mining, rheological processes in salt and above-salt horizons developing upon the long-term altered stress-strain state result in surface deformations, i.e., local land subsidence, shift zones, sinkholes and collapses. At the same time, the surface deformations result from the hypergenic decompaction of ground massifs due to fracturing, weathering, groundwater seepage, leaching, suffusion, etc. The values and velocity of surface subsidence depends on the process stage (background deformations, the initial stage of the earth surface subsidence, the active stage with

sinkhole formation, or the terminal stage), as well as on the site allocation in respect to the epicenter of the collapse sinkhole, i.e., the peripheral or the central part of the forming sinkhole zone. In the peripheral zones of sinkholes, the rates of surface deformation range within 20–40 mm/month. Within the zones of active influence of developing sinkholes, the surface subsidence rate rises to 50–80 mm/month. In the central parts of sinkholes, the deformation rates are maximal reaching 100–200 mm/month.

In terms of geomechanics, these features are explained by the development of, first, creep, flow processes changing the rock density and gradually decreasing the rock strength and next rock destruction and failure in the massifs overlying mine workings. Upon vast and voluminous mine workings, zones of significant subsidence (up to 3–4.5 m) are formed at the day surface, with their depth increasing from year to year. The ground collapses proper develop catastrophically quickly, being accompanied by the formation of round-shaped cavities with nearly vertical walls.

Their dimensions usually vary from 5 to 20 m in size and 15–20 m in depth. Further, their surface dimensions increase up to 100–150 m, more rarely to 300–400 m, with depth reaching 80–100 m. This depth corresponds to the lower boundary of the supergenesis zone and the terrigenous-carbonate bedrock horizon occurring at the surface, as registered by the drilling and geophysical data. Collapse progress is often accompanied by methane and hydrogen sulfide gas and gas-dust emissions, which is observed visually and by smell (Fig. 2).

### 3.2 Geophysical

The development of subsidence troughs and collapse sinkholes may be predicted geophysically. These methods permit researchers to allocate, control and predict the geomechanical processes, including those developing at the sites prone to surface deformations and collapses. Figure 3 shows the results of electric survey profiling at the site of future collapse within the undermined territory of potassium mine. The results were obtained a year before the collapse happened there. The profile shows vividly a substantial transformation in their electric field within the limits of the future sinkhole with the changed direction of strata manifesting different specific electric resistance.

The areal seismological control over the processes in the rock massifs in the areas disturbed by mining activity is carried out within the potentially hazardous sites using a network of mobile seismological stations with deepened registration sensors of seismic events (blows, shocks, or failures) caused by the destruction of weathered, fractured weak rock massifs either above or near the mine workings and karst voids.



**Fig. 2** Emission of gas in the formation of a dip in the mine

The epicenter coordinates and energy parameters of seismic events are registered. Increasing frequency and magnitude of seismic event points to the intensification of the collapse process.

The abnormal zone in the structure of impermeable rock strata protecting the salt beds from dissolution are revealed from geological and geophysical data. These zones may be specified by a small thickness or absence of aquicludes in the geological cross-section at the studied site; by the presence of major tectonic faults or densely fractured zones; by the impact of seismic or tectonic processes, or technogenic impact.

### 3.3 Hydrogeological

Hydrogeological investigations provide important data on the features and stages of deformations in the rock massif. The groundwater level monitoring in the hydrogeological and engineering geological drillholes within the sites of formed sinkholes above the flooded mine workings reveals an abnormal decrease in the groundwater table in the above-salt strata 15–45 days prior to the collapse at the day surface. This is explained by a powerful downward

groundwater flow filling mine workings (Trofimov and Kochneva 2012), which under certain conditions (large volumes, high gradients and high velocities of groundwater filtration, heterogenic texture, composition and high fracturing of rocks) induces karst and suffusion, which in their turn, produce open (washed off) fractures, voids, and openings. As a rule, all surface water bodies disappear in the zone influences by the collapse sinkhole.

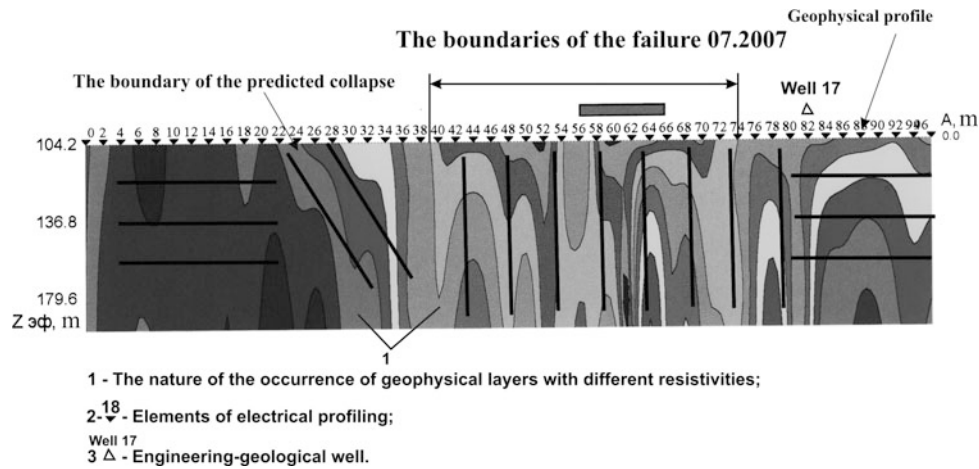
Substantial deformations, surface collapses, and high fracturing of rocks in the hypergenesis zone favor the intense mixing up groundwater and overflow between aquifers, including in the upward direction. This may be connected with the salt strata failure into the flooded mine workings and extrusion of brine from the deep horizons, which results in groundwater ponding and level rise.

Changing groundwater regime at the collapse sites is accompanied by the noticeable changes in its chemical composition and mineralization. The hydrogeochemical studies in the observation wells drilled within the collapse sites attest to a substantial increase in the mineralization and concentration of certain chemical elements in the groundwater (i.e., bromine, calcium, potassium, etc.) in the upper part of geological cross-section prior to the sinkhole formation at the surface (Osipov et al. 2016). The collapse sites and the adjacent zones show an elevated content of hydrocarbonates in groundwater (ranging within 0.5–1.4 g/l), whereas their background content in the groundwater at this mineral deposit field usually does not exceed 0.1–0.3 g/l (Mustel and Shlendova 2016). The rock failure in the flooded mine workings must extrude highly mineralized water from deep aquifers upwards to the surface and to the karstified rock massifs overlying the salt beds. Shortly operating ascending water flows arise, which bring high mineralized water upward, which is registered in the observation wells. This phenomenon may be regarded as the indicator or precursor of the accelerating rock massif failure at the depth prior to the sinkhole formation at the surface.

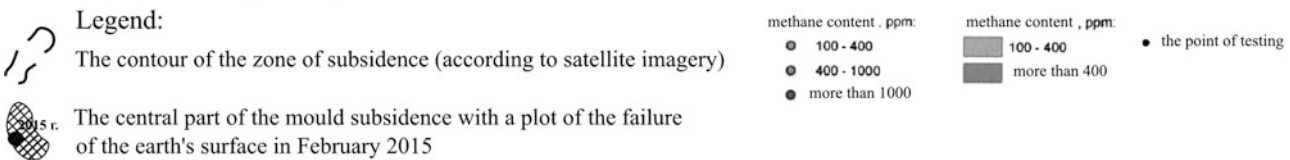
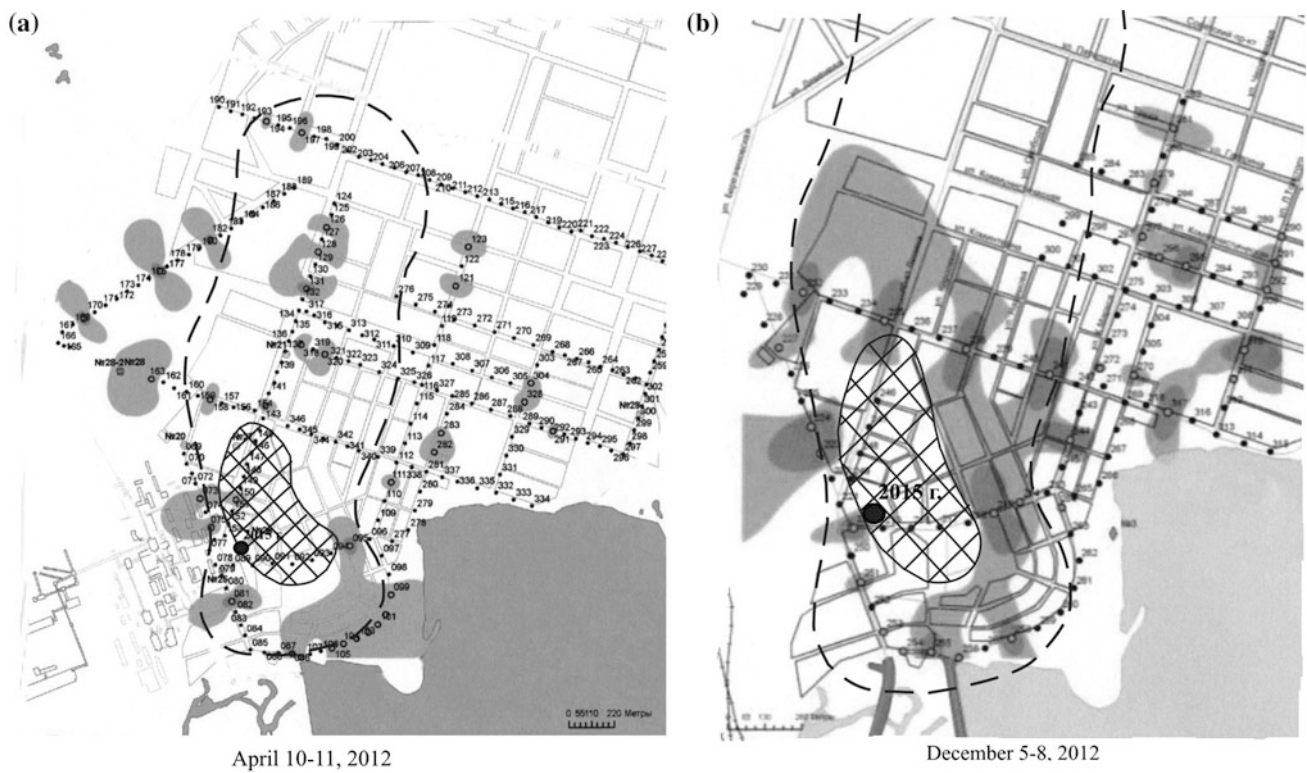
### 3.4 Gas and Geochemical

As proceeds from gas geochemical studied of subsoil gases, the deformation and destruction of salt rock massifs are accompanied by their degassing and emission of scattered and bound gases, i.e., methane, carbon dioxide, hydrocarbons (C1–C5), hydrogen sulfide, etc. Methane appears to be the principle gaseous indicator of the discussed processes. Gases enter the subsoil and soil forming the abnormal gas saturated zones usually confined to the zones of high fractured deposits, along which the mass transfer of gases goes upon the deformations in rock massifs in the salt and above-salt strata. At the initial stage of subsidence troughs formation, small zones of abnormal gas saturation are spread





**Fig. 3** The profile of apparent resistances (profile no. 1) across the future collapse site



**Fig. 4** The results of gas geochemical monitoring in the southwestern part of Berezniki town in different periods of time (according to the data of Mining Institute, Urals Division RAS, supplemented)

evenly and chaotically (Fig. 4a). As the subsidence troughs develops above the underground voids, the central parts of these troughs show either low concentrations of hydrocarbons in the subsoil air or their absence at all. On the contrary, in the periphery of subsidence troughs, numerous abnormal zones are registered, being often united to enlarge the abnormal areas (Fig. 4b).

Gas geochemical anomalies for methane point to the intensely going processes of deformation, dissolution and mass transfer in rock massifs, as well as to the highly fractured zones in the above-salt strata. The low concentrations of methane in the subsoil air indicate to the attenuation or absence of leaching salts and geodynamic processes.

#### 4 Conclusions

The above-described regularities in the geological processes in the undermined areas of potassium salt deposits may be considered as the prediction features of hazardous deformations and rock mass failures with possible surface collapses. These regularities are important for allocating the hazardous sites and zoning territory by the technonatural hazard degree, elaboration of protective measures for territories and engineering structures, and planning residential and industrial districts within the territory of developed potassium salt mines.

The revealed regularities in the development of geological processes in many respects are based on the perennial complex monitoring and measurements. The applied monitoring methods may differ for different engineering structures and territories; however, they should supplement each other and should be carried out permanently, which permits controlling and predicting the geohazards and to undertake the preventive measures timely.

**Acknowledgements** The research was supported by Russian Scientific Foundation (Project No. 16-17-00125).

#### References

- Mustel, I.P., Shlendova, T.K.: Transformation of hydrogeological conditions upon the accidental deformation of undermined rock mass (by the example of BKPRU-1 mine). *Gornyi zhurnal*, No. 6, pp. 32–39 (2016). (in Russian)
- Osipov, V.I., Baruyach, A.A., Sanfirov, I.A., Mamaev, Yu.A., Yastrebov, A.A. Hydrogeomechanical conditions of karst collapse development in the territory of potassium mines in Berezniki, Perm krai. *Geoekologiya*, No. 2, pp. 142–148 (2016). (in Russian)
- Trofimov, V.I., Kochneva, M.N.: Hydrogeological prediction of karst processes at the BKPRU-1 “Uralkalii” mine. *Gornoe echo*, Perm, Mining Institute Urals Division RAS, no. 2, 2012, pp. 33–45 (in Russian)

# The Petrographic and Geotechnical Properties of a Dolerite Intrusion in the Assessment of Its Blasting Performance at the Magdalena Colliery, Dundee, South Africa

Quinton Nankua , Egerton Daniel Christian Hingston, Sihle Mtshali, and Cebolenkosi Khumalo

## Abstract

The presence of dolerite intrusions in underground collieries often causes damage to mining equipment, delays in mining schedules and loss in production. This is often exacerbated by inadequate pull from the blasting operations along the intrusion. Thus, the proficient removal of dolerite intrusions through efficient blasting techniques play a vital role in the economic output of a colliery. This study is focused on one such intrusion within the Magdalena Colliery, wherein a 13.88 m dolerite dyke resulted in the replacement and displacement of the Alfred seam. Selected sampling was conducted along the length of the intrusion in order to determine the petrographic and geotechnical properties influencing the blasting performance of the dyke. A detailed petrographic analysis was done by analyzing thin sections of the dolerite in order to identify the major minerals present. X-ray diffraction (XRD) analysis was also conducted to determine the percentage composition of minerals along the intrusion. Geotechnical tests were also conducted in order to assess the technical properties of the dolerite. The geotechnical tests conducted included point load test, sound velocity test, uniaxial compressive strength test and Brazilian disc strength test. The study conducted demonstrates that a strong correlation exists between the blasting performance and geotechnical and petrographic properties of the dyke.

## Keywords

Alfred seam • Blasting • Dolerite intrusion • Pull

## 1 Introduction

South Africa is one of the largest coal producers in the world, where coal mining has been going on a commercial basis since 1857. Whilst in-roads are being made into clean energy, coal remains the primary energy source in South Africa for domestic power generation, and is set to dominate energy demands for the foreseeable future (Hancox and Götz 2014). Buffalo Coal currently operates two collieries in Dundee, South Africa; the Magdalena Colliery and the Aviemore Colliery, which are hosted within the Klip River coalfield. The Aviemore Colliery extracts high-grade anthracite coal while the Magdalena Colliery extracts high-grade bituminous coal (Muller et al. 2013). The focus of this study was the Magdalena Colliery, which has been mining bituminous coal since 2005.

Two coal seams, which are referred to as the Alfred seam and the Gus seam of the Vryheid Formation, are currently being mined at the Magdalena Colliery. Mining is by the bord and pillar method, also referred to as the room and pillar method, whereby a continuous miner is used to extract bituminous coal from the Alfred seam and the Gus seam. The bord and pillar mining method involves the extraction of coal from relatively flat-lying deposits, whereby the excavation is carried out to produce a network of rooms between pillars of coal that are left behind to support the overlying strata (Brady and Brown 2006; Esterhuizen et al. 2013; Clemente et al. 2013). The rooms that are produced as a result of excavation of the coal seams act as access openings, haul roads, and ventilation paths.

It is well known that igneous intrusions, mostly dolerite dykes and sills, are ubiquitous within the coal bearing formation (Roberts 1987). These intrusions within the coal, result in damage to mining equipment and significant loss in production. This study is focused on one such occurrence within Panel 417, Section 1 of the Magdalena Colliery, wherein a dolerite intrusion spanning a length of 13.88 m was encountered, resulting in both replacement and

Q. Nankua · E. D. C. Hingston (✉)  
University of KwaZulu-Natal, King George V Ave, Durban, 4041,  
South Africa  
e-mail: hingstone@ukzn.ac.za

S. Mtshali · C. Khumalo  
Buffalo Coal, Dundee, South Africa

displacement of the coal seam. This caused a significant delay in the mining schedule and was exacerbated by inadequate pull from the blasting operations along the intrusion. The proficient removal of dolerite intrusions through efficient blasting techniques thus play a vital role in the economic output of the colliery.

The main aim of this study was to assess the influence of the petrographic and geotechnical properties of the dolerite on its blasting performance. A detailed petrographic analysis of the intrusion was conducted in order to determine the primary minerals present as well as the nature of minerals present. X-ray diffraction (XRD) analysis was also conducted to determine the percentage composition of minerals along the intrusion. Laboratory tests were conducted on selected samples obtained along the intrusion in order to determine the geotechnical properties along the course of the dolerite intrusion. The geotechnical properties determined were the density, porosity, point load strength, uniaxial compressive strength and Brazilian disc test. Assessment of the blasting advance was done using a laser distometer.

## 2 Location of the Study Area

The study area is located within the Magdalena Colliery, which is approximately 22 km north of the central town of Dundee, in the KwaZulu-Natal Province ( $27^{\circ} 58' 24''$  S and  $30^{\circ} 11' 51''$  E), South Africa (Fig. 1). The towns of Hattingspruit, Normandien, and Fort Mistake lie to the south, west-southwest, and southwest respectively of the Magdalena Colliery.

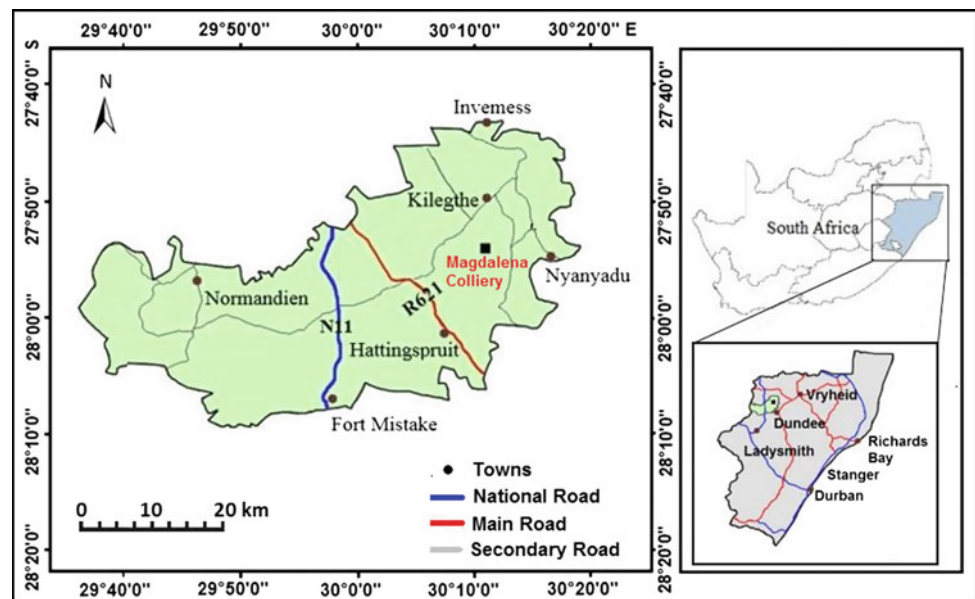
## 3 Geology of the Study Area

The study area lies within the Vryheid Formation of the Ecca Group, a subdivision of the Karoo Supergroup, which is of Carboniferous age (320–180 Ma) (Johnson et al. 1997). The Vryheid Formation comprises feldspathic sandstone, grey micaceous shale, and mudstone (Fig. 2) (Muller et al. 2013). The Vryheid Formation contains five coal seams that persist throughout the Formation (Venter 1994). The coal seams currently located at the collieries belong to the Klip River coalfield. These represent the two most economically minable seams, the upper Alfred seam and the lower Gus seam (Muller et al. 2013). The Alfred seam is more developed than the Gus seam, as it ranges in thickness from 1.5 m in the south to 3.3 m in the north, whereas the less developed Gus seam ranges in thickness from 0.5 m in the south to 2 m in the north (Muller et al. 2013).

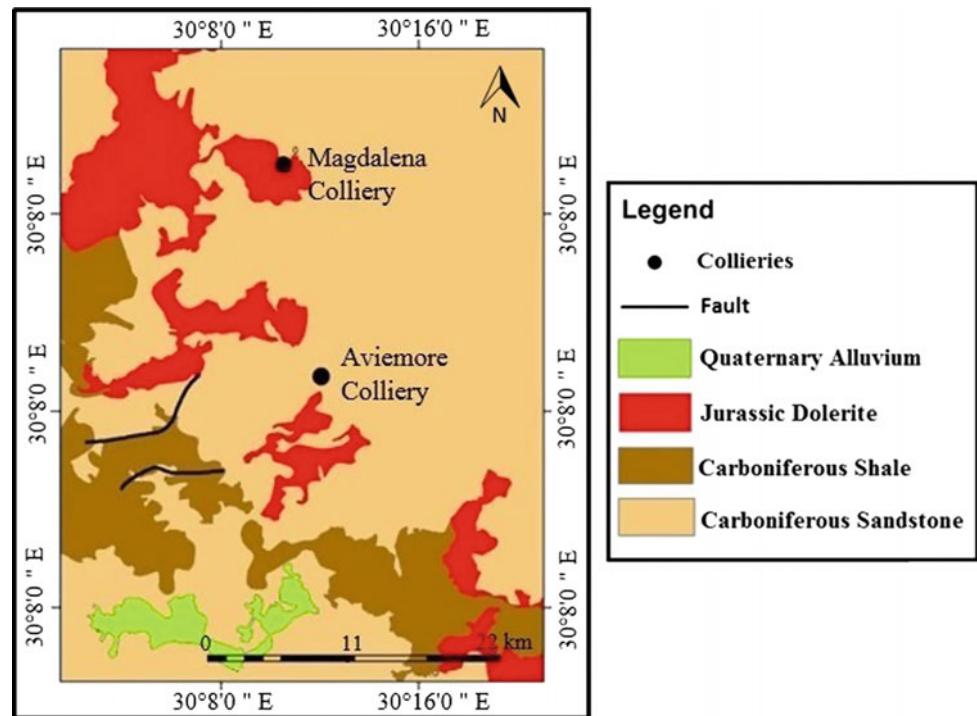
It is well known that mostly dolerite dykes and sills of Jurassic to early Cretaceous age, are ubiquitous within the early Permian Vryheid Formation (Roberts 1987). In South Africa, difficulties with intrusions in coal were recognized as early as 1899 and approximately 90% of the Natal coalfields are affected by intrusions (Heslop 1924). Blignaut (1952) estimated that 40% of KwaZulu-Natal's coal has been destroyed in this manner, and concluded that the limiting factor in the life of every colliery is the presence of intrusions.

A series of dolerite intrusions is present in the Magdalena area, represented by the Ingogo dolerite sill as well as a network of widely spaced dolerite dykes, (Clemente et al. 2013; Muller et al. 2013). The Ingogo dolerite sill extends

**Fig. 1** Location map of Magdalena Colliery



**Fig. 2** Local geology of the Magdalena colliery (modified after Council for Geoscience 1997)



over a large area, with a transgressive spilt from the base of the sill. In certain regions of the area, the sill has been removed by erosion. Within the eastern region of the Magdalena area, a phenomenal change in the sill's characteristics is observed, where the sill transgresses into a dyke, cross-cutting the lithology and then returns to its sill-like habit, lying concordantly with the lithology. This change in placement relative to the coal seams has caused a displacement in the seams pushing the seams by a distance equal to the thickness of the sill. As a result of exposure, the coal seams in this region have been eroded away (Clemente et al. 2013).

Within Section 1, Panel 417 at the Magdalena Colliery, a dolerite intrusion spanning 13.88 m caused both replacement and a 13.3 m displacement of the Alfred seam (Fig. 3). The unexpected occurrence of the dyke during the mining operation caused a significant delay in the mining operation and considerable loss in production. As a result of the intrusion, the involvement of a specialist team was required in order to remove the dyke by blasting. The blasting method employed involved the use of a wedge cut solid blasting technique, which utilizes synchronized delay intervals between blastholes. Due to the sensitive environment and associated dangers within a coal mining environment, such as the presence of methane and highly combustible coal dust, the blasting operations have limited flexibility. Therefore, a total permitted amount of 1000 g of Seamex® water gel explosives was used in the blasting operations. Other controllable blasting parameters such as the drill hole diameter

(38 mm), stemming material (clay), stemming length (200 mm), drill hole depth (1.8–2.2 m) and explosive delay intervals (0–400 ms) were kept constant throughout the blasting operation of the dolerite.

#### 4 Methodology

Selected sampling was conducted along the length of the intrusion and three sampling points; A<sub>2</sub>, A<sub>6</sub>, A<sub>9</sub>, were chosen at strategic locations of the dolerite as shown in Fig. 3.

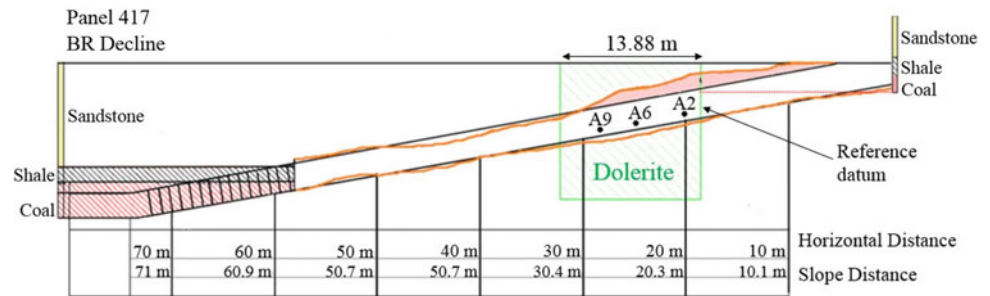
Detailed petrographic analysis of thin sections, using an Olympus BX41 microscope, was done on seven samples taken from the dolerite. XRD analysis was conducted on five samples, three of which were taken from the geotechnical sampling points. Sample preparation was carried out as prescribed by Jenkins and Snyder (1996) and Darling (2011). The analysis was done using a PANalytical Empyrean diffractometer, with data interpretation using the High Score Plus software.

The preparation and assessment of all samples used for geotechnical analysis were completed in accordance with the ISRM (1981) procedures. The geotechnical properties determined were the dry density, porosity, Brazilian disc strength, uniaxial compressive strength (UCS) test, point load test and sound velocity.

In order to quantify the blasting performance, measurements were taken from a known point of reference after each blast advance, using a laser distometer. In order to ensure the



**Fig. 3** Cross section along BR decline, Section 1, Panel 417



accuracy of each measurement, three measurements were taken along the face, with the average value used as a representation of the blast advance.

## 5 Results and Discussion

### 5.1 Petrographic Analysis of the Dolerite

Results obtained from thin section analysis, indicate that the dolerite comprises anorthite (65–80%), augite (10%) and enstatite (5%) as the essential minerals, and accessories of calcite, devitrified glass and opaque minerals (5%).

Plagioclase feldspar being the main constitute, occur as subhedral tabular crystals with pyroxene, glass and opaque minerals occupying the spaces between the plagioclase laths giving rise to an interstitial texture. The samples at the contacts were much finer grained with an average grain size of 0.25 mm than at the centre of the intrusion with average grain size of 0.75 mm (Fig. 4).

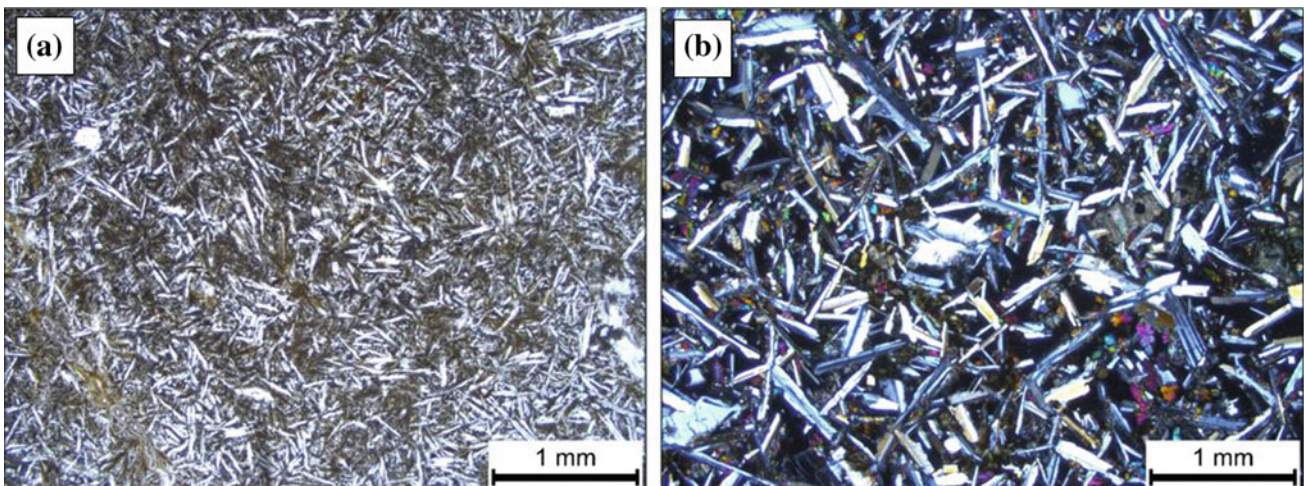
A notable difference in the thin sections prepared from samples taken along the contact of the intrusions from those taken at the centre, was the presence of calcite infillings

(Fig. 5). It was observed that the percentage of calcite reduces from the contact to the centre of the intrusion with little or no calcite present at the centre. This was also confirmed by XRD analysis (Fig. 6).

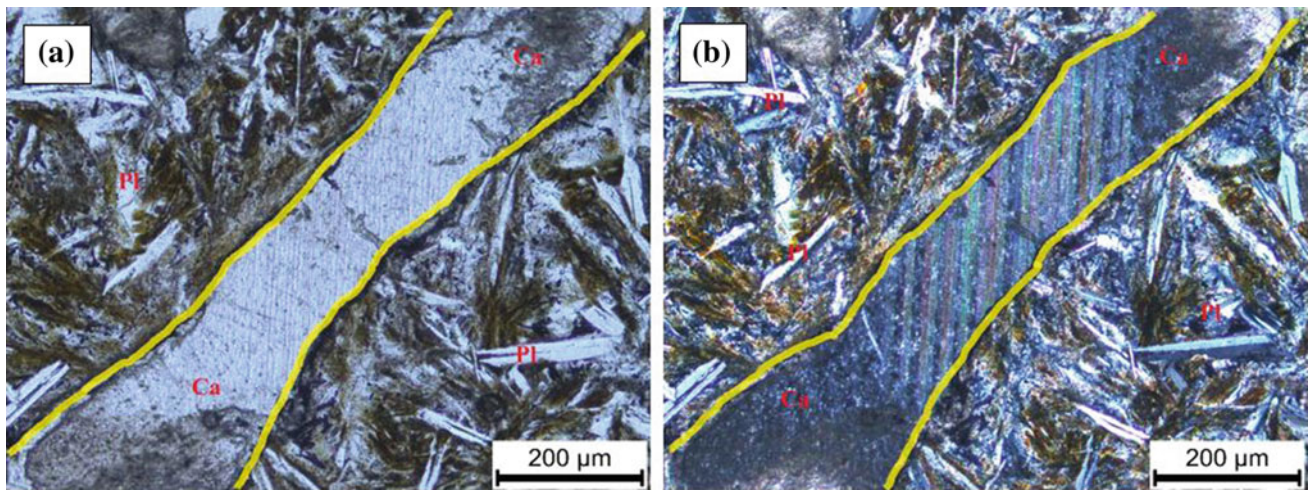
According to research conducted on dolerite intrusions within the Klip River coalfields, Roberts (1987) indicated a similar observation stating that the intrusions within the coalfields exhibited evidence of late stage reaction with a mobile fluid phase along intrusive contacts with coal. This resulted in many of the intrusions being altered to carbonate and other secondary minerals by endometamorphism. At the dolerite-coal contacts, the intrusions were described as being brecciated and penetrated by a series of calcite veins (Roberts 1987).

### 5.2 Geotechnical Properties of the Dolerite

A summary of the geotechnical properties obtained from the various tests conducted on the dolerite intrusion are shown in Table 1. The UCS and Brazilian disc strength values show that the dolerite is stronger at the centre than at the margins. The relatively low strength values at the margins

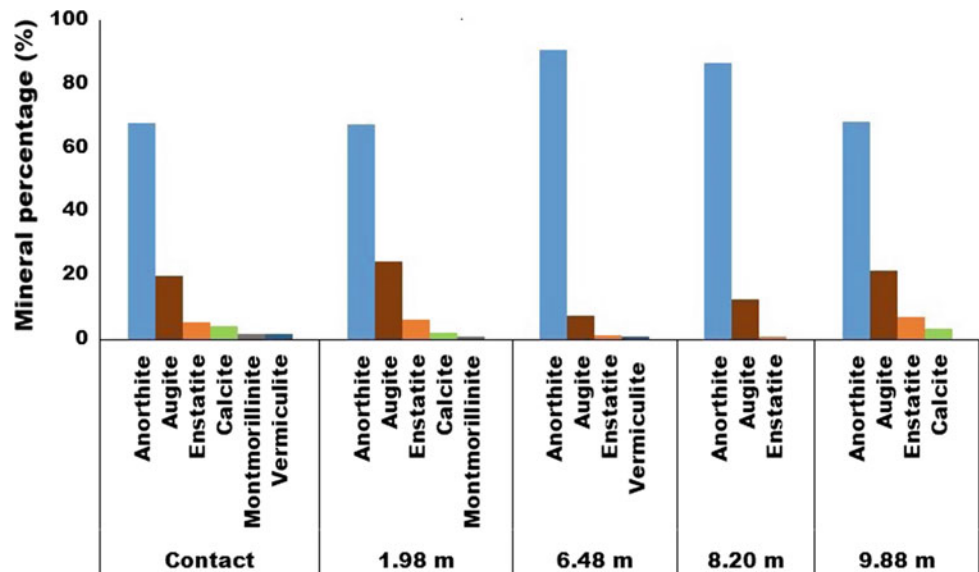


**Fig. 4** a Photomicrograph of sample taken along contact, magnification 2× under cross-polarized light showing interstitial texture; b Sample A<sub>6</sub> Photomicrograph of sample taken at the centre, magnification 2× under cross-polarized light showing interstitial texture



**Fig. 5** a Sample A<sub>2</sub> photomicrograph magnification 10× under plane polarized light showing calcite infilling (yellow); b Sample A<sub>2</sub> photomicrograph magnification 10× cross polarized light showing calcite infilling (yellow)

**Fig. 6** Modal mineral percentages for samples taken along length of intrusion



could be attributed to the presence of calcite infillings, which compromise the strength of the rock. Based on the average UCS and Brazilian disc strength values, the blastability index, which is the ratio of the UCS to tensile strength, was obtained for the dolerite at the sampling points. The values obtained show that the blastability indices at the margins were found to be higher than at the centre which suggests a higher expected advance at the margins than at the centre of the intrusion.

### 5.3 Blasting Analysis

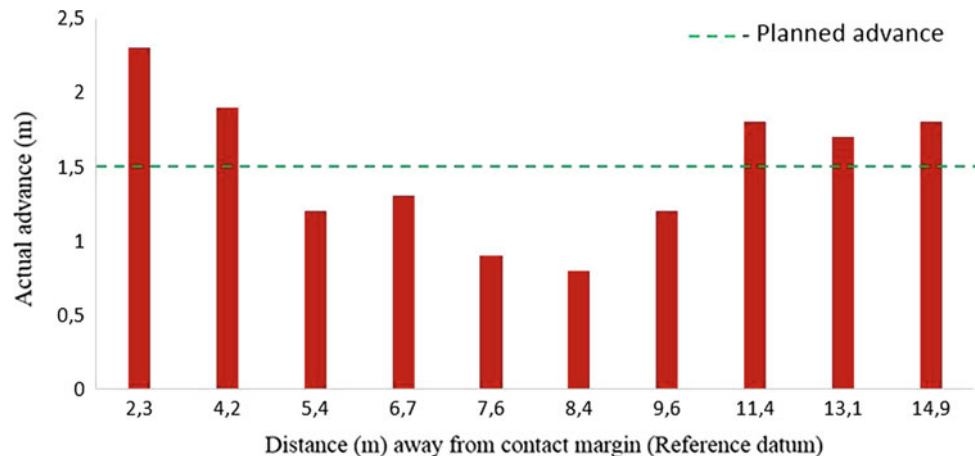
Blasting advance recorded along the length of the intrusion indicate a distinctive trend in the amount of pull received

during excavation of the intrusion (Fig. 7). According to the empirically calculated planned blasting advancement (i.e. 1.5 m), actual advances recorded indicate a decrease from the margin towards the centre of the intrusion. Thus, the blasting performance was shown to be greatest at the margins of the intrusion and progressively decrease towards the centre. It is evident that although the dolerite was subjected to identical energy input from explosives throughout, different results were obtained in the advance. This is indicative of different resistance of the dolerite to blasting along its length due to its variability in mineralogy, grain size and geotechnical properties along the length of the intrusion.

Several authors (e.g. Hino 1959; Jimeno et al. 1995; Bhandari 1997; Olofsson 1999) have pointed out that the ease of fragmentation of a rock can be indicated by its

**Table 1** Geotechnical properties of the dolerite intrusion

Sample		A <sub>2</sub>	A <sub>6</sub>	A <sub>9</sub>
Density (g/cm <sup>3</sup> )	Average	2.72	2.64	2.69
	Range	2.72–2.73	2.61–2.65	2.65–2.72
	No. of samples	3	3	5
Porosity (%)	Average	0.79	0.96	0.98
	Range	0.78–0.81	0.93–1.02	0.87–1.28
	No. of samples	3	3	5
Sound velocity P-wave (m/s)	Average	5211	5344	5668
	Range	–	5336–5352	–
	No. of samples	1	2	1
UCS (MPa)	Average	143.49	160.89	156.86
	Range	–	159–162	–
	No. of samples	1	2	1
Point load index Is <sub>50</sub> (MPa)	Average	6.46	7.88	7.48
	Range	5.34–7.34	6.32–9.51	5.34–8.71
	No. of samples	5	7	5
Correlated UCS by Broch and Franklin (1972) (MPa)	Average	155.04	189.12	179.52
	Range	128–176	151–228	128–209
	No. of samples	5	7	5
Brazilian disc strength (MPa)	Average	13.38	20.91	19.13
	Range	11.60–16.78	20.28–21.59	18.29–20.38
	No. of samples	3	3	5
Blastability index	Average	11.58	9.04	9.38

**Fig. 7** Blasting advance measurements taken along Panel 417, Section 1

blastability index, which is defined as the ratio of the uniaxial compressive strength to the tensile strength. According to the blastability index calculated for the sampling points along the length of the intrusion, a higher than the planned advance along the intrusion contact was found to correspond to a higher blastability index in comparison to the centre of the intrusion.

## 6 Conclusion

A dolerite intrusion within Panel 417, Section 1 of the Magdalena Colliery resulted in both replacement and displacement of the Alfred seam. The intrusion resulted in a delay in the mining schedule. This was further exacerbated



by inadequate pull from the blasting operations along the intrusion. Thus, the study was focused on investigating the influence of petrographic and geotechnical properties in the assessment of its blasting performance. Petrographic analysis revealed that the main minerals in the dolerite comprises anorthite, augite and enstatite, with accessories of calcite, devitrified glass and opaque minerals. A notable difference was observed in thin sections prepared from the margins of the intrusion, which revealed the presence of calcite infillings due to endometamorphism. According to the geotechnical analysis conducted, the results indicate that the mechanical strength of the intrusion was compromised along the margins of the intrusion. This was shown to have a significant effect on the blasting performance, whereby greater pull was obtained along the margin of the intrusion margin as compared to the centre. Thus, the investigation demonstrates that a strong relationship exists between the blasting performance and the geotechnical and petrographic properties of the dolerite. Thus, the variation in pull from the blasting operations of the dolerite can be attributed to the influence of its geotechnical and petrographic properties.

## References

- Bhandari, S.: *Engineering Rock Blasting Operations*. CRC Press, Rotterdam (1997)
- Blignaut, J.J.G.: Field relationships of the dolerite intrusions in the Natal coalfields. *S. Afr. J. Geol.* **55**(1), 19–27 (1952)
- Brady, B.H.G., Brown, E.T.: *Rock Mechanics for Underground Mining*, 2nd edn. Springer, Dordrecht (2006)
- Broch, E., Franklin, J.A.: The point-load strength test. *Int. J. Rock Mech. Min. Sci.* **9**(6), 669–697 (1972)
- Clemente, D., Muller, C.J., Odendaal, N.J., Heerden, D.: An independent Qualified Person's Report on Forbes Coal Dundee Operations in the KwaZulu-Natal Province, Minxcon, South Africa (2013)
- Council for Geoscience.: 1:250 000 Geological Series Sheet, 2830 Dundee. Government printer, Pretoria (1997)
- Darling, P.: *SME Mining Engineering Handbook*. Society of Mining, Metallurgy and Exploration, Colorado (2011)
- Esterhuizen, G.S., Bajpayee, T.S., Ellenberger, J.L., Murphy, M.M.: Practical estimation of rock properties for modeling bedded coal mine strata using the Coal Mine Roof Rating. In: *Proceedings of the 47th US Rock Mechanics/Geomechanics Symposium*, pp. 13–154. American Rock Mechanics Association, San Francisco (2013)
- Hancox, P.J., Götz, A.E.: South Africa's coalfields—a 2014 perspective. *Int. J. Coal Geol.* **132**, 170–254 (2014)
- Heslop, W.T.: Coal in South Africa. *J Chem Metall Min Soc* **25**(6), 151–172 (1924)
- Hino, K.: *Theory and practice of blasting*. Nippon Kayaku Co, Japan (1959)
- ISRM. Brown, E.T. (ed.): *Rock Characterisation, Testing and Monitoring, ISRM Suggested Methods*. Pergamon Press, Oxford (1981)
- Jenkins, R., Snyder, R.L.: *Introduction to X-ray Powder Diffractometry*. Wiley, Canada (1996)
- Jimeno, E.L., Jimino, C.L., Carcedo, A.: *Drilling and Blasting of Rocks*. CRC Press, Rotterdam (1995)
- Johnson, M.R., Van Vuuren, C.J., Visser, J.N.J., Cole, D.I., Wickens, H.D.V., Christie, A.D.M, Roberts, D.L.: The Foreland Karoo Basin, South Africa. In: Shelly, R.C. (ed.) *Sedimentary basins of the Africa*. Elsevier, Amsterdam (1997)
- Muller, C.J., van Heerden, D., Odendaal, N.J., Clemente, D.: An Independent Qualified Person's Report on Forbes Coal Dundee Operations in the KwaZulu-Natal Province, South Africa. Minxcon, South Africa (2013)
- Olofsson, S.O.: *Applied Explosives Technology for Construction and Mining*. Applex, Sweden (1999)
- Roberts, J.R.D.R.: The effect of dolerite dykes on coal seams of the Klip River Coalfield. Ph.D. thesis (unpublished), University of Natal, South Africa (1987)
- Venter, B.J.: Assessment of the permeability of Vryheid Formation sediments. M. Sc. thesis, University of Natal (1994)

# Preliminary Study of the Adsorption Capacity of Pb, Zn and Cd Through Zeolite and Organic Compost

Jacqueline Zanin Lima<sup>✉</sup>, Isabela Monici Raimondi<sup>✉</sup>,  
and Valéria Guimarães Silvestre Rodrigues<sup>✉</sup>

## Abstract

Reactive materials have been used as a solution to prevent potentially toxic metal contamination stemming from mining waste disposal. These materials are characterized by a high cation exchange capacity (CEC) and a predominance of negative charges, favoring their potential utilization in metal cation immobilization. Therefore, the aim of this study is to compare the sorption capacity of common metals in mining areas (Pb, Zn and Cd) with zeolite, an inorganic material traditionally studied and used for this purpose, and compost, a low-cost organic material, that in comparison to zeolite, has been sparsely researched. Two Cuban commercial clinoptilolite zeolites were evaluated: natural zeolite (NZ) and NaCl treated zeolite (TZ). Two municipal solid waste-derived composts were also assessed with differences in the composting method: windrow (WC) and static pile (SPC). Batch equilibrium experiments showed that the selectivity of removal of TZ, WC and SPC followed the order Pb > Cd > Zn. The only exception was NZ (Pb > Zn > Cd). In general, all materials presented higher performances than Pb (with adsorption efficiency more than 95%). The SPC was revealed to be the best adsorbent of Pb, but with a similar removal percentage for the TZ. The TZ was significantly more efficient in retaining Zn. In the case of the Cd, the WC and TZ showed the highest removal percentage. These results suggest that compost, a low-cost byproduct, can adsorb a considerable

concentrations of metals, and thus is able to compete with zeolites for use, isolated or combined with other materials, as an effective sorbent in metal contamination.

## Keywords

Reactive materials • Batch equilibrium • Contaminated mine areas

## 1 Introduction

Potentially toxic metals naturally occur in the earth's crust at geogenic concentrations. However, mining accelerates the release of these elements into the environment, affecting the natural ecological balance (Salomons 1995), resulting in soil contamination by a wide range of elements, such as arsenic (As), cadmium (Cd), lead (Pb), copper (Cu), chromium (Cr), mercury (Hg), selenium (Se) and zinc (Zn) (Förstner and Wittmann 1983).

It is estimated that Europe contains about 2.5 million potentially contaminated sites. The waste disposal and treatment are the main contributors to soil contamination (38%) and potentially toxic metals account for approximately 35% of the soil contamination and 31% of the groundwater contamination (Van Liedekerke et al. 2014). In Latin America, natural metal concentration in soil is high and diverse. On the one hand, this countries have a long mining history, but without adequate environmental laws. Regulations for natural resources protection have improved since the 1980s in Brazil and since the 1990s in some countries, such as Bolivia, Chile, Peru and Ecuador. Therefore, does not exist the complete inventory presenting polluted sites in the region, only several metal contamination problems examples (Utmazian and Wenzel 2006; MMSD América del Sur 2002). In Brazil, there are several abandoned mining areas, such as the Ribeira Valley region, where the Pb, Zn and Ag extraction, produced millions of tons of waste (tailing and slags) (Kasemodel et al. 2016).

J. Z. Lima (✉) · I. M. Raimondi · V. G. S. Rodrigues  
São Carlos School of Engineering, University  
of São Paulo, São Carlos, SP 13566-590, Brazil  
e-mail: jacqueline.zanin.lima@usp.br

V. G. S. Rodrigues  
e-mail: valguima@usp.br

The remediation is generally not a priority in these countries, due to technical and financial implications. Furthermore, the metal mining industry has not only been important in the last decades, currently, new investments in ore exploration has still been made (MMSD América del Sur 2002). Thus, it is necessary to develop different technological approaches able to treat and stabilize contaminants in an efficient, eco-friendly, and cost effective way.

In addition, an alternative to the final disposal of mining wastes are landfills, which aim to reduce the migration of contaminants through a liner and barrier covering (Sharma and Lewis 1994). The use of constructive materials with high adsorption potential may be favorable, since it increases the safety of structures. In this category are the reactive materials of an inorganic character, such as zeolites, and of an organic character, such as the composts originated from composting.

Zeolite minerals are crystalline and hydrated aluminosilicates with microporous crystalline structures, which can also be produced synthetically (Pabalan et al. 2001). In contrast, organic compost, resulting from composting, is the product of organic waste management and is a considerable portion of the municipal solid waste (Epstein 1997).

Zeolites have been shown to have great potential to remove cationic metal species, associated with ion-exchange, in their characteristically large surface areas (Pabalan et al. 2001; Simantiraki and Gidarakos 2015). Some studies have also confirmed the high capacity of immobilization of metallic contaminants by the composts as a function of the humic substances, such as humic and fulvic acids (Simantiraki and Gidarakos 2015; Paradelo and Barral 2012).

The purpose of this study was to evaluate the equilibrium adsorption of clinoptilolite zeolites and municipal solid waste-derived composts to compare the adsorption efficiency of these reactive materials for Pb(II), Zn(II) and Cd(II). This metal cations were chosen because they are important and frequent contaminants in metal ore mining residues. This research was conducted with the hope that it might help develop alternatives for the recuperation of abandoned and contaminated mining areas using a single or multi type, low cost and environmentally friendly material.

## 2 Materials and Methods

The compost samples were made using food waste submitted to two different composting processes: windrow composting (WC) and static pile compost (SPC). The second type of adsorbent material was zeolite (clinoptilolite) extracted from a mine in Cuba by the Brazilian company (CELTA Brasil Ltda). Two types of zeolite were evaluated: natural zeolite (NZ) and chemically treated zeolite using sodium hydroxide (NaCl) (TZ).

### 2.1 Materials Characterization

The pH (H<sub>2</sub>O and KCl), redox potential (Eh) and electrical conductivity (EC) were determined according to the methodology proposed by EMBRAPA (2011), using ratio of 1:2.5 (mass:volume), with stirring of the samples and standing for 60 min. Then, the  $\Delta$ pH is calculated using the difference between the pH in KCl and the pH in H<sub>2</sub>O. The determination of the composts cation exchange capacity (CEC) followed the titulometry method (MAPA 2013) and the zeolite CEC was provided for the supplier. The specific surface area ( $S_{\text{BET}}$ ) and porosity (average pore radius and total pore volume) were found by determining the nitrogen adsorption/desorption isotherm using a Quantachrome NOVA 1000. The specific surface area was calculated using the Brunauer-Emmett-Teller (BET) method. The total pore volume was estimated from the amount of nitrogen adsorbed at a relative pressure of  $P/P_0 = 0.98$ . The X-Ray Fluorescence (XRF) was determined in an X-Ray Fluorescence Spectrometer (Axios Advantage, Panalytical).

### 2.2 Metal Sorption Experiment

Equilibrium adsorption studies were conducted through contact between the composts (particles smaller than 2.0 mm and oven dried for 48 h at 50 °C) and zeolites in single-solute systems, for a predetermined contact time. Single contaminant solutions containing Pb(II), Zn(II) or Cd (II) (frequent contaminants in metal ore mining residues) were prepared after dissolving the corresponding chloride salts with deionized water, achieving concentrations around 150 mg L<sup>-1</sup>. In 50 mL Falcon tubes, 1 g of each reactive material, which had been continuously stirred with 50 mL of each contaminant solution (optimum adsorbent:solution ratio of 1:50) was added to a horizontal shaker at a rate of 10–20% at room temperature (approximately 25 °C). After agitation for 24 h, the extracts were centrifuged and filtered through Unifil filter paper (weight of 80 g m<sup>-2</sup> and particle retention of 4–12  $\mu$ m).

The physicochemical parameters (pH and CE) were monitored with measurements of the initial values (immediately after contact of the adsorbent with the contaminant solution) and final values (after 24 h of contact, immediately after filtration). The concentrations of Pb, Zn and Cd present in the filtered extracts were analyzed in the Atomic Absorption Spectrophotometer (PinAAcle 900F PerkinElmer). For the calibration curves, three points were used with different concentrations, obtained from the dilution of the respective PerkinElmer standards in deionized water. All calibration curves have a correlation coefficient greater than 0.995.

With the results obtained, it was possible to calculate the respective removal percentage and removal capacity of each metal, using the following formulas (Soares and Casagrande 2000):

$$q_e = \frac{[V_{\text{solution}}(C_0 - C_e)]}{M_{\text{reactive material}}} \quad (1)$$

$$R = \left[ \frac{C_0 - C_e}{C_0} \right] \times 100 \quad (2)$$

Wherein  $q_e$  is the adsorbed concentration or the removal capacity after equilibrium ( $\text{mg g}^{-1}$ );  $V_{\text{solution}}$  is the volume of solution (L);  $C_0$  and  $C_e$  are the initial concentrations and equilibrium concentrations ( $\text{mg L}^{-1}$ );  $M_{\text{reactive material}}$  is the exact mass of the reactive material sample (g) and R is the removal percentage (%).

### 3 Results and Discussion

#### 3.1 Materials Characterization

The physicochemical properties of organic and inorganic materials, which affect the metal removal, are presented in Table 1. In the present study, all the materials showed low acidity, wherein composts have higher pH values (7.4 and 6.4) compared to zeolites (6.2 and 5.6); oxidizing conditions and predominance of negative charges, principally the NZ ( $\Delta\text{pH} = -2.5$ ). These characteristics facilitate high cation retention. Sorption is the most dominant mechanism in determining the effective removal of metals (Yong and Mulligan 2004). Thereby, the specific surface area ( $S_{\text{BET}}$ ) and cation exchange capacity (CEC) are the most indicative parameters to predict this process. According to the results, the CEC of NZ demonstrated to be higher ( $180 \text{ cmol}_c \text{ kg}^{-1}$ ) than both compost samples ( $34$  e  $29 \text{ cmol}_c \text{ kg}^{-1}$ ). The CEC of zeolite is similar to the theoretical value of clinoptilolite ( $220 \text{ cmol}_c \text{ kg}^{-1}$ ), considering the isomorphous substitution and its typical unit cell (Pabalan et al. 2001). The alkali-treatment of the zeolite provided an increase in the  $S_{\text{BET}}$  ( $60.09 \text{ m}^2 \text{ g}^{-1}$  for the NZ and  $76.82 \text{ m}^2 \text{ g}^{-1}$  for the TZ). The  $S_{\text{BET}}$  for composts presented a wide range of values ( $5.69 \text{ m}^2 \text{ g}^{-1}$  for the WC and  $62.99 \text{ m}^2 \text{ g}^{-1}$  for the SPC). The X-Ray Fluorescence (XRF) analysis of zeolites indicated that its main components are clinoptilolite with more than 80%  $\text{SiO}_2$  and  $\text{Al}_2\text{O}_3$ . The composts were also primarily composed of the oxides,  $\text{SiO}_2$  and  $\text{Al}_2\text{O}_3$  (55.5% for the WC and 70% for the SPC).

#### 3.2 The pH of Solutions Before and After Agitation

The pH of a solution considerably affects the degree and extent of adsorption, in so far as it regulates the adsorption force of  $\text{H}^+$  and  $\text{OH}^-$  ions and the degree of ionization (Weber 1972). This adsorption study did not adjust the solutions' pH. The pH values varied between 4.7 and 6.3 in the solutions containing Pb; between 5.0 and 6.3 in the solutions containing Zn; and between 4.5 and 6.1 in the solutions containing Cd (Fig. 1). According to Dick et al. (2016) in pH values ranging from 4.0 to 5.0 dissociation occurs in most of the COOH groups. Therefore, the pH conditions of this study favored cation exchange. In addition, the decrease in pH with agitation (as observed for Zn) may be indicative of the predominance of the ion exchange mechanism, releasing more  $\text{H}^+$  ions and, consequently, leaving more sites free for adsorption (Bartczak et al. 2015). Nevertheless, the increase in pH values (as observed for Pb and Cd) may be related to the release of  $\text{OH}^-$  ions due to the adsorption of metal cations (Sharma and Forster 1993) or metal ions being withdrawn from the solution and  $\text{H}^+$  ions are also removed. Furthermore, other adsorption mechanisms may also be acting, such as the electrostatic attraction of the negative charges present on the surface of the adsorbents (Table 1) by the metal cations or the physical adsorption related to porosity (Table 1).

#### 3.3 The Electrical Conductivity (EC) of Solutions Before and After Agitation

For all the metals studied (Pb, Zn and Cd), the samples containing the reactive materials and the contaminant solutions had higher EC values compared to the respective blank solutions (Fig. 2). With agitation, there was also an increase in the EC values (Fig. 2). This increase may be due to an inherent mechanism of adsorption which is the cation exchange, anteriorly reported, with the release of various previously adsorbed cations and the subsequent binding of the metal cations present in the synthetic solution. Therefore, this increase of cations in the solution may have increased EC values.

#### 3.4 Removal Percentage of Pb, Zn and Cd

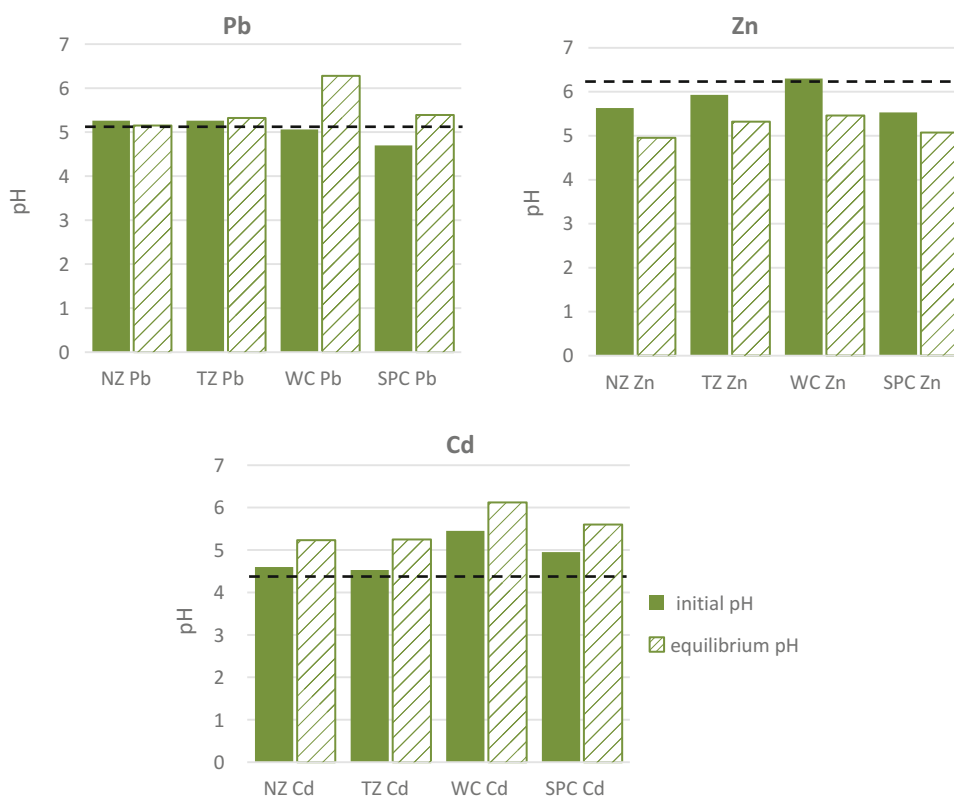
With the exception of NZ, the trend of the removal on the reactive materials (TZ, WC and SPC) followed the order

**Table 1** Physicochemical properties of zeolites (NZ = natural zeolite, TZ = treated zeolite) and organic composts (WC = windrow compost, SPC = static pile compost)

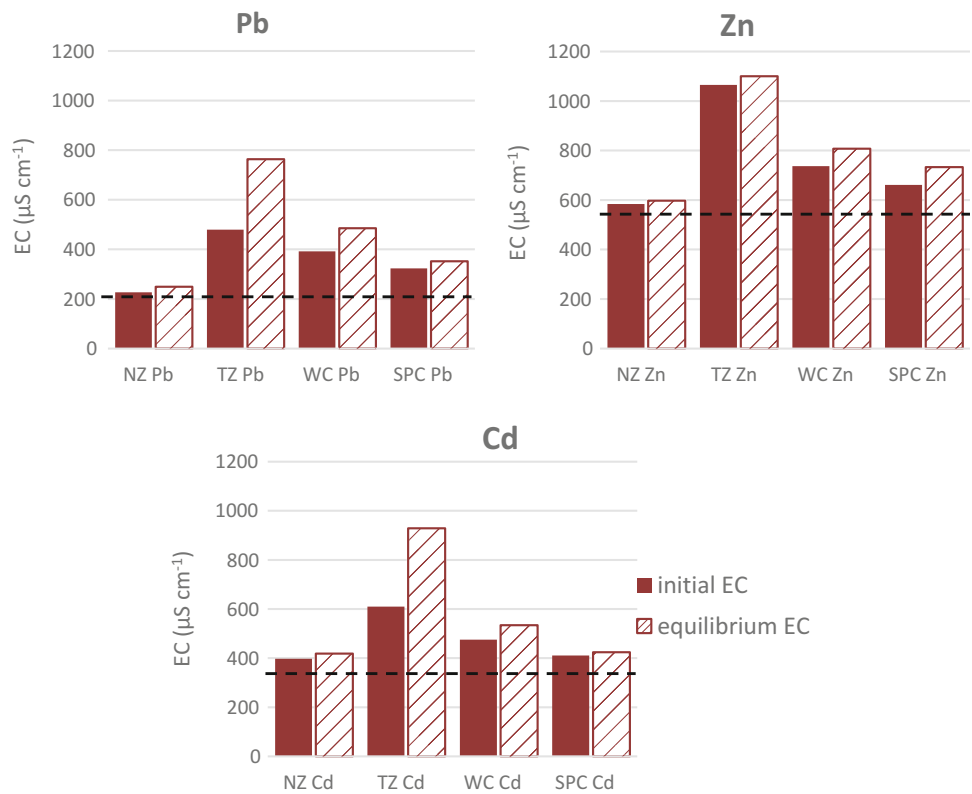
Parameters	Zeolites		Composts	
	NZ	TZ	WC	SPC
pH (1:2.5 in H <sub>2</sub> O)	6.2	5.6	7.4	6.4
pH (1:2.5 in KCl)	3.7	4.8	6.4	5.5
$\Delta$ pH (pH <sub>KCl</sub> -pH <sub>H<sub>2</sub>O</sub> )	-2.5	-0.8	-1.0	-0.9
Eh (mV)	+297	+275	+268	+330
EC ( $\mu$ S cm <sup>-1</sup> )	67	6000	665	157
CEC (cmol <sub>c</sub> kg <sup>-1</sup> )	180	ND	34	29
S <sub>BET</sub> (m <sup>2</sup> g <sup>-1</sup> )	60.09	76.82	5.69	62.99
V <sub>pores</sub> (cm <sup>3</sup> g <sup>-1</sup> )	0.08301	0.13880	0.03341	0.01113
R <sub>pores</sub> (Å)	27.63	36.13	117.50	35.33
XRF	SiO <sub>2</sub> (75.4%); Al <sub>2</sub> O <sub>3</sub> (13.5%); CaO (4.0%); K <sub>2</sub> O (2.1%)	SiO <sub>2</sub> (72.0%); Al <sub>2</sub> O <sub>3</sub> (12.6%); K <sub>2</sub> O (3.8%); CaO (1.9%)	SiO <sub>2</sub> (44.5%); Al <sub>2</sub> O <sub>3</sub> (11.0%); Fe <sub>2</sub> O <sub>3</sub> (5.8%); CaO (1.6%)	SiO <sub>2</sub> (55.2%); Al <sub>2</sub> O <sub>3</sub> (14.8%); Fe <sub>2</sub> O <sub>3</sub> (6.7%); CaO (0.8%)

Eh: redox potential; EC: electrical conductivity; CEC: cation exchange capacity; S<sub>BET</sub>: specific surface area; V<sub>pores</sub>: total pore volume; R<sub>pores</sub>: average pore radius; XRF: X-Ray Fluorescence  
 ND = Not determined

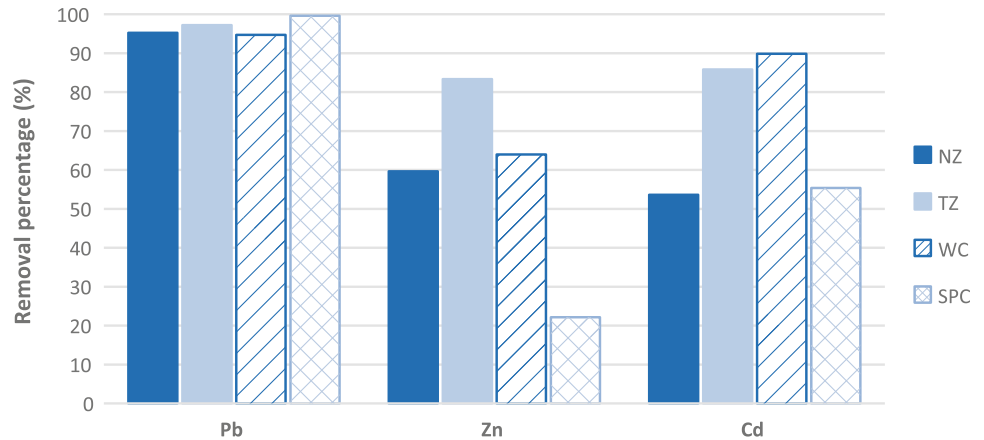
**Fig. 1** The pH values of solutions containing Pb, Zn or Cd before agitation (initial pH) and after agitation (equilibrium pH). The dashed line represents the initial pH value of the blank metal solution. NZ = natural zeolite, TZ = treated zeolite, WC = windrow compost, SPC = static pile compost



**Fig. 2** The electrical conductivity (EC) values of solutions containing Pb, Zn or Cd before agitation (initial EC) and after agitation (equilibrium EC). The dashed line represents the initial EC value of the blank metal solution. NZ = natural zeolite, TZ = treated zeolite, WC = windrow compost, SPC = static pile compost



**Fig. 3** Removal percentage of Pb, Zn or Cd in zeolites (NZ = natural zeolite, TZ = treated zeolite) and organic composts (WC = windrow compost, SPC = static pile compost)

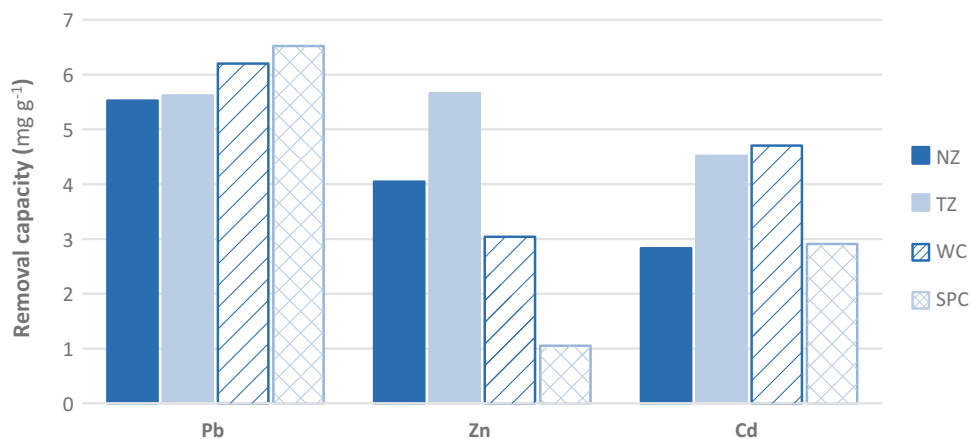


Pb > Cd > Zn (Fig. 3). All of the materials performed well in Pb retention (with adsorption efficiency of more than 95%). The SPC revealed to be the most adsorbent of Pb (99.6% of removal). The TZ presented the highest rate of adsorption of Zn (83.4%). The WC demonstrated the highest percentage of Cd removal (89.8%), but with similar values to those of TZ (85.9%). Both zeolites have similar efficiency for Zn and Cd sorption.

### 3.5 Removal Capacity of Pb, Zn and Cd

Sorption studies are usually conducted with different types of reactive materials and under different conditions, like pH values, temperatures, concentration solutions and optimum adsorbate/solution ratio, which makes direct comparisons of the results difficult. A general trend of best removal of Pb by zeolite and compost has been observed by other researchers

**Fig. 4** Removal capacity of Pb, Zn or Cd in zeolites (NZ = natural zeolite, TZ = treated zeolite) and organic composts (WC = windrow compost, SPC = static pile compost)



(Paradelo and Barral 2012; Nguyen et al. 2015). In this study, the Pb removal capacity values ranged from 5.525 (NZ) to 6.521 mg g<sup>-1</sup> (SPC) (Fig. 4). The maximum removal capacity of these materials is likely higher in saturation conditions. The Pb maximum removal capacity by zeolite from a single metal solution obtained by Nguyen et al. (2015) was 9.97 mg g<sup>-1</sup> and by compost presented by Paradelo and Barral (2012) was 196 mg g<sup>-1</sup>. In the case of Zn, contrary to the results of this study (Fig. 4), Simantiraki and Gidaracos (2015) showed a higher Zn maximum removal capacity by compost (1.11 mg g<sup>-1</sup>) compared to zeolite (0.97 mg g<sup>-1</sup>). The selectivity order of Cd maximum removal capacity in this study (Fig. 4) is in agreement with Simantiraki and Gidaracos (2015) (1.46 mg g<sup>-1</sup> for zeolite < 2.96 mg g<sup>-1</sup> for compost). Therefore, zeolites and composts are efficient adsorbents in the removal of metals. However, the best immobilization capacity is determined by the physicochemical, chemical and hydraulic properties, associated with the origin of these materials.

## 4 Conclusions

The comparative assessment of this study showed that the removal percentage and removal capacity of Pb, Zn and Cd by zeolites and composts yielded the following ranking: Pb > Cd > Zn (the only exception is NZ: Pb > Zn > Cd). All of the materials indicated a higher performance for Pb (with adsorption efficiency of more than 95%). The SPC, TZ and WC performed better in terms of removal of Pb, Zn and Cd, respectively. According to the results, composting may not only be a viable and efficient alternative to waste management, but also be used as adsorbents in contaminated mining areas, ensuring social and economic benefits. The composts, unlike extracted zeolites from specific sites, have the advantage that they can be made at the using site. However, further research is required to

know the adsorption potential in other concentrations and the desorption of Pb, Zn, or Cd from compost materials. The over time composts' stability is an important consideration and a possible limitation of use that should be better evaluated.

**Acknowledgements** The authors gratefully acknowledge the São Paulo Research Foundation (FAPESP) for granting a scholarship (2015/02529-4) and for a research fellowship (2014/07180-7) and the National Council for Scientific and Technological Development (CNPq) for a Ph.D. fellowship (54134/2016-3) and for financial support (305096/2015-0).

## References

- Bartczak, P., Norman, M., Klapiszewski, L., Karwańska, N., Kawalec, M., Baczyńska, M., Wysokowski, M., Zdarta, J., Ciesielczyk, F., Jesionowski, T.: Removal of nickel(II) and lead(II) ions from aqueous solution using peat as a low-cost adsorbent: a kinetic and equilibrium study. *Arab. J. Chem.* (2015)
- Dick, D.P., Novotny, E.H., Diechow, J., Bayer, C.: *Química Da Matéria Orgânica Do Solo*. In: Melo, V.F., Alleoni, L.R.F. (eds.) *Química e mineralogia do solo: Parte II—Aplicações*. 1st edn. Viçosa, Minas Gerais (2016)
- Empresa Brasileira de Pesquisa Agropecuária—EMBRAPA: *Manual de Métodos de Análise de Solo*. 2nd edn. Rio de Janeiro (2011)
- Epstein, E.: *The Science of Composting*. CRC Press LLC (1997)
- Förstner, U., Wittmann, G.T.W.: *Metal Pollution in the Aquatic Environment*. Springer-Verlag (1983)
- Kasemodel, M.C., Lima, J.Z., Sakamoto, I.K., Vareshe, M.B.A., Trofino, J.C., Rodrigues, V.G.S.: Soil contamination assessment for Pb, Zn and Cd in a slag disposal area using the integration of geochemical and microbiological data. *Environ. Monit. Assess* 188 (12) (2016)
- MMSD América del Sur: *Minería, Minerales y Desarrollo Sustentable en América del Sur*. Graphis Ltda, Bolivia (2002)
- Ministério da Agricultura, Pecuária e Abastecimento—MAPA: *Manual de Métodos Analíticos Oficiais para Fertilizantes e Corretivos*. Brasília (2013)
- Nguyen, T.C., Loganathan, P., Nguyen, T.V., Vigneswaran, S., Kandasamy, J., Naidu, R.: Simultaneous adsorption of Cd, Cr, Cu, Pb, and Zn by an iron-coated Australian zeolite in batch and fixed-bed column studies. *Chem. Eng. J.* 270, 393–404 (2015)



- Pabalan, R.T., Bertetti, F.P.: Cation-exchange properties of natural zeolites. In: Bish, D.L., Ming, D.W. (eds.). *Reviews in Mineralogy and Geochemistry* vol. 45, pp 453–518 (2001)
- Paradelo, R., Barral, M.T.: Evaluation of the potential capacity as biosorbents of two MSW composts with different Cu, Pb and Zn concentrations. *Bioresources Technol* **104**, 810–813 (2012)
- Salomons, W.: Environmental impact of metals derived from mining activities: processes, predictions, prevention. *J. Geochem. Explor.* **52** (1–2), 5–23 (1995)
- Sharma, D.C., Forster, C.F.: Removal of hexavalente chromium using sphagnum moss peat. *Water Res.* **27**(7), 1201–1208 (1993)
- Sharma, H.D., Lewis, S.P.: *Waste Containment Systems, Waste Stabilization, and Landfills: Design and Evaluation*. Wiley, New York (1994)
- Simantiraki, F., Gidarakos, E.: Comparative assessment of compost and zeolite utilisation for the simultaneous removal of BTEX, Cd and Zn from the aqueous phase: Batch and continuous flow study. *J. Environ. Manage.* **159**, 218–226 (2015)
- Soares, M.R., Casagrande, J.C.: Adsorção e modelos. In: Ribeiro, M. R., Nascimento, C.W.A., Ribeiro Filho, M.R., Cantalice, J.R.B. (eds.) *Tópicos em ciência do solo*. Sociedade Brasileira de Ciência do Solo, Viçosa, MG (2000)
- Utmazian, M.N.S., Wenzel, W.W.: Phytoextraction of metal polluted soils in Latin America. *Environmental Applications of Poplar and Willow Working Party*. Available at: <http://www.fao.org/forestry/11114-07881fab8de72bc1ae18a2f90c9367d2f.pdf> (2006). Last accessed 2018/02/12
- Van Liedekerke, M.; Prokop, G., Rabl-Berger, S., Kibblewhite, M., Louwagie, G.: *Progress in the management of contaminated sites in Europe*. Reference Report by the Joint Research Centre of the European Commission, 2014
- Weber Jr., W.J.: *Physicochemical Processes for Water Quality Control*. Wiley-Interscience, New York (1972)
- Yong, R.N., Mulligan, C.N.: *Natural Attenuation of Contaminants in Soil*. Lewis Publishers (2004)



# A Comparison of Two Methods of Sequential Extraction in a Former Mining Waste Deposit of Pb—Adrianópolis (Brazil)

Mariana Consiglio Kasemodel<sup>✉</sup>  
and Valéria Guimarães Silvestre Rodrigues<sup>✉</sup>

## Abstract

Sequential extraction methods (SEM) have been developed to study potentially toxic metal (PTM) fractionation in soil. Although many procedures have been suggested in literature, these methods are usually developed for temperate soils. Thus, the objective of this study was to compare a SEM developed for temperate soils with a SEM developed for tropical soils. The soil samples chosen for this comparison were collected in a former deposit of slag enriched in lead (Pb) and zinc (Zn), located in Adrianópolis (Brazil—tropical soil). These samples were collected in profile to verify metal mobility in depth. Since it is known that soil characteristics affect metal mobility, the soil pH, the soil organic matter content (SOM), the cation exchange capacity (CEC) and the pseudo-total concentration of Pb and Zn were determined. Zn and Pb were predominantly associated with Fe–Mn oxides and the residual fraction. Using methodology developed for tropical soils, it was possible to distinguish Fe–Mn oxides and verify that Pb and Zn were mainly associated with the less mobile form (crystalline Fe oxides). Metal associated with the mobile fraction varied significantly, being more abundant when using the temperate soil method. It is concluded that the procedure for tropical soils is more adequate for distinguishing different forms of Fe–Mn oxides in soil, but the temperate soils procedure was more effective in extracting exchangeable and organic matter fractions.

## Keywords

Lead (Pb) • Slag • Contamination • Zinc (Zn)

M. C. Kasemodel · V. G. S. Rodrigues (✉)  
São Carlos School of Engineering, University of São Paulo, São Carlos, SP 13566-590, Brazil  
e-mail: valguima@usp.br

M. C. Kasemodel  
e-mail: makasemodel@yahoo.com.br

## 1 Introduction

The total or pseudo-total concentration of metals may indicate the overall level of metal in soils, however, this method does not provide information about the mobility and reactivity of the metal in the soil (Silveira et al. 2006; Anju and Banerjee 2011). The mobility and bioavailability of Pb and Zn in the environment depends strongly on their chemical forms (Lu et al. 2015). Sequential extraction methods (SEM) are widely used to determine the fractioning of metal bound to pre-established chemical forms in the solid phase. These chemical phases range from water soluble to insoluble forms immobilized in mineral lattices (Silveira et al. 2006).

The extraction of metal in each chemical form is dependent on various conditions, such as the reagent used, the concentration and pH of the extracting solution, duration of the contact between the extractant solution and the soil, and the natural conditions of the soil (Silveira et al. 2006; Tessier et al. 1979; Cardoso Fonseca and Ferreira Da Silva 1998). Aside from that, there are many methods described in the literature, making it difficult to discuss and compare results due to the lack of uniformity in the experiment conditions.

The choice of the reagent used in each step is variable depending on the methodology chosen. Procedures may vary depending on the soil used to establish the methodology. For instance, the widely used procedure suggested by Tessier et al. (1979) was originally developed for sediment samples from Canada with mineralogy dominated by quartz, plagioclase, and K-feldspar. While the methodology proposed by Silveira et al. (2006) was proposed for soils with a wide range of physical-chemical properties collected in São Paulo state (Brazil).

In this context, the objective of this study was to evaluate two distinctive SEM to evaluate the mobility of Pb and Zn in a former Pb mining waste deposit in Adrianópolis (Brazil).

## 2 Materials and Methods

Samples were collected in the city of Adrianópolis (the state of Paraná, Brazil), in an area that was used for the disposal of slags from a mining company that operated in the city from 1945–1995. For this study, samples from 3 soil profiles (P1, P2 and P3) were collected. Profiles P1 and P2 were collected to a depth of 100 cm and profile P3 was collected to a depth of 80 cm. Each profile was subsampled at every 20 cm.

Samples were collected using auger (Dutch model). For the analysis conducted, samples were air dried at room temperature, disintegrated with agate mortar and subsequently quartered and sieved (2 mm).

The soil samples collected were characterized (Table 1) and then subjected to the two distinctive SEM (Table 2).

The chemical fractionation of Pb and Zn in the soil were determined using two procedures described in the literature: (i) a classical SEM proposed by Tessier et al. (1979) and (ii) a SEM proposed for tropical soils by Silveira et al. (2006). Both methods were carried out using 1 g of soil and divided into several steps (Table 2).

The extracts obtained at each step of the sequential extraction were analyzed for the concentration of Pb and Zn in FS-AAS (Varian AA240FS) as described in Method B3111 Standard Methods for the Examination of Water and Wastewater (APHA 1998).

## 3 Results and Discussion

### 3.1 Soil Physicochemical Characterization

Results obtained for the soil pH, SOM, CEC and pseudo-total concentration of Pb and Zn are summarized in Table 3. The values for pH varied from 6.5 to 7.3 (slightly acidic to neutral). Therefore, the mobilization of PTM in this soil will be less expressive than in acidic soils.

SOM varied from 0.8 to 3.8 g kg<sup>-1</sup>. SOM content is important since it has both cationic exchange and chelation abilities, and it may be responsible for the accumulation of PTM (Adriano 1986; Othmani et al. 2015).

Soil CEC varied from 2.7 to 21.6 cmol<sub>c</sub> kg<sup>-1</sup>. Higher values were usually obtained in samples collected at deeper depths, indicating the presence of clay minerals (mainly kaolinite) and Fe–Mn oxides, typically present in tropical soils.

Pb concentration varied from 24.6 to 7139.0 mg kg<sup>-1</sup>. The pseudo-total concentration of Pb was significantly higher in surficial samples where slag was present. The Zn concentration varied from under 3.3 mg kg<sup>-1</sup> (equipment detection level) to 34,290.0 mg kg<sup>-1</sup>. The concentration of Pb and Zn in the slag deposit are mainly associated with the presence of galena (PbS) and sphalerite (ZnS) minerals in the mining wastes (Kasemodel 2017).

### 3.2 Pb and Zn Chemical Fractionation

When using the methodology proposed by Tessier et al. (1979) Pb and Zn were mainly associated with the residual fraction (Table 4). However, a considerable portion of Pb and Zn were associated with the exchangeable fraction in samples collected at depths of 40–100 cm. High concentration of metals in the carbonate fraction was observed throughout the soil samples, which is expected due to the embedding rocks of the region which are mainly carbonates.

Tropical soils are usually rich in Fe–Mn oxides, and when using Tessier et al. (1979) SEM for tempered sediments, Fe–Mn oxides fractions varied between 1.4 and 13.4% for Pb; and from 1.7 to 28.1% for Zn.

Frentiu et al. (2008) analyzed several soils with distinctive mineralogical composition using the method of Tessier et al. (1979) which compared the sum of the fractions with the XRF analysis, and then evaluated the results using Bland and Altman charts for repeated measures (Kasemodel 2017). According to these authors, the comparison is useful when Pb contents are over 250 mg kg<sup>-1</sup>, however, the comparison was only valid for lower concentration of Zn (Kasemodel 2017). The differences between the sum of the extraction fractions and concentrations obtained through XRF analysis might rely on the fact that XRF is a semi qualitative method. The authors attributed the poorer reproducibility of the Pb extraction to the differences among the samples regarding

**Table 1** Characterization analysis conducted in in the samples collected in the former area of slag disposal

Analysis	Description	Reference
Soil pH	Soil and distilled water solution (1:2.5 ratio) stirred constantly for 5 min and then left for 60 min before pH determination (Digimed DM21)	EMBRAPA (1997)
SOM	Hydrogen peroxide (H <sub>2</sub> O <sub>2</sub> ) attack	Eusterhues et al. (2005)
CEC	Methylene blue adsorption test	Arab et al. (2015)
Pseudo-total concentration of Pb and Zn	HNO <sub>3</sub> and HCl 50% (3:1 ratio) digestion. Results were read on FS-AAS (fast sequential atomic spectrometer—Varian AA240FS)	Method 3030F and 3111B (APHA 1998)

**Table 2** SEM used to determine Pb and Zn fractionation in the soil

Fraction	Solution	Equilibrium conditions
Method 1:	Tessier et al. (1979)	
F1. Exchangeable	8 mL 1 M MgCl <sub>2</sub> (pH 7)	1 h, room temperature
F2. Carbonates	8 mL 1 M NaOAc (pH 5)	5 h, room temperature
F3. Fe and Mn oxides	20 mL 0.04 M NH <sub>2</sub> OH/HCl in 25% (v/v) HOAc	6 h, 96 °C
F4. Organic matter	3 mL 0.02 M HNO <sub>3</sub> + 5 mL 30% H <sub>2</sub> O <sub>2</sub> (pH 2) 5 mL 3.2 M	3 h, 85 °C 20 min, room temperature
F5. Residual	HNO <sub>3</sub> -HCl digestion	
Method 2:	Silveira et al. (2006)	
F1. Soluble-exchangeable	15 mL 0.1 M CaCl <sub>2</sub>	2 h, room temperature
F2. Surface adsorbed	30 mL 1 M NaOAc (pH 5)	5 h, room temperature
F3. Organic matter	5 mL NaOCl (pH 8.5)	30 min, 90–95 °C
F4. Mn oxides	30 mL 0.05 M NH <sub>2</sub> OH/HCl (pH 2)	30 min, room temperature
F5. Poor crystalline Fe oxides	30 mL 0.2 M oxalic acid +0.2 M NH <sub>4</sub> oxalate (pH 3)	2 h, dark
F6. Crystalline Fe oxides	40 mL 6 M HCl	24 h, room temperature
F7. Residual	HNO <sub>3</sub> -HCl digestion	

**Table 3** Mean values for pH, SOM, CEC and pseudo-total concentration of metals (Pb and Zn) in the samples collected in the former area of slag disposal

Profile	Depth (cm)	pH	SOM (g kg <sup>-1</sup> )	CEC (cmol <sub>c</sub> kg <sup>-1</sup> )	Concentration (mg kg <sup>-1</sup> )	
					Pb	Zn
P1	0–20	6.7	1.2	7.6	4262.0	15,100.0
	20–40	6.5	2.6	3.4	2859.0	3654.0
	40–60	6.7	1.0	2.7	45.5	31.6
	60–80	6.8	3.4	17.6	27.5	8.1
	80–100	6.8	3.8	21.6	24.6	<3.3
P2	0–20	6.9	2.8	7.6	3727.0	6763.0
	20–40	6.9	1.8	6.2	1950.0	5585.0
	40–60	6.7	1.9	5.2	48.1	40.4
	60–80	6.7	1.1	4.3	28.7	6.1
	80–100	6.7	0.8	6.0	31.0	7.2
P3	0–20	7.3	1.8	5.7	6480.0	14,890.0
	20–40	7.3	1.2	5.6	7139.0	34,290.0
	40–60	7.2	1.7	7.6	52.7	71.4
	60–80	7.2	2.3	14.0	37.0	56.6

both their general mineralogical composition and the diversity of identified Pb types.

The methodology of Silveira et al. (2006) allows for the identifications of different oxide forms. Although, the use of SEM with more steps can provide useful information about metal speciation, it can also mask the results, since sample loss during the transfer of one step to another is likely to occur.

When using the methodology proposed by Silveira et al. (2006) for tropical soils, Pb and Zn were mainly associated with the residual fraction and crystalline Fe oxides (Table 5).

From a chemical standpoint, crystalline Fe oxides is a less active component in the geochemical cycling of trace elements (Silveira et al. 2006). Pb and Zn associated with Mn oxides and poorly crystalline Fe oxides were less abundant. Although, Fe–Mn oxides are usually considered a less available chemical form, the distinguishing of these forms allows a broad view of the chemical speciation. When considering the sum of the three oxide fractions extracted using Silveira et al. (2006) methodology (Table 5) as the total of Fe–Mn oxides in the samples, Pb associated with Fe–Mn oxides varied from 28.0–51.9% and Zn from

**Table 4** Chemical fractioning of Pb and Zn using Tessier et al. (1979) methodology in soil samples collected in the former area of slag disposal

Profile	Depth (cm)	F1 - %		F2 - %		F3 - %		F4 - %		F5 - %	
		Pb	Zn	Pb	Zn	Pb	Zn	Pb	Zn	Pb	Zn
P1	0–20	0.4	0.4	25.4	31.7	13.4	28.1	10.8	9.8	50.0	30.0
	20–40	0.9	0.3	32.8	47.3	7.9	5.6	13.4	6.7	45.0	40.0
	40–60	10.2	2.6	18.4	36.6	9.7	7.6	16.7	9.5	45.0	43.7
	60–80	13.7	6.5	20.3	23.6	11.4	6.4	5.9	19.6	48.7	43.9
	80–100	10.8	5.0	19.8	23.9	10.3	9.0	5.8	17.1	53.3	45.0
P2	0–20	0.1	0.2	34.0	39.2	2.1	4.8	8.8	8.8	55.0	47.0
	20–40	1.1	0.5	34.8	53.4	3.1	8.2	11.0	7.9	50.0	30.0
	40–60	6.5	3.5	28.3	33.1	6.7	8.6	8.5	11.0	50.0	43.8
	60–80	7.0	1.2	27.8	35.3	6.1	8.4	6.0	11.0	53.2	44.1
	80–100	8.8	3.3	24.9	23.1	7.5	10.0	7.0	19.7	51.8	43.9
P3	0–20	0.2	0.2	34.1	46.6	6.5	4.3	9.2	8.9	50.0	40.0
	20–40	0.9	0.1	36.2	43.4	1.4	1.7	16.5	9.9	45.0	45.0
	40–60	11.0	4.0	24.1	26.9	9.1	10.6	10.8	11.9	45.0	46.7
	60–80	8.9	4.4	24.6	28.1	8.2	8.9	11.5	13.5	46.8	45.1

Color scale:								55%
--------------	--	--	--	--	--	--	--	-----

Note F1 (exchangeable); F2 (carbonates); F3 (Fe–Mn oxides); F4 (organic matter); F5 (residual)

33.5–66.4%. These values are greater than those obtained using the Tessier et al. (1979) methodology, indicating that the tropical soils methodology is more efficient in extracting Fe–Mn oxides.

Like the results obtained using method 1, the Pb and Zn soluble-exchangeable fraction was higher in the deeper portion of the profile (40–100 cm) rather than in the surficial samples. The Pb and Zn surface-adsorbed fraction was also more significant in the 40–100 cm portion, where the CEC was also higher (Table 3). Higher concentrations of Pb (mean: 3.8%) were obtained in the soluble-exchangeable fraction when compared to the Zn concentration (mean: 1.6%). The concentration of Pb (mean: 3.9%) and Zn (mean: 5.1%) adsorbed in the surface was higher than in the soluble-exchangeable fraction.

The fraction of Pb and Zn associated with organic matter was very low when extracted with NaOCl. Results using the reagents proposed by Tessier et al. (1979) were considerably higher. However, the concentration of SOM obtained using H<sub>2</sub>O<sub>2</sub> attack is similar to the results obtained using Silveira et al. (2006) SEM. The higher concentration of metals bound to the organic matter fraction in the temperate sediment method can be due to the pH conditions and the extraction period, higher than the one used by Silveira et al. (2006).

He et al. (2013) compared the SEM proposed by Tessier et al. (1979) with that of Silveira et al. (2006) in contaminated soils near a mining area in China (Frentiu et al. 2008).

According to the results obtained by the authors, Zn was more bound to the insoluble forms and both of the SEMs yielded similar results in the chemical speciation of Zn (Frentiu et al. 2008). Zn bound to the organic fraction, extracted using both SEMs, was low, unlike the results obtained in this study.

Usero et al. (1998) indicated that the levels of metals (Cu, Zn, Mn, Cr, Pb and Fe) bound to iron and manganese oxides (reducible fraction) were influenced by the efficiency and selectivity of the reagents used in the previous stages (He et al. 2013). Therefore, the concentration of Fe–Mn oxides may be higher if the metals bound to carbonates have not been completely dissolved in the previous fraction (He et al. 2013).

Considering the high concentration of Pb and Zn in the soil samples, a simple way to assess the risk in the area is using the Risk Assessment Code (RAC) described by Perin et al. (1985) and Usero et al. (1998). The RAC is obtained using the sum of the first two extraction products in percentages. According to the authors, there is no risk when the sum of the fractions is less than 1%; low risk when in the range of 1–10%; medium risk when in the range of 11–30%; high risk when varying from 31 to 50%; and very high risk when the sum is above 50%. The medium RAC for Pb (13.1%) and Zn (11.0%) was higher using the SEM proposed by Tessier et al. (1979) (Table 6). Using the Silveira et al. (2006) SEM, RAC was 7.7% (Pb) and 6.7% (Zn),

**Table 5** Chemical fractioning of Pb and Zn using Silveira et al. (2006) methodology y in soil samples collected in the former area of slag disposal

Profile	Depth (cm)	F1 - %		F2 - %		F3 - %		F4 - %		F5 - %		F6 - %		F7 - %	
		Pb	Zn	Pb	Zn	Pb	Zn	Pb	Zn	Pb	Zn	Pb	Zn	Pb	Zn
P1	0-20	0.6	0.0	6.2	1.6	1.5	0.9	19.6	1.7	10.6	1.9	14.5	62.8	47.0	31.0
	20-40	0.7	0.1	1.6	1.3	0.3	0.1	5.9	1.6	7.1	2.0	37.5	56.9	46.8	38.0
	40-60	7.0	1.4	9.0	2.9	0.8	0.2	5.0	5.0	7.0	4.5	26.8	41.9	44.3	44.0
	60-80	9.2	3.9	7.4	14.1	1.1	0.9	7.1	5.4	5.5	3.5	21.8	31.2	47.9	41.0
	80-100	7.6	4.4	7.1	15.4	5.3	3.6	3.9	2.4	3.3	3.7	20.8	27.5	52.1	43.0
P2	0-20	0.3	0.1	2.9	1.1	2.6	1.7	6.4	1.5	4.3	2.1	36.1	49.5	47.5	44.0
	20-40	0.4	0.1	0.8	1.8	0.6	2.0	2.7	1.8	3.2	2.2	42.4	61.1	49.9	31.0
	40-60	5.6	2.0	3.9	7.7	4.8	3.3	6.2	6.2	8.7	8.8	27.0	26.0	43.8	46.0
	60-80	5.3	3.3	3.3	11.2	3.4	4.6	3.2	5.4	4.8	6.3	28.8	28.2	51.2	41.0
	80-100	5.8	3.6	3.3	10.1	3.9	3.2	2.8	4.1	4.8	6.2	23.9	32.9	55.4	40.0
P3	0-20	0.2	0.0	3.6	2.0	2.0	1.0	6.9	2.0	1.7	3.3	37.4	59.7	48.2	32.0
	20-40	1.0	0.1	1.7	1.9	1.3	1.2	11.6	2.8	8.9	3.5	31.4	57.5	44.1	33.0
	40-60	3.3	0.2	1.7	0.6	2.1	0.3	5.0	1.3	6.7	1.2	31.6	60.4	49.7	36.0
	60-80	6.4	3.5	2.4	0.0	5.1	5.0	6.4	5.6	5.2	6.2	27.1	36.6	47.3	43.0

Color scale:		62.8%
--------------	--	-------

Note F1 (soluble-exchangeable); F2 (surface adsorbed); F3 (organic matter); F4 (Mn oxides); F5 (poor crystalline Fe oxides); F6 (crystalline Fe oxides); F7 (residual)

**Table 6** RAC calculated using different SEM in soil samples collected in the former area of slag disposal

Profile	Depth (cm)	RAC (%) - Method 1		RAC (%) - Method 2	
		Pb	Zn	Pb	Zn
P1	0-20	25.8	32.1	6.8	7.8
	20-40	33.7	47.6	2.4	3.0
	40-60	28.6	39.2	16.0	13.3
	60-80	34.0	30.1	16.6	25.4
	80-100	30.6	28.9	14.6	26.9
P2	0-20	34.1	39.4	3.1	4.1
	20-40	35.9	53.9	1.3	2.7
	40-60	34.8	36.6	9.5	13.6
	60-80	34.8	36.5	8.6	17.8
	80-100	33.7	26.4	9.1	17.0
P3	0-20	34.3	46.8	3.8	5.6
	20-40	37.1	43.5	2.7	3.7
	40-60	35.1	30.9	5.0	2.5
	60-80	33.5	32.5	8.9	5.9

Color scale:		Low		Medium		High		Very high
--------------	--	-----	--	--------	--	------	--	-----------

which is classified as low risk (1–10%). In this case, the choice of SEM influences the RAC.

### 3.3 Statistical Treatment

The results obtained in each fraction of both SEM tested were subjected to statistical treatment to verify the similarity between them. The statistical treatments used were paired Student t-test and correlation Pearson index (Table 7). As in each method it is obtained distinguished fractions, in order to compare it was deducted that the exchangeable fraction (F1) from Tessier et al. (1979) is similar to the soluble-exchangeable fraction (F1) from Silveira et al. (2006) the carbonate (F2) from Tessier et al. (1979) is similar to the surface adsorbed (F2) from Silveira et al. (2006) Fe–Mn oxides (F3) from Tessier et al. (1979) is similar to the sum of the Mn oxides (F4), poor crystalline Fe oxides (F5) and crystalline Fe oxide (F6) from Silveira et al. (2006) the organic matter (F4) from Tessier et al. (1979) is similar to the organic matter (F3) from Silveira et al. (2006) and the residual fraction (F5) from Tessier et al. (1979) is similar to the residual fraction (F7) from Silveira et al. (2006).

Considering the significance level 5% ( $p = 0.05$ ), when comparing Pb fractionation, the null hypothesis is rejected in comparison (1) and (4). Considering Zn fractionation, the null hypothesis is rejected in comparison (4).

The Pearson correlation index was low for comparison (1) of Pb and Zn and comparison (2) of Zn. However, a positive linear correlation was observed in comparisons (3), (4), (5) and (6).

## 4 Conclusion

The use of SEM to study the chemical speciation of metal in contaminated soils is essential for understanding the binding of metal to different chemical forms. However, there are many procedures described in the literature. The SEMs suggested in the literature are usually developed for specific soils. The choice of method depends on soil characteristics. Methods developed for tropical soils are adequate to fractionate Fe–Mn oxides, which are usually described as a singular fraction in methods developed for temperate soils.

The efficiency of the extraction method is often discussed because some reagents may extract other chemical forms. However, a broad view of the scenario is possible in the slag deposit. Using both methods, it is noticeable that Pb and Zn are more bound to the residual fraction. However, when comparing the first two fractions, it is noticeable significant differences. The Tessier et al. (1979) method extracted more Pb and Zn in the first two fractions, than did the Silveira et al. (2006) method. Significant differences were also observed when comparing organic matter fractions, Tessier et al. (1979) method extracted more metals bound to the organic matter than did the Silveira et al. (2006) method. The higher extraction efficiency for organic matter in the temperate sediment method can be due to the low pH conditions, which makes metals more available in the solution, and to the extraction period, much superior than the one used in the tropical soils method.

Using statistical treatment, the comparison between the two methods was valid for the residual fraction and when considering that all oxides forms extracted in the Silveira

**Table 7** Paired Student t-test and Pearson correlation index ( $R^2$ )

Comparison		p	$R^2$
(1) Methods 1 (F1) and Method 2 (F1)	Pb	<b>&lt;0.001</b>	<b>–0.052</b>
	Zn	0.193	<b>0.625</b>
(2) Methods 1 (F2) and Method 2 (F2)	Pb	0.061	0.942
	Zn	0.234	<b>0.747</b>
(3) Method 1 (F3) and Method 2 (F4 + F5 + F6)	Pb	0.821	0.868
	Zn	0.052	0.919
(4) Methods 1 (F4) and Method 2 (F3)	Pb	<b>0.038</b>	0.943
	Zn	<b>0.046</b>	0.910
(5) Method 1 (F5) and Method 2 (F7)	Pb	0.277	0.899
	Zn	0.068	0.945
(6) Method 1 (F1 + F2 + F3 + F4 + F5) and Method 2 (F1 + F2 + F3 + F4 + F5 + F6 + F7)	Pb	0.273	0.894
	Zn	0.118	0.967

The bold defines  $R^2 < 0.85$  and  $p < 0.050$



et al. (2006) method was equivalent to the Fe–Mn oxide fraction from Tessier et al. (1979).

The method of Tessier et al. (1979) is widely used, and for this specific case was more adequate for extracting exchangeable, carbonates and organic matter fractions. However, the Silveira et al. (2006) method was adequate to fractionate the different Fe and Mn oxides in the soil, and to verify that Pb and Zn are more abundant in the crystalline Fe oxide form, a less available form of oxide.

The accurate choice of SEM used to determine metal speciation in the soil is very important. The use of data from SEM to assess metal availability in the soil, such as RAC, can be influenced by the SEM. The comparison of different methods is valid for determining the accuracy of an extraction method.


**Acknowledgements** The authors are grateful for the support provided by the São Paulo Research Foundation (FAPESP) in the research fellowship 2014/07180-7, scholarship 160934/2012-5 provided by the National Council for Scientific and Technological Development (CNPq) and the scholarship provided by Coordination for the Improvement of Higher Education (CAPES).

## References

- APHA. Standard methods for the examination of water and wastewater. 20th edn. APHA, Washington, D. C. (1998)
- Adriano, D.C.: Trace Elements in the Territorial Environment. Springer-Verlag, New York (1986)
- Anju, M., Banerjee, D.K.: Associations of cadmium, zinc, and lead in soils from a lead and zinc mining area as studied by single and sequential extractions. *Environ. Monit. Assess.* **176**, 67–85 (2011)
- Arab, P.B., Araújo, T.P., Pejon, O.J.: Identification of clay minerals in mixtures subjected to differential thermal and thermogravimetry analyses and methylene blue adsorption tests. *Appl. Clay Sci.* **114**, 133–14 (2015)
- Cardoso Fonseca, E., Ferreira Da Silva, E.: Application of selective extraction techniques in metal-bearing phases identification: a South European case study. *J. Geochem. Explor.* **61**, 203–212 (1998)
- EMBRAPA. Manual de Métodos de Análise de Solo. EMBRAPA, Rio de Janeiro (1997)
- Eusterhues, K., Rumpel, C., Kögel-Knabner, I.: Stabilization of soil organic matter isolated by oxidative degradation. *Org. Geochem.* **36**, 1567–1575 (2005)
- Frentiu, T., Ponta, M., Levei, E., Gheorghiu, E., Kasler, I., Cordos, E. A.: Validation of the Tessier scheme for speciation of metals in soil using the Bland and Altman test. *Chem. Pap.* **62**(1), 114–122 (2008)
- He, Q., Ren, Y., Mohamed, I., Ali, M., Hassan, W.: Assessment of trace and heavy metal distribution by four sequential extraction procedures in a contaminated soil. *Soil Water Res.* **8**(2), 71–76 (2013)
- Kasemodel, M.C.: Avaliação integrada da contaminação por metais potencialmente tóxicos em área de disposição de resíduo de mineração de chumbo—Adrianópolis (PR). Ph.D. thesis, São Carlos School of Engineering (Geotechnical Engineering department) (2017)
- Lu, S., Teng, Y., Wang, Y., Wu, J., Wang, J.: Research on the ecological risk of heavy metals in the soil around a Pb–Zn mine in the Huize County, China. *Chin. J. Geochem.* **34**(4), 540–549 (2015)
- Othmani, M.A., Souissi, F., Durães, N., Abdelkader, M., Da Silva, E. F.: Assessment of metal pollution in a former mining area in the NW Tunisia: Spatial distribution and fraction of Cd, Pb and Zn in soil. *Environ. Monit. Assess.* **187**, 523–540 (2015)
- Perin, G., Craboledda, L., Lucchese, M., Cirillo, R., Dotta, L., Zanetta, M.L., Oro, A.A.: Heavy metal speciation in the sediments of northern Adriatic sea. A new approach for environmental toxicity determination. In: Lakkas T.D. (ed.). *Heavy Metals in the Environment*, Vol. 2. CEP Consultants, Edinburgh (1985)
- Silveira, M.L., Alleoni, L.R., O'Connor, G.A., Chang, A.C.: Heavy metal extraction methods—a modification for tropical soils. *Chemosphere* **64**(11), 1929–1938 (2006)
- Tessier, A., Campbell, P.G.C., Bisson, M.: Sequential extraction procedure for the speciation of particulate trace metals. *Anal. Chem.* **51**, 844–851 (1979)
- Usero, J., Gamero, M., Morillo, J., Gracia, I.: Comparative study of three sequential extraction procedures for metals in marine sediments. *Environ. Int.* **24**(4), 487–496 (1998)



# Stability Evaluation and Grouting of Abandoned Coal Mines Used for Building Constructions

Wanghua Sui , Jiawei Liu, and Guangtao Cai

## Abstract

This paper presents a case study of the grouting improvement of high-rise buildings built over an abandoned coal mine where several seams were mined out. The engineering behavior of the subsided land and its stability before and after grouting plays an important role in its use for construction and ecological development. The stability, suitability, and grouting efficiency for a case study of the Hupan Buildings built over an abandoned mined-out area in Xuzhou, Jiangsu, China were investigated through an in situ investigation and a theoretical analysis. Grouts with water-solid ratios of 1:1 and 1:1.5 were injected into the abandoned mined-out panels through 185 boreholes. The study area can be divided into three zones with different stability and suitability. Four detection boreholes were drilled for evaluating the grouting efficiency. The results show that the stability of the mined-out area was improved by grouting. The study provides a good basis for the construction and ecological use of subsided land.

## Keywords

Grouting • Abandoned mined-out area • Grouting efficiency • Stability • Construction

## 1 Introduction

China is witnessing an increasing demand for construction and ecological development on abandoned coal mining lands in addition to the urbanization and development of transformation of mining areas. Some structures have to be built on mined-out areas because of low land availability. Before construction, the stability of the abandoned mined-out area

should be comprehensively investigated, and improvement measurements always be to sure safety.

Underground mining significantly disturbs the in situ stresses in rock mass and results in stress redistribution. The subsidence induced by the movement of overlying strata in mined-out areas does not stop immediately after mining. The residual subsidence and deformation is related to the magnitude of the increment in stress and is mainly affected by geological and mining conditions, including mining methods, coal seam occurrence, and other factors (Tong et al. 2016; Lee et al. 2013). The duration of residual subsidence under repeated mining conditions is shorter than that after the initial mining or that under the stratified first layer (Singh and Singh 1998). Residual subsidence persists for a longer period as the depth of the seams increases, and persists for a shorter while as the overburden strength increases (Kies et al. 2006; Yao and Reddish 1994).

The disturbance caused by human engineering activity will increase the deformation of the subsidence area and the deterioration of the environment. Changes in hydrogeological conditions, including the water quality, in the subsidence area affect not only the human living environment, but also the deformation of the rock and soil mass (Tiwary 2001; Johnson 2003; Szwedzicki 1999; Bell and Bruyn 1999). After complete the normal subsidence, the faults caused naturally or by coal mining may still be re-activated when the external environment changes, causing damage to constructions and transportation corridors (Donnelly 2009).

Grouting is an effective means of improving abandoned mined-out areas (Salimian et al. 2017). In grouting operation, grout fills crack openings to improve the mechanical properties of rock mass and control groundwater flow or seepage underground (Kikuchi et al. 2010; Sui et al. 2015). It can improve the structure and engineering properties of fractured rock mass, and effectively control the “activation” of abandoned mined-out areas. Measures to improve abandoned mined-out areas for construction mainly include grouting filling the mined-out area, reinforcing the overburden structure, building grouting columns and employing

W. Sui (✉) · J. Liu · G. Cai  
School of Resources and Geosciences, China University of Mining and Technology, Xuzhou, 221116, Jiangsu, China  
e-mail: suiwanghua@cumt.edu.cn

high-energy dynamic compaction for the caving zone (Guo et al. 2000). The range that needs to be grouted is mainly determined by the angle of critical displacement induced by mining activities (Lu et al. 2008).

However, because of the concealment, random spatial distribution, and uncertainty of the abandoned mined-out areas, accurate detection of the occurrence, volume, and boundaries of these areas are key issues for stability evaluation and grouting improvement. At present, in situ investigation, geophysical survey, and drilling technology are the main methods for detecting abandoned mined-out areas (Bharti et al. 2016). In engineering practices, efficiency evaluation for grouting improvement includes analytical methods, borehole and sampling, and geophysical prospecting methods (Zhang et al. 2006).

This work delves into the stability evaluation of abandoned mined-out areas and grouting improvement based on a case study of construction above a mined-out area. For this purpose, a theoretical analysis, an in situ investigation, and borehole drilling were carried out in the study area.

## 2 Overview of the Abandoned Coal Mine and the Hupan Buildings

The Hupan Buildings are located in the Jiawang District, Xuzhou City, Jiangsu Province. The total area of this project is 79,342.9 m<sup>2</sup>, with a total overall floorage of approximately 123,800 m<sup>2</sup>. There are 17 residential buildings in this area.

However, the subsidence induced in the abandoned mined-out area of the Lianshui Coal Mine seriously threatens the stability of the buildings. Grouting improvement can be adopted before constructing buildings here to guarantee their stability.

### 2.1 Hydrogeological and Engineering Geological Conditions

Geologically, the Jiawang District is located in the Xusu Settings of the Luxi District, which is located on the North China Platform, with a single synclinorium. The specific stratum structure is presented in Table 1. The main coal seams in this area are Nos. 20 and 21 in the Taiyuan Formation. The roofs of seams Nos. 20 and 21 coal seams are composed of shale and limestone, respectively, while the floor is sandy shale for both seams. These two coal seams have an average thickness of 0.69 and 0.73 m, respectively. The overburden deposited under the unconsolidated Neogene is mainly sandstone, shale, and mudstone.

The hydrogeological sections of the Jiawang District mainly contain groundwater in the Quaternary layer and the

karst-fissured limestone in the Carboniferous Taiyuan Formation, which can be categorized as layers with low and medium water abundance, respectively.

### 2.2 Historical Mining Activities and Distribution of Abandoned Panels

Mining at the Lianshui Coal Mine started in 1983. Coal seams of the Taiyuan Formation were mined by caving method. Unfortunately, a groundwater inrush occurred in 1988, and the mine was flooded in 1990. The mined-out area was buried at a depth of 30–150 m, with a cutting thickness of 0.7 m. The mine has since been filled with groundwater. The rock mass in the mined-out area was not compacted, and the residual voids were distributed locally. Therefore, mining subsidence was the main factor influencing the stability of the mined-out area. Figure 1 shows the distribution of the abandoned mined-out area.

## 3 Method

### 3.1 Empirical Evaluation of the Stability of the Abandoned Mined-Out Area

No mining activity has been conducted in the study area for more than 27 years; the process of main subsidence and residual deformation have been completed. However, the abandoned mined-out area may be activated because of the influence of factors such as human engineering activities, earthquakes, and changes in the groundwater level, deforming the ground in the mined-out area.

The angle of critical displacement is used as the angular parameter for the influence zone of the mined-out area. According to the empirical parameters obtained from the rock strata movement in Xuzhou coalmines, the angle of critical displacement for the loose layer is  $\varphi = 40^\circ$ , and the angles for upward and downward of rock strata are  $\gamma = 54.5^\circ$  and  $\beta = 53.5^\circ$ , respectively.

### 3.2 Theoretical Analysis

The scope and depth of grouting improvement can be theoretically analyzed according to the “Technical code for ground treatment of buildings in coal mine goaf” (Ministry of Housing and Urban-Rural Development of the People’s Republic of China, et al. 2017). Grout should penetrate the floor of the abandoned mined-out area. The void volume that should be filled by grouts can be calculated as follows.

$$\Delta V = s \cdot b \cdot \eta_1 \cdot \eta_2 \quad (1)$$

**Table 1** Stratigraphy features and mechanical properties of the overburden

Stratigraphy	Lithology	Thickness (m)	Description	Unit weight (kN/m <sup>3</sup> )	Elasticity modulus (MPa)	Angle of internal friction (°)	Cohesion (KPa)
Neogene	Top soil	0.75	Variogated and loose, mainly the broken brick for buildings	–	–	–	–
	Clay	1.35	Yellow-brown to reddish-brown, plastic to hard plastic	18.6	5.0	9.7	68.0
	Sandy clay with gravel	4.08	Yellow, consisting of 30–70% gravel with a particle size of 0.5–5 cm	19.0	9.0	10.8	91.0
	Clay	2.29	Brown, hard plastic	19.7	11.0	17.3	82.0
	Silty clay	2.46	Brown and plastic, contain a large number of gravels with a particle size of 0.5–5 cm	19.3	4.0	25.0	80.0
	Residual soil	2.71	Yellow, hard, containing a lot of gravel with a particle size of 1–70 cm, and locally with a plate-like cementation, easily softened with water	–	–	–	–
Permian	Sandstone	188.00	Gray and grayish yellow, a strong weathered zone is deposited on this layer	24.3	–	30.03	910.0
	Shale	–	Gray–yellow to gray–black, with a weak capacity of resistance to water influencing	22.0	–	34.16	235.0

–: Not applicable

where  $\Delta V$  is the void volume;  $s$  is the area that needs grouting;  $b$  is the thickness of the coal seam;  $\eta_1$  is the mining rate; and  $\eta_2$  is the mined-out area residential voidage.

The grouting volume can be calculated as follows.

$$Q = A \cdot \Delta V \cdot \eta / c \quad (2)$$

where  $A$  is the grouting losing coefficient;  $\eta$  is the coefficient of grouting, and  $c$  is the grout stone rate.

Considering the expansion of the slurry during grouting, and the filling in the fissures of the overlying strata, the parameters for the mined-out area and grouting amount are presented in Table 2.

### 3.3 Field Tests

Grouting efficiency was investigated by drilling and imaging and through a wave velocity test and laboratory experiments.

Four boreholes were employed for coring for the uniaxial compressive strength (UCS) tests, borehole imaging and the wave velocity test. The layout of the drilling holes is shown in Fig. 2.

The wave velocity test was performed to obtain the shear wave velocity. The filling efficiency and stone rate in and around the borehole were determined using the shear velocity. In each borehole, the space between measuring points was 1.0 m, and the testing sequence was from bottom

to top according to the source. The results should be reviewed from bottom to top at intervals of 5 m.

For these detection boreholes, the borehole imaging technology was used to observe directly the lithology, integrity of grouting stone and rock mass, and the distribution of cracks and voids.

Additionally, uniaxial compressive strength tests were performed on the grouting stones obtained from the boreholes to determine whether the strength of the grouting stones meet the design requirements.

## 4 Results

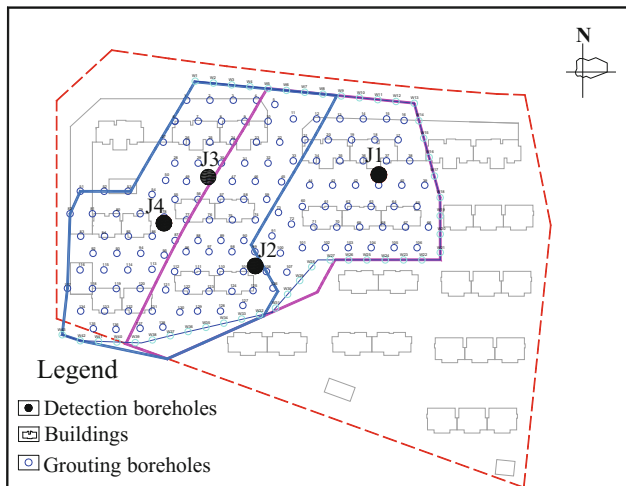
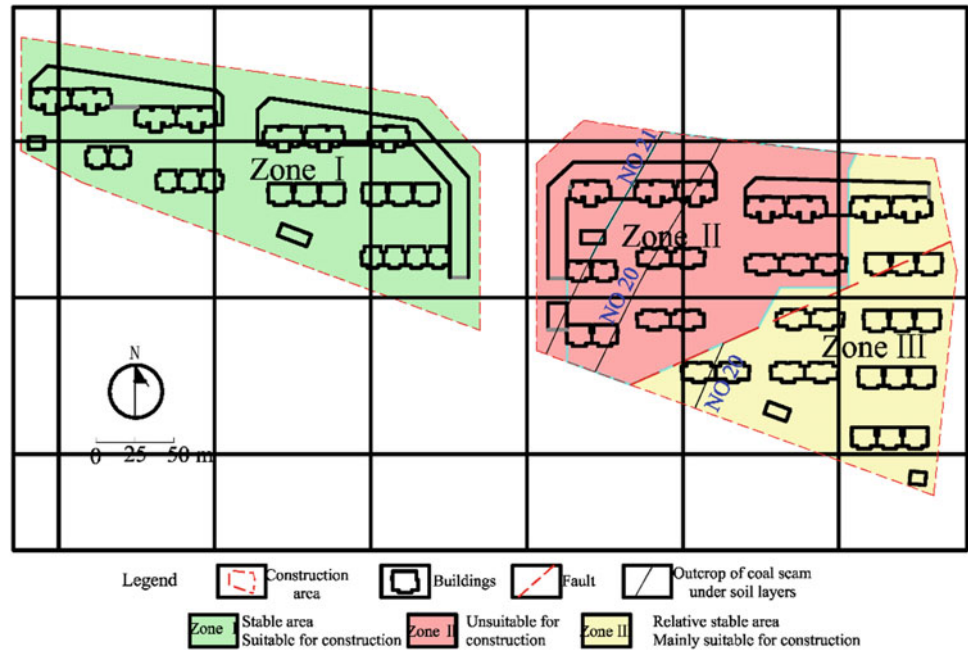
### 4.1 Stability of the Abandoned Mined-Out Area

Based on stability, the abandoned mined-out area in the study area can be divided into three zones, namely zones I, II, and III (Fig. 1).

Zone I is located in the western part of the study area without coal seams. Therefore, it is not affected by the mined-out area.

Zone II is located in the western part of the study area over the coal seams. It corresponds to a residual deformation period due to the influence of the abandoned mined-out area. In this zone, the rock mass was not compacted, and the ratio of mining depth to height exceeded 30, indicating that this

**Fig. 1** Stability of the abandoned mined-out area



**Fig. 2** Layout of the grouting and detection boreholes

zone is relatively stable. However, because of the low buried depth, further variations in hydrogeological conditions, and residual deformation of the abandoned mined-out area, this zone is not suitable for construction.

Zone III is located in the eastern part of the study area, and it is significantly affected by the subsidence of the mined-out area. However, as the burial depth of the mined-out area in this zone was high, the zone is considered relatively stable.

Zones II and III require improvement by grouting, in order to guarantee the stability of the structures.

## 4.2 Grouting Efficiency

Grout is composed of water, cement, fly ash, and a water reduction agent. The water should be clean. Muddy water should not be used. Cement type PR32.5 is used to guarantee the quality level. The water-solid mixture proportion ranges 1:1–1:1.5, and the cement accounted for 20–30% of the solid, while the fly ash accounted for 70–80%.

There are 185 drilling boreholes in the study area. These include 143 grouting boreholes and 42 curtain boreholes. The total footage of the drilling holes is approximately 9952.5 m, and the grouting volume is 9546 m<sup>3</sup>. The layout of the grouting boreholes is shown in Fig. 2.

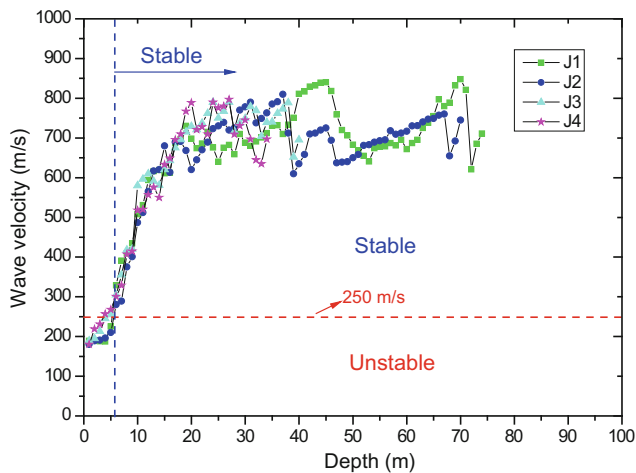
Four detection boreholes were drilled to identify the geotechnical and mechanical properties of the rock and soil layers. These holes were bored slowly, and there were generally stably, and drill falling or suction did not occur. The mined-out area was filled with solidified grout. The results of drilling indicate that the grouting efficiency is good and that no void and larger fractures remain.

UCS tests of the solidified grouts sampled from boreholes show that UCS ranges from 0.78 to 1.15 MPa, with an

**Table 2** Parameters of the mined-out area and grouting volume

Seam No.	Thickness of seam (m)	Mining rate	Residential voidage	Grouting area (m <sup>2</sup> )	Residential void (m <sup>3</sup> )	Grouting losing coefficient	Coefficient of grouting	Grout stone rate	Grout take (m <sup>3</sup> )
20	0.7	0.85	0.35	14,243	2966	1.35	0.9	0.75	4805
21	0.7	0.85	0.35	14,051	2926	1.35	0.9	0.75	4740
Total	—	—	—	28,295	5892				9546

—: Not applicable

**Fig. 3** Wave velocities of four detection boreholes

average value of 0.96 MPa, which is larger than the designed value of 0.5 MPa.

The wave velocity test was conducted in these detection holes to determine the effects of filling and grouting. Shear wave velocity is an important index to evaluate the effect of grouting. It can be used to judge whether there are any unfilled voids around and also to quantify the grouting efficiency. Figure 3 shows the wave velocity of the rock mass in the range of influence within the abandoned mined-out area. The results show that the wave velocity ranges from 610 to 655 m/s, this range greatly exceeds 250 m/s (Ministry of Housing and Urban-Rural Development of the People's Republic of China 2016). The results

indicate that the grouting efficiency can satisfy the design requirement.

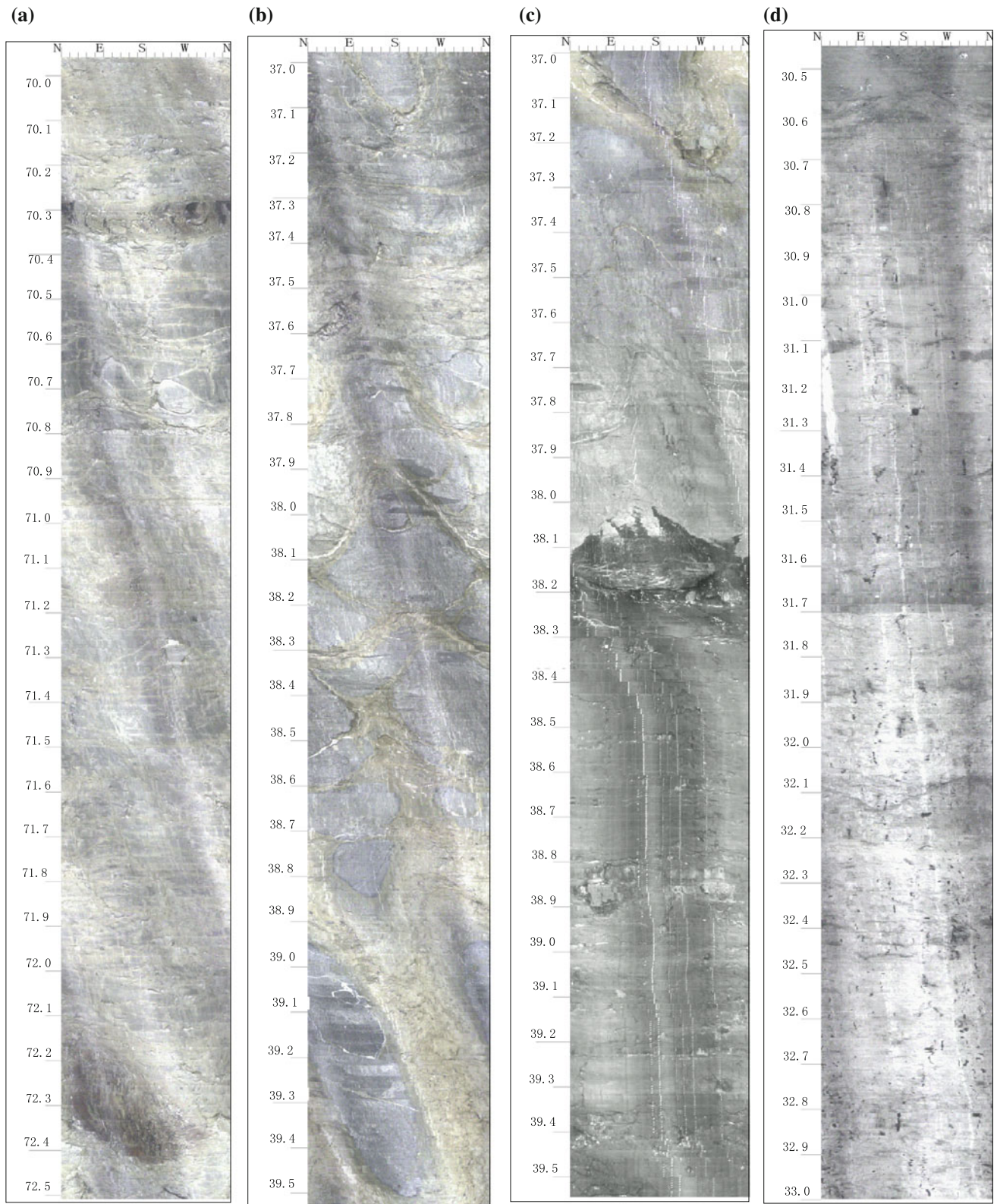
Figure 4 shows images from four boreholes. These images present the structure of rock mass in the whole section. The results indicate that there are no obvious unfilled fissures and that the rock mass around the borehole is integrant. The filling rate exceeds 90%, indicating good grouting quality.

## 5 Conclusions

Abandoned mines with multiple layers of mined-out area may pose a serious threat to construction activities. This paper presents a case study of the application of grouting to improve the stability of an abandoned mined-out area.

- (1) The influence of surface movement and deformation on construction and damage level is related to factors such as the features of the abandoned mined-out area and the influence of activation of the area on constructions. Therefore, stability evaluation of the abandoned mined-out area should be comprehensively analyzed based on the evolution of the hydrogeology.
- (2) The study area can be divided into three zones based on stability and suitability level. Zone I is the stable area. Zone II is unstable and is not suitable for construction; grouting should be applied here. Zone III is relatively stable and is mainly suitable for construction; although grouting is not necessary, some anti-deformation measures should be taken here.





**Fig. 4** Drilling imaging of the four detection boreholes **a** borehole J1, **b** borehole J2, **c** borehole J3, **d** borehole J4



(3) In all, 185 grouting boreholes were available for improving the abandoned mined-out area. Four detection boreholes were employed for evaluating grouting efficiency. The results indicate that the grouting efficiency is good and that no empty voids and large fissures are present in the rock mass.

**Acknowledgements** The authors would like to acknowledge the financial support from the National Natural Science Foundation of China under Grant No. 41472268.

## References

- Bell, F.G., Bruyn, I.A.: Subsidence problems due to abandoned pillar workings in coal seams. *Bull. Eng. Geol. Env.* **57**, 225–237 (1999)
- Bharti, A.K., Pal, S.K., Priyam, P., et al.: Detection of illegal mine voids using electrical resistivity tomography: the case-study of Raniganj coalfield (India). *Eng. Geol.* **213**, 120–132 (2016)
- Donnelly, L.: J: A review of international cases of fault reactivation during mining subsidence and fluid abstraction. *Q. J. Eng. Geol. Hydrogeol.* **42**(1), 73–94 (2009)
- Guo, G., Deng, K., He, G., Yue, J.: Grouting consolidation and detection of fractured rockmass foundation over abandoned mine goaf. *J. China Univ. Min. Technol.* **3**, 293–296 (2000). (in Chinese)
- Johnson, D.: Chemical and microbiological characteristics of mineral spoils and drainage waters at abandoned coal and metal mines. *Water Air Soil Pollut.* **3**(1), 47–66 (2003)
- Kies, A., Storoni, A., Tosheva, Z.: Radon measurements as a monitoring possibility for mining subsidence occurrence. *J. Min. Sci.* **42**(5), 518–522 (2006)
- Kikuchi, K., Mito, Y., Adachi, T., Hakoishi, N.: In situ experimental study on grouting effects on mechanical properties of rock masses. *Proc. JSCE* **517**(517), 117–124 (2010)
- Lee, D.K., Mojtabai, N., Lee, H.B., Song, W.K.: Assessment of the influencing factors on subsidence at abandoned coal mines in South Korea. *Environ. Earth Sci.* **68**(3), 647–654 (2013)
- Lu, Z., Deng, K., Jin, Y.: Determination of grouting filling area in goaf with longwall mining. *J. Min. Saf. Eng.* **25**(4), 499–501 (2008). (in Chinese)
- Ministry of Housing and Urban-Rural Development of the People's Republic of China, et al.: Technical code for ground treatment of buildings in coal mine goaf (GB 51180-2016). China Planning Press, Beijing, China (2017). (in Chinese)
- Ministry of Housing and Urban-Rural Development of the People's Republic of China: Code for seismic design of buildings (GB 50011-2010). China Building Industry Press, Beijing, China (2016). (in Chinese)
- Salimian, M.H., Baghbanan, A., Hashemolhosseini, H., et al.: Effect of grouting on shear behavior of rock joint. *Int. J. Rock Mech. Min. Sci.* **98**, 159–166 (2017)
- Singh, K.B., Singh, T.N.: Ground movements over longwall workings in the Kamptee coalfield, India. *Eng. Geol.* **50**, 125–139 (1998)
- Sui, W., Liu, J., Hu, W., et al.: Experimental investigation on sealing efficiency of chemical grouting in rock fracture with flowing water. *Tunn. Undergr. Space Technol. Incorporating Trenchless Technol. Res.* **50**(1), 239–249 (2015)
- Szwedzicki, T.: Pre-and post-failure ground behavior: Case studies of surface crown pillar collapse. *Int. J. Rock Mech. Min. Sci.* **36**, 351–359 (1999)
- Tiwary, R.: Environmental impact of coal mining on water regime and its management. *Water Air Soil Pollut.* **132**(1), 185–199 (2001)
- Tong, L., Lian, L., Amatya, B., Liu, S.: Risk assessment and remediation strategies for highway construction in abandoned coal mine region: lessons learned from Xuzhou, China. *Bull. Eng. Geol. Env.* **75**(3), 1045–1066 (2016)
- Yao, X.L., Reddish, D.J.: Analysis of residual subsidence movements in the UK coalfields. *Q. J. Eng. Geol. Hydrogeol.* **27**(1), 15–23 (1994)
- Zhang, M., Zhang, W., Sun, G.: Evaluation technique of grouting effect and its application to engineering **25**(2), 3909–3918 (2006). (in Chinese)

# Detection of Subsidence by Radar Interferometric Data in the Seruci-Nuraxi Figus Coal Mine Area (Sardinia, Italy)

Serena Tessitore, Diego Di Martire, Nicola Mondillo,  
Lorenzo Ammirati, Maria Boni, and Domenico Calcaterra

## Abstract

In the present work, an Advanced Differential Interferometric Synthetic Aperture Radar (DInSAR) technique has been used to measure deformations related to Seruci-Nuraxi Figus underground coal mine, located in the Carbonia-Iglesias mining district (Sardinia region, Italy). Specifically, COSMO-SkyMed (CSK) data, obtained in the framework of the Third Not-ordinary Plan of Environmental Remote Sensing project by PSP-IFSAR technique, have been used to analyze the deformations occurring between 2011 and 2014 in the study area to improve the phenomenon knowledge. Availability of images acquired in ascending and descending geometries has permitted to calculate the vertical displacement component. Accordingly, a maximum subsidence of about 25 cm has been measured in the time span 2011–2014. Furthermore, time-lapsed vertical deformation profiles have also been carried out to analyze the dynamic ground-deformation development. DInSAR measurements have allowed obtaining information on the spatial and temporal development of a

phenomenon, very useful to the cause-effect mechanism understanding aimed to improve the resources management.

## Keywords

InSAR • Coal mine • Monitoring • Subsidence • Underground mining

## 1 Introduction

Extraction activities are usually related to deformation phenomena which can mainly result in mine collapses and subsidence (Ng et al. 2012). Mine subsidence can also involve buildings (Bell 1992; Clarke et al. 2006) or infrastructures, impact groundwater and induce economic and life losses. Thus, the management of the consequences of mining activities represents a major concern issue (Raucoules et al. 2007). Several countries worldwide can be cited where coal mining provoked subsidence, like Poland, United Kingdom and Belgium (Graniczny et al. 2015), Illinois, Pennsylvania and Virginia (Pickering and Owen 1994). Mining activities can also have consequences after their cessation as occurred in the upper Silesian coal basin in Southern Poland (Graniczny et al. 2015) or in Belgium (Vervoort 2016). Therefore, monitoring of active or abandoned mining areas is a key point as to detect and forecast potential and actual geological hazards, or to improve their environmental rehabilitation (Winterhalder 1996). In the last years, Advanced Differential Interferometric Synthetic Aperture Radar (A-DInSAR) techniques have been effectively used to measure surficial deformations related to underground mining activity (Herrera et al. 2010; Tomás et al. 2014; Yerro et al. 2014; Fan et al. 2015; Przyłucka et al. 2015) being very useful to identify the extension of the area of influence also for longwall mining (Duro et al. 2013). Longwall mining represents a total extraction method which can result in failure, depending on the mine geometry as well as on the coal

S. Tessitore · D. Di Martire · N. Mondillo · L. Ammirati  
M. Boni · D. Calcaterra (✉)  
Department of Earth Sciences, Environment and Resources,  
Federico II University of Napoli, Largo San Marcellino, 10,  
Naples, 80138, Italy  
e-mail: domenico.calcaterra@unina.it

S. Tessitore  
e-mail: serena.tessitore@unina.it

D. Di Martire  
e-mail: diego.dimartire@unina.it

N. Mondillo  
e-mail: nicola.mondillo@unina.it

L. Ammirati  
e-mail: ammiratilorenzo@gmail.com

M. Boni  
e-mail: maria.boni@unina.it

physical properties (Gee et al. 2017). In fact, this method results in the immediate collapse of the roof and overlying rock into the obtained void and this can have as consequence a ground areal subsidence.

In this work, an A-DInSAR technique has been used to study the surficial deformations occurred between 2011 and 2014 in the Seruci-Nuraxi Figus area (Carbonia-Iglesias, Sardinia region, Italy—Fig. 1), where a large underground coal longwall mine was active until 2013. For this study, COSMO-SkyMed data (2011–2014) obtained in the framework of the Third Not-ordinary Plan of Environmental Remote Sensing project (Piano Straordinario di Telerilevamento Ambientale, PST-A-3 in Italian) promoted by the Italian Ministry for the Environment, Land and Sea (Costantini et al. 2017; Di Martire et al. 2017) have been used. Specifically, 99 images (41 and 58, respectively acquired in ascending and descending geometries) were processed by PSP-IFSAR algorithm (Persistent Scatterers Pair Interferometry SAR—Costantini et al. 2008) and has allowed first analyses of the deformations measured in the

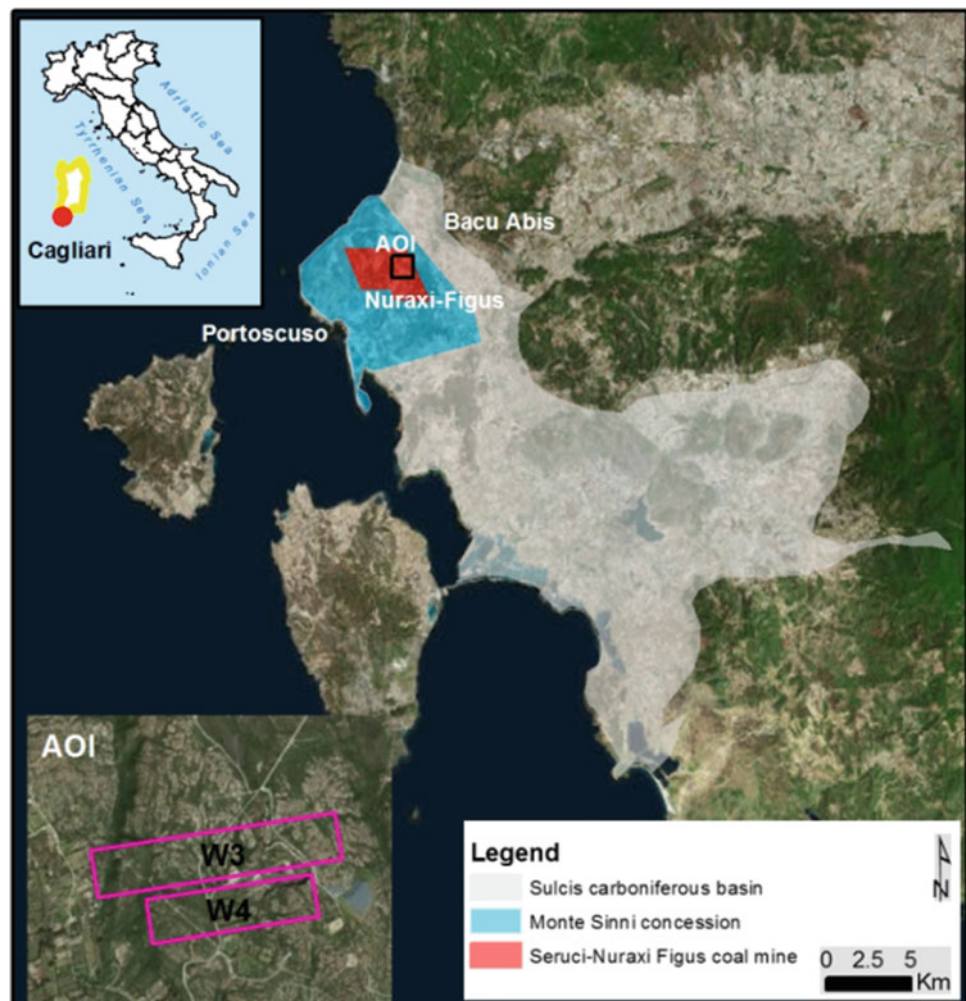
study area. At first, deformation measurements, projected along the satellite Line of Sight (LoS) direction (ascending and descending acquisitions), have been combined together to obtain vertical deformation maps and profiles. The availability of such kind of data can be very useful to the cause-effect mechanism understanding in order to improve the active deformation phenomena monitoring.

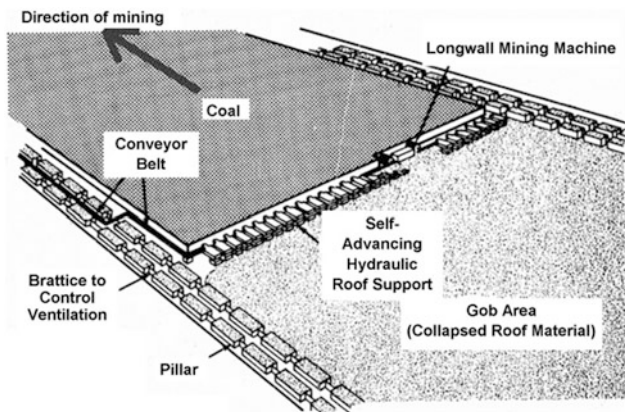
## 2 Study Area

### 2.1 History of Mining District

The Seruci-Nuraxi Figus coal mine is located in a historic coal mining district, which was active since the 1850 (Fig. 1). In the Seruci-Nuraxi Figus area the underground mining started at the end of the 1950. Since the 1976 the mining license has been owned by Carbosulcis S.p.A., which mined the coal seams in several sectors of the Seruci-Nuraxi Figus concession (also named “Monte Sinni”

**Fig. 1** Location of the study area





**Fig. 2** Longwall mining technique scheme

concession) until 2012, to supply coal fuel to the nearby thermal electric power station, owned by ENEL. Between 1996 and 2012, Carbosulcis S.p.A. mined several panels by using the longwall technique (Fig. 2).

Panels W3 and W4, within the Area of Interest (AOI, Fig. 1), are located at a depth of about 500 m below the ground surface, having average extent of about 0.1–0.2 km<sup>2</sup> (length of 500–900 m, width of 200–250 m) and height of ca. 3 m. According to the mining activity records reported in the Carbosulcis S.p.A. website, panels W3 and W4 were mined before and during the InSAR monitoring time-window, object of this study. In detail, panel W4 was completely mined out between 2008 and 2011, whereas panel W3 was only partially mined in the period 2011–2013. Between March 2013 and June 2015 the extraction activities of the W3 panel had to stop for long periods of time due to technical reasons, which prevented any further excavation of the panel and allowed only to carry out limited maintenance works to the main and tail tunnels.

On 1th October 2014, at the end of a EU procedure aimed to reveal if illegal state aid had supported the Carbosulcis operations in Sardinia, the European Commission finally approved a closure plan of the Seruci-Nuraxi Figus coal mine, which intends to definitely stop coal mining before the end of 2018 and to complete an environmental remediation plan before the end of 2027 (<http://www.carbosulcis.eu/>). Thus, from April to October 2014 the coal production was minimised and the activities were mainly focused on the maintenance and safety measures without new tunnel excavations.

## 2.2 Geological Setting

The Seruci-Nuraxi Figus coal mine is geologically located in the so-called “Sulcis carboniferous basin”, a tectonic depression covering an area of ca. 100 km<sup>2</sup>, which in the

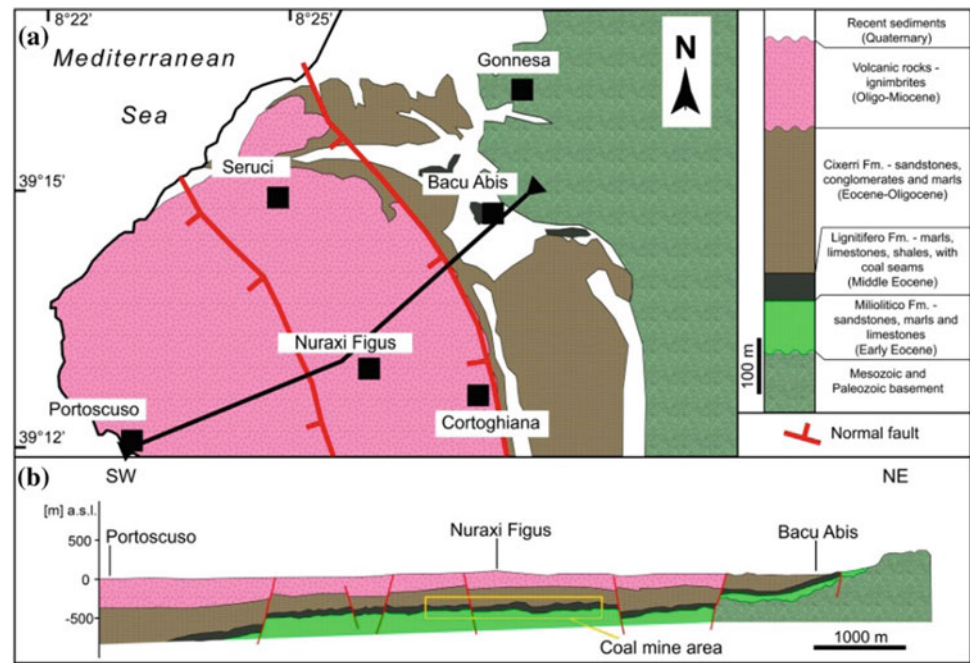
Paleogene (66–23 Ma before present) was filled by a thick (up to 700 m) pile of continental-marine sediments (Fig. 3a). The basin is surrounded by Paleozoic to Mesozoic rocks (the basement), which mainly crop out on the eastern and northern borders of the basin (Pasci et al. 2012). The sedimentary succession filling the basin, uncomfortably covering the basement, can be subdivided from the bottom to the top, in four Formations of Paleogene age: *Calcari a Macroforaminiferi* Fm., (limestones—identified only in very deep drill holes); *Miliolitico* Fm., consisting of sandstones, marls and limestones (20–70 m thick; Early Eocene age); *Lignitifero* Fm., an association, 70–150 m thick, of clays, marly limestones, bituminous limestones, marls and conglomerates, interbedded with coal seams (Early-Middle Eocene age), and *Cixerri* Fm., consisting of sandstones, conglomerates and marls (average thickness = 300 m) (Eocene-Oligocene age; Pasci et al. 2012). The Lignitifero Fm., coal seams have a thickness comprised between 1 and 10 m, and consist of pure coal layers commonly 10 cm thick, rarely reaching 30–50 cm of thickness, interbedded with clays. In the Seruci-Nuraxi Figus area, the mined horizon is located at 350–450 m below the surface (Fig. 3b). Sedimentary rocks are covered by 100–300 m of volcano-pyroclastic rocks and ignimbrites (Oligocene-Miocene age; Fadda et al. 1994; Pasci et al. 2012). This area is crossed by several regional faults which seems not have interacted with the cultivation activities.

## 3 Satellite Data

In this work, the PSP-IFSAR algorithm (Costantini et al. 2008) has been applied to 41 high-resolution CSK images acquired in ascending and 58 in descending orbit modes, respectively covering the periods May 2011–January 2014 and May 2011–March 2014. InSAR results consist of LoS-projected deformation maps, profiles and time series (TS). The 2011–2014 subsidence rate (projected along the LoS) for the AOI is presented in Fig. 4a, while the LOS-projected deformation TS of the points labeled in Fig. 4a have been plotted in Fig. 4b. It is important to note that, in the central part of the monitored area, deformation velocities exceed the detection limits (Massonnet and Feigl 1998) and no satellite-based measurements are available (Fig. 4a). Cumulated satellite-based LoS displacements vary between –131 and +29 mm (until January 2014) and between –293 and +22 mm (until March 2014) in ascending and descending geometries, respectively. Specifically, cumulated measured displacements (for each observation period) are of  $-6 \pm 16$  mm (ascending) and of  $-13 \pm 32$  mm (descending) on average for the whole study area. According to Fig. 4a, as expected, the highest deformation rates ( $>5$  cm/year) are observed in the center of the



**Fig. 3** Geological sketch map (a); geological cross-section (b)



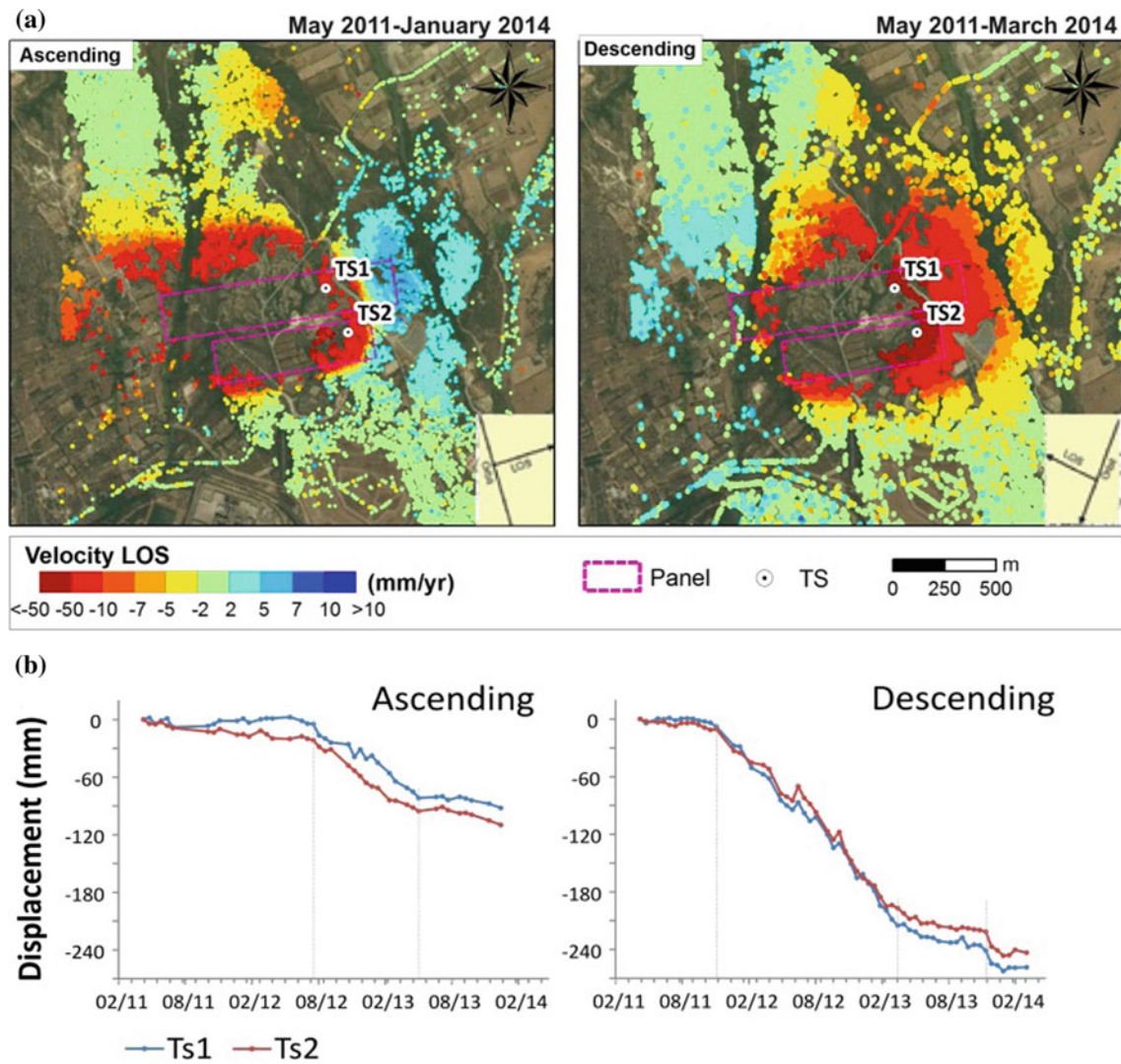
subsiding area, circumscribed to the mined panels W3 and W4. TS reported in Fig. 4b show several deformation trend changes during the monitoring windows; after a first stable period (until December 2011), an acceleration can be observed until May 2013; then the deformation rate decreased until December 2013 when a rapid settlement of about 3 cm has been detected by descending data.

## 4 Results and Discussion

Longwall mining activities are characterized by a special ground deformation behaviour due to the excavation technique; in fact, longwall face advances induce a strong movement pattern in the excavation surrounding area (Duro et al. 2013). In Seruci-Nuraxi Figus coal mine, in spite of the high thickness of the cover (Fig. 2b), an aerial subsidence has been detected by means of satellite-based measurements in correspondence of W3 and W4 panels (Fig. 4a). The availability of both ascending and descending acquisition geometries has permitted to obtain a vertical projection of displacement data, reported in Fig. 5. Maximum cumulated vertical displacements are of about 3 cm until January 2012, 14 cm until January 2013 and 24 cm until January 2014 (Fig. 5). As previously observed (see Sect. 3), no data in correspondence of the center of the panels are available; this issue does not allow to fully characterize the phenomenon and an integration with complementary InSAR techniques is needed to correctly estimate the maximum subsidence in the center of the study area.

Furthermore, as a first simplified analysis aimed to verify the possible causes of the observed phenomenon, the theory described in O'Reilly and New (1982) concerning the relations between tunneling depth and settlement geometries has been used. Specifically, by considering DInSAR deformation profile B–B' (orthogonal to the excavation direction), it is possible to obtain the length of the deformed area, the maximum displacement and the settlement inflection point. Such geometrical profile characteristics are related to the depth of the deformation causes which, in this case, has resulted located at  $-380$  m to the ground. Of course, especially for the great error related to the maximum displacement in the central part of the profiles, further analyses will be carried out.

Nevertheless, to support this hypothesis, the observed deformation trend changes showed in Fig. 4b seem to be related with the excavation development. In fact, W3 panel was mined from 2011 to 2013 and the highest deformation velocities have been detected between December 2011 and May 2013; then, just a possible collapse has been observed by satellite in December 2013. Also in this case, the interferometric fringes integration would allow to better understand the event. Moreover, accordingly with Peng (1992), considering the deformation mechanisms upon a mined area, 4 zones can be identified where a proportion with the panel height ( $H$ ) can be found: (a) caving zone ( $2-8 H$ ); (b) fractured zone ( $30-50 H$ ); (c) bending zone; (d) soil zone. Taking into account such relations, for the Seruci-Nuraxi Figus area (see Fig. 3b), upon the mined horizon (located at 380 m below the surface), the caving zone “a” should be



**Fig. 4** InSAR mean velocity maps along the LoS direction in the ascending (left) and descending (right) acquisition geometries (a); TS of deformation (b)

completely included in the Lignifero formation, while the fractured zone “b” should affect a part of the Cixerri formation; a residual part of Cixerri formation and the Volcanic-pyroclastic rocks should belong to bending zone “c”. Further analyses will be needed in order to found the specific relations for the geological settings of Seruci-Nuraxi Figus area.

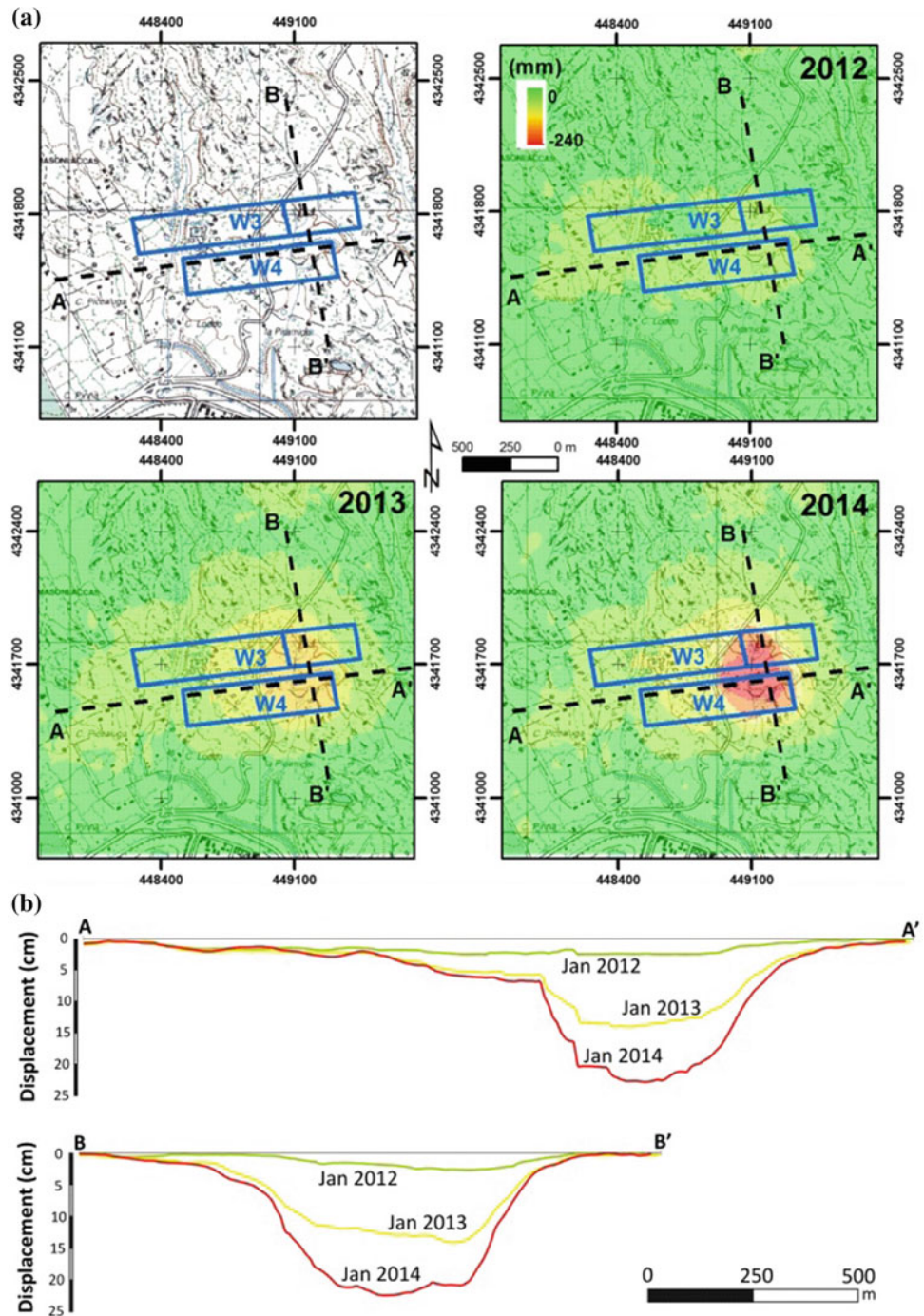
## 5 Conclusions and Future Goals

Recently, the improvement of satellite and sensor technologies, the easier access to the data and the higher acquisition frequency have brought to an increase in the use

of remote sensing for Earth Observation (Tomás and Li 2017). A-DInSAR results (i.e. deformation velocity maps, profiles and TS) have turned out to be very useful for the hazard management. In this preliminary study concerning the possible deformation related to longwall coal mining, satellite-based measurements have allowed to identify a possible extension of the area of influence, deformation trend changes and vertical profiles. In the following of the present work, A-DInSAR processing will be performed with a coherence-based technique and deformation monitoring updated nowadays; then, in order to obtain displacement information at the centre of the longwall panels, where probably movements exceed the detection limits, InSAR fringes will be integrated. To analyse in depth the observed



**Fig. 5** InSAR vertical deformation maps (a) and vertical deformation profiles (b) cumulated in the periods May 2011–January 2012, May 2011–January 2013 and May 2011–January 2014; black dashed lines in the figure represent the profiles cross-sections



phenomenon and better understand the cause-effect mechanism, external data should be acquired; as usual, also in situ surveys should be carried out to improve the knowledge of the nature of the ground motion and interpret the areas where predominantly horizontal and vertical components have been observed. Accordingly to existing regulations, mines monitoring is mandatory also after their closure. DInSAR could

be considered as a complementary tool to detect existing potential risks and to plan possible rehabilitations.

**Acknowledgements** COSMO-SkyMed data have been used thanks to a cooperation protocol between Italian Ministry for the Environment, Land and Sea (MATM) and Federico II University of Napoli. The authors are grateful to Carbosulcis S.p.A. for allowing publication of mine data.

## References

- Bell, F.G.: Salt mining and associated subsidence in mid-Cheshire, England, and its influence on planning. *Bull. Assoc. Eng. Geol.* **22**, 371–386 (1992). <https://doi.org/10.2113/gseegeosci.xxix.4.371>
- Carbosulcis S.p.A. website: <http://www.carbosulcis.eu/> (last consultation 05/10/2017)
- Clarke, B.G., Welford, M., Hughes, D.B.: The threat of abandoned mines on the stability of urban areas. In: Proceedings of the 10th Congress of the International Association for Engineering Geology and the Environment, IAEG2006, Nottingham, UK, 6–10 September 2006; Geological Society, London, UK (2006)
- Costantini, M., Falco, S., Malvarosa, F., Minati, F.: A new method for identification and analysis of persistent scatterers in series of SAR images. In: IGARSS 2008-2008 IEEE International Geoscience and Remote Sensing Symposium vol. 2, 449 p (2008)
- Costantini, M., Ferretti, A., Minati, F., Falco, S., Trillo, F., Colombo, D., Novati, F., Malvarosa, F., Mammone, C., Vecchiolli, F., Rucci, A., Fumagalli, A., Allievi, J., Ciminelli, M.G., Costabile, S.: Analysis of surface deformations over the whole Italian territory by interferometric processing of ERS, Envisat and COSMO-SkyMed radar data. *Remote Sens. Environ.* in press (2017). <https://doi.org/10.1016/j.rse.2017.07.017>
- Di Martire, D., Paci, M., Confuorto, P., Costabile, S., Guastaferrò, F., Verta, A., Calcaterra, D.: A nation-wide system for landslide mapping and risk management in Italy: the second not-ordinary plan of environmental remote sensing. *Int. J. Appl. Earth Obs. Geoinf.* **63**, 143–157 (2017). <https://doi.org/10.1016/j.jag.2017.07.018>
- Duro, J., Albiol, D., Mora, O., Payàs, B.: Application of advanced InSAR techniques for the measurement of vertical and horizontal ground motion in longwall minings. In: Proceedings of 13th Coal Operators' Conference, University of Wollongong, The Australasian Institute of Mining and Metallurgy & Mine Managers Association of Australia, pp. 99–106 (2013)
- Fadda, A., Ottelli, L., Perna, G.: The Sulcis Carboniferous Basin—Geology, Hydrogeology, Mines. Carbosulcis s.p.a, Cagliari, Italy (in Italian) (1994)
- Fan, H., Gao, X., Yang, J., Deng, K., Yu, Y.: Monitoring mining subsidence using a combination of phase-stacking and offset-tracking methods. *Remote Sens.* **7**, 9166–9183 (2015). <https://doi.org/10.3390/rs70709166>
- Gee, D., Bateson, L., Sowter, A., Grebbly, S., Novellino, A., Cigna, F., Marsh, S., Banton, C., Wyatt, L.: Ground motion in areas of abandoned mining: application of the intermittent SBAS (ISBAS) to the Northumberland and Durham Coalfield, UK. *Geosciences* **7**(3), 85 (2017). <https://doi.org/10.3390/geosciences7030085>
- Graniczny, M., Colombo, D., Kowalski, Z., Przyłucka, M., Zdanowski, A.: New results on ground deformation in the Upper Silesian Coal Basin (southern Poland) obtained during the DORIS Project (EU-FP 7). *Pure. Appl. Geophys.* **172**, 3029–3042 (2015). <https://doi.org/10.1007/s00024-014-0908-6>
- Herrera, G., Tomás, R., Vicente, F., Lopez-Sanchez, J.M., Mallorquí, J.J., Mulas, J.: Mapping ground movements in open pit mining areas using differential SAR interferometry. *Int. J. Rock Mech. Min. Sci.* **47**, 1114–1125 (2010). <https://doi.org/10.1016/j.ijrmms.2010.07.006>
- Massonnet, D., Feigl, K.L.: Radar interferometry and its application to changes in the Earth's surface. *Rev. Geophys.* **36**, 441–500 (1998). <https://doi.org/10.1029/97RG03139>
- Ng, A.H.-M., Ge, L., Zhang, K., Li, X.: Estimating horizontal and vertical movements due to underground mining using ALOS PALSAR. *Eng. Geol.* **143–144**, 18–27 (2012). <https://doi.org/10.1016/j.enggeo.2012.06.003>
- O'Reilly, M.P., New, B.M.: Settlements above tunnels in the United Kingdom: their magnitude and prediction. In: Proceeding of Tunnelling 82 Symposium. London, pp. 173–181 (1982)
- Pasci, S., Carmignani, L., Pisanu, G., Sale, V.: Notes to 1:50,000 Geological Map of Italy, Sheet 564, Carbonia. Servizio Geologico d'Italia - ISPRA and Regione Autonoma della Sardegna (2012). (in Italian)
- Peng, S.S.: Surface Subsidence Engineering. Society for Mining, Metallurgy, and Exploration, Inc. Littleton, USA. 161 pp (1992)
- Pickering, K.T., Owen, L.A.: An Introduction to Global Environmental Issues. Routledge, London, New York (1994)
- Przyłucka, M., Herrera, G., Graniczny, M., Colombo, D., Béjar-Pizarro, M.: Combination of conventional and advanced DInSAR to monitor very fast mining subsidence with TerraSAR-X Data: Bytom City (Poland). *Remote Sens.* **7**, 5300–5328 (2015). <https://doi.org/10.3390/rs70505300>
- Raucoules, D., Colesanti, C., Carnec, C.: Use of SAR interferometry for detecting and assessing ground subsidence. *C.R. Geosci.* **339**(5), 289–302 (2007). <https://doi.org/10.1016/j.crte.2007.02.002>
- Tomás, R., Li, Z.: Earth observations for geohazards: present and future challenges. *Remote Sens.* **9**(3), 194 (2017). <https://doi.org/10.3390/rs9030194>
- Tomás, R., Romero, R., Mulas, J., Marturià, J.J., Mallorquí, J.J., Lopez-Sanchez, J.M., Herrera, G., Gutiérrez, F., González, P.J., Fernández, J., Duque, S., Concha-Dimas, A., Cocksley, G., Castañeda, C., Carrasco, D., Blanco, P.: Radar interferometry techniques for the study of ground subsidence phenomena: a review of practical issues through cases in Spain. *Environ. Earth Sci.* **71**, 163–181 (2014). <https://doi.org/10.1007/s12665-013-2422-z>
- Vervoort, A.: Surface movement above an underground coal longwall mine after closure. *Nat. Hazards Earth Syst. Sci.* **16**, 2107–2121 (2016). <https://doi.org/10.5194/nhess-16-2107-2016>
- Winterhalder, K.: Environmental degradation and rehabilitation of the landscape around Sudbury, a major mining and smelting area. *Environ. Rev.* **4**, 185–224 (1996). <https://doi.org/10.1139/a96-011>
- Yerro, A., Corominas, J., Monells, D., Mallorquí, J.J.: Analysis of the evolution of ground movements in a low densely urban area by means of DInSAR technique. *Eng. Geol.* **170**, 52–65 (2014). <https://doi.org/10.1016/j.enggeo.2013.12.002>

# Field Observation of the Unsaturated Characteristics in a Mine Waste Dump During Rainfall

Young-Suk Song<sup>✉</sup> and Yong-Chan Cho<sup>✉</sup>

## Abstract

Field monitoring sensors and an instrumentation system were installed in a mine waste dump slope at the Imgi mine in South Korea to investigate and analyze the surficial seepage and unsaturated soil behavior at the vadose zone. The field instrumentation consisted of a data acquisition system, a solar charging system, and measuring sensors. The rainfall, matric suction, and volumetric water contents were continuously measured from the units in the site and analyzed with the soil water characteristic curve (SWCC) estimated from laboratory experiments. The variations in matric suction and volumetric water content were primarily affected by the rainfall intensity. At the surface of the waste dump slope, the largest increase and decrease in the changes of matric suction and volumetric water content were observed during the wetting and drying processes, respectively. The measured matric suction and volumetric water content data from the field monitoring site were compared with the SWCCs obtained from the laboratory test, and the measured data was located between the drying and wetting paths. The drying and wetting paths obtained from the laboratory test are regarded as the primary drying and wetting curves, respectively. Therefore, the measured data with a nonlinear relationship between matric suction and volumetric water content could be defined as scanning curves, which are located near the primary drying and wetting curves. In particular, the characteristics of unsaturated soil near ground surface were dominantly associated with the primary wetting curve.

## Keywords

Field monitoring • Matric suction • Rainfall • Volumetric water content • Waste dump slope

Y.-S. Song (✉) · Y.-C. Cho  
Korea Institute of Geoscience and Mineral Resources,  
Daejeon, 34132, South Korea  
e-mail: yssong@kigam.re.kr

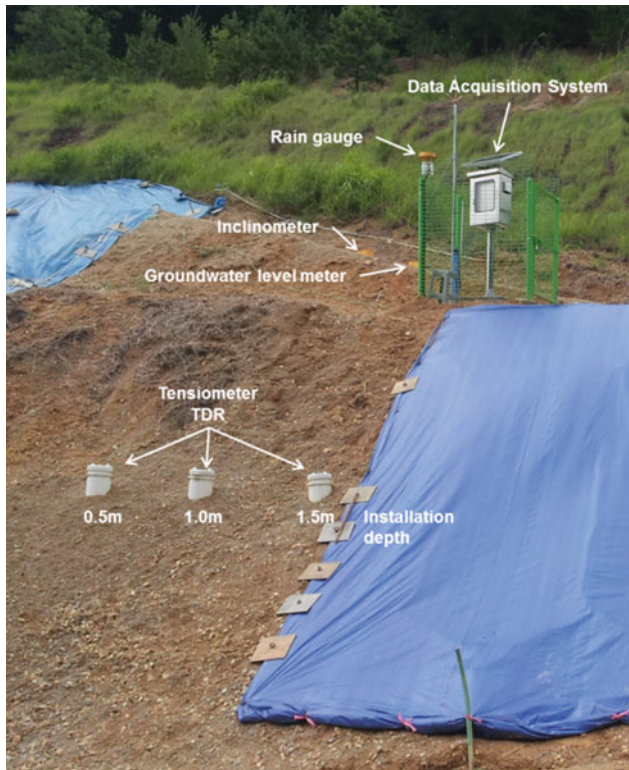
## 1 Introduction

Slope failures often occur during the rainy season, suggesting that rainfall is a primary factor causing slope failure. In general, deep-seated slope failures can be triggered by a rising the underground water level due to rainfall infiltration. However, shallow slope failures often occur after the wetting front caused by rainfall infiltration reaches the critical depth. Fredlund and Rahardjo (1993) reported that localized heavy rain resulted in an increase in only the surface underground water level, and thus, an increase in the underground water level at a deep depth could not cause shallow slope failure. Because the unsaturated characteristics of the slope can vary due to rainfall infiltration, the field measurement data for matric suction and volumetric water content in the slope are required to predict slope failure.

## 2 Field Instrumentation

The mine waste dump slope was located in Imgi-ri, Cheolma-myeon, Gijang-gun, Busan. Since the mine was abandoned, there has been no specific plan for preventing environmental damage by the mine, and thus, the surface of the mine waste dump slope has experienced seepage erosion and slope failure. In this area, rainfall infiltration and unsaturated soil movement were measured during rainfall using the field instrumentation system. Figure 1 demonstrates the instrumented slope to monitor the unsaturated soil characteristics. The tensiometers and TDR sensors were installed in the middle of the slope to measure the changes in matric suction and volumetric water content during rainfall. In particular, the tensiometers and TDR sensors were placed at depths of 0.5, 1.0, and 1.5 m to observe the behavior of the wet front and the variations in matric suction and volumetric water content according to depth during rainfall. The inclinometer and groundwater level meter were installed to measure the slope displacement and groundwater level





**Fig. 1** Setup for the measuring device on the mine waste dump slope

changes, respectively. The rain gauge was installed next to the groundwater level meter. The data acquisition system and solar charging system were placed to collect and transmit the field data. Detailed information for the installation sensors is provided in Table 1.

### 3 Engineering Properties of Mine Tailings

#### 3.1 Physical Properties

A series of laboratory tests, including unit weight, specific gravity, grain size analysis, liquid and plastic limits, and compaction tests, were performed to determine the engineering properties of the tailing mine waste at the Imgi mine. According to the Unified Soil Classification System, the sample was silty sand (SM), and the field dry unit weight was  $1.59 \text{ t/m}^3$ . The physical properties of the mine tailings are summarized in Table 2.

#### 3.2 Unsaturated Properties

The automated SWCC apparatus was employed to investigate the unsaturated properties of the tailing at the Imgi mine

(Song et al. 2012; Wayllace and Lu 2012). Based on the results of the automated SWCC test, the model developed by van Genuchten (1980) was chosen to estimate the SWCC because pore-water pressure was recorded according to matric suction, and the van Genuchten model (VG model) was the best model to predict the SWCCs for the given soil condition (Song et al. 2010). The estimated equation is shown in Eq. (1).

$$S_e = \frac{\theta - \theta_r}{\theta_s - \theta_r} = \left[ \frac{1}{1 + [\alpha(u_a - u_w)]^n} \right]^m \quad (1)$$

where  $\theta_r$  is the residual value of the soil-water content,  $\theta_s$  is the saturated value of the soil-water content,  $u_a$  is the pore air pressure,  $u_w$  is pore water pressure,  $\alpha$  is the parameter related to the air-entry value (AEV),  $n$  is the parameter related to the slope of the SWCC,  $m$  is the parameter related to the residual water content, and  $R^2$  is the coefficient of determination. The SWCC for mine waste dump slope tailing in the drying and wetting paths was estimated based on Eq. (1) and the parameters in Table 3.

Figure 2 shows the SWCCs calculated by the van Genuchten model (VG model) above for drying and wetting paths. As shown in Fig. 2, the SWCCs of the drying and wetting paths were not matched. The volumetric water content of the drying path is higher than that of the wetting path at the same matric suction. The difference of SWCCs in the drying and wetting paths is referred to as hysteresis. The SWCCs of drying and wetting paths in Fig. 2 could be regarded as the primary drying and wetting curves, respectively, proposed by Muraleetharan et al. (2009).

### 4 Results and Measurement Analysis

#### 4.1 Measurement Results

Figure 3 represents the variation in volumetric water content at different depths according to rainfall intensity. The volumetric water content was greatly influenced by the rainfall intensity. The volumetric water content increased as a result of rainfall infiltration for the wetting period and decreased for the drying period. For rainfall, the volumetric water content was the highest at the surface and decreased with depth. However, for the drying period, the highest volumetric water content was observed at a depth of 1.0 m, while volumetric water content was the lowest at a depth of 0.5 m. The primary reason that the lowest volumetric water content was measured at a depth of 0.5 m appeared to be that the evaporation at the surface can result in a decrease in volumetric water content (Rahardjo et al. 2013). In other words,

**Table 1** Instrumentation sensors

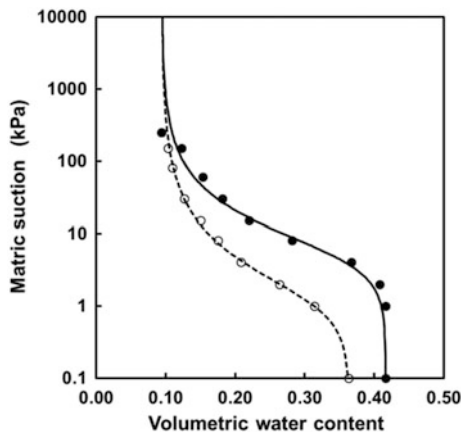
Item	Measurement sensor	Model (Manufacturer)
Rainfall	Rainfall tipping bucket	Te525MM-L23 (Campbell)
Matric suction	Tensiometer	Jet-fill 2725 (Soil moisture)
Volumetric water contents	TDR	TRIME PICO 64 (IMCO)
Groundwater level	Groundwater level meter	CWL-5 (ZIS)
Soil displacement	Automated inclinometer	SMI-5 (ZIS)

**Table 2** Physical properties of the mine tailings

Property	Symbol	Unit	Measured value
Specific gravity	$G_s$	–	2.73
Natural water content	$w$	%	6.87
Total unit weight	$r_t$	t/m <sup>3</sup>	1.70
Dry unit weight	$r_d$	t/m <sup>3</sup>	1.59
Effective particle size	$D_{10}$	mm	0.0064
USCS	–	–	SM

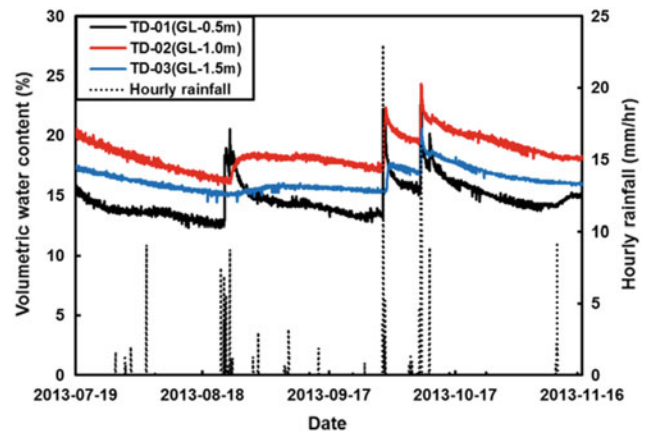
**Table 3** Best curve-fitting parameters from the van Genuchten model

Path	$\alpha$ (kPa <sup>-1</sup> )	$n$	$m$	$R^2$
Drying	0.180	1.811	0.448	0.994
Wetting	0.787	1.670	0.401	0.998

**Fig. 2** SWCC of tailings at the mine waste dump slope

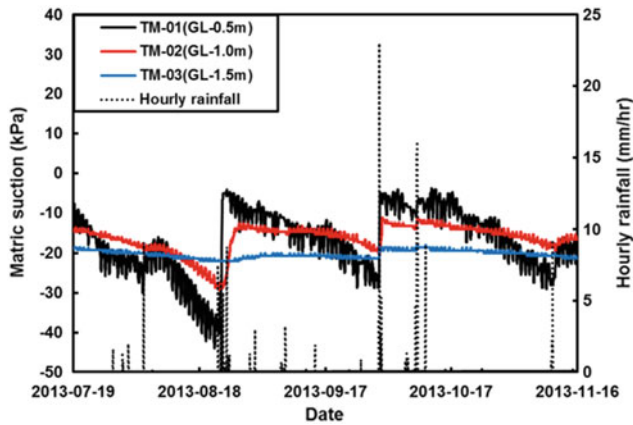
the variation range in volumetric water content was the largest between the surface and a depth of 0.5 m for both the drying and wetting periods, and the amount of the variation was approximately 10%.

The variation in matric suction measured from the tensiometers at different depths is shown in Fig. 4. Matric suction was also affected by the rainfall intensity. The pattern of variation in matric suction was the same as that of the volumetric water content. The maximum amount of variation in matric suction for the drying and wetting periods was approximately 40 kPa.

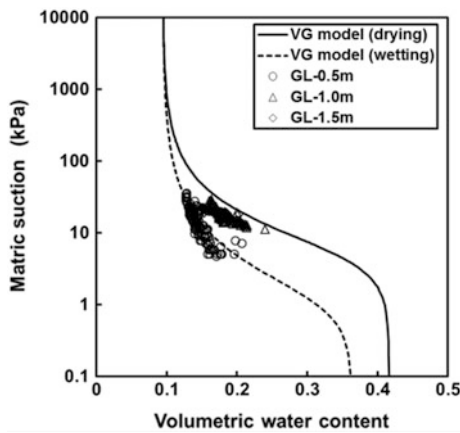
**Fig. 3** Variation in volumetric water content at different depths according to rainfall intensity

#### 4.2 Relationship Between Matric Suction and Volumetric Water Content

In general, the relationship between matric suction and volumetric water content was estimated by the result from the automated SWCC apparatus. The stress state of the unsaturated soil can be simply predicted based on the estimated SWCC. In this section, the estimated SWCC was compared with the measured volumetric water content and matric suction.



**Fig. 4** Variation in matric suction at different depths according to rainfall intensity



**Fig. 5** Comparison between measured data from the field and SWCC from the laboratory

The estimated SWCC, the measured matric suction, and the observed volumetric water content at different depths are plotted together in Fig. 5. All measured data for matric suction and volumetric water content were located below the drying path of the estimated SWCC. In particular, the most of measured values were located near the drying and wetting paths of the estimated SWCC. The data measured at depth of 0.5 m were similar to the gradient of wetting path and the data measured at depths of 1.0 and 1.5 m were similar to the

gradient of drying path. The drying and wetting paths obtained from the laboratory test were regarded as the primary drying and wetting curves, respectively. Therefore, the measured data with a nonlinear relationship between matric suction and volumetric water content could be defined as scanning curves, which are located near the primary drying and wetting curves.

## 5 Conclusion

The goal of this study was to understand the surficial seepage and unsaturated soil characteristics at the vadose zone in a waste dump slope during rainfall. To analyze the variations in the unsaturated features of a waste dump slope at the Imgi mine according to rainfall infiltration, field measurement sensors and a system for the unsaturated soil of the slope were installed at the site. Rainfall, volumetric water content, and matric suction were measured and analyzed. Then, the relationship between the SWCCs estimated from the laboratory experiments and the observed data were investigated. The detailed results are as follows:

1. During rainfall, the variation in matric suction and volumetric water content was influenced by rainfall intensity. In particular, the variation increased and then decreased at the surface of the slope during the drying and wetting processes. The increase in the variation during rainfall was primarily due to rainfall infiltration.
2. All of the matric suction and volumetric water content measured in the field were located below the drying path of the SWCC estimated from the laboratory test. In particular, the most of measured values were located near the drying and wetting paths of the estimated SWCC. The observed matric suction and volumetric water content were 5–35 kPa and 0.12–0.24, respectively.
3. The measured data with a nonlinear relationship between matric suction and volumetric water content could be defined as scanning curves, which are located near the primary drying and wetting curves. In particular, the characteristics of unsaturated soil near ground surface were dominantly associated with the primary wetting curve.



## References

- Fredlund, D.G., Rahardjo, H.: *Soil Mechanics for Unsaturated Soils*. Wiley, New York (1993)
- Muraleetharan, K.K., Liu, C., Wei, C., Kibbey, T.C.G., Chen, L.: An elastoplastic framework for coupling hydraulic and mechanical behavior of unsaturated soils. *Int. J. Plast.* **25**, 473–490 (2009)
- Rahardjo, H., Satyanaga, A., Leong, E.: Effects of flux boundary conditions on pore-water pressure distribution in slope. *Eng. Geol.* **165**, 133–142 (2013)
- Song, Y.S., Hwang, W.K., Jung, S.J., Kim, T.H.: A comparative study of suction stress between sand and silt under unsaturated conditions. *Eng. Geol.* **124**, 90–97 (2012)
- Song, Y.S., Lee, N.W., Hwang, W.K., Kim, T.H.: Construction and application of an automated apparatus for calculating the soil water characteristics curve. *J. Korean Geotech. Soc.* **20**, 281–295 (2010)
- van Genuchten, M.T.: A closed-form equation for predicting the hydraulic conductivity of unsaturated soils. *Soil Sci. Soc. Am. J.* **44**, 892–898 (1980)
- Wayllace, A., Lu, N.: A transient water release and imbibitions method for rapidly measuring wetting and drying soil water retention and hydraulic conductivity functions. *Geotech. Test. J.* **35**(1), GTJ103596 (2012)

---

**Part II**  
**Aggregates**

# Petrographic Characterization of Waste Rocks: Applicability as Concrete Aggregates

Maria del Pilar Durante Ingunza, Antonio Carlos Galindo, and Ana Beatriz Azevedo de Medeiros

## Abstract

Petrographic characterization showing mineralogical, textural and structural aspects of rocks is an essential technique in the study of the performance of concrete aggregates, specifically on the investigation of the alkali-aggregate reaction (AAR). The assessment of this deleterious reaction, considered as one of the most important pathologies, is a required test in the waste utilization programs. In this paper, waste rock samples of a feldspar mine were studied by optical microscopy, approaching aspects related to morphology, texture and alteration degree to determine the potential alkali reactivity for use as aggregates in cementitious mixtures. The rock studied shows characteristics that make it susceptible to be a reactive aggregate, due to, mainly, the strained quartz and the microcrystalline quartz. However, these results must be confirmed by standard mechanical test methods.

## Keywords

Petrographic characterization • Waste rocks • Concrete aggregates

## 1 Introduction

Nowadays, sustainable mining is increasingly considered as a more accessible challenge. To include mining waste in sustainable management practices is a global consensus.

Mining industry produces a large amount of waste rocks with different properties related to formation processes. Specifically, crystalline rocks are widely used as ornamental

stone and as raw material in civil construction, mainly as concrete aggregate, due to their suitable properties.

ASTM defines aggregates as granular materials of mineral composition such as sand, gravel, shell, slag or crushed stone used with a cementing medium to form mortars or concrete (ASTM Standard 2016a). The use of aggregates for concrete is widely regularized by ASTM Standard (2009, 2011, 2013, 2014a, b, c, 2016b).

On the other hand, alkali-aggregate reactivity (AAR) is considered one of the most important pathologies in civil construction. Two types of Alkali-aggregate reactivity are commonly defined, the alkali-silica reaction (ASR), where there are two variants, depending on the velocity of the reaction and the alkali-carbonate reaction (ACR). Both are complex reactions of aggregates and alkali hydroxides in concrete that create expansion processes, and provoke, potential structural damages.

Although ASR pathologies in structures have been reported around the world related to crystalline aggregates (Ian Sims and Poole 2017) these materials are commonly used in civil construction, having obtained successful results.

Table 1 summarizes the main reactive minerals and the respective occurrence rocks. Clearly, potential reactive minerals occur in just about all the common rocks, which emphasizes the importance of accurate analysis in aggregates.

The U.S. Department of Transportation (2012) defines the combination of petrographic examination, expansion testing and field performance as required actions to confirm the non-deleteriously-reactive nature of the aggregates.

Petrographic description of aggregates is a very well known method to identify its reactivity. It is due, basically, to the reliability and quickness that this technique provides. However, it is strongly recommended to confirm the results by other methods, specifically mechanical tests as the accelerated mortar test (ASTM Standard 1994).

Recently, Sanchez et al. (2017) have stood out microscopic techniques as important complementary tools in the AAR assessment. In addition, microscopic examination is

M. del Pilar Durante Ingunza (✉) · A. C. Galindo · A. B. A. de Medeiros  
Federal University of Rio Grande do Norte (UFRN), Natal, RN  
59078-970, Brazil  
e-mail: durante@ct.ufrn.br

**Table 1** Some potential reactive minerals

Reactive material	Occurrence rocks
Chalcedony, micro and cryptocrystalline quartz Macrogranular strained quartz, rich in inclusion, intensely fractured with microcrystalline quartz in grain contacts	Volcanic rocks with devitrified glass or cryptocrystalline Igneous rocks: granite, granodiorite and charnockite Sedimentary Rocks: sandstone, grauvaque, siltite, argillite, shale, phyllite and slate Metamorphic rocks: gneiss, shale, quartzite, phyllite and slate

Modified from ABNT (2008)

highlighted as the appropriated measurement of deformation intensity (Murlidhar et al. 2016).

Specifically for rocks with quartz, the undulatory extinction in quartz is a criterion strongly used for identifying potentially alkali-reactive reactions (Dolar-Mantuani 1981). Consequently, rocks with micro and cryptocrystalline quartz moderately to strongly strained are considered as susceptible to AAR (ABNT 2008; CSA 1994).

The amount of strained and microcrystalline quartz needed to provoke potential reactivity reaction is variable. There are no defined values, consensually. Many factors can contribute to ASR-induced damage; consequently, cases should be studied separately. In this way, Brazilian norm suggested values of 5% of strained quartz, 3% of chalcedony, 1% of tridymite-cristobalite, 3% volcanic glass, 0.5% opal. Under these values, the aggregate is considered potentially innocuous. These values can be changed by petrographer considerations (ABNT 2008).

The aim of this paper is to evaluate the applicability as concrete aggregates of waste rocks by petrographic characterization in the context of sustainable mining.

## 2 Materials and Methods

Locally, the study area is geologically inserted in the Structural Province of Borborema (Fig. 1), with composition and organization essentially Neoproterozoic (Brasiliano Domain). The stratigraphic units in this area are predominantly composed by formations inserted in the Seridó Group, associated to the Brasiliano/Pan-African Orogeny, including the Itaporanga intrusive suite, resulting of a Brasiliano plutonism (Angelim 2007).

Tectonically, the Seridó Group experienced three deformational events causing compositional banding, geological folds and NNE-SSW foliation, respectively. The last one corresponding to the Brasiliano transcurrent Kinematic, with shear areas (Jardim de Sá 1984, 1987, 1994).

Samples of waste rocks from feldspar mining at Parelhas/RN, Brazil were collected. The samples are included in the intrusive suite Itaporanga. Geologically, the rock is classified as granite gneiss. Petrographic examination of

samples was performed according to Brazilian norm (ABNT 2008) based in international standards (ASTM Standard 2012) with a Polarizing Microscope Nikon Eclipse E200MV POL. Table 2 shows the procedures followed.

## 3 Results and Discussion

Figures 2, 3, 4, 5 and 6 show thin sections of the rock samples. The minerals identified are quartz, k-feldspar, plagioclase, biotite, opaques, apatite, and zircon. Mostly, the rock presents a medium-grained texture, inequigranular, with the largest crystals of quartz, without a clear out mineral orientation, although biotite crystals show slightly preferential orientation (Fig. 2).

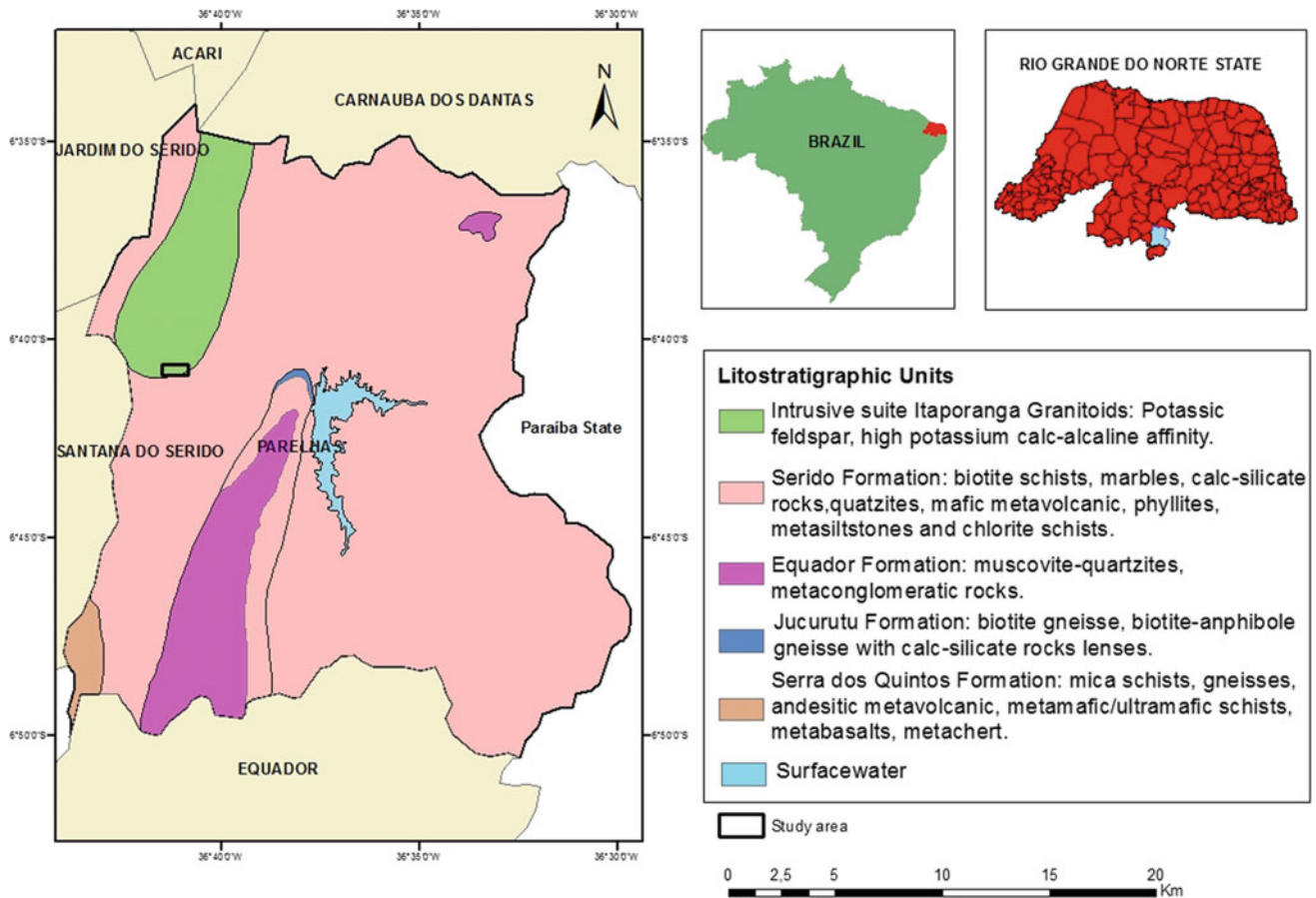
The predominant mineral is quartz (Table 3) appearing essentially, as xenomorphic crystals, clear and colourless, with undulatory extinction and with fractures, which are occasionally filled by fine micaceous material, with bright birefringence colours (Fig. 3).

The second most abundant mineral, K-feldspar, appears as xenomorphic-hypidiomorphic microcline crystals, with characteristic cross-hatched twinning. The crystals are of varied size, generally larger than 0.3 mm, some crystals reaching 1.0–1.5 mm (Fig. 4). Further, some K-feldspar crystals show some characteristic textures as string perthite (Fig. 5).

Plagioclase arises generally as hypidiomorphic crystals, usually with twin lamellae, polysynthetic, showing a low degree of alteration and, commonly composing aggregates with triple junction contacts (Fig. 6).

The mafic mineral in the rock is, predominantly, biotite (Fig. 2) which occurs in general as hypidiomorphic crystals, with pallet shapes showing, discreetly, preferential orientation. Its colour is yellow with pleochroism in brown tones. Biotite shows low degree of secondary alteration. In addition, biotite crystals contain apatite, zircon and opaques inclusions.

Opaques occur as small crystals (<0.3 mm) with dark colours, usually idiomorphic, in quadratic sections, suggestive of being magnetite.



**Fig. 1** Location and geological characterization of the study area. *Source* Modified from Angelim et al. (2006)

**Table 2** Procedures in thin sections

Characteristic	Observations
Mineralogical composition	Description of main and subordinate minerals. Including opaques Percentages (estimative)
Texture	Identification of myrmekite and perthitic textures
Granulation	Classification: fine-medium-coarse
Deleterious minerals <sup>(a)</sup>	Description of deleterious mineral and phases Percentages (estimative)
Microfractures	Classification: low-moderate-high
Alteration degree	Description of altered minerals

Modified from ABNT (2008)

<sup>(a)</sup> as described in Table 1

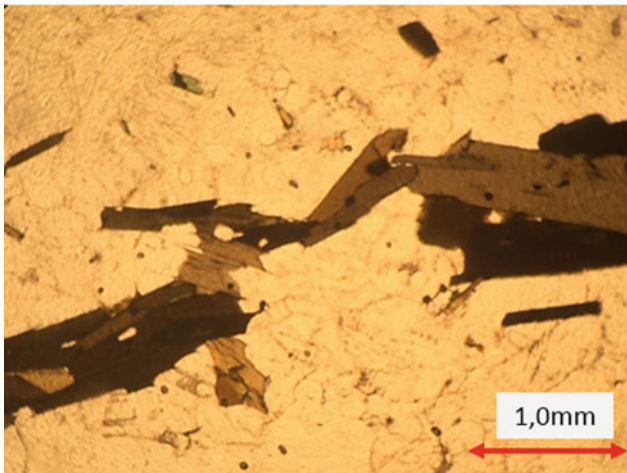
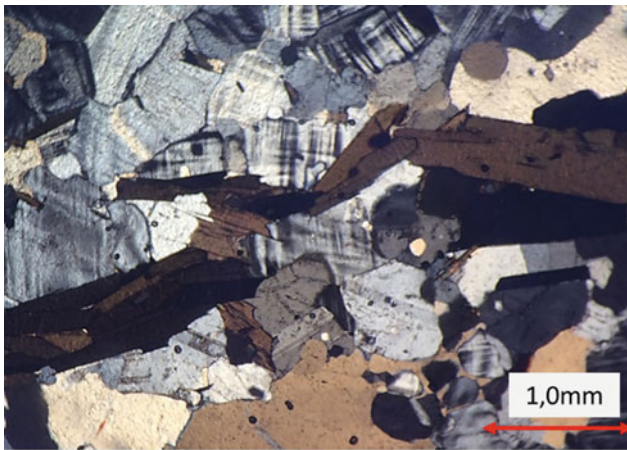
Apatite and Zircon are present in lower amounts (1%) and small crystals (<0.1 mm) essentially idiomorphic and included in biotite. Apatite is colourless and high relief with rounded hexagonal crystals.

Zircon is slightly colourful, quadratic to prismatic elongated, with strong birefringence colours.

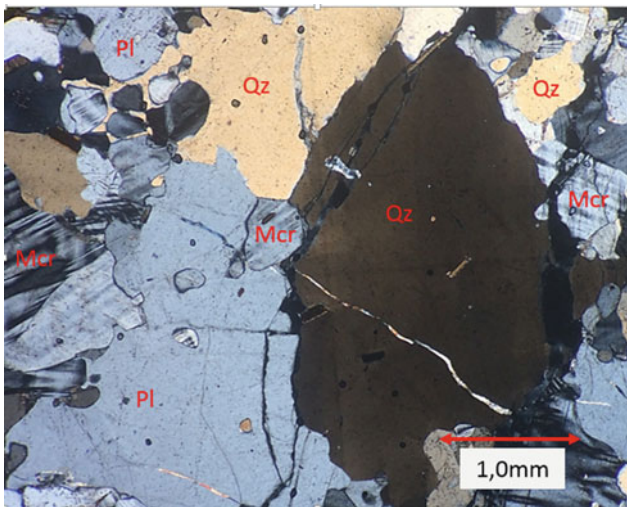
## 4 AAR Reactivity

Two types of deleterious minerals have been found: strained quartz, as shown in Fig. 3 and microgranular quartz. The maximum undulatory extinction angle was 17°.

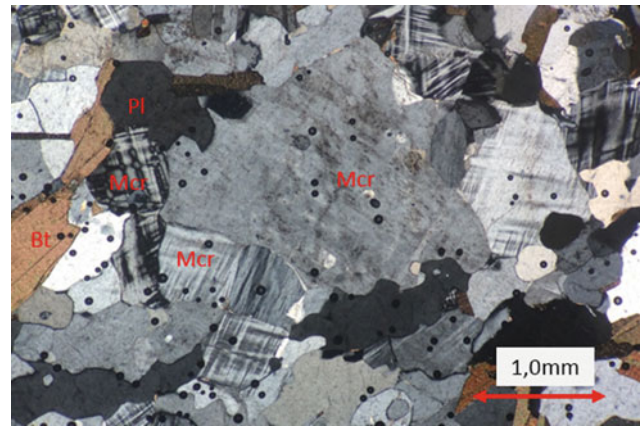




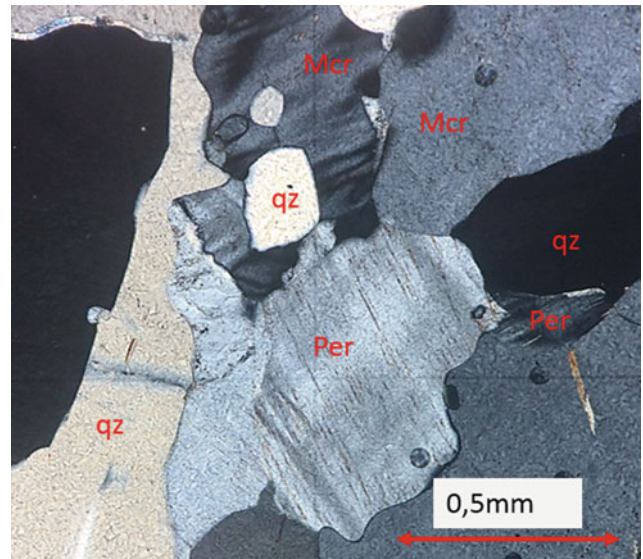
**Fig. 2** General overview. Biotite crystals show, slightly, preferential orientation. Crossed polarized light (upper photograph), plane-polarized light (lower photograph).



**Fig. 3** Xenomorphic crystals of quartz, with undulatory extinction and micaceous material filling a fracture, with bright birefringence colours (crossed polarized light). Qz: quartz; Mcr: microcline; Pl: plagioclase



**Fig. 4** Xenomorphic-hypidiomorphic microcline crystals showing cross-hatched twinning (crossed polarized light). Bt: biotite; Mcr: microcline; Pl: plagioclase



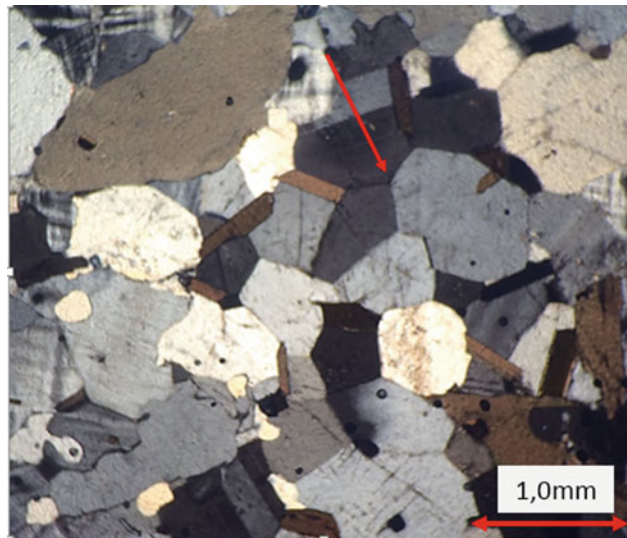
**Fig. 5** Large alkali feldspars with string perthite (crossed polarized light). Per: perthite; qz: quartz; Mcr: microcline

The percentage found for strained quartz was 15%, which transcends the recommended values in Brazilian standards of 5% (ABNT 2008). Regarding to microcrystalline quartz, the percentage found was 1%.

Perthitic texture is considered potentially reactive for AAR in the specific case of flame Perthite, as it indicates deformation processes. In all the samples studied, there is no evidence of that specific texture. However, string perthite—not suggestive of AAR—is commonly found (Fig. 5).

The textural and mineralogical characteristics of the protolith—probably a syenogranite—due to the high amount of K-feldspar and low percentage of mafics—have certainly influenced on the potential alkali-aggregate reactivity of the





**Fig. 6** Crystals of plagioclase with slight alteration and triple junctions (crossed polarized light)

**Table 3** Modal percentage of minerals

Mineral	Modal percentage (%)
Quartz	40
K-Feldspar	30
Plagioclase	17
Biotite	10
Opaques	2
Apatite, Zircon	1

samples studied. In this respect, petrographic description indicates stability of the protolith.

The rock is classified as potentially reactive due to the percentage of strained quartz and the undulatory extinction angle, with low degree by Brazilian Standards (ABNT 2008). However, these results must be confirmed by standard mechanical test methods.

## 5 Conclusions

The rock studied shows characteristics that make it susceptible to be a reactive aggregate mainly, strained quartz, undulatory extinction angle and microcrystalline quartz. Furthermore, the materials show slight alteration processes, which also have to be considered.

In addition, the rock formation processes and the protolith characteristics have influenced, considerably, the low potential reaction degree of the rock.

Finally, as established in international standard norms, these results must be confirmed by standard mechanical tests (ASTM Standard 1994).

## References

- ABNT (Brazilian Association of Standards Specification) Standard ABNT NBR 15577, 1-5, 2008: Alkali Reactivity of Aggregates. ABNT, Rio de Janeiro, Brazil, (2008)
- Angelim, L.A.A.: Geology and Mineral Resources of Rio Grande do Norte State (Brazil). Scale 1:500.000. Recife: CPRM–Brazilian Geological Service (2007)
- Angelim, L.A.A., Medeiros, V.C., Nesi, J.R.: Brazilian Geology Program. Geology and Mineral Resources of RN Project. Geological Map of RN State. Scale 1:500.000. Recife: CPRM/FAPERNA (2006)
- ASTM Standard C1260, 1994: Test method for potential alkali reactivity of aggregates (mortar bar method). ASTM International, West Conshohocken, PA. [www.astm.org](http://www.astm.org) (1994)
- ASTM Standard C332, 2009: Specification for Lightweight Aggregates for Insulating Concrete. ASTM International, West Conshohocken, PA. [www.astm.org](http://www.astm.org) (2009)
- ASTM Standard C144, 2011: Specification for Aggregate for Masonry Mortar. ASTM International, West Conshohocken, PA. [www.astm.org](http://www.astm.org) (2011)
- ASTM Standard C295/C295M, 2012: Standard Guide for Petrographic Examination of Aggregates for Concrete. ASTM International, West Conshohocken, PA. [www.astm.org](http://www.astm.org) (2012)
- ASTM Standard C33/C33M, 2013: Specification for Concrete Aggregates. ASTM International, West Conshohocken, PA. [www.astm.org](http://www.astm.org) (2013)

- ASTM Standard C330/C330M, 2014: Specification for Lightweight Aggregates for Structural Concrete. ASTM International, West Conshohocken, PA. [www.astm.org](http://www.astm.org) (2014a)
- ASTM Standard C331/C331M, 2014: Specification for Lightweight Aggregates for Concrete Masonry. ASTM International, West Conshohocken, PA. [www.astm.org](http://www.astm.org) (2014b)
- ASTM Standard C637, 2014: Specification for Aggregates for Radiation-Shielding Concrete. ASTM International, West Conshohocken, PA. [www.astm.org](http://www.astm.org) (2014c)
- ASTM Standard D8, 2016: Terminology Relating to Materials for Roads and Pavements. ASTM International, West Conshohocken, PA. [www.astm.org](http://www.astm.org) (2016a)
- ASTM Standard C1797, 2016: Specification for Ground Calcium Carbonate and Aggregate Mineral. ASTM International, West Conshohocken, PA. [www.astm.org](http://www.astm.org) (2016b)
- CSA (Canadian Standard Association) A23.2-4, 1994: Appendix B Alkali-Aggregate Reaction: Concrete Materials and Methods Of Concrete Construction, Toronto, Ont. (1994)
- Dolar-Mantuani, L.M.M.: Undulatory extinction in quartz used for identifying potentially alkali-reactive rocks. In: Proceedings on International conference on alkali-reaction in concrete, 5. Cape Town, Pretoria (1981)
- Ian Sims, I., Poole, A.B. (ed.): Alkali-Aggregate Reaction in Concrete: A World Review. CRC Press (2017)
- Jardim de Sá, E.F.: Seridó Region geology: data compilation. In: Symposium of Northeast Geology, Natal, Brazil (1984)
- Jardim de Sá, E.F.: Proterozoic granitoids in a polycyclic setting: the Seridó region, NE Brazil. In: International Symposium on Granites and Associated Mineralizations-IGAM, 1, Salvador (1987)
- Jardim de Sá, E.F.: Seridó faixa (Borborema Province) geodinamical meaning on Braziliam/Pan-African System. Doctoral thesis. Brasília, 803 p (1994)
- Murlidhar, B.R., Mohamad, E.T., Armaghani, D.J.: Potential alkali silica reactivity of various rock types in an aggregate granite quarry. *Measurement* **81**, 221–231 (2016)
- Sanchez, L.F.M., Fournier, B., Jolinb, M., Mitchell, D., Bastien, J.: Overall assessment of alkali-aggregate reaction (AAR) in concretes presenting different strengths and incorporating a wide range of reactive aggregate types and natures. *Cem. Concr. Res.* **93**, 17–31 (2017)
- U.S. Department of Transportation; Federal Highway Administration: Alkali-aggregate reactivity (AAR) workshops for engineers and practitioners reference manual (2012)

# The Search for New Aggregate Sources in Hong Kong

Kitty Chan and Stuart Millis

## Abstract

Hong Kong is often described as a ‘concrete jungle’ and aggregate sourced from local hard rock quarries has formed an essential construction material for the development of the cityscape seen today. However, the continual expansion of the urban area coupled with increasing environmental controls and awareness means that most of the local quarry sites providing aggregate to the construction sector have been closed down and rehabilitated over the last 20 years and, despite an abundance of hard igneous rock suitable for aggregate generation, no new local quarries have been established in almost 50 years. The decline of aggregate supply from local sources arising from this has resulted in an increased reliance on imported materials, with associated implications in terms of supply, cost and quality control as well as a reduced ability to sustainably process good quality rock generated by construction projects. With these concerns in mind the HKSAR Government initiated a review of short and long-term aggregate supply strategies for Hong Kong, including territory-wide searches for potential aggregate reserves, both surface and underground, that took due account of the associated technical, environmental and socio-political aspects affecting reserve accessibility and extraction potential. This paper explores some of the key factors associated with the past, present and future supply of aggregate in Hong Kong and outlines some of the ways in which the future of quarrying might be considered for the territory.

## Keywords

Aggregates • Quarry • Hong Kong

K. Chan · S. Millis (✉)  
Ove Arup & Partners Hong Kong Ltd., Kowloon Tong,  
Hong Kong  
e-mail: stuart.millis@arup.com

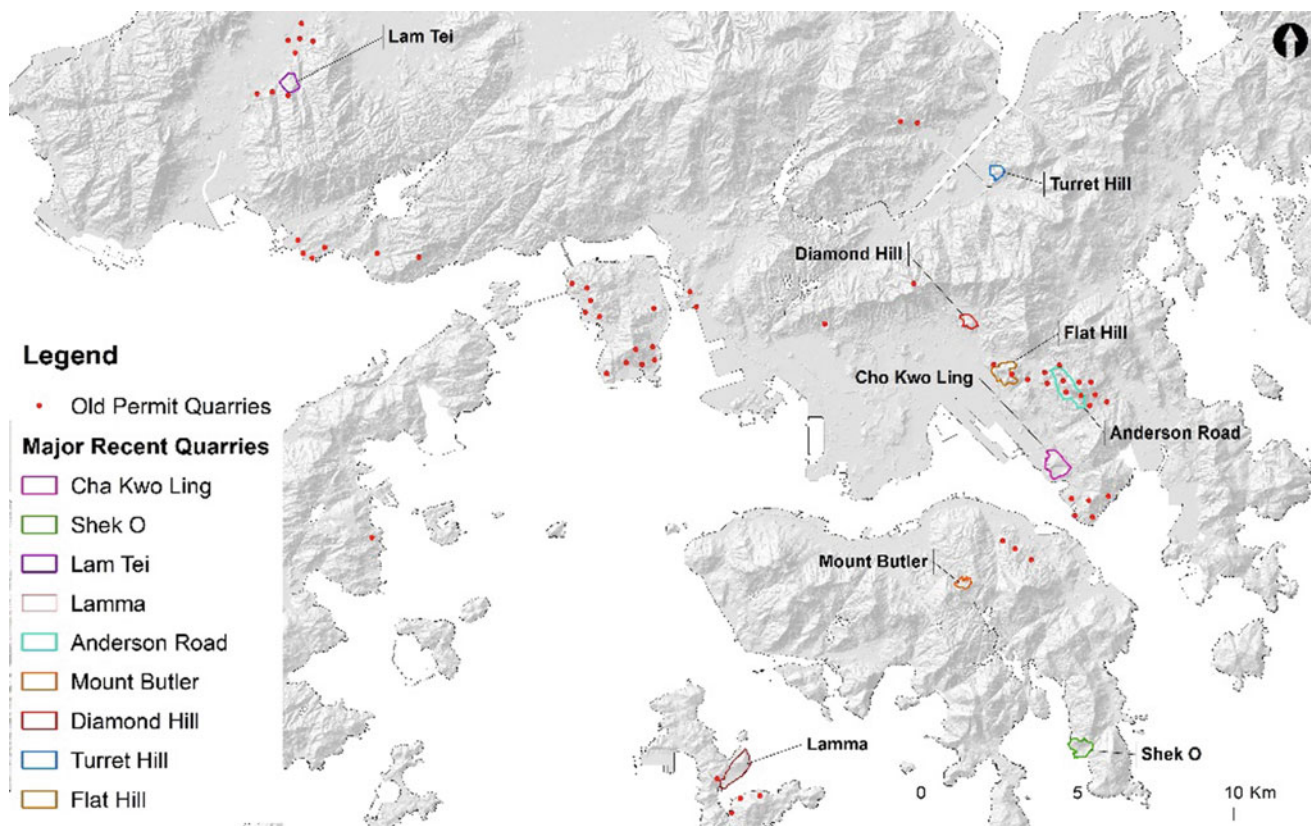
K. Chan  
e-mail: kitty.chan@arup.com

## 1 Introduction

Hong Kong possesses one of the highest density of skyscrapers in the world. Crushed rock for concrete has been one of the fundamental materials needed to build the impressive skyline and also forms an essential component in many other construction materials that make up the foundation and fabric of the city. Crushed rock in Hong Kong has been obtained through surface quarrying using a process of blasting, crushing and screening to form aggregate of varying sizes. As a result of this, local quarries have played a significant role in the development of Hong Kong over the last 150 years, not only through the extraction, processing and provision of crushed rock for use as aggregate, but also through the temporary provision of land to house quarrying related facilities. Upon closure, the quarry sites have also provided useful land for residential developments and other valuable uses. However, with no new local quarries established for over 50 years and existing quarries being progressively rehabilitated and closed over the past two decades, is there a future for the quarrying industry in Hong Kong?

## 2 Quarrying and Crushed Rock Supply in Hong Kong

Quarrying is one of the oldest industries in Hong Kong, dating back to the Qing Dynasty (1644–1912). Poon et al. (2011) reports that stone quarrying was very active along the coastal areas of northern Hong Kong Island in the 1890s, with the well-known Quarry Bay area being named because of this trade. In the early days, these works were typically labour intensive, permit based operations and by the 1950s numerous small-scale permit quarries had been established throughout the territory (PWD 1966). However, an increasing public concern over the visual and environmental impacts of quarry operations from the 1970s onwards led the



**Fig. 1** Location of major quarries in Hong Kong since the 1950s

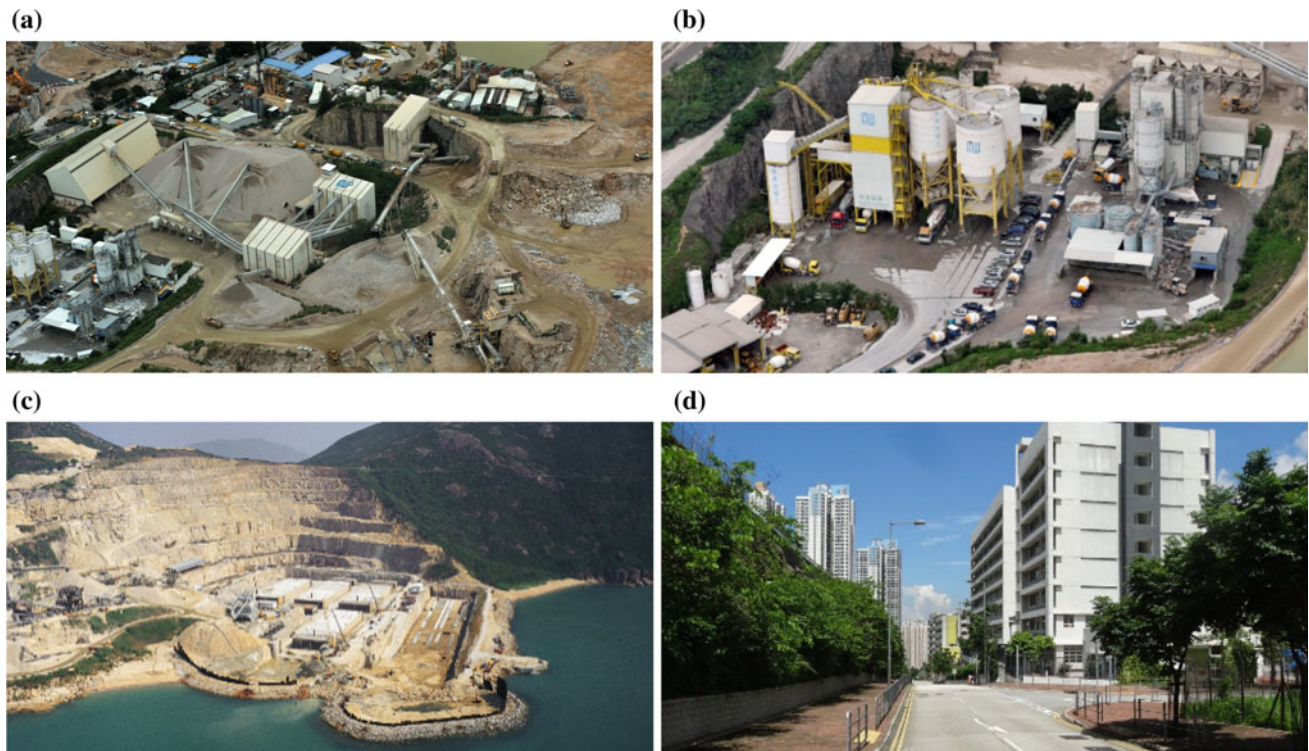
Government to implement tighter control on quarry operation and restoration, first through a period of Contract Quarries and later through the use of Quarry Rehabilitation Contracts (Chan et al. 2007). These approaches focussed on cleaning up the scars left by the permit quarries through the use of large-scale modern operations that delivered a final restored landform merging with the surrounding environment and yielding platforms suitable for future development. Figure 1 presents the quarry locations in Hong Kong since the 1950s.

Currently, the only active quarry site in Hong Kong is at Lam Tei, which will close in 2022. The limited production capacity from this remaining quarry site and spiking demands has resulted in dramatic increases in the proportion of crushed rock supplied from mainland China, which has accounted for over 80% of crushed rock consumed since 2013. With limited local rock supply available and a strong dependence on imported products, there is little the HKSAR Government can currently do to ensure a consistent supply of rock at a reasonable price for the city.

### 3 Benefits of Quarries

In addition to the direct benefit of local supply of aggregate, quarries in Hong Kong have also supported the construction industry and local population in a number of other ways. Foremost amongst these is ability to stockpile and process surplus high quality rock from various site formation and tunnelling projects (Fig. 2a) into aggregate for reuse in production of concrete in a sustainable manner. This has supplemented the local supply of crushed rock from quarries with over 14 Mt of additional rock over the last decade. The various quarries in Hong Kong have also been used to house batching plants for a number of industries reliant on crushed rock (Fig. 2b). Without the quarries, these facilities would have otherwise had to occupy valuable waterfront sites to receive imported crushed rock delivered by barge. In addition, on several occasions drop-cuts formed in the floors of coastal quarry sites have been used as casting basins for the construction of pre-cast tunnel segments used for immersed





**Fig. 2** Services rendered by the local quarries

tube projects, such as the Eastern and Western Harbour Crossings (Fig. 2c) and, more recently, the MTRC Sha Tin to Central Link.

However, undoubtedly the biggest asset gained from the quarry sites is the developable land they yield upon completion of quarrying (Fig. 2d). This value has been realised with the former quarries at Diamond Hill, Jordan Valley and Turret Hill having been used to great effect to facilitate multi-developments. The combined footprint of the quarries operated in Hong Kong since 1970s comprises around 328 ha, of which about 150 ha is developable land.

#### 4 Future Demand Estimates and Supply Strategies

Periodic forecasts on the demand for crushed rock in Hong Kong and potential supply sources have been conducted on several occasions. However, the continually evolving social situations mean the strategies devised from these seldom remain applicable over the longer term. Whilst reliable short-term forecasts could be made based on the programme for committed major works, longer term forecasts (up to 2039) needed to make use of other economic indicators to provide a reasonable estimate of crushed rock demand. To achieve this, a number of indices were reviewed to

determine which provided the best correlation with crushed rock consumption, including Gross Domestic Product, Population, Gross Value of Construction Works, Property Completion, Consumer Price Index and Cost of Material Price Index. Making use of the Government's long-term projection on population growth (C&SD 2014), these figures suggest a long-term annual crushed rock demand of about 15–18 Mt (Fig. 3).

In contrast to the high demand forecast, the closure of many local quarry sites means there has been a noticeable decrease in local supply, with post-2016 production accounting for less than 10% of total supply and no confirmed local supply sources in place post-2022. The lack of quarry sites will also result in a diminishing capacity to process surplus rock from construction projects, reducing the likelihood of such material being re-used in a sustainable manner. Because of this the local construction industry will become increasingly reliant on the import of rock from the mainland if it is to achieve the various building and infrastructure development targets currently scheduled. In recognition of this and to maintain a degree of control in terms of crushed rock supply security, quality and cost, there is a need from a strategic development perspective to maintain a healthy proportion of local supply of rock for construction use. It is likely that one or more new quarry sites will need to be developed in Hong Kong to yield the targeted proportion of local rock supply.

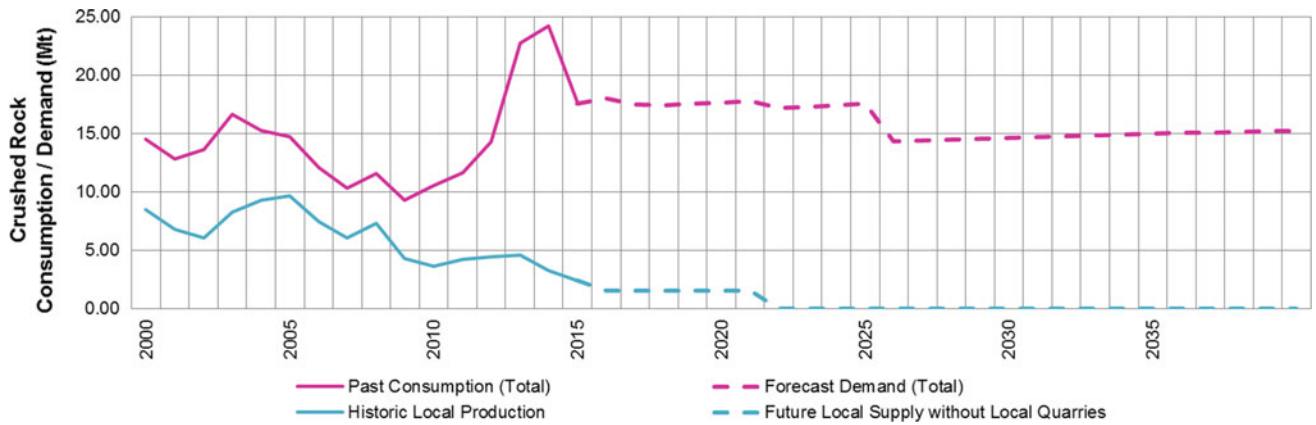


Fig. 3 Projected demand for crushed rock up to 2039

### 5 Finding the Right Surface Quarry Site

Virtually all previous quarries in Hong Kong have been in areas of fine-grained to medium-grained granitic rock due to issues associated with alkali silica reactivity (ASR) when using volcanic aggregates for concrete. Although advances in concrete technology mean that many of these issues can now be overcome using additives such as PFA or GGBS, the construction industry in Hong Kong has generally still not

yet prepared for the move with respect to the supply chain, quality assurance framework and clients' acceptance, except for specialist high strength concrete under closely controlled conditions with limited exposure to moisture. For this reason, the Rock Resource Map (Fig. 4) developed during the site search was limited to areas recorded as granitic rocks that account for about 26% of the Hong Kong land mass. However, it was also recognised that there are many existing and proposed land use constraints that could significantly limit the feasibility of new quarry development. These no-go

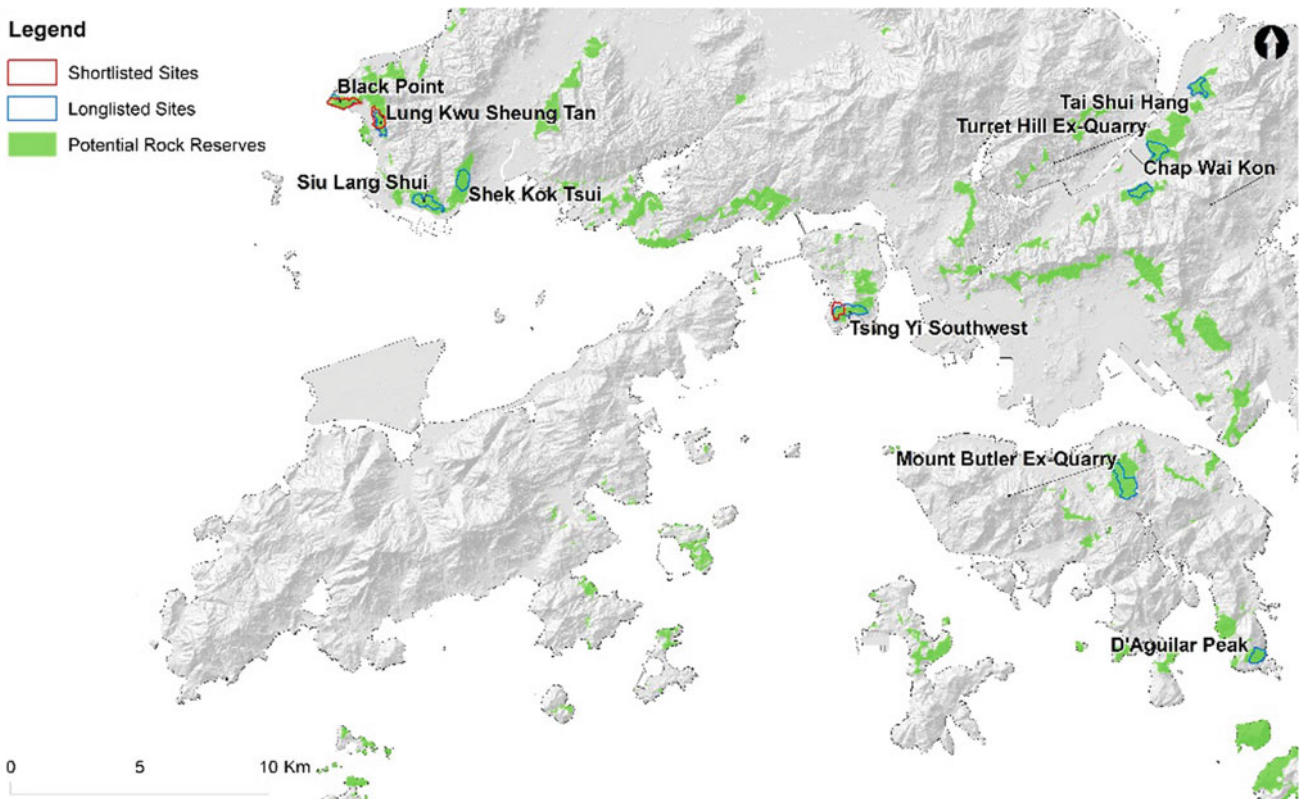


Fig. 4 Potential quarry sites considered



areas, plus several additional quarry specific no-go zones defined based on other local land planning requirements, accounts for about 76% of the area of the HKSAR. The territory-wide rock reserves were identified based on these two datasets and indicate that just 3% of the land area can be considered as having broad suitability for quarry development.

Further screening of the potentially suitable areas in the territory-wide rock reserve map was then conducted to identify commercially viable sites with good connectivity to existing transport distribution networks. This second round of screening identified only ten sites with potential for quarry development. Broad technical studies for these sites were then conducted to evaluate and shortlist the sites with respect to their prospect for development as new quarries. Based on the various technical and social constraints present, only three of the ten sites were found worthy of taking forward for more detailed technical and financial feasibility assessment. If confirmed as feasible, these three sites are anticipated to yield a total of about 70 Mt of rock over the coming two decades, and would also eventually yield about 36 ha of land for future developments.

---

## 6 Underground Quarrying Options

The potential to develop underground quarrying has also been explored in several ongoing and recent studies. This approach can shield the public from many of the unfavourable nuisance aspects of quarrying such as landscape and visual impact, dust and noise, and has been successfully implemented on a commercial basis in several overseas countries. With the current strong emphasis on underground space creation in Hong Kong, a combination of rock cavern development with underground quarrying and rock processing could be considered a win-win situation. However, the overall business case for such a commercial operation needs to be studied in more detail such that it aligns with local regulations and approaches for underground excavation in Hong Kong. As the cost of such a venture will be higher than a bulk surface quarry operation, the business case and the overall value of the rock caverns formed require further review in detail to determine whether the costs associated with such a scheme can be balanced with the positive aspects of space formation under such an approach.

---

## 7 The Way Forward

The identification of several sites with apparent feasibility for quarry development means that Hong Kong can secure its own source, from its own reserves, of suitable rock to allow the construction industry to supply a healthy

proportion of crushed rock production and thus to avoid relying entirely on the use of imported products. To outline the ways in which this could be achieved a Quarry Development Master Plan was developed. This outlined both the strategic and technical approaches recommended to facilitate future crushed rock supply in terms of: (i) the development and implementation programme for the potential new local quarry sites; (ii) the capacity within these sites to process surplus rock from construction projects, where available; and (iii) the remaining quantity of rock likely to be required from import. The relative proportions that can be achieved from each of these supply sources are shown in Fig. 5.

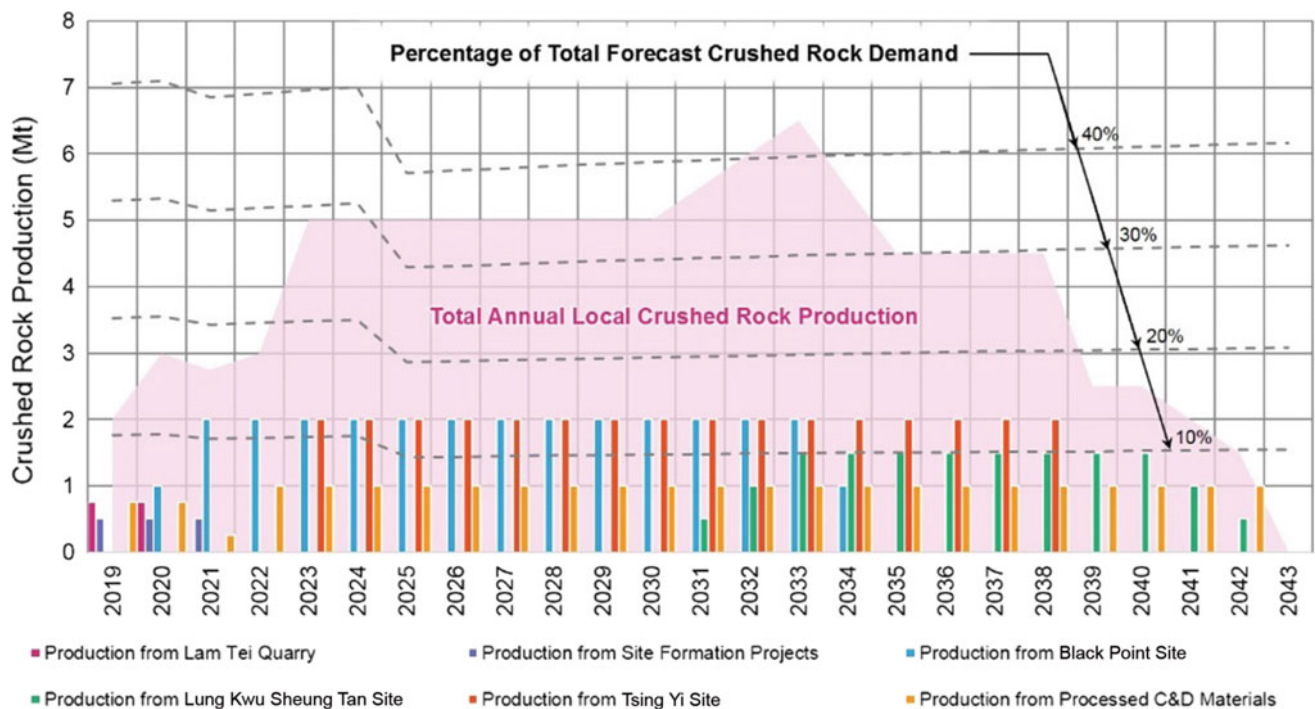
This indicates that rock extraction and processing within the potential new local quarry sites could supply about 30–40% of the total projected crushed rock demand in Hong Kong up to 2038 and can largely achieve the desired strategic goals. The dilemma that is faced is how to balance these benefits against an ever-present desire to enhance and expand the city whilst at the same time reducing nuisance and improving the living environment with better air quality, reduced visual impact and reduced noise.

---

## 8 Conclusions

Crushed rock is an essential construction raw material, and a reliable and secure supply is required to ensure the maintenance, development and prosperity of any modern city. Hong Kong has a rich history of quarrying that has helped shape the cityscape we see before us today. However, limited land area and strong concerns on the environmental impacts of quarrying has meant that nearly all local quarry sites have been rehabilitated and closed, with no new quarry operations established to offset the diminishing local supply this has resulted in. With significant demand for crushed rock forecast, there are merits for Hong Kong to achieve between 20 and 40% of total crushed rock supply from local sources, such that it can maintain a degree of control on the local crushed rock market. The development of new local quarry sites is a fundamental component of the mechanisms required to achieve this and can still provide various other benefits.

Although Hong Kong has an abundant resource of rock suitable for use as aggregate, a territory-wide site search and screening revealed relatively few sites with significant potential for quarry development, with just three high potential sites identified. Preliminary technical studies for these sites indicate that the rock reserves within them, together with a nominal allowance for the processing of high quality rock from construction projects, would be sufficient to achieve the strategic goals set for about the next 25 years. Although the implementation of new local quarries is by no means guaranteed, the option to consider underground



**Fig. 5** Projected supply of crushed rock in Hong Kong from local sources

quarrying hints at a future that may comprise a balance between surface and underground quarrying to meet the city's needs. It appears that there's still life in Hong Kong's quarrying industry yet.

**Acknowledgements** This paper is published with the kind permission of the Head of the Geotechnical Engineering Office and the Director of the Civil Engineering and Development Department of the Government of the Hong Kong Special Administrative Region.

## References

Census and Statistics Department: Statistics table 001: population by sex. Demographic statistics section. C&S Department, Hong Kong (2014)

Chan G, Pallot D, Hogan D: The evolution of the quarrying industry in Hong Kong. In: Providing a Visionary Approach to the "Life Cycle of a Site". 2007 Institute of Quarrying Australia Conference, Hobart, Australia (2007)

Poon SW, Ma KY, Man KF and Tsin TW: The quarry licensing system in Hong Kong 1841–1941. In: Hong Kong Quarrying Conference 2011: Revelations of the Hong Kong Quarrying Industry, Yesterday, Today & Tomorrow. The Institute of Quarrying (Hong Kong Branch), Hong Kong. Conference Notes (2011)

Public Works Department (PWD): Quarry Report. Roads & Drainage Division, Civil Engineering Office, Public Works Department, Hong Kong, p. 23 (1966)

# Abrasiveness Properties at Different Temperatures of Basalt, Marble and Limestone in Turkey

Candan Alptekin Bilen, Selman Er, Murat Yılmaz, Erdi Avcı, and Atiye Tugrul

## Abstract

Turkey is a bridge between Europe and Asia. There are numerous historical monuments in Turkey that were built by using natural stones. Due to the geographical features of Turkey, natural stones were exposed to different climatic conditions over time. Temperature and humidity changes have affected physical and mechanical properties of natural stones. The aim of this study is to investigate the physical and mechanical properties of basalt, marble and limestone, which are frequently used in historical buildings in Turkey, in saturated and dry state at different temperatures. For this purpose, basalt, marble and limestone samples were collected from their today's quarries. The obtained samples were dried and saturated with water, cooled to  $-15\text{ }^{\circ}\text{C}$  and heated to  $105\text{ }^{\circ}\text{C}$ . In every 5 min temperature values of samples were measured to reach up to room temperature (about  $23\text{ }^{\circ}\text{C}$ ), thus their CERCHAR abrasiveness index were determined. According to the results obtained CERCHAR abrasiveness index increased when the temperature value exceeded  $40\text{ }^{\circ}\text{C}$ . In water saturated samples CERCHAR abrasiveness index didn't change when the temperature value exceeded  $30\text{ }^{\circ}\text{C}$ .

## Keywords

Basalt • Marble • Limestone • Temperature • Abrasiveness

## 1 Introduction

Istanbul city has been an important settlement for civilizations throughout history. Due to the geographic location often it has been the capital of the civilization. Many

buildings were built in Istanbul, which was the capital of the last Ottoman Empire. Mostly natural stone is preferred when constructing. Among the natural stones Marmara Marble and Küfeki stone quarries are the most preferred stone because of their location close to the construction to be built. Constructions built with these rock are able to weather over time due to climatic conditions or place of use. Rock surface exposed to sunlight can reach a very high temperature. In this case a temperature difference occurs between the inner and outer surfaces. Temperature difference, expansion and contraction create internal pressures in different directions and across the grain. As a result, the capillary cracks begin to develop. The rock developed by the cracks is fragmented and crumbled in physical terms (İ.T.Ü Development Foundation 2000). The CERCHAR Abrasivity Index is determined as the abrasion of a metal pin after scratching over the freshly broken surface of a rock. This pin is made of certain steel quality ( $200\text{ kg/mm}^2$ , Rockwell Hardness 54–56) and is terminated by a 900 “infinitely” conical point, sharpened on a high precision lathe (Suana and Peters 1982). Valantin (1973) defines the CERCHAR Index as follows: “During one second and under a static load of 7 kg, this pin is pulled over one centimeter of the fresh fracture surface of rock. The diameter of the resulting abraded flat on the steel point, measured in  $1/10\text{ mm}$ , determines the Index of CERCHAR Abrasivity”. International Rock Mechanics Association (International Rock Mechanics Society), the meeting held in Montreal on September 3, 1987 CERCHAR abrasion and CERCHAR hardness index test standards in terms of cutability, punctureability and excavatability of rocks in space (Yaralı and Akçın 2005; Bilgin 1989). The aim of this study is to investigate abrasiveness properties of Marmara marble, Küfeki stone and Kayseri basalt in different temperature and to evaluate the results. For this purpose, marble from the Marmara Island and Küfeki stone samples from Edirne Süloğlu region, which are actively working today, were collected. First of all, petrographical analysis and then physical and mechanical experiments carried on the samples.

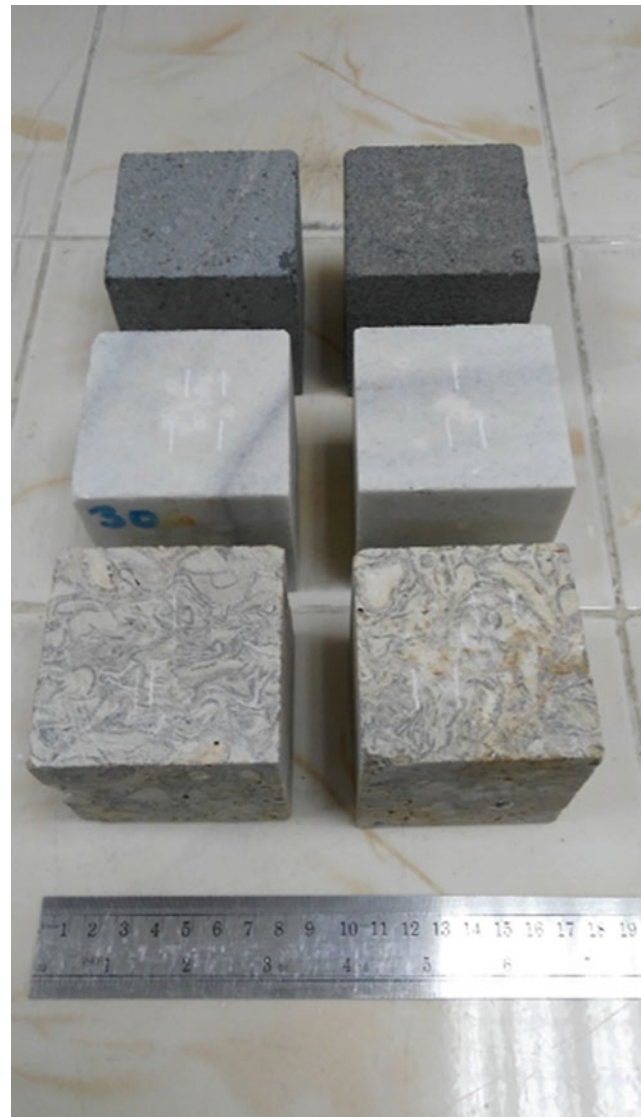
C. A. Bilen (✉) · Selman Er · M. Yılmaz · E. Avcı · A. Tugrul  
Department of Geological Engineering, Istanbul University,  
Istanbul, Turkey  
e-mail: candanalptekin@gmail.com

## 2 Material and Method

The abrasivity of rock is a factor of significant importance for excavation in tunnelling, underground construction, mining or quarrying. Abrasion can be defined as wearing or tearing away of particles and material from the solid surface. The CERCHAR abrasivity test is a laboratory method to quantify the rock abrasivity. It allows to determine an index called CERCHAR Abrasivity Index (CAI) for the rock's abrasivity which can be used for evaluate the wear of excavation equipment in different application such as mining, tunnelling and drilling. Surface of a rough rock sample over a distance of 10 mm under static load of 70 N. In the original CERCHAR setup (1986). The pin and the dead load are moved across the rock surface. The test is then carried out by relative displacement of the pin on the rock surface across 10 mm at given time intervals. After the test, the pin is carefully removed and the tip flat wear is measured. The method was initially developed in 70s by the Laboratoire du Centre d'Etude et Recherches des Charbonnages (CERCHAR) de France for coal mining purposes (<http://www.geotechdata.info/geotest/Cerchar-Abrasivity-test.html>). Böhme is used for determining the abrasion resistance of concrete and natural stone products used for internal or external paving. The machine consists of a grinding wheel of approx. 750 mm diameter, a removable testing weight of 30 kg and a clamping device for the sample. The machine is equipped with an adjustable counter ( $30 \pm 1$  rpm) and an automatic cut-off system which stops the machine after 22 rotations (<https://cooper.co.uk/shop/aggregate-testing/bohme-abrasion-testing-machine/>).

Samples were taken from the quarries where the production still in progress to determine the physical and mechanical properties of Marmara Marble, Küfeki stone and Kayseri basalt. For the Marmara Marble, samples were taken from Marmara Island area, Küfeki stone from the Süloğlu region of Edirne, and for the Kayseri basalt from the Develi region of Kayseri (Fig. 1). The studies on the samples were carried out according to TS 699 (2009) norms in the Natural Building Materials Laboratory of the Department of Geological Engineering of Istanbul University. The obtained results are given in Table 1.

In order to determine the petrographical properties of Marmara Marble, Küfeki stone and Kayseri basalt, thin sections were prepared and mineral contents were determined by modal analysis method. The content of the Marmara Marble is composed of calcite minerals ( $\text{CaCO}_3$ ), which mostly provide carlsbad twinning. The size of these minerals varies between 0.5 and 2.5 mm (Fig. 2a). Graphite zones in the form of bands were also determined in thin sections. According to the petrographic analysis on the thin sections of the Küfeki stone, these rocks contain abundant



**Fig. 1** General view of the samples (upper: basalt, middle: marble, bottom: limestone)

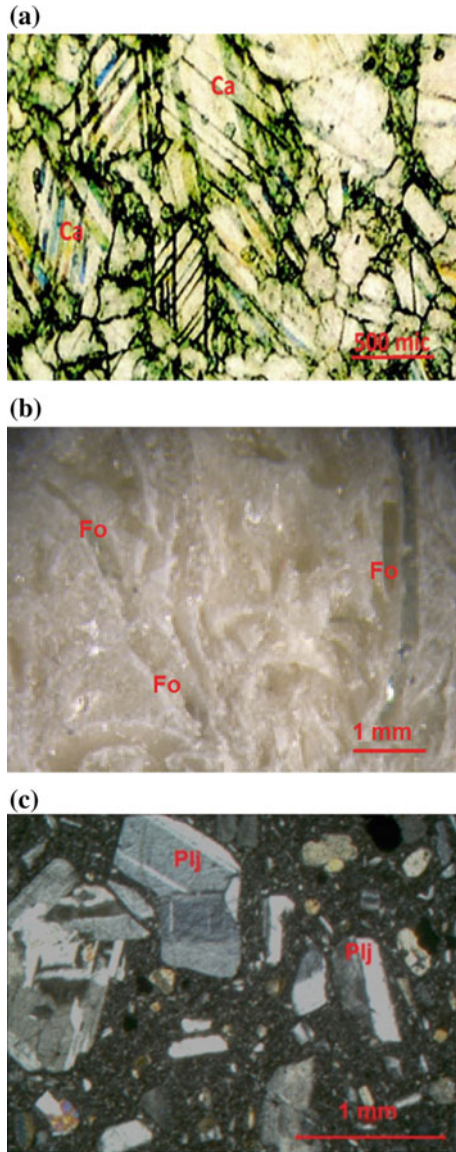
amounts of feldspar (maetra fossil) and small amount of opaque minerals and locally secondary calcite occurrences which have biosparite composition and widespread voids (Fig. 2b). According to the petrographic analysis results, it has been seen that the predominant chemical composition of the two rocks is calcium carbonate ( $\text{CaCO}_3$ ). According to the results of the modal analysis obtained by petrographic studies, phenocrystal minerals in the basalt having 52.42% of matrix percentage; pyroxene (21.29%) plagioclase (15.62%) and opaque minerals (1.55%). In addition, the samples contains 9.12% dissociated minerals (Fig. 2c).

The samples were then dried and saturated with water, cooled to  $-15$  °C and heated to  $105$  °C. Cooling process were done in deep freeze. The dry heating process is performed in an oven and the wet heating process is performed in the water tank



**Table 1** Results of physico-mechanical tests of Marmara marble, Küfeki stone and Kayseri basalt

Physical properties	Marmara marble	Küfeki stone	Kayseri basalt
Dry unit weight (kN/m <sup>3</sup> )	26.18–27.15	19.3–25.8	26.6–27.7
Water absorption by weight (%)	0.08–0.2	4.2–13.2	0.2–0.4
Total porosity (%)	0.11–0.28	5.5–32.8	0.3–0.5
P wave velocity (m/s)	4658–4712	2875–4270	4275–4450
Compressive strength (MPa)	78–95	18–58	110–155
Tensile strength (MPa)	12–19	2.1–9.8	18–25

**Fig. 2** View of thin sections **a** Marmara marble (Ca; calcite) **b** Küfeki stone (Fo; fossil) **c** Kayseri basalt (Plj; plagioclase)

(Fig. 3a). The temperature of the samples were measured every 5 min until reaching room temperature (approx. 23 °C). At the same time, together with its temperature CERCHAR

abrasiveness indexes of the samples were also determined (Fig. 3b). Since the CERCHAR abrasiveness test is generally used for predicting metal abrasiveness, Böhme abrasiveness values were determined with an Eq. (1) (this equation applied for marble but there is no another equation for the other type of rocks in the literature, so the authors used this equation for all rocks) proposed by Deliormanlı (2012).

$$BA^* = -4.64 \times CAI^{**} + 25.06 \quad (1)$$

\*(BA) Böhme Abrasiveness

\*\* (CAI) CERCHAR Abrasivity Index

### 3 Result and Discussion

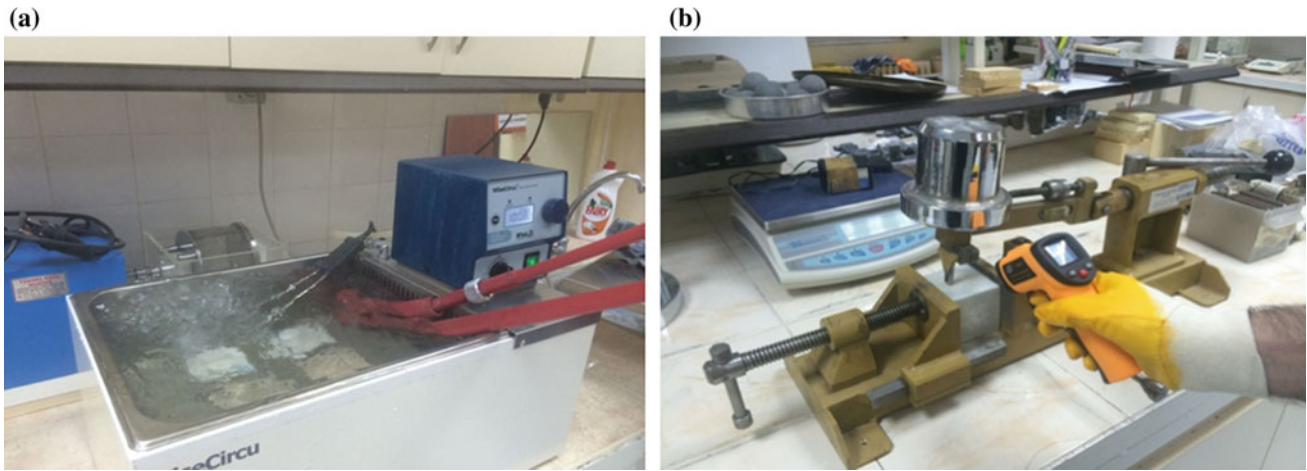
In dry condition, abrasiveness of Marmara Marble starts to increase after 40°, slows down after 60° (Fig. 4), in Küfeki stone the abrasiveness increases after 40°, it is also determined that after 80° it slows down (Fig. 5). When the change in abrasiveness is examined, it is seen that there is no change after 30 °C. It is thought that in the absence of change, the space of the expanding material is filled with water. The abrasiveness values do not change after 40° when the basalts are in dry condition (Fig. 6a). When the basalts are saturated with water, the abrasiveness values show a decrease until 50°, after this temperature there is no significant change (Fig. 6b).

### 4 Conclusion

The CERCHAR and Boehme abrasion tests, are test techniques that give information about the abrasion resistance of rocks, used by many researchers in their researches from past to the present. In this study, changes were tried to be observed in the abrasion resistance of marble, limestone and basalt rocks under different temperature conditions.

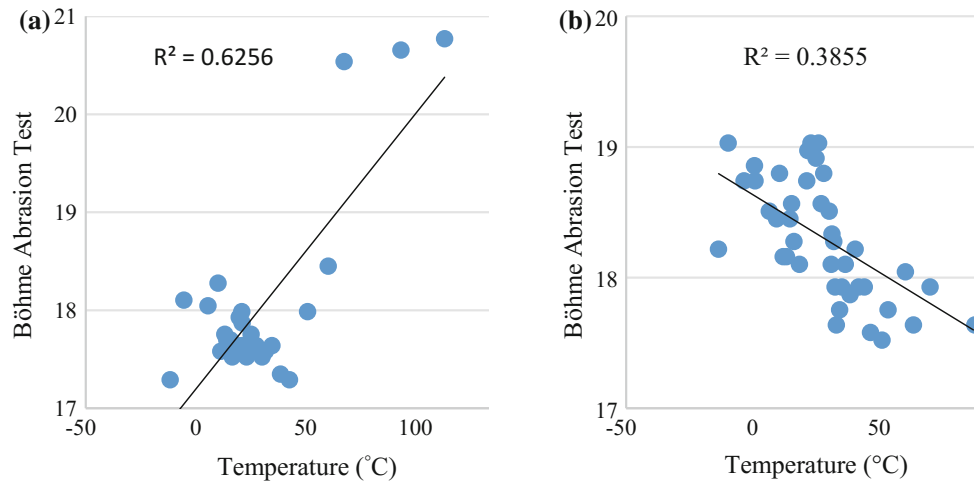
The aim of this study is to investigate the effect of different heat conditions on the abrasion resistance of rock



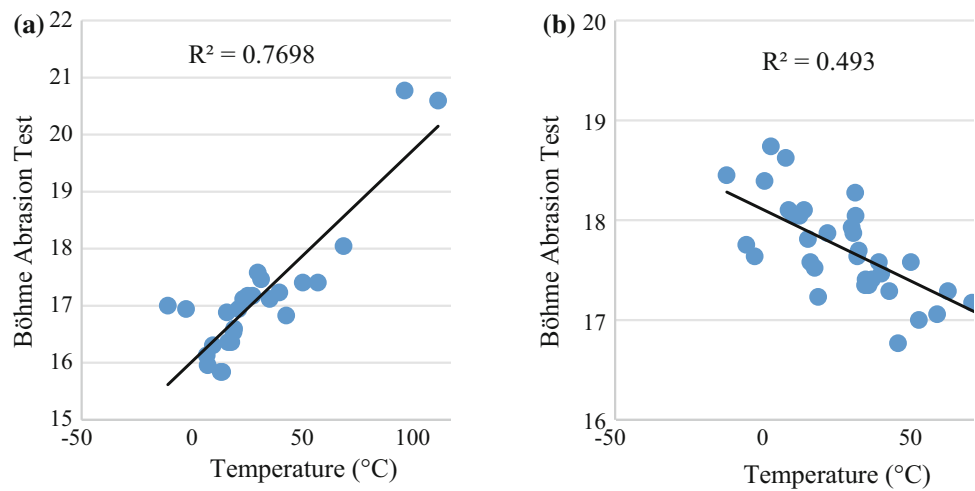


**Fig. 3** View of tests **a** boiling in water tank **b** CERCHAR abrasiveness test

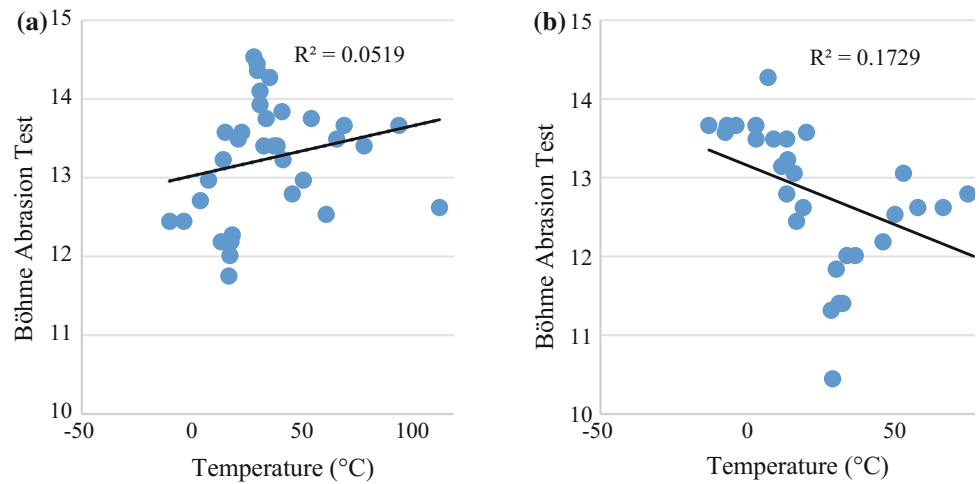
**Fig. 4** The abrasiveness values of the Marmara marble at different temperatures **a** dry abrasiveness change, **b** saturation abrasiveness change



**Fig. 5** The abrasiveness values of the Küfeki stone (limestone) at different temperatures **a** dry abrasiveness change, **b** saturation abrasiveness change



**Fig. 6** The abrasiveness values of the basalts at different temperatures **a** dry abrasiveness change, **b** saturation abrasiveness change



samples which are frequently used in outer coverings, flooring, baths such as areas exposed to temperature and water effects, and in historical buildings have different climatic conditions. In the dry conditions (Figs. 4a and 5a) for marble and limestone specimens, the abrasion index with increasing heat ( $R = 0.79$ ,  $R = 0.88$ ) for the same samples were in saturated condition (Figs. 4b and 5b) showed a negative relationship ( $R = 0.62$ ,  $R = 0.70$ ). In the basalt samples, it was found that the heat change did not have much effect on the abrasion resistance ( $R = 0.23$ ,  $R = 0.41$ ) in dry and saturated conditions (Fig. 6a–b).

## References

- Bilgin, N.: İnşaat ve Maden Mühendisleri İçin Uygulamalı Kazı Mekaniği, Birsen Yayınevi, İstanbul, 192 s (1989)
- Cerchar - Centre d'Études et des Recherches des Charbonages de France: The Cerchar abrasiveness index. Verneuil (1986)
- Delioranlı, A.H.: CERCHAR abrasivity index (CAI) and its relation to strength and abrasiveness test methods for marble stones. *Constr Build Mater* **30**, 16–21 (2012)
- İ.T.Ü Development Foundation: Determination of Protection Conditions and Causes of Weathering of the Rocks Used at Dolmabahçe Palace. Project Final Report of Protection and Instauration Methods, İstanbul (2000)
- Suana, M., Peters, T.: The CERCHAR abrasivity index and its relation to rock mineralogy and petrography. *Rock Mech* **15**, 1–7 (1982)
- TS 699: Natural building stones—investigation and laboratory test methods. TSE, Ankara (2009)
- URL 1: <http://www.geotechdata.info/geotest/Cerchar-Abrasivity-test.html>
- URL 2: <https://cooper.co.uk/shop/aggregate-testing/bohme-abrasion-testing-machine/>
- Valantin, A.: Test CERCHAR pour la mesure de la dureté et de l'abrasivité des roches. Annexe de l'exposé présenté aux Journées de Information "Techniques de creusement", Nov 1973, Luxembourg (1973)
- Yaralı, O., Akçın, N.A.: Kayaçların CERCHAR Sertlik İndeks Değerleri İle Dayanım Özellikleri Arasındaki İlişkilerin Belirlenmesi, Türkiye 19. Uluslararası Madencilik Kongresi ve Fuarı, IMCET2005. İzmir, Türkiye, 09–12 Haziran 2005

# Aggregate Mining in Megacities and Existing Problems: An Example from İstanbul, Turkey

Atiye Tugrul and Murat Yilmaz

## Abstract

In addition to the increasing population and structuring in the growth/development process of a country or megacity, the obligation to maintain industrial and infrastructure investments makes aggregate (crushed stone, etc.) one of the most consumed building materials per capita. Crushed stone, cement and ready-mixed concrete are the basic building blocks of the construction sector and have a great contribution to the development of the industry as well as the increase in national income and employment. However, work safety, environmental problems and increased social opposition to aggregate (crushed stone) open pit mines is intensive and unplanned/irregular urbanization areas are hampering the future sustainable production of medium and large sized enterprises in technical, environmental and economic aspects. The city of İstanbul which has a high aggregate production (90 million tone/year) provides a good example of those issues. In order to maintain efficient and sustainable aggregate resources in İstanbul and its surrounding region, plan and program should be reviewed and new strategies evaluated to facilitate the sustainable management of resources. In this regard, the importance of existing resources and their possibilities, determining operable new resources and their management have been considered.

## Keywords

İstanbul • Aggregate • Quarry • Resource planning • Aggregate management

## 1 Introduction

İstanbul is the largest city in Turkey, constituting the country's economic, cultural, and historical heart. With a population of 15.5 million, the city forms one of the largest urban agglomerations in Europe and is among the largest cities in the world.

Over the last three decades İstanbul, has grown quickly and its population density has increased. This means that many quarries that were once rural are now located in suburban areas (Fig. 1). In addition, surface mining activities have destroyed much of the natural countryside around both sides of İstanbul (i.e. either side of the Bosphorus Strait). Because of this, İstanbul provides an important example of the effects on land cover and land use due to mining and the impacts this has on the natural environment. Therefore, the assessment of the environmental impact of a quarry is now an important prerequisite for the any future operations (Kuzu and Ergin 2005).

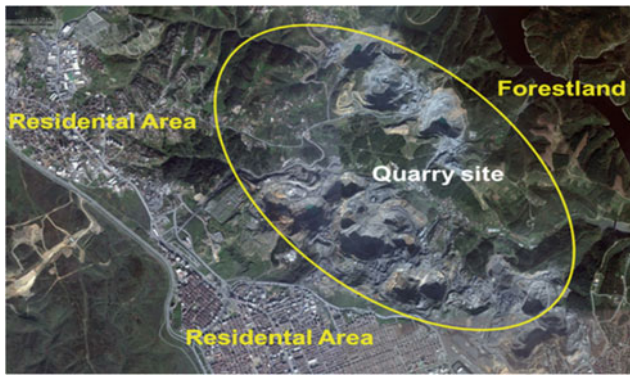
Determination of the impact of aggregate mining activities on the environment is a major issue in sustainable development and management of resources in megacities. The conflict between mining activities and environmental protection has intensified over recent years, emphasizing the need for improved information on the nature of impacts at regional and local scales (Latifovica et al. 2005).

This paper focuses aggregate mining in İstanbul and describes the available aggregate mining activities and existing problems and outlines the main considerations when planning for future aggregate supply.

## 2 Aggregate Mining Activities in İstanbul

Crushed stone has been produced in the İstanbul since the early twentieth century. Today, there are nearly 40 crushed stone quarries on both sides of İstanbul, from which approximately, 79 million ton of crushed stone is produced

A. Tugrul (✉) · M. Yilmaz  
İstanbul University, İstanbul, Turkey  
e-mail: tugrulative@gmail.com



**Fig. 1** General view of the quarry area and its surroundings in İstanbul

annually. Beside this, there are also approximately 25 sand quarries producing nearly 14.1 million ton of sand and gravel annually (Tugrul et al. 2012).

One way to understand the importance of the aggregates industry in İstanbul is to look at their production in the context of all mining. On the basis of either weight or volume, aggregates accounted for all nonfuel minerals produced in the İstanbul. In western side of the İstanbul, the amount of aggregate production is nearly 36 million ton in 2016 whereas, in the eastern part of the İstanbul, this production is nearly 33 million ton. On the other hand, total amount of crushed stone aggregate consumption is nearly 25 million ton whereas, in the eastern part of the İstanbul, this consumption was nearly 20 million ton.

### 3 Existing Problems

Rapidly growing population, increasing industrialization and the need for buildings, highways, railroads and other structures in İstanbul have resulted in intensive construction activity in recent years. To meet İstanbul's development needs, large quantities of aggregates have been required which have always been obtained almost entirely from quarries within the provincial border. However, this is becoming increasingly problematic for the following reasons:

- Rapidly reducing aggregates resources from existing sources (i.e. quarries are being worked out)
- Until ten years ago, aggregates quarries were located not far from the urban centres. But now, quarry sites are located near or around the residential areas (Fig. 1). Because of this, the closure of quarries near to the city centre is a key element of government policy.
- Need for urban renewal
- Potential for a substantial earthquake affecting İstanbul
- Increasing standards requiring higher quality aggregate

- Rapidly increasing requirements for greater quantities of aggregates to support future development (with the need for ready concrete, high strength concrete, highways, railways, airports, new projects, etc.).

On the other hand, quarry operations and aggregate productions have many significant environmental impacts in İstanbul:

- The use of land for the production of aggregates is severely limited and there are overriding environmental constraints on the establishment and operation of quarries in both the urban and rural areas.
- Since aggregates are produced mainly from surface mines, there is a direct impact on the natural landscape notably landform and drainage.
- Quarries damage natural water recharge and can lead to reduced quantity and quality of underground and surface water (Fig. 2).
- Blasting generally provides aggregates and this causes noise and dust pollution.
- Blastings in quarries causes ground vibration and create fly rocks (Fig. 3).
- Dust emission arising from extraction, processing operations and transportation activities has negative effects on air quality, soils, people and habitats around quarry areas (Figs. 3 and 4).
- Transportation of aggregates in İstanbul is carried out by trucks. Nearly 1500 dump trucks are circulating within



**Fig. 2** Surface water flow into the quarry area





**Fig. 3** Environmental effects of blasting in a quarry area



**Fig. 4** Dust emissions arising from production plant

the city adding to the already heavy traffic congestion and leading to increased noise and air pollution.

- The wastes generated during quarrying operations are mainly in the form of topsoil and weathered materials, which are dumped into nearby empty pits or slopes, riverbeds, pasturelands and agricultural fields leading to widespread environmental pollution (Fig. 5).

## 4 Suggestions

Accurate planning and management are important issues for megacities such as İstanbul. As indicated by Persson (2002), the planning of natural resources in an area, region or



**Fig. 5** The wastes generated during quarrying operations

country provides economic as well as environmental benefit. The use of the right material for the right purpose is highly advantageous.

Ideally aggregate reserves should be identified with low levels of waste. For different rock conditions, suitable production techniques must be selected. These should be aimed at increasing the quality of aggregates and also decreasing the amount of waste materials.

The high demand for aggregate, the limited production facilities, the lack of good quality aggregate and the rapid urban development has forced aggregate suppliers to find new resource areas in İstanbul. In recent years, different rock types, which have not been used previously, have been investigated as potential aggregates (Tugrul and Zarif 1997, 1999, 2002; Zarif and Tugrul 2004; Tugrul et al. 2010, 2012; Tugrul 2011; Tugrul and Yilmaz 2012; Yilmaz and Tugrul 2012). However, there are considerable rock reserves between the quarries and these reserves should be assessed. As an example of such conditions can be found in the Cebeci Region, which is one of the important aggregate production areas for İstanbul and is presented in Fig. 6.

Undoubtedly quarry operations and aggregate production have significant environmental impact, in particular as noise, dust and visual impacts. Due to these negative impacts, developing environmentally friendly mining activities is important for megacities (Fig. 7). To decrease environmental impacts, new conditions on the planning and operation of quarries are needed, as discussed below.

The main potential sources of dust include the processing plant, stockpiles, traffic on internal haul roads, stripping and overburden storage. In order to prevent dust emission; enclosing the conveyor belts and the processing plants, providing a dust removal system for the plant, using water sprays and appropriate dust filter systems are generally applied in İstanbul. In addition there are new closed aggregate preparation system. Due to this system fine material is



**Fig. 6** Abandoned rock reserves between the quarries



**Fig. 7** An example of environmentally friendly mining in eastern part of İstanbul



no longer stockpiled in open areas, therefore dust pollution is reduced (Fig. 8). The dust produced is collected by the filtering unit of the system and provided to the concrete or asphalt plant as filler material instead of scattering in the air.

Noise in quarrying usually comes from two major sources: machinery (stationary, e.g. crushers or moving e.g. trucks) and blasting. Good practices include regular monitoring of noise and comparison to current legislation limits and use of appropriate blasting techniques. As with dust, to minimize noise effects, conveyor belts and crushing/screening equipment is closed in most of the quarries around İstanbul.

When assessing the potential impacts of aggregate extraction activities on society and nature, it is important to note that these impacts may concern not just the extraction site itself but also all associated infrastructure and other facilities such as access roads, conveyor belts, crushers, storage sites, etc. As indicated by Chalkiopoulou and Hatzilazaridou (2011), good planning requires the successful design of the whole operation and detailed planning of aggregate quarrying activities for İstanbul, consideration of all legislative, technical, environmental, economic and social factors.



**Fig. 8** A closed aggregate preparation system

## 5 Conclusions

The construction industry is an important sector of the İstanbul economy. It uses large quantities of construction aggregates, obtained from a variety of sources. Because of this, the planning, management, rational utilization of natural resources is critical to reaching the objective of sustainable economic and social development in İstanbul. For this, a newly guideline should be focused on not only quarry regulations and rules including quarry opening, during the mining but also resource planning and efficiency,

development of a strategy related to resource usage, good quality product at usage area, usability of alternative resources, transportation from resources and environmentally friendly mining, including creation of suitable decommissioning schemes.

## References

- Chalkiopolou, F., Hatzilazaridou, K.: How to achieve aggregates resource efficiency in local communities. The reports prepared within Work Package 3 of the SARMA Project “Sustainable Aggregates Resource Management” (SEE/A/151/2.4/X) (2011)
- Kuzu, E., Ergin, H.: An assessment of environmental impacts of quarry-blasting operation: a case study in İstanbul, Turkey. *Environ. Geol.* **48**, 211–217 (2005)
- Latifovica, R., Fytasb, K., Chenc, J., Paraszczakb, J.: Assessing land cover change resulting from large surface mining development. *Int. J. Appl. Earth Obs. Geoinf.* **7**, 29–48 (2005)
- Persson, L.: Rock materials for construction: resources, properties, heterogeneity and suitability for use: examples and issues from the Precambrian of Sweden. In: *Proceedings of 9th IAEG Congress*, pp. 105–120, Durban, South Africa (2002)
- Raisanen, M.: Quality assessment of a geologically heterogeneous rock quarry in Pirkanmaa county, southern Finland. *Bull. Eng. Geol. Env.* **64**, 409–418 (2005)
- Tuğrul, A., Zarif, İ.H.: The Influence of Mineralogical and Textural Characteristics on the Durability of Selected Sandstone in İstanbul, Turkey, p. 87. *International Symposium on Geology and Environment, İstanbul* (1997)
- Tuğrul, A., Zarif, İ.H.: Aggregate properties of Devonian limestone for use in concrete in İstanbul, Turkey. *J. Nepal Geol. Soc. Abstr. Vol. Int. Symp. Eng. Geol. Hydrogeol. Nat. Disasters Emphas. Asia Kathmandu-Nepal* **20**, 92–93 (1999)
- Tuğrul, A., Zarif, İ.H.: Aggregate production in İstanbul, Turkey. In: *Proceedings of International Symposium on Industrial Minerals and Building Stones*, pp. 609–616, İstanbul, Turkey (2002)
- Tuğrul, A., Ündül, Ö., Yılmaz, M.: Correlation of different sandstone aggregates from the point of alkali-silica reactivity in concrete. In: Williams, A.L., Pinches G.M., Chin, C.Y., McMorran, T.J., Massey, C.I. (eds.) *Geologically Active, Proceedings, 11th Congress of the International Association for Engineering Geology and the Environment*, pp. 4553–4561, Auckland, New Zealand. CRC Press/Balkema, Taylor & Francis Group, London, UK (2010)
- Tuğrul, A.: Aggregate production in İstanbul. In: *Sustainable Aggregates Resource Management International Conference Ljubljana*, pp. 20–22, Slovenia, September (2011)
- Tuğrul, A., Sönmez, İ., Hasdemir, S., Yılmaz, M.: Aggregate requirements in İstanbul, existing problems and their solution. In: *34th International Geological Congress*, vol. 154, pp. 5–10, Brisbane, Australia (2012)
- Tuğrul, A., Yılmaz, M.: Assessing the quality of sandstones for use as aggregate in concrete. *Mag. Concr. Res.* **64**, 1–12 (2012)
- Yılmaz, M., Tuğrul, A.: The effects of different sandstone aggregates on concrete strength. *Constr. Build. Mater.* **35**, 294–303 (2012)
- Zarif, İ.H., Tuğrul, A.: Aggregate properties of Devonian limestones for use in concrete in İstanbul, Turkey. *Bull. Eng. Geol. Env.* **62**, 379–388 (2004)

# Study of Hungarian Rocks Regarding Potential Reactivity to Alkalis

Isabel Fernandes, Maria dos Anjos Ribeiro, and Ákos Török

## Abstract

The durability of concrete can be affected due to internal reactions between the alkalis of the cement paste and certain forms of silica present in the aggregates. Petrographic examination provides a useful tool to assess the alkali reactivity of aggregates. In the present work Hungarian stones that are used as aggregates were analyzed for alkali reactivity. Sandstone, two granitic rocks, one andesite and one diabase were studied using petrographic microscopy in order to identify the presence of potentially reactive forms of silica and to classify these rocks accordingly. Complementary methods such as scanning electron microscopy were also applied. Our results confirm that all studied rocks, except diabase, contain silica that has a potential of alkali reaction. Hence analyzed rocks are classified to Class II from the alkali reactivity point of view, while diabase is in Class I.

## Keywords

Alkali-silica reactions • Aggregates • Silica • Petrography • SEM

## 1 Introduction

Concrete can be affected by internal reactions between the alkalis of the cement paste and certain forms of silica present in the aggregates, reducing the durability of the concrete and

I. Fernandes (✉)

Faculty of Sciences of University of Lisbon, Department of Geology, Instituto Dom Luiz, Lisbon, Portugal  
e-mail: mifernandes@fc.ul.pt

M. A. Ribeiro

Faculty of Sciences of University of Porto, DGAOT, ICT, Porto, Portugal

Á. Török

Department of Engineering Geology and Geotechnics, Budapest University of Technology and Economics, Budapest, Hungary

the service life of the structures. The aggregates can therefore be classified as innocuous, of reactivity uncertain or potentially alkali-reactive, depending on the forms of silica they contain. The alkali-silica reaction can occur just a few years or some decades after the construction and the potentially reactive aggregates are accordingly named fast reactive (e.g. when opal is present) or slow reactive (e.g. aggregates containing deformed quartz or volcanic glass).

The potential alkali reactivity of aggregates can be studied with the petrographic examination; mineralogical and textural description of the samples. The reactivity of some rocks containing silica, such as sandstone, greywacke and gneiss (Fernandes et al. 2016) is well known but there are other rocks, such as the carbonate and some volcanic rocks that need to be further studied. In fact, the reaction between the cement paste and the carbonate rocks is not yet well understood and lately it has been considered that deterioration of concrete with these rocks was due to the presence of cryptocrystalline quartz spread in the rocks (Katayama 2010; Sanchez et al. 2012). The deleterious behavior of some under-saturated volcanic rocks has been attributed to the chemical composition of the volcanic glass they contain. Some authors consider a threshold of 65% SiO<sub>2</sub> for the composition of the volcanic glass (Wakizaka 2000).

In Hungary most of the aggregates are exploited from alluvial deposits of sand and gravel, which are considered as non-potentially reactive. Crushed aggregates are composed of igneous rocks and sedimentary carbonates. From igneous rocks Eocene-Miocene andesite, and late-Miocene basalt are common, while granite is found in smaller areas (Török 2007). Andesite and basalt have been used for prestressed prefabricated elements, wherever the tensile strength is of importance, but andesite has shown to be potentially reactive.

The present work summarizes the results of the petrographic characterization of seven selected samples, four of sedimentary rocks and three under-saturated igneous rocks.



## 2 Materials and Methods

For this study one sandstone, two granitic rocks, one andesite and a diabase were studied. These lithotypes occur at various locations in Hungary representing wide geographic range (Fig. 1). The granitic rocks, the andesite and the diabase are used as aggregate (Török 2015). The andesite has excellent aggregate properties with mean Los Angeles abrasion values of 13 (Török and Czinder 2017), while diabase performs even better with a Los Angeles abrasion value of 11, which is much lower than that of the granite (Török 2007).

Petrographic microscope using plane polarized (PPL) and crossed polarized light (XPL) were used in order to identify the presence of potentially reactive forms of silica and to classify these rocks accordingly. When necessary, complementary methods such as scanning electron microscope with energy dispersive spectrometry (SEM/EDS) were also applied.

## 3 Results and Discussion

The studied samples represent wide-ranges of lithologies with various micro-fabric (Fig. 2) containing different forms of silica that can be potentially reactive to alkalis. The sandstone is composed of angular clasts of quartz, quartzite and chert. The interstitial spaces are filled with micro- to cryptocrystalline quartz, abundant feather-like clay minerals, some mica and ferruginous cement.

The monzogranite contains quartz, perthitic K-feldspar, zoned plagioclase, biotite and hornblende, with minor epidote, chlorite and calcite. The rock is deformed, showing undulatory extinction in the larger crystals of quartz and

subgraining with formation of microcrystalline strained quartz. The altered granitic rock is intensely tectonized and is composed of quartz with abundant subgraining, perthitic K-feldspar and plagioclase. Abundant secondary calcite is present in the borders of the larger crystals of the main constituents.

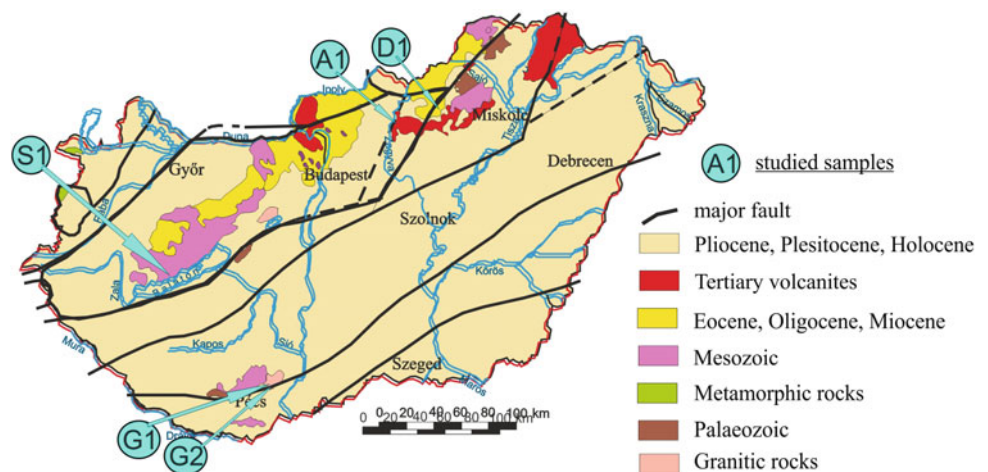
The andesitic rock is a porphyric igneous rock of intermediate composition with phenocrysts of zoned plagioclase, ortho- and clinopyroxene. Some crystals are partially altered to clay minerals and carbonates. The fine-grained groundmass shows small laths of plagioclase. SEM/EDS analyses were carried out in order to identify the components of the groundmass. The spectra and element mapping obtained show the presence of quartz intergrowths with feldspars (Fig. 3).

The greenish grey diabase/dolerite sample is composed of phenocrysts of plagioclase and pyroxene. The groundmass is very fine grained, with laths of plagioclase and abundant fibrous greenish mineral which resulted from the alteration of a primary mineral. According to SEM/EDS analyses chlorite is the main mineral in the groundmass (Fig. 4). This mineral is responsible for the greenish colour of the rock. No free silica was detected in this rock.


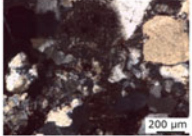

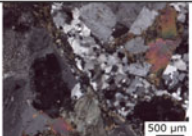

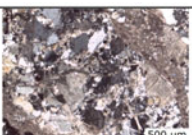



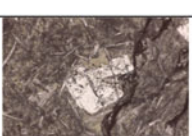
## 4 Conclusions

Sedimentary and igneous rocks from Hungary were studied by petrographic methods to assess the potential reactivity to alkalis. The sandstone contains micro- to cryptocrystalline quartz, besides the clasts of chert and is Class II. From the igneous rocks, the diabase is the only one that does not contain free silica minerals and is therefore Class I. All the other rocks contain cryptocrystalline quartz and deformed, subgrained quartz and are classified as Class II.

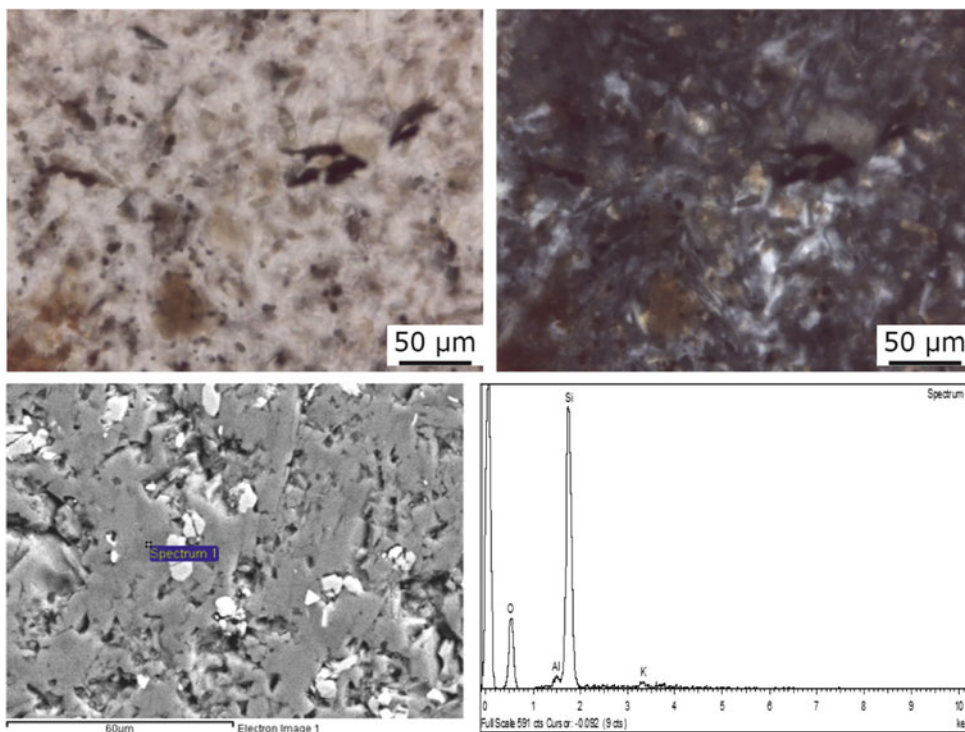
**Fig. 1** Simplified geological map of Hungary (modified after Haas 2001 and Török 2015) showing the sample sites (S1-sandstone, A1-andesite, D1-diabase, G1 and G2 granite, see Fig. 2 for details)



**Fig. 2** Studied lithologies and their microscopic image (XPL) (see location of sampling sites on Fig. 1)

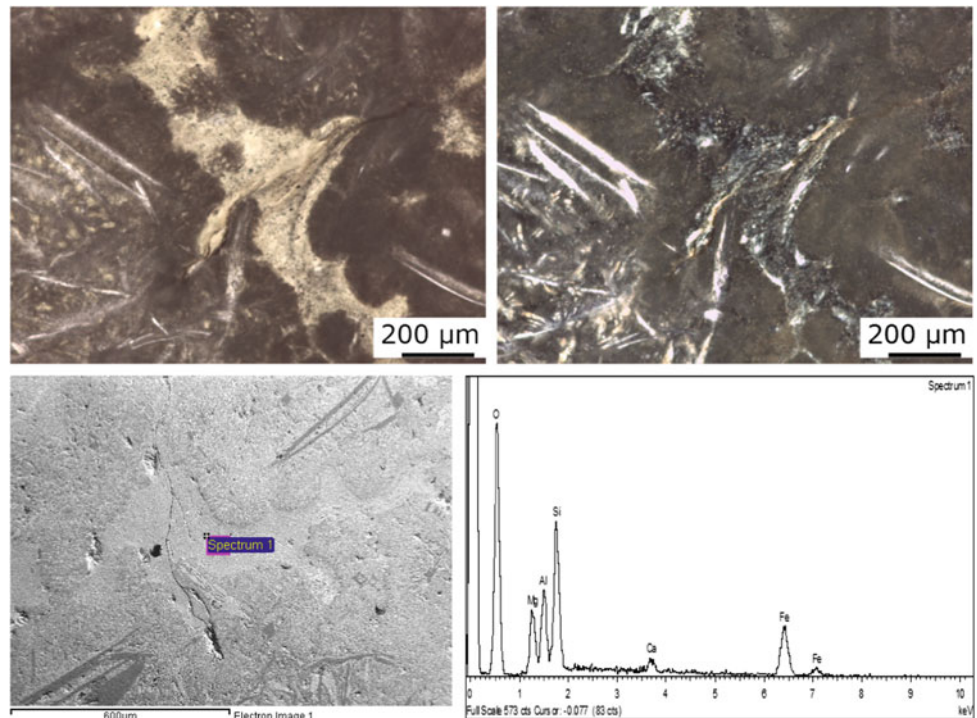
	Location/Age	Hand sample	Thin section
S1	Red sandstone Balatonrendes/Permian  Potentially reactive		
G1	Granitic rock (Monzogranite) Bátaapáti/Carboniferous  Potentially reactive		
G2	Altered granite Bátaapáti/Carboniferous  Potentially reactive		
A1	Andesite Gyöngyössolymos  Potentially reactive		
D1	Diabase Egerbakta  Non-reactive		

**Fig. 3** Groundmass of the andesite, composed of microcrystalline quartz and feldspar. Photomicrographs under PPL (left) and XPL (right), image obtained by SEM and EDS spectrum





**Fig. 4** Diabase with intense alteration to chlorite. Photomicrographs under PPL (left) and XPL (right), image obtained by SEM and EDS spectrum




**Acknowledgements** This publication is supported by FCT-project UID/GEO/50019/2013—IDL (IF) and Hungarian National Research, Development and Innovation Fund (K 116532) (ÁT).

## References

- Fernandes, I., Ribeiro, M.A., Broekmans, M.A.T.M., Sims, I.: Petrographic Atlas: Characterisation of aggregates regarding potential reactivity to alkalis. In: RILEM TC 219-ACS Recommended Guidance AAR-1.2 for Use with the RILEM AAR-1.1 Petrographic Examination Method. Springer, Dordrecht, the Netherlands, p. 191 (2016)
- Haas, J.: Geology of Hungary. Eötvös Kiadó, Budapest, 316 p. (2001)
- Katayama, T.: The so-called alkali-carbonate reaction (ACR)—its mineralogical and geochemical details, with special reference to ASR. *Cem. Concr. Res.* **40**(4), 643–675 (2010)
- Sanchez, L., Salva, P., Fournier, B., Jolin, M., Pouliot, N., Hovington, A.: Evaluation of damage in the concrete elements of the Viaduct “Robert-Bourassa-Charest” after nearly 50 years in service. In: Drimalas, T., Ideker, J.H., Fournier, B. (eds.) Proceedings of the 14th International Conference on Alkali-Aggregate Reactivity in Concrete, Austin, Texas, USA, 2012, 081511-FOUR-01, pp. 10 (2012)
- Török, Á.: Geológia mérnököknek (Geology for Engineers). Műegyetemi Kiadó, Budapest, 384 p. (2007). ISBN 978-963-420-934-8 (In Hungarian with English Summary)
- Török, Á.: Los Angeles and micro-deval values of volcanic rocks and their use as aggregates, examples from Hungary. In: Lollino, G., Manconi, A., Guzzetti, F., Culshaw, M., Bobrowsky, P., Luino, F. (eds.) Engineering Geology for Society and Territory—Volume 5: Urban Geology, Sustainable Planning and Landscape Exploitation. 12th IAEG Congress, Torino, Springer Switzerland, pp. 115–118 (2015)
- Török, Á., Czinder, B.: Relationship between density, compressive and tensile strength and aggregate properties of andesites from Hungary. *Environ. Earth Sci.* **76**, 639 (2017). <https://doi.org/10.1007/s12665-017-6977-y>
- Wakizaka, Y.: Alkali-silica reactivity of Japanese rocks. *Eng. Geol.* **56**, 211–221 (2000)

# Long-Term Wear of Aggregates Assessed by Micro-Deval Tests

Balázs Czinder and Ákos Török 

## Abstract

Aggregate tests are used worldwide to assess the durability of crushed stone. These standardized test methods aim to determine the resistance to wear by using given rotations as it is described in the European Norm of Micro-Deval test (EN 1097-1:2012). It recommends 12,000 rotations to determine the Micro-Deval coefficient of a rock. The present paper goes a step further since it aims to describe the long-term wear resistance of tested volcanic rocks (Nógrádkövesd, Hungary). Micro-Deval coefficients were determined after gradual increase of rotations from the suggested 12,000–780,000. The material loss was recorded in 65 steps, i.e., after each increment of 12,000 rotations. Not only the material loss but also grain shapes were documented. As it was expected the grains became smaller and more subspherical with the increasing number of rotations. Regression analyses were used to describe the material loss. Correlation between the number of rotations and the Micro-Deval coefficients were also outlined. Pearson coefficient of correlation was also calculated. Our test results suggest that during the long-term Micro-Deval tests the aggregate durability properties change due to long-term wear. The regression analyses of the results give a strong indication that polynomial and exponential curves are suitable to describe the changes in Micro-Deval coefficients on a long-term wear. These tests also demonstrate that it is possible to predict the

long-term behaviour/wear of andesite under investigation by using the applied equations.

## Keywords

Andesite • Aggregate • Durability • Micro-Deval test

## 1 Introduction

Though dimension stone has lost its significance as building a material, aggregates are indispensable in construction industry. Andesite is the most common igneous rock in Hungary, and its properties make it applicable for use as aggregate in asphalt, concrete, railway ballast, or armour stones in hydraulic engineering.

Several test methods have been developed to investigate the different properties of the aggregates. Some of these tests are widespread in the world (e.g., particle size distribution test, water content test), others are only used in local regions (e.g., Nordic test, aggregate impact value test). One of the most important properties of the aggregates is the resistance against abrasion. The durability can be analysed by numerous laboratory tests: slake durability test (Miščević and Vlastelica 2011), Nordic test (Krutilová and Příkryl 2017), aggregate impact and aggregate crushing value test (Palassi and Danesh 2016). Los Angeles (LA) and Micro-Deval (MDE) tests are the most common methods used to assess the durability of andesite in the EU and also in Hungary (Gálos and Kárpáti 2007). The different standards require different sets of the laboratory tests, therefore, the test results are not comparable; Gökalp et al. (2016) revealed that the Micro-Deval coefficient determined according to the EN standard is higher than that of the ASTM.

The different rock mechanical and aggregate properties may correlate with each other. Rigopoulos et al. (2013) found logarithmic dependence between the uniaxial compressive strength (UCS) and the Los Angeles abrasion values of ophiolite complexes from Greece. According to

---

B. Czinder · Á. Török (✉)  
Department of Engineering Geology and Geotechnics, Budapest  
University of Technology and Economics, 1111, Műegyetem  
rkp. 3, Budapest, Hungary  
e-mail: torokakos@mail.bme.hu

B. Czinder  
e-mail: czinder.balazs@epito.bme.hu

Capik and Yilmaz (2017) the UCS correlate with the MDE values but they took into account the test results of various rock types including igneous and sedimentary rocks. The MDE values also correlated with the point-load index, the Brazilian tensile strength, the apparent porosity, the void ratio, and the Schmidt hammer rebound (Capik and Yilmaz 2017). Dependence was found between the LA and MDE values of Hungarian andesite and basalt (Török 2015).

The alteration of the particle shape was also analysed. Bobály and Gálos (2016) found that the flakiness index and the shape index correlate linearly with both the LA and MDE values of andesite aggregates in the case of 31.50/40.00 mm sized grains. The dependence between the flakiness index and the MDE value was also determined by Rigopoulos et al. (2013).

The behaviour of the aggregates undergoing continuous abrasive impact is changing significantly, and therefore, long-term durability tests are needed to describe it. Erichsen (2015) analysed jasper and greenstone with Los Angeles tests, increasing the number of rotations to 900 from 100. The residual LA values showed significant decreasing tendency owing to the shape alteration, the decreasing flakiness of the grains. Slake durability index ( $I_d$ ) can also describe the aggregate durability. The alteration of the  $I_d$  according to the number of rotations was assigned in the case of Croatian marls (Mišević and Vlastelica 2011) and Turkish clay-bearing rock types (Gökçeuglo et al. 2000). Based on the results of long-term Micro-Deval tests with raised number of rotation Czinder and Török (2017) revealed that quadratic models are suitable to describe the initial phase of the abrasion of andesites from Hungary. Tanyu et al. (2017) analysed the short-term behaviour of different aggregates (diabase, limestone, andesite, marble, tuff and slate) by decreasing the number of rotations, and they found linear correlations between the number of rotations and the loss in material.

The investigation of aggregate abrasion is interesting and important from geological aspect, too. The abrasion of the grains of the river-beds could be described by aggregate abrasion tests in laboratory condition. The volume reduction of the grains is described in exponential form (Morris and Williams 1999; Szabó et al. 2013; Domokos et al. 2014). Domokos et al. (2014) analysed the weight loss and shape evolution of a cuboid specimen which was abraded in a Los Angeles drum. According to their results, the abrasion occurs in two phases: in the first phase, the edges of the specimen round without changes in the axis dimensions, and in the second phase the axis of the rounded specimen are reduced.

## 2 Materials and Methods

For this study, andesite aggregate was used for the Micro-Deval abrasion tests. The samples were collected from the eastern part of Hungary, from the Nógrádköves quarry. The quarry exposes a Miocene andesite that was formed during the Carpathian volcanic activity. A more detailed lithological description of the andesite and some rock mechanical parameters are given by Török and Czinder (2017). The aggregate samples were made from larger aggregates by crushing.

Micro-Deval tests were used to analyse the abrasion of the aggregate samples. The relevant European standard is EN 1097-1:2012. The samples were made from 150 g of 10.0/11.2 mm sized and 350 g of 11.2/14.0 mm sized grains. The aggregates were tested in steel drums (diameter: 154 mm, height: 200 mm). The abrasive processes are modelled by the rotation of the drums (100 rotations per minute) (Fig. 1). The intensity of the abrasion is enhanced by adding 5000 g of steel balls (diameter: 10 mm) and 2500 ml of water into the drum. According to the relevant EN standard (EN 1097-1:2012), 12,000 rotations should be applied. After the rotations the grains which are smaller than 1.6 mm should be removed from the samples. The result of the Micro-Deval test is Micro-Deval coefficient ( $M_{DE}$ ) which is the ratio of the abraded mass and the original mass of the aggregates. Other standards, like the American ASTM D 6928 require different grain-size and mass compared to Micro-Deval tests.

The long-term durability properties were tested by additional rotations. The number of the rotations of Micro-Deval tests was increased up to 780,000. The Micro-Deval tests were repeated on the same aggregate sample until 99% of the original mass of the aggregate samples was abraded. The mass reduction and the long-term Micro-Deval value (MDE) was calculated after each of the 12,000 rotations. The Micro-Deval tests were made simultaneously on two samples, the average values of the MDE coefficients were used for the subsequent analyses.

Correlation and regression analyses were used to determine the mathematical models which can describe the behaviour of the aggregate sample under abrasive impact. The relationship between the number of rotations and the mass reduction is described by the Pearson-coefficient ( $R^2$ ). The calculated functions do not contain constant members, and the first point (when the MDE value and the number of rotations are zero) was considered as a fix point of the curves.

**Fig. 1** The Micro-Deval test machine with four steel drums



### 3 Results and Discussion

The long-term MDE test results showed significant changes of the grain shape and the mass of the aggregate specimens (Fig. 2), and the mass reduction reached 99%.

Previous studies (Czinder and Török 2017) proved that quadratic curves fitted well to the MDE test results at the initial phase of the abrasion (from 0 to 12,000 rotations, the Pearson-coefficient of the quadratic function was 0.995) (Fig. 3, POLY-2), but the whole process of the abrasion could not be described by parabolic curves. The expansion of the degree of polynomial functions resulted in better curve fitting as the  $R^2$  value is 0.999 in the case of a polynomial function of degree 6 (Fig. 3, POLY-6). The polynomial function:

$$\begin{aligned} \text{MDE}_{\text{POLY-6}} = & -9.495\text{E} - 33 \cdot N^6 + 2.6115\text{E} - 26 \cdot N^5 \\ & - 2.890\text{E} - 20 \cdot N^4 + 1.663\text{E} - 14 \cdot N^3 \\ & - 5.396\text{E} - 09 \cdot N^2 + 1.011\text{E} - 03 \cdot N \end{aligned} \quad (1)$$

The previously introduced visualization form is not suitable for the presentation of exponential functions because it would not be able to consider the first fixed point in zero. Figure 4 shows the relative residual mass ( $m_{\text{res}}$ ) according to the number of rotations:

$$m_{\text{res}} = 100 - \text{MDE} [\%] \quad (2)$$

Three regression curves were determined: the previously introduced polynomial function (POLY-6), and two exponential functions, one without (EXP-1) and one with (EXP-2) the consideration of the fixed point at the initial phase. The  $R^2$  values were 0.989 and 0.958. Though previous research results suggested the application of exponential regression, the polynomial function provided better curve fitting. The exponential functions:

$$\text{EXP-1: } \text{MDE}_{\text{EXP-1}} = 64.117 \cdot e^{-5.552\text{E}-06 \cdot N} \quad (3)$$

$$\text{EXP-2: } \text{MDE}_{\text{EXP-2}} = 100 \cdot e^{-6.400\text{E}-06 \cdot N} \quad (4)$$

According to the test results, the fitted regression curves (Figs. 3 and 4) and the alteration of the grain shapes (Fig. 2),



**Fig. 2** The grains of the aggregate samples during the long-term Micro-Deval tests (N: number of rotations, MDE: Micro-Deval value)



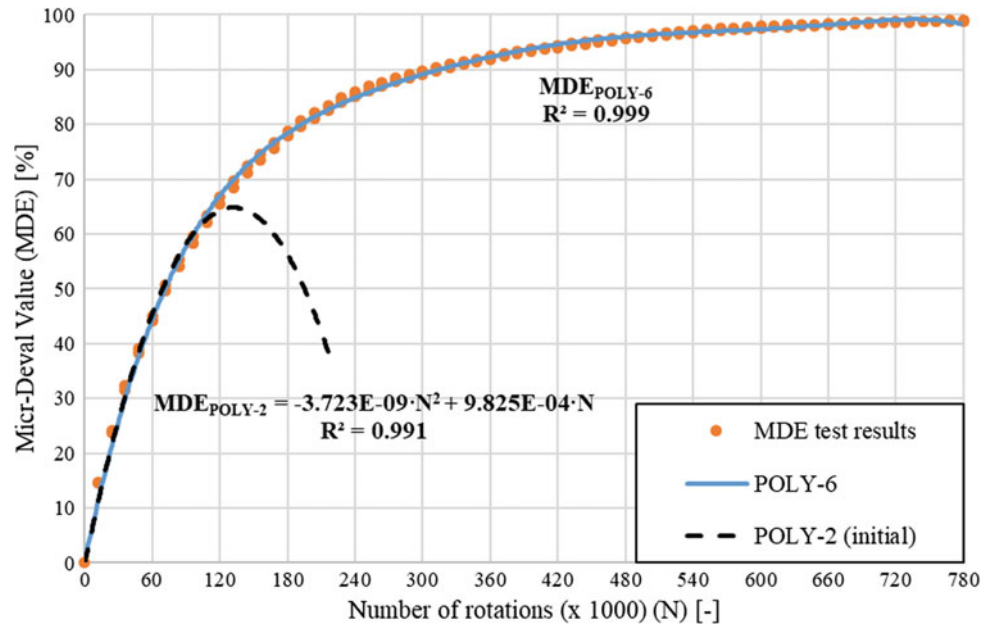
the two-phased model introduced by Domokos et al. (2014) is suitable to describe the abrasion caused by long-term Micro-Deval tests. The rapid mass reduction of the aggregate samples in the initial phase could be explained by the rounding of the edges of the grains without significant changes in the grain size. In the next phase, the slower mass reduction is related to the size reduction without significant rounding.

#### 4 Conclusions

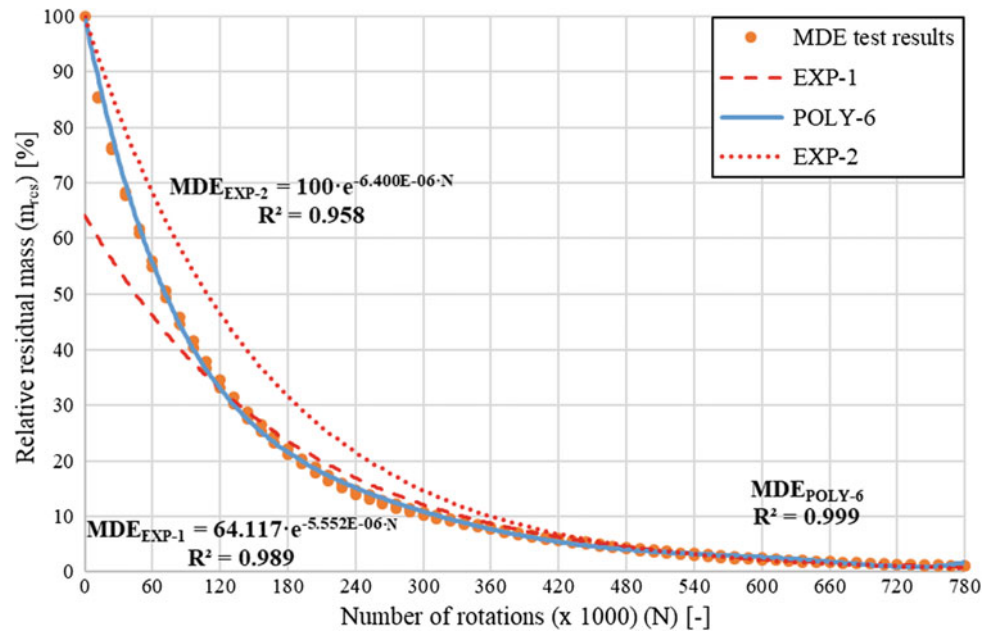
Micro-Deval durability tests are applicable for the analyses of the long-term behaviour of aggregates. This paper shows the alteration of the Micro-Deval test results modelled by increasing number of rotations. Long-term properties are important from engineering and geological perspectives, too.



**Fig. 3** The MDE values and the fitted polynomial functions according to the number of rotations (POLY-6: polynomial function of degree 6, POLY-2: polynomial function of degree 2 fitted at the initial phase) (POLY-2 curve is after Czinder and Török 2017)



**Fig. 4** The relative mass reduction according to the number of rotations, the fitted polynomial and exponential functions (POLY-6: polynomial function of degree 6, EXP-1: exponential function without the consideration of the first fix point, EXP-2: exponential function with the consideration of the first fix point)



Aggregates in road or railway constructions and the particles of river-beds are subjected to continuous abrasive impact and such long-term abrasive tests provide valuable information on the wear of particles. The suggested 12,000 rotations in the European Norm (EN 1097-1:2012) seems not to describe the complete wearing process. The number of rotations during the long-term Micro-Deval tests increased to 780,000, allowing a better understanding of long-term wear.

Our test results confirm the findings of Domokos et al. (2014), namely that the abrasion of the aggregate samples

follows a two-phase abrasion model. The size reduction of the grains was relatively slow, while the rounding of the edges speeded up the degradation in the first phase.

Similar to previous studies, the tendency of the abrasion can be described by exponential curves. The  $R^2$  value is 0.958. The Micro-Deval test results showed that better curve fitting was available by the application of polynomial functions. In the initial phase of the long-term tests quadratic curves were suitable, but expansion to the 6th degree of the polynomial was needed to describe the total course of abrasion. At degree 6, the Pearson-coefficient was 0.999.

**Acknowledgements** The authors are indebted to László Ézsiás and COLAS Északkő Ltd. for providing andesite aggregate for the laboratory tests. Gyula Emszt and Bálint Pálinkás helped in laboratory analyses. The financial support of the Hungarian National Research, Development and Innovation (NKFI) Fund (K 116532) is appreciated.

## References

- Bobály, J., Gálos, M.: Szemalak hatása a vasúti Los Angeles- és a vasúti mikro-Deval vizsgálatok eredményeire. *Sínek világa* **58**(5), 8–14 (2016). MÁV Ltd. Chief Executive Officer, Budapest
- Capik, M., Yilmaz, A.O.: Modeling of Micro-Deval abrasion loss based on some rock properties. *J. Afr. Earth Sci.* **134**, 549–556 (2017). <https://doi.org/10.1016/j.jafrearsci.2017.04.006>
- Czinder, B., Török, Á.: Long-term durability tests of andesite aggregates from Hungary. *Cent. Eur. Geol.* **60**(3), 333–343 (2017). <https://doi.org/10.1556/24.60.2017.010>
- Domokos, G., Jerolmack, D.J., Sipos, A.Á., Török, Á.: How river rocks round: resolving the shape-size paradox. *PLoS ONE* **9**(2), e88657 (2014). <https://doi.org/10.1371/journal.pone.0088657>
- Erichsen, E.: Plotting aggregate degradation results from the Los Angeles test on a triangular diagram: proposal of a new quality ranking for aggregates. *Bull. Eng. Geol. Environ.* **74**, 667–671 (2015). <https://doi.org/10.1007/s10064-014-0655-z>
- Gálos, M., Kárpáti, L.: Testing of Hungarian aggregates for railway ballast according to MSZ EN 13450. *Cent. Eur. Geol.* **50**(4), 353–361 (2007). <https://doi.org/10.1556/CEuGeol.50.2007.4.5>
- Gökalp, İ., Uz, V.E., Saltan, M.: Testing the abrasion resistance of aggregates including by-products by using Micro Deval apparatus with different standard test methods. *Constr. Build. Mater.* **123**, 1–7 (2016). <https://doi.org/10.1016/j.conbuildmat.2016.06.141>
- Gökçeuglo, C., Ulusay, R., Sönmez, H.: Factors affecting the durability of selected weak and claybearing rocks from Turkey, with particular emphases on the influence of the number of drying and wetting cycles. *Eng. Geol.* **57**, 215–237 (2000). [https://doi.org/10.1016/S0013-7952\(00\)00031-4](https://doi.org/10.1016/S0013-7952(00)00031-4)
- Krutilová, K., Příkryl, R.: Relationship between polished stone value (PSV) and Nordic abrasion value (AN) of volcanic rocks. *Bull. Eng. Geol. Environ.* **76**, 85–99 (2017). <https://doi.org/10.1007/s10064-015-0814-x>
- Miščević, P., Vlastelica, G.: Durability characterization of marls from the region of Dalmatia, Croatia. *Geotech. Geol. Eng.* **29**, 771–781 (2011). <https://doi.org/10.1007/s10706-011-9416-y>
- Morris, P.H., Williams, D.J.: A worldwide correlation for exponential bed particle size variation in subaerial aqueous flows. *Earth Surf. Process. Landf.* **24**(9), 835–847 (1999). [https://doi.org/10.1002/\(sici\)1096-9837\(199908\)24:9](https://doi.org/10.1002/(sici)1096-9837(199908)24:9)
- Palassi, M., Danesh, A.: Relationships between abrasion/degradation of aggregate evaluated from various tests and the effect of saturation. *Rock Mech. Rock Eng.* **49**, 2937–2943 (2016). <https://doi.org/10.1007/s00603-015-0869-9>
- Rigopoulos, I., Tsikouras, B., Pomonis, P., Hatzipanagiotou, K.: Determination of the interrelations between the engineering parameters of construction aggregates from ophiolite complexes of Greece using factor analysis. *Constr. Build. Mater.* **49**, 747–757 (2013). doi:<https://doi.org/10.1016/j.conbuildmat.2013.08.065>
- Szabó, T., Fityus, S., Domokos, G.: Abrasion model of downstream changes in grain shape and size along Williams River, Australia. *J. Geophys. Res. Earth Surf.* **118**, 2059–2071 (2013). <https://doi.org/10.1002/jgrf.20142>
- Tanyu, B.F., Yavuz, A.B., Ullah, S.: A parametric study to improve suitability of Micro-Deval test to assess unbound base course aggregates. *Constr. Build. Mater.* **147**, 328–338 (2017). <https://doi.org/10.1016/j.conbuildmat.2017.04.173>
- Török, Á.: Los Angeles and Micro-Deval values of volcanic rocks and their use as aggregates, examples from Hungary. In: Lollino, G., Manconi, A., Guzzetti, A.F., Culshaw, M., Bobrowsky, P., Luino, F. (eds.) *Engineering Geology for Society and Territory* (Vol. 5, Urban Geology, Sustainable Planning and Landscape Exploitation), pp. 115–118. Springer International Publishing, Basel (2015). [https://doi.org/10.1007/978-3-319-09048-1\\_23](https://doi.org/10.1007/978-3-319-09048-1_23)
- Török, Á., Czinder, B.: Relationship between density, compressive strength, tensile strength and aggregate properties of andesites from Hungary. *Environ. Earth Sci.* **76**, 639 (2017). <https://doi.org/10.1007/s12665-017-6977-y>

---

**Part III**  
**Karst**

# Bacterial Processes in Oil-Polluted Karst Environments in Perm Region (Russian Federation)

Nikolay Maksimovich , Olga Meshcheriakova , and Vadim Khmurchik

## Abstract

Rocks and groundwater of karst areas are weakly protected from any pollution. The most common pollutants within them are oil hydrocarbons. Microbial populations of karst rocks and groundwater are able to degrade a large number of contaminants under the existing redox conditions, often used in biotechnological methods of remediation. The authors investigated oil polluted karst territories of the Perm region (Russian Federation) to develop methods of remediation. Two sites of karst rocks and groundwater with different redox conditions and impacted by oil and oil-products were studied. Aerobic hydrocarbon-oxidizing bacterial processes occurred in the first site, and this paper describes the complex method of mechanical and microbiological cleaning to achieve complete oil removal. Anaerobic degradation of oil hydrocarbons during sulfate reduction process was detected in the second place. One of the products of this process, hydrogen sulfide, is very toxic to water fauna but readily oxidative in air. The authors recommend constructing special oxidizing and precipitating ponds to improve the environment.

## Keywords

Karst rock • Oil pollution • Hydrocarbon-oxidizing bacteria • Bacterial sulfate reduction • Remediation

## 1 Introduction

Karst rocks, such as limestone and gypsum, are well developed on the Earth and occupy its vast territories (approx. 31.5% or 47,000,000 km<sup>2</sup>). Rocks and groundwater of karst areas are weakly protected from any pollution, and the remediation of them is difficult and costly. The most common pollutants of groundwater are hydrocarbons and other compounds of oil and oil products. Microbial populations of groundwater are active in situ and able to degrade a large number of contaminants under the existing redox conditions. The presence of sufficient electron acceptors is a principal factor in the degradation of organic contaminants. There are two main biotechnological methods of oil polluted natural habitats remediation: the first one is stimulation of natural microbial hydrocarbon-degrading populations by nutrient supplies (especially N and P), and the second method is introduction of active hydrocarbon-degrading bacteria (and nutrient supplies) into polluted environments in regions of cold and temperate climate, where the warm season is not long (Koronelli 1996). It is known that bacterial populations can utilise oil and oil products both in aerobic and anaerobic conditions. The capability of some bacteria to metabolize hydrocarbons in the absence of molecular oxygen was first recognized about 20 years ago. Since then, the number of hydrocarbon compounds shown to be catabolized anaerobically by bacterial cultures has been steadily increasing. Anaerobic degradation of oil and oil products proceeded during nitrate-reducing (Callaghan et al. 2009), denitrifying (Rabus et al. 2001), iron-reducing (Dawn et al. 2011), sulphate-reducing (Dorota and Borkowski 2007), and methanogenic (Aitken et al. 2013) bacterial processes. So, mentioned bacterial groups could be used to remediate oil polluted natural habitats. However, some products of these bacterial processes are environmentally toxic, i.e. hydrogen sulphide, the product of sulfate reduction process, therefore thorough study of conditions and environmental engineering of additional measures is needed.

N. Maksimovich · O. Meshcheriakova (✉) · V. Khmurchik  
Institute of Natural Sciences of Perm State, Natural Research  
University, 15 Bukireva St., Perm, 614990, Russia  
e-mail: olgam.psu@gmail.com

N. Maksimovich  
e-mail: nmax54@gmail.com

V. Khmurchik  
e-mail: khmurchik.vadim@mail.ru

The aim of our study was to research oil polluted karst territories of the Perm region (Russian Federation) and to develop methods of remediation.

## 2 General Characteristics of the Region Karst

Karst rocks such as limestone, gypsum and salt occur within vast areas of the Western Urals (Russian Federation). Modern and ancient karst is widespread there. Three geological structures are presented in this area: the eastern margin of the East European Platform, the CisUrals Foredeep and the Urals' Folded Zone. Sulphate karst and to a lesser extent carbonate karst occur mainly on the Platform. Salt and gypsum karst developed in the CisUrals Foredeep, whereas dolomite and limestone karst, and somewhere marble karst, are registered in the Urals' Folded Zone. Karst rocks are covered by eluvial and deluvial deposits, and overlapped in river valleys by alluvial deposits or non-karstic rocks of a relatively small thickness. Seldom karst rock remains uncovered.

The territory of the Western Urals undergoes strong technogenic impact, which alters significantly the conditions and factors of karst development due to irreversible transformation of relief and rocks, pollution of surface and groundwater, and vegetation degradation.

The Perm region occupies an area of about 160,000 km<sup>2</sup>. The karstified rocks, i.e., paleozoic limestones, dolomites, gypsums, anhydrites, and rock salts, are either exposed or lie close to the surface in the area of about 30,000 km<sup>2</sup>. The Perm region is one of the areas where oil deposits are development also—oil deposits are distributed in a large part of its territory. A considerable number of oil deposits are located on the catchment area of the Kama River and its tributaries (see Fig. 1). In this area, the groundwater is poorly protected from oil and oil products pollution due to the intense karst development. Karst regions have some features, creating peculiar conditions of oil pollution distribution due to rock fracturing and permeability of rocks, vertical zonality of water exchange rate. Lithological composition of karst rocks have an indirect impact on oil pollution—it mainly determines the chemical type and mineralization of groundwater, which in turn both influence on migration capability of oil products and determine the distribution conditions and the scale of pollution (for example, an increase in water salinity decreases the solubility of oil in water). Contaminated karst groundwater discharges to rivers which results in pollution of the river and adjacent areas.

We studied two sites of karst rocks and groundwater polluted with oil and oil products and differed in redox conditions.

## 3 Aerobic Oxidation of the Oil in Karst Rocks

The first studied site is situated in the Polazninskiy karst area of gypsum and carbonate-gypsum karst in central part of the Perm region. This area encloses the left coastal side of the Kama water reservoir. Karst development in the region was promoted by the formation of the Kama water reservoir in 1954, which induced the water level rise of 20–22 m. 1691 karst forms are found on the area of 28.1 km<sup>2</sup>, 97% of them are sinkholes. Other karst forms, such as karrs, karst trenches, hollows, gullies, dry river channels and lakes also occur within this area. The relative average density of karst forms reach 60 per km<sup>2</sup>. The existing karst forms are renewed and new ones appear. The bulk of karst cavities occur within the zone of seasonal fluctuation of fractural-karst water, where dissolution of rocks develop most intensely (Milanovic 2000; Pecherkin 1969).

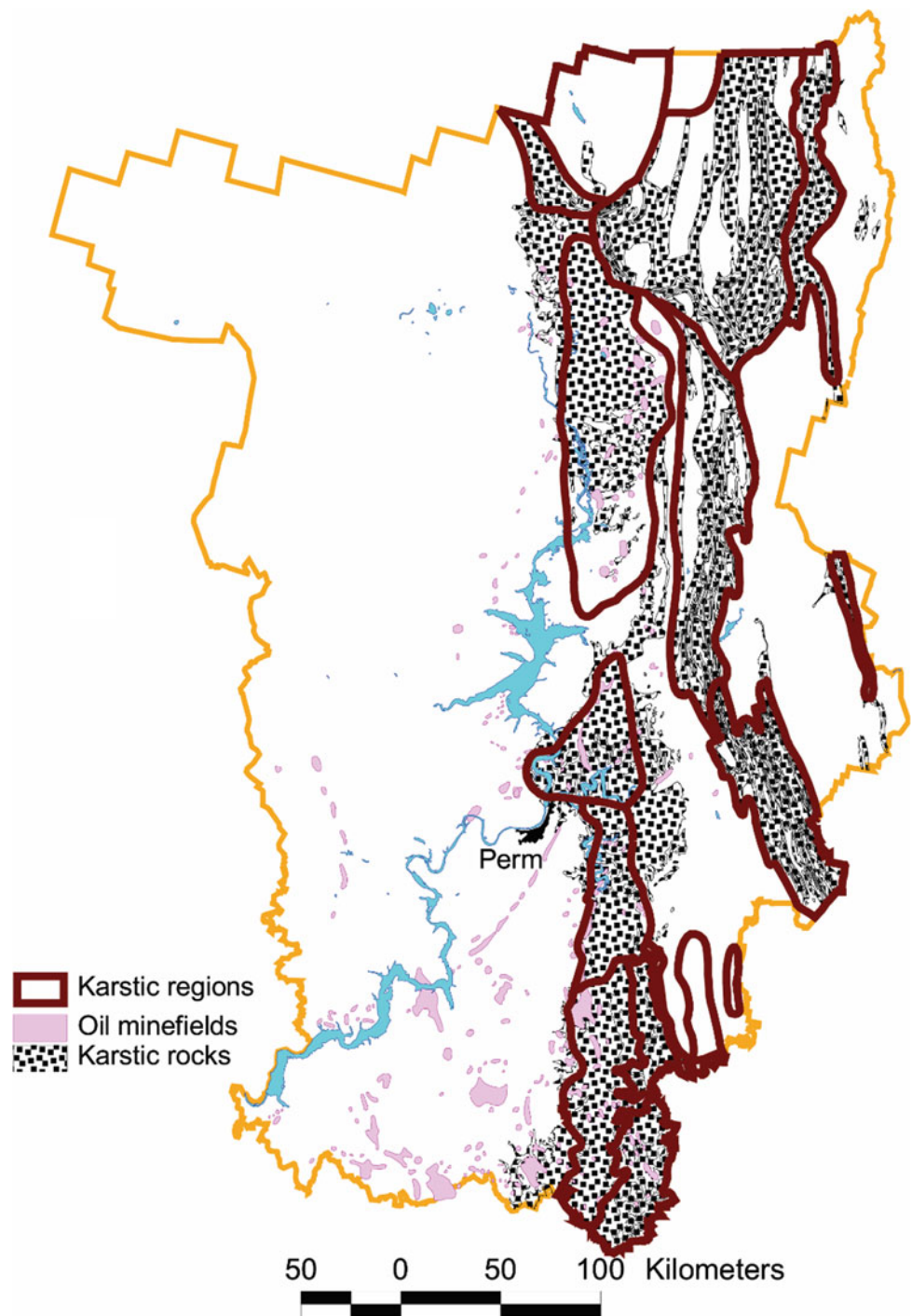
There are oil deposits beneath the banks of the Kama water reservoir. During a 50-year period of oil deposit exploration the oil lens (thickness up to 2–3 m) was formed within karst rocks on the surface of the water table and became a source of pollution of the Kama water reservoir. Investigations revealed that the most probable and basic source of formed oil lens were spills and discharges of oil on the ground surface during initial stages of deposit exploitation.

There is a direct connection between the karstic groundwater water table and the Kama water reservoir level: fluctuations of water level in the Kama water reservoir induce the karstic groundwater movement into rock massif and backward in the reservoir, that is favourable to maintain aerobic redox conditions in groundwater. Oxidative weathering and bacterial degradation of lens' hydrocarbons as well as the fluctuation of water table within karst massif led to the formation of bituminous film on the walls of the lens containing cavity, which prevents the direct flow of lens' hydrocarbons to the Kama water reservoir. Water-dissolved oil products discharge as springs to the reservoir freely. The intensity of discharge is controlled by the level of water in the Kama water reservoir (see Fig. 2).

To improve the ecological situation the technology of mechanical and microbiological cleaning of polluted waters was utilized, consisting of the pumping oil out of the lens using a special technique and the biochemical destruction of oil using the natural biodegradation based on activation of



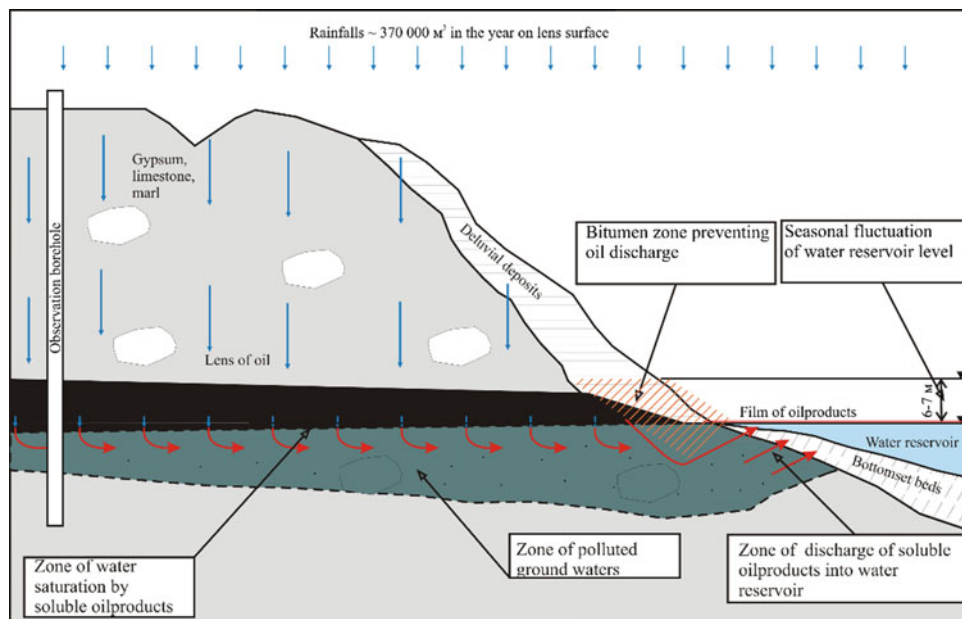
**Fig. 1** Karst territories in Perm Region



aerobic oil-degrading bacteria in groundwater. The work consisted of several stages: the isolation of active hydrocarbon-oxidizing bacteria from karstic groundwater and the study of their oil degrading capability; the development of bacterial preparation based on isolated

hydrocarbon-oxidizing bacteria; the stimulation of groundwater hydrocarbon-oxidizing microflora with inorganic nutrients supplies; and the introduction of developed bacterial preparation into groundwater to achieve complete oil removal (Maximovich and Khmurchik 2009).

**Fig. 2** Mechanism of pollution of the Kama water reservoir by oil products in the Polazninskiy karst area



#### 4 Anaerobic Oxidation of the Oil in Karst Rocks

The second studied site is situated in the Iremsky karst district in the south part of the Perm region. Forms of karst in the district are diverse. Karst depressions concentrate surface runoff and feed karst groundwater, which in turn discharges to rivers. Karst rivers are typical to the Iremsky karst district, most of them are tributaries of the Iren river. Effluents of these rivers are represented by the karst springs arising at the foot of the gypsum rocks (Gorbunova et al. 1992). The Turaevka and the Kamenka karst rivers flow on the territory of the Iremsky karst district. Part of the riverbeds are underground and discharge as karst springs. The Kokuyskoye oil deposit occupies part of the territory of the Iremsky karst district, its oil-producing wells are located in the catchment area of the Turaevka and the Kamenka rivers.

Until the 1990s the water in the rivers was clean and used as potable. Numerous accidental spills of oil and technical fluids on the surface and leaks of oil through broken sides of oil-producing wells led to pollution of karstified rocks with oil and oil products. Now water of the Turaevka and the Kamenka rivers contains saturated and unsaturated hydrocarbons, hydrocarbon acids, ethers, alcohols, and halogenated derivatives. The bottom of the rivers are covered with a thin layer of dark brown oil tar for tens of meters downstream from their discharges from the rocks, and sub-aquial springs in the riverbeds periodically discharge.

A strong smell of hydrogen sulfide comes from the water of these rivers, as well as the deposition of elemental sulfur covers the underwater part of the river plants.

In our opinion, these features indicate the development of bacterial sulfate-reducing process where oil hydrocarbons serve as carbon and energy sources to bacteria. So, there is natural bioremediation process developed under anaerobic environmental conditions. These conditions established in the underground part of riverbeds after the depletion of water-dissolved oxygen in oxidative processes. The product of bacterial sulfate-reducing process, hydrogen sulphide, is very toxic to river fauna, but readily oxidizable on air. The product of hydrogen sulphide oxidation is elementary sulphur undissolved in water. Therefore we recommended construction of oxidizing and precipitating ponds downstream of the rivers' discharges from the rocks to improve the environment.

#### 5 Conclusion

Karst territories occupy approximately one third of the Earth surface. Karst rocks and water are weakly protected from any pollution, including from the surface. The remediation of karst territories is often technically difficult and expensive.

Karst rocks and water contain natural bacterial populations, which could degrade a great number of various

pollutants. The most common pollutants of karst rocks and water are hydrocarbons and other compounds of oil especially in oil industry regions.

As natural bacterial populations can degrade oil and oil products both in aerobic and anaerobic conditions, environment oil pollution of any origin—natural, man-made or both—could cause the activation of aerobic or anaerobic microflora of water and rocks. So, this capability of natural bacteria could be used in bioremediation technologies. However, some products of these bacterial processes could be environmentally toxic, therefore thorough study of environment conditions and engineering of additional measures could be needed.

Authors studied two sites of oil polluted karst territories of the Perm region (the Western Urals, Russian Federation). Aerobic bacterial degradation of oil products occurred at the first studied site and anaerobic one at the second site. The complex method of mechanical and biotechnological remediation of the first site was elaborated: a bulk of oil was eliminated with pumping; natural hydrocarbon-oxidizing bacterial populations were stimulated with inorganic nutrients supplies; hydrocarbon-oxidizing bacteria were isolated and bacterial preparation was made and applied to achieve complete oil removal. Recommendations on engineering of additional constructions were made to improve the environment at the second studied site.

**Acknowledgements** Work was financially supported by the RFBR (project 16-35-00104 mol\_a).

## References

- Aitken, C.M., Jones, D.M., Maguire, M.J., Gray, N.D., Sherry, A., Bowler, B.F.J., Ditchfield, A.K., Larter, S.R., Head, I.M.: Evidence that crude oil alkane activation proceeds by different mechanisms under sulfate-reducing and methanogenic conditions. *Geochim. Cosmochim. Acta* **109**, 162–174 (2013)
- Callaghan, Amy V., Tierney, M., Phelps, C.D., Young, L.Y.: Anaerobic biodegradation of n-hexadecane by a nitrate-reducing consortium. *Appl. Environ. Microbiol.* **75**(5), 1339–1344 (2009)
- Dawn, H.E., Rizzo, C., Smith, J.A., Lovley, D.R.: Anaerobic Oxidation of Benzene by the hyperthermophilic archaeon *Ferroglobus placidus*. *Appl. Environ. Microbiol.* **77**(17), 5926–5933 (2011)
- Dorota, W., Borkowski, A.: The geomicrobiological role of sulphate-reducing bacteria in environments contaminated by petroleum products. *Geomicrobiol. J.* **24**(7–8), 599–607 (2007)
- Gorbunova, K.A., Andreichuk, V.N., Kostarev, V.P., Maximovich, N. G.: Karst and caves in Perm region. Perm University Publishing House, Perm, 200 p. (1992) (in Russian)
- Koronelli, T.V.: The principles and methods of intensification of biological degradation of hydrocarbons in environment (review). *Appl. Biochem. Microbiol.* **32**(6), 579–585 (1996) (in Russian)
- Maximovich, N.G., Khmurchik, V.T.: Groundwaters clarification experience from oil pollution by biological methods. *Ind. Saf. Ecol.* **4**(37), 34–36 (2009)
- Milanovic, P.T.: Geological in Karst: dams, reservoirs, grouting, groundwater protection, water tapping, tunneling. Zebra, Belgrad, 347 p. (2000)
- Pecherkin, I.A.: Geodynamics of the coasts of the Kamsky reservoirs, vol. 2. Geological processes, Perm, 308 p. (1969) (in Russian)
- Rabus, R., Wilkes, H., Behrends, A., Armstroff, A., Fischer, T., Pierik, A.J., Widdel, F.: Anaerobic initial reaction of n-alkanes in a denitrifying bacterium: Evidence for (1-methylpentyl) succinate as initial product and for improvement of an organic radical in n-hexane metabolism. *J. Bacteriol.* **183**(5), 1707–1715 (2001)

# The Influence of Technogenic Factors on the Intensification of Karst on the Eastern Slope of the Urals in Russia

S. N. Elokhina and S. V. Gorbova

## Abstract

This article deals with two aspects of increased karst risk, at the border of Europe and Asia, caused by the processes of leaching and dissolution of rocks. Their activation and occurrence enhance under man-made conditions, including in areas of mining. Territories refer to the first group in limits karst rocks, where technical activization of a karst is created by the following technical factors: chemical, geodynamic, mechanical and hydrodynamic. The territories of the second group are not associated with natural karst rocks. Here, the processes of dissolution and leaching of rocks occur outside the zone of development of karst rocks in various subsurface and surface cavities flooded with groundwater in the post-operational period of mining production. Similarly to karst massifs, under certain conditions, an outflow of mine waters is formed from flooded mine workings, similar to karst siphon springs, with increased salinity, and other parameters. The activity of destruction and offset mineral components exceed natural conditions by 1–2 order, according to the analysis of leachings with sulphuric acid.

## Keywords

Karst • Karst risk • Mining activities • Ural region of Russia

## 1 Introduction

In Russia, karstic rocks occupy 66.5% of the territory. When mapping emergency situations, karst processes are not considered as extremely dangerous (catastrophic), although 13%

S. N. Elokhina (✉) · S. V. Gorbova (✉)  
 FBGU “Hydrospetsgeology”. Branch of the Ural Regional Center  
 of the State Mining Inspectorate, Yekaterinburg, Russia  
 e-mail: Elokhina.s@mail.ru

S. V. Gorbova  
 e-mail: Gorbova@gmsn-ural.ru

of karst areas are in the zone of destructive, 17%—dangerous, 70%—locally dangerous natural and technogenic phenomena (Dublynsky and Dublyanskaya 1992).

Increase of anthropogenic load on karst territory leads to technogenic activation of the process. We are studying the karst of a part of the Trans-Ural karst province, where the karstic rocks are represented by carbonate deposits of the lower and middle Carbon. Figure 1 shows this area as zone V.

For the first time the karst regionalization of the Urals was carried out in 1958 by Maksimovic (1968). In 1960, according to the results of detailed studies, the zoning of the Eastern slope of the Middle Urals was supplemented by Gevierts (1960). The zoning is based on tectonic, geomorphological and climatic features, the lithological composition of the karst rocks, the age and morphology of the karst.

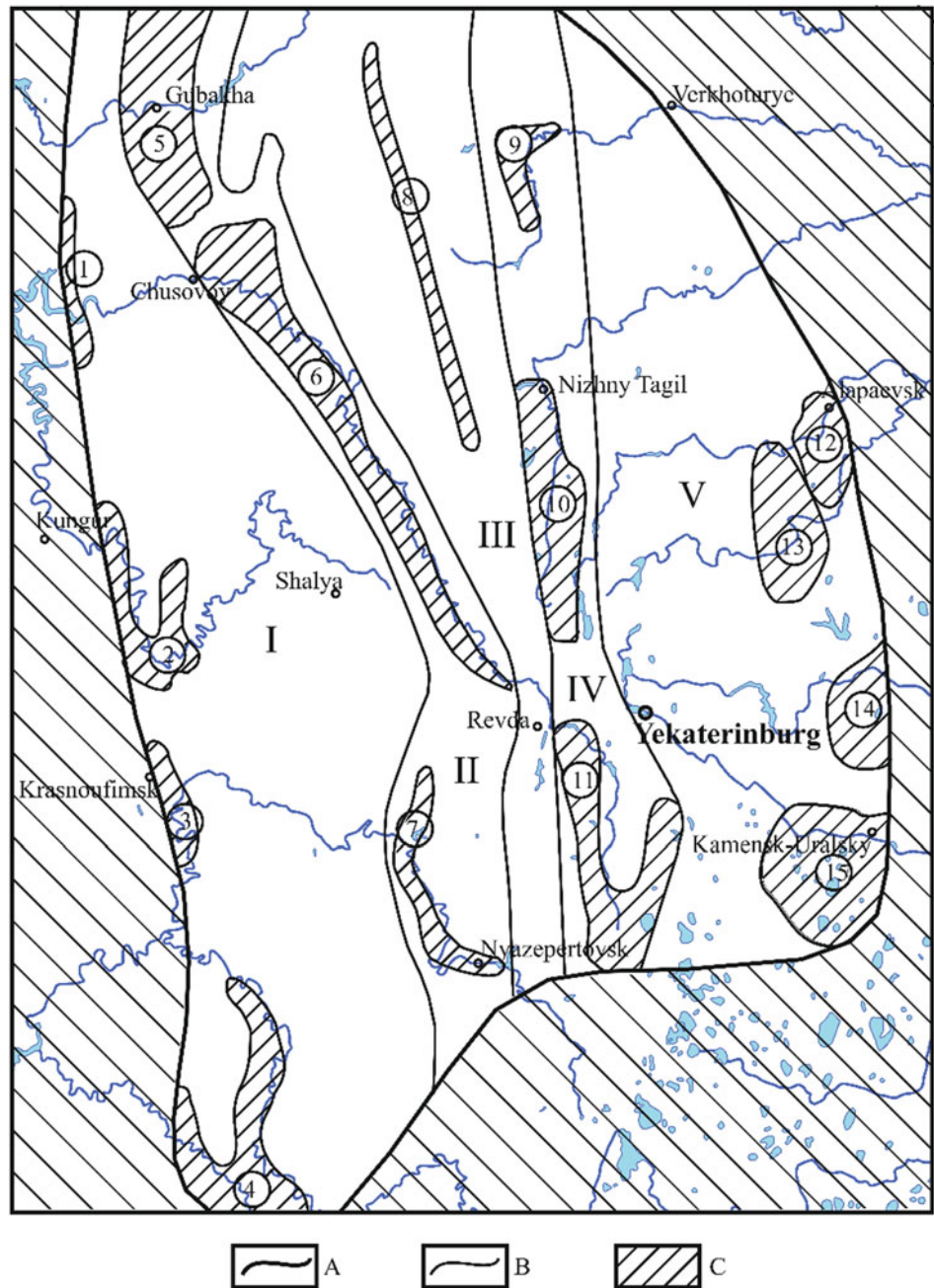
## 2 Regularities of Karst Development in the Study Area

The main revealed patterns of karst development on the eastern slope of the Urals are as follows:

1. Depending on paleoclimatic and tectonic conditions, two main periods of active development of karst are distinguished. The first epoch (C<sub>2</sub>–K<sub>2s</sub>) includes two stages: the Middle Carboniferous and Middle Jurassic—the beginning of the Upper Cretaceous. In the second epoch (P–Q), two stages are also singled out up to the present day: Oligocene and Pliocene. The most active and long stage of karst formation was a period corresponding to the time of the Middle Jurassic—the beginning of the Upper Cretaceous.
2. The ancient karst is located under loose sediments of the Quaternary age, therefore it is expressed only in the relief of the roof of the Paleozoic basement. It is represented by funnels made by Late Mesozoic continental deposits overlain by marine sediments of the Upper Cretaceous–Paleogene.



**Fig. 1** Scheme of karst regionalization of the Middle Urals



A - the boundary in the middle Urals karst region; B - the boundaries of karst provinces;  
C - the karst areas of the Middle Urals

I - Ural karst province (areas: 1 - Kulikovskiy, 2 - Sylvanskiy, 3 - Krasnoufimskiy, 4 - Isco-Yuryuzanskiy); II - karst province Western slope (areas: 5 - Kizelovskiy, 6 - Pashijsko-Chusovskiy, 7 - Ufa-Serginskiy); III - the Central Urals karst province (areas: 8 - Koivo-Serebryanskiy); IV - the karst province of the Eastern slope (areas: 9 - Verkhne-Turinskiy, 10 - Tagilo-Nevyanskiy, 11 - Top-Chusovskiy); V - Trans-Ural karst province (areas: 12 - Alapaevskiy, 13 - Rezhhevskiy, 14 - Sukholovskiy, 15 - Kamenskiy)



3. The development areas of the Mesozoic karst were superimposed on the Paleozoic karst. The karst is confined to the Oligocene river valleys and is represented by karstic funnels filled with Oligocene continental sediments, often covered by younger covering formations.
4. Karsting rocks are represented by carbonate sediments of the lower and middle carbon. In different stratigraphic subdivisions, carbonate rocks differ in color, texture-structural features, quality and quantity of organogenic detritus, species composition and proportion of organic residues, different intensity of dolomitization and silicification processes, as well as secondary changes (recrystallization, calcification), which causes their different susceptibility to karst processes, creating differences in the degree of karstological danger.
5. Theoretically, high carbonate sediments with insignificant content of insoluble residue have a higher ability for karst formation. However, the analysis of the karst formation of the carbonate strata in deposits of carbonate raw materials in the Bogdanovich region showed that all varieties of limestone are crusted to approximately the same extent and the lithological factor is not clearly manifested in conditions of a thick strata of carbonate rocks (Ford and Williams 2007; Gorbova 2006).
6. The degree of watering of carbonate massifs determines the possibility of karst development. The location of carbonate rocks in the form of strips of meridional strike with a common latitudinal direction of flow of underground and surface waters, facilitates the interception and accumulation of surface and underground runoff. As a whole, for the eastern slope of the Urals, the karst is characterized as an ancient decaying one, but in some areas, despite the mild and sometimes cold climate of the 4th stage, the karst development continues.
7. The activity of the karst process is determined by the presence or absence of an equilibrium between groundwaters and limestones, which can be estimated by the method of Savarensky (1995). For example, groundwater from wells in the Sukholozhsko-Kamensky karst area is aggressive with respect to karstic rocks, the lack of water saturation with calcium carbonate is from 0.035 to 0.078  $\mu\text{-eq/dm}^3$  (Gorbova 2006). Virtually all groundwater in karst aquifers is characterized by increased rigidity and the presence of a noticeable amount of suspended matter.
8. Complex tectonic structure, fragmentation and fissuring of rocks contributed to the penetration of surface waters into significant depths and intensive development of karst in the past geological epochs. In the Sukholozhsko-Kamensky region, many of the known karst forms have been drilled, such as funnels, karst-erosion logs, caves, buried poles and paleoclastic remains and ridges, as well as zones of destroyed rocks, cavities and cracks expanded by karst, etc. (Gorbova 2006).
9. The most common type of surface karst are funnels. In the microdistrict 13-a city of Kamensk-Uralsky, their number reaches 12–15 per 1 km<sup>2</sup>. To the north of Bogdanovich on an area of 12 km<sup>2</sup>, more than 160 karstic manifestations have been identified, which makes up density of 13.3 karst forms per 1 km<sup>2</sup>. Funnels are concentrated along the zones of increased fracturing, faults, contacts of limestones with terrigenous rocks, in valleys of rivers. It was established by the detailed research on Kamensky site (Gorbova 2006), that the leading factor in formation and development of karst cavities was tectonic fracturing.
10. In the massif of carbonate rocks of the Kamenskoye and Bogdanovichsky sections of detailed studies based on drilling data (Gorbova 2006), underground disturbances (buried funnels, filled, partially filled and unfilled cracks and cavities), as well as intermediate cavities in the covering deposits, representing a potential natural hazard were uncovered (Fig. 2). In the structure of the sandy-argillaceous strata covering the carbonate rocks, traces of repeated deformations in the form of a sharp decrease in their thickness, as well as complete absence of the underlying layer above the karst cavities in some places were revealed.

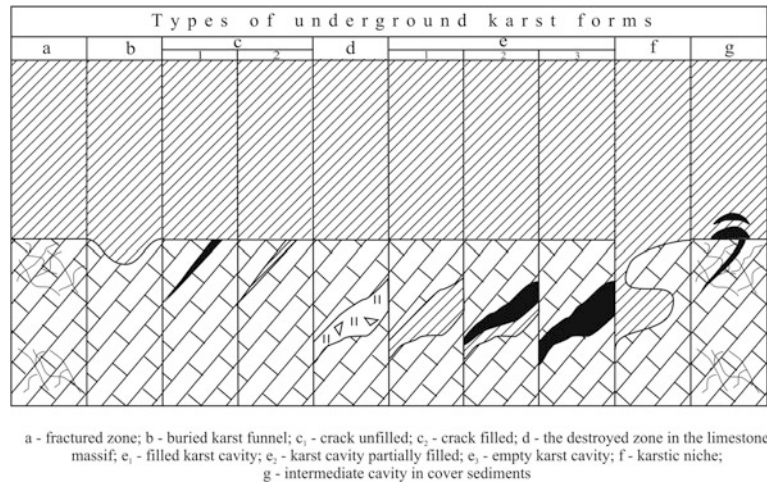
### 3 Technogenic Activation of Karst Process

In the era of technogenesis, the processes of dissolution and leaching of rocks (karst) have not only natural but also technogenic origin, expanding the areas of karst damage. As a result, karst and karst-like forms occur outside the natural provinces of the active natural karst process. Examination of the activation of karst processes in the considered territory of the Urals allows to highlight the main triggering factors. They make up two large groups.

Group I—technogenic activation of the natural karst process, which occurs only within the boundaries of karst rocks (Elokhina and Elokhin 2014). There are four factors that determine the technogenic activation of this process:

I-1. Chemical, i.e. agents of technogenic origin, entering the area of development of karst rocks, first, due to leaks from surface objects (slurry accumulators, pulp pipelines, etc.) enriched with acids or other active substances; secondly, by infiltration of contaminated atmospheric and surface waters (for example, acid rains).

**Fig. 2** Types of underground karst forms on the Kamensky site



**Fig. 3** Karst failure on 1914 km of the Bogdanovich-Pyshminskaya railroad of the Sverdlovsk Railway, August 22, 2001



I-2. Geodynamic, arising, for example, as a result of vibration (movement on railways and roads, construction, etc.) (Fig. 3) (Gorbova 2006).

I-3. Mechanical, disrupting the continuity of the rock massif, for example, by means of mine workings, which leads to activation of the access of leaching and dissolution agents to new rock surfaces, and to an increase in the rate of subterranean flow, and the like. For example, at mining facilities in the Urals (Elokhina 2013).

I-4. Hydrodynamic, associated with a sharp change in pressure gradients in the underground flow, including the change in the marks of the erosion base (Elokhina 2013), as well as the

violation of surface runoff and the creation of foci of concentrated infiltration in the reserves of linear structures (Fig. 4).

Group II—the formation of new technogenic karst-like forms on the area of development of rocks that are not subjected to karst in natural conditions. Such manifestations of man-made forms are the result of leaching and dissolution of rocks in artificial underground and surface cavities at the passive stage of mining technogenesis (Elokhina 2013), collapse and subsidence of the roof of underground excavations with the formation of a special terrain (Fig. 5).

Technogenic cavities represent different kinds of mining: vertical, horizontal, etc., most often interconnected. Under



**Fig. 4** Karst-suffusion failure on the 8th kilometer of the road Bogdanovich—Sukhoy Log



**Fig. 5** Failure over the mine field of the Krylatovsky mine, Sverdlovsk region



certain conditions, the spilling of mine waters from flooded excavations to the surface of the earth, similar to karst siphon sources, is formed. In some areas, for example, at pyrite deposits, acidic mine waters with different from natural conditions parameters are formed. For example, it has been established on a number of objects in the Urals that the activity of sulfuric acid leaching at the passive stage of technogenesis (after flooding of mines) is approximately one or two orders higher than under natural conditions and is accompanied by an increase in the concentration of suspended solids, total hardness, total salt content, as it was described above, which is typical for the sites with the

development of a natural karst process. The underground component of the water balance of the flooded mines is also increasing, which approximates the natural non-karst massifs of rocks to karst.

---

## 4 Conclusion

Thus, technogenesis changes the level of karst risk associated with the threat of formation of dips, and requires mandatory consideration of man-made factors in its assessment, even beyond the limits of the development of karst rocks.

## References

- Dublyansky, V.N., Dublyanskaya, G.N.: Mapping, Regionalization, and Engineering Geological Assessment of Karstified Terrains, Novosibirsk (in Russian) (1992)
- Elokhina, S.N.: Hydrogeological consequences of mining technogenesis in the Urals. Ekaterinburg: LLC "UIPTs", 187 p (2013)
- Elokhina, S.N., Elokhin, V.A.: Natural-technogenic geological processes in the underground spaces of the flooded Ural mines// "Complex use and protection of underground spaces"—Sat. reports of the International. scientific-practical. conf., dedicated to the centenary of the scientific and tourist-excursion activities in the Kungur Ice Cave and the 100th anniversary of the birth of V.S. Lukin (May 26–31, 2014). GI UB RAS: Perm, pp. 310–316 (2014)
- Ford, D., Williams, P.: Karst Hydrogeology and Geomorphology. Wiley, The Atrium, Southern Gate, Chichester, West Sussex PO19 8SQ, England, 578 p (2007)
- Gevirts, M.I.: Zoning of the Karst of the Eastern slope of the Middle Urals. Reports of the Perm Department of the Geographical Society of the USSR, Vol. 1, No. II–IV. Perm (1960)
- Gorbova, S.V.: Carbonate Karst of the Sukholozhsko-Kamensky District (Eastern slope of the Middle Urals). Thesis for the degree of candidate of geological and mineralogical sciences. Ekaterinburg: UGGGA (2006)
- Maksimovich, G.A., Kostarev, V.P.: The Karst of Ural and Transurals// Materials of the All-Urals Meeting. Perm (1968)
- Savarensky, I.A.: Mironov NA guide to engineering and geological surveys in the areas of karst development, p. 165. PNIIS, Moscow (1995)

# The Effectiveness of an Inverse Wenner-Schlumberger Array for Geoelectrical Karst Reconnaissance, on the Swabian Alb High Plain, New Line Wendlingen–Ulm, Southwestern Germany

Constantin Prins, Kurosch Thuro, and Michael Krautblatter

## Abstract

On the Swabian Alb high plain, new line Wendlingen–Ulm, southwestern Germany, 2D electrical resistivity tomography (ERT) measurements were performed during construction at the excavation bottom level in addition to the standard investigation program (including microgravimetric and seismic methods) to test the effectiveness of an inverse Wenner-Schlumberger array for exploring geological defective karst voids and other karstic features in a highly heterogeneous karstic environment. The 2D ERT survey (ABEM Terrameter SAS 4000, inverse Wenner-Schlumberger array, 2.0 m electrode spacing, roll-along technique, robust inversion, RMS error: 1.61% for a maximum of 5 iterations) provided a high-resolution image of the subsurface, revealed the size, shape and spatial distribution of conductive clayey/loamy deposits (<60  $\Omega\text{m}$ ) and delineated them from an intensely fractured and/or highly weathered limestone bedrock (60–240  $\Omega\text{m}$ ), respectively. In addition, the 2D ERT profile indicated several resistive zones of moderately fractured and/or medium weathered limestone bedrock (240–960  $\Omega\text{m}$ ) as well as the general absence of intact limestone bedrock (>1000  $\Omega\text{m}$ ) and air-filled voids (>2000  $\Omega\text{m}$ ). These observations were confirmed by extensive direct probing investigations (1 exploration drilling, 4 core drillings, 19 destructive drillings, 2 trial pits). Moreover, the 2D ERT data coincided with the microgravimetric and seismic results of the previously conducted standard investigation program to a high degree. The exact spatial distribution with depth as well

as the internal structure of the detected anomalies (clayey/loamy deposits, moderately fractured and/or medium weathered limestone bedrock) could, however, only be obtained from the 2D ERT data. The 2D ERT measurements conducted with an inverse Wenner-Schlumberger array provided a decisive contribution to karst reconnaissance in a highly heterogeneous karstic environment like the Swabian Alb high plain, on the new line Wendlingen–Ulm.

## Keywords

Karst • Limestone • Drilling • Electrical resistivity tomography (ERT) • Inverse Wenner-Schlumberger array • Microgravimetry • Seismics

## 1 Introduction

The new line from Wendlingen to Ulm, part of the new trans-European Main Line from Paris to Budapest, is presently under construction. This new line is designed for running speeds of up to 250 km/h and has a total length of approximately 60 km with about 50% running through tunnel constructions (Kielbassa et al. 2015a: 27). One significant project section on the new line is the PFA 2.3 Alb high plain, which ranges from line km 53 + 811 near Hohenstadt over Merklingen and Temmenhausen to line km 75 + 250 near Dornstadt (Fig. 1). The approximately 21.4 km long Alb high plain is mainly characterized by open-air line and smaller tunnels. The excavation bottom level on the Alb high plain is predominantly situated in limestones of the Upper Jurassic, which are primarily affected by karstification and can be classified as slightly to heavily karstified (Kielbassa et al. 2015b: 130f.). In order to determine the dimension of karstification of the Alb high plain, comprehensive, independent and complementary indirect geophysical investigations including microgravimetric and seismic methods were previously conducted at

C. Prins (✉) · K. Thuro · M. Krautblatter  
Department of Civil, Geo and Environmental Engineering, Chair of Engineering Geology, Technical University of Munich, Munich, Germany  
e-mail: constantin.prins@mytum.de

K. Thuro  
e-mail: thuro@tum.de

M. Krautblatter  
e-mail: m.krautblatter@tum.de



the excavation bottom level (Kielbassa et al. 2015b: 132f.). In the course of the present research study, 2D electrical resistivity tomography (ERT) measurements conducted with an inverse Wenner-Schlumberger array were performed in addition to the standard investigation program to explore geological defective karst voids and other karstic features including (i) their geometry (size, shape, spatial distribution) and (ii) their type of filling (non, partially or almost completely filled with soil material and/or water). The 2D ERT results were subsequently compared with the results of the previously conducted microgravimetric and seismic methods. Direct probing investigations (1 exploration drilling, 4 core drillings, 19 destructive drillings, 2 trial pits) served for calibration and discussion.

## 2 Methodology

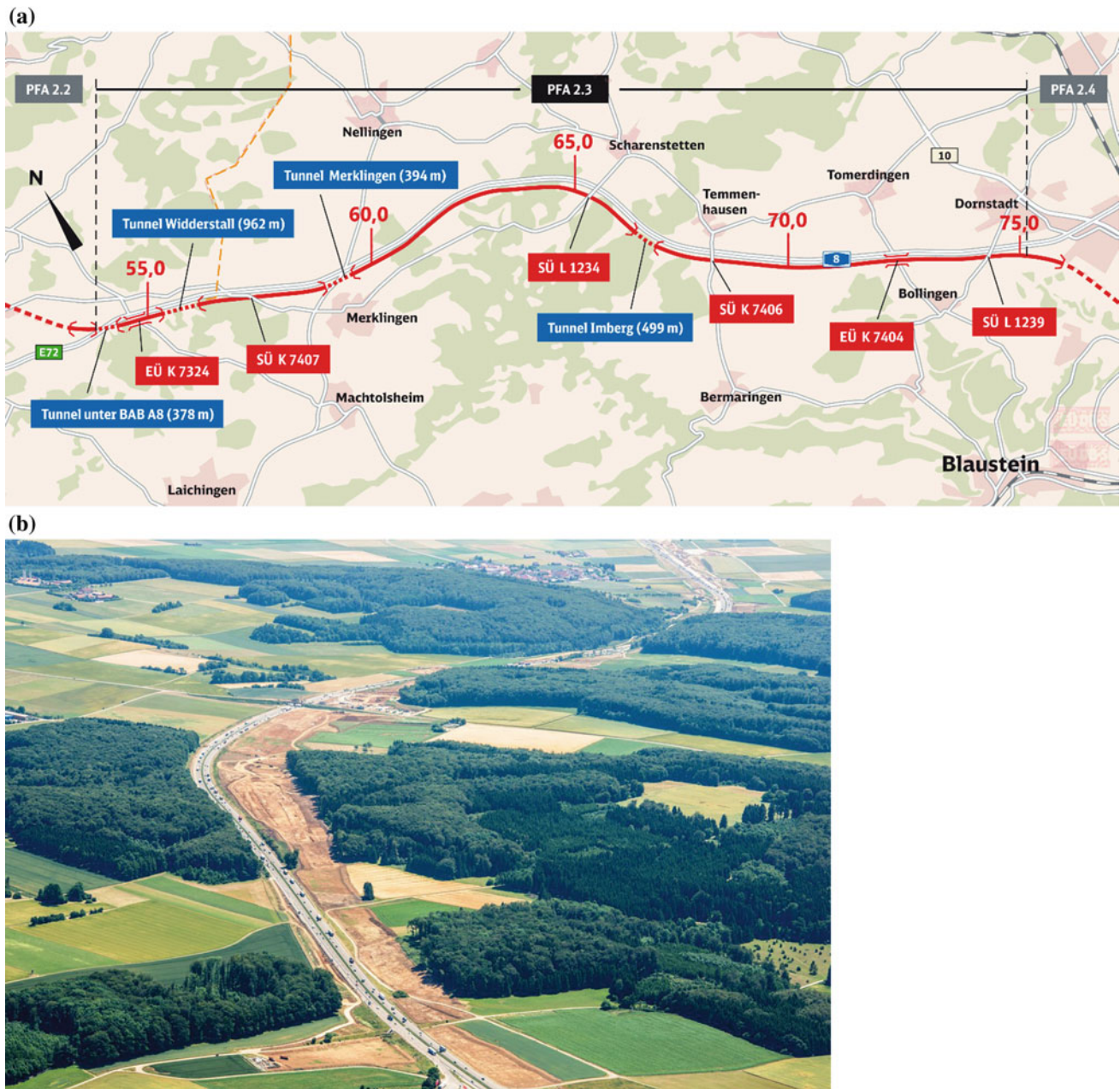
The purpose of geoelectrical resistivity measurements is to determine the resistivity distribution in the subsurface. By introducing an artificial current into the ground via point electrodes, the potentials at other electrodes (geometrically arranged) can be measured and the effective or apparent resistivity of the subsurface can be derived. By using a controlled source of specific dimensions, quantitative results are obtained.

In carbonate karst terrains, geoelectrical imaging methods are routinely used to characterize the (for common) highly heterogeneous subsurface, inter alia composed of undisturbed soils, carbonate rock, clay in-fills and air-filled voids, all generally characterized by very different resistivity values. Clays and clayey deposits/infills tend to retain moisture and generally show a comparatively high ion concentration to conduct electricity; they are usually characterized by low resistivities (less than 100  $\Omega\text{m}$ ), with variable resistivity values depending on moisture content, purity and unit shape/size (Ismail and Anderson 2012: 282, 291; Telford et al. 1990: 283ff.; Zhou et al. 2000: 761). Residual soils are typically characterized by intermediate resistivities (between 25 and 600  $\Omega\text{m}$ ), with variable resistivity values depending on clay and moisture content (Ismail and Anderson 2012: 282). Weathered to intact carbonate rock is generally characterized by higher resistivities (typically more than 400  $\Omega\text{m}$ , but variable depending on layer thickness, moisture content and impurities) (Ismail and Anderson 2012: 282). Relatively intact carbonate rock in general has a significantly higher resistivity than clayey soils due to its much smaller primary porosity and fewer interconnected pore spaces; it is characterized by high resistivities (typically

more than 1000  $\Omega\text{m}$ , but again variable depending on layer thickness, moisture content and impurities) (Ismail and Anderson 2012: 291; Telford et al. 1990: 283ff.; Zhou et al. 2000: 761). Dry air-filled voids (such as fractures, conduits and cavities) always provide a significant resistivity contrast between the void and the surrounding host rock; they are generally characterized by very high resistivities (typically more than 2000  $\Omega\text{m}$ ), depending on the conductivity of the encompassing material and the size/shape of the void (Ismail and Anderson 2012: 282; Kidanu et al. 2016: 107; Yassin et al. 2014: 71).

The acquisition system used for the 2D ERT survey was composed of an ABEM Terrameter SAS 4000, an ES10-64C electrode selector and 41 electrodes in one layout. The survey contained one 320 m long section (2.0 m inter-electrode spacing) along the southwestern line track (direction Stuttgart to Ulm). Electrode locations/elevations were obtained by differential GPS measurements. An inverse Wenner-Schlumberger electrode array was applied. The only significant disadvantage of this array in comparison to the standard Wenner-Schlumberger array is the increased telluric noise/the possibly minimized resolution at large potential electrode spacings. This might be the reason why the inverse Wenner-Schlumberger array is yet very rarely used for karst reconnaissance, although it can be applied in a multi-channel system and thus reduces the survey time significantly. The inverse Wenner-Schlumberger protocol used and exhibited in this paper totaled 2516 measurement points. The acquisition time was 0.5 s and the delay time was 0.3 s. The injection intensity ranged between 100 and 200 mA according to the ground resistance. During acquisition, the measurement was stacked until two times.

The 2D apparent resistivity pseudosections were matched using a finite-difference forward modeling subroutine and inverted with a non-linear least-squares optimization technique (Degroot-Hedlin and Constable 1990; Loke and Barker 1996). The 2D finite-element inversion program RES2DINV ver. 3.54 (Loke and Barker 1996; Loke 2004) was used to automatically subdivide the subsurface into a large number of rectangular cells of calculated apparent resistivity values (with dimensions in the order of the electrode spacing). RES2DINV iteratively changed the resistivity of the model cells in order to minimize the difference between the measured and calculated apparent resistivity values; this difference was quantified by the Root-Mean-Square (RMS) error, respectively. Only a few bad datum points were gradually removed and model cells with widths of one unit electrode spacing were used. Further model refinements (meaning the use of model cells with widths of

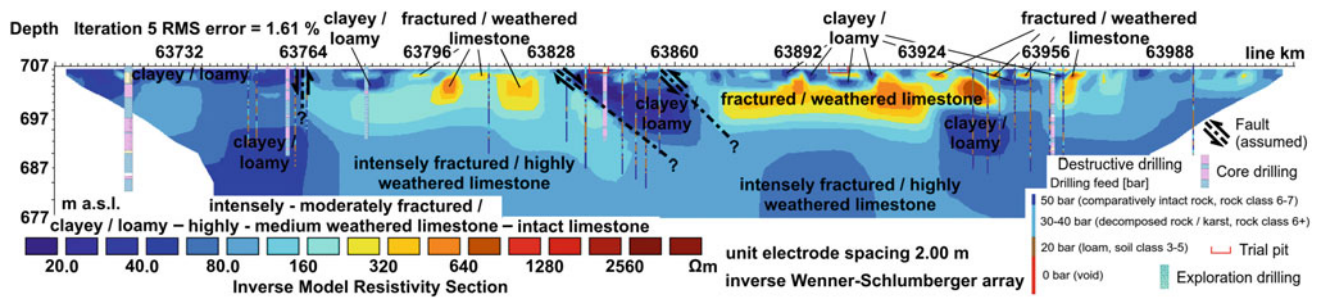


**Fig. 1** **a** Overview of the PFA 2.3 Alb high plain, **b** Aerial photograph, 2nd line section, view from Merklingen to Temmenhausen (DB Projekt Stuttgart–Ulm GmbH © 2014/2015)

half the unit electrode spacing) were not applied, because this approach produced small near-surface artifacts, which significantly disturbed the data set. In comparison with the smoothness-constrained least squares method (L2-norm criterion) (Degroot-Hedlin and Constable 1990), the robust inversion routine (L1-norm criterion) (Farquharson and Oldenburg 1998; Loke et al. 2003) yielded consistently more accurate results with lower RMS errors and, therefore, was used to invert the acquired resistivity data.

### 3 Results and Discussion

The 2D ERT results are shown with the used electrode array, the number of iterations required for the solution and the RMS error (Fig. 2). The used inverse Wenner-Schlumberger array (2.0 m inter-electrode spacing) allowed an investigation depth of up to 30 m. The average RMS error was 1.61% after 5 iterations.



**Fig. 2** Interpreted 2D ERT results, obtained from the 320 m long profile along the southwestern line track (direction Stuttgart to Ulm). Directly adjoining exploration drillings, core drillings, destructive

drillings (indicating the drilling feed) and crossing trial pits were incorporated onto the ERT section

Numerous near-surface and a few deep-reaching, spatially limited conductive zones with low resistivity values ( $<60 \Omega\text{m}$ ) are indicated in the 2D ERT section. These conductive zones were interpreted as clayey/loamy deposits, whose existence could subsequently be confirmed by visual inspection of the excavation bottom level and by directly adjoining boreholes (3 core drillings, 13 destructive drillings). These conductive zones were distinguishable from the more resistive surrounding with resistivity values ranging from 60 to  $240 \Omega\text{m}$ , respectively. In conjunction with the available borehole and trial pit investigations, this more resistive environment could be assigned to an intensely fractured and/or highly weathered limestone bedrock. Its comparatively low resistivity values were most probably caused by frequently recurring clayey/loamy (and thus conductive) fracture and void infillings with increasing depth, as indicated by the superimposed borehole logs; these observations also coincide with the results presented by Ismail and Anderson (2012: 287f.) and Prins et al. (2017: 376). Only in areas where the limestone bedrock is of high quality (i.e. with very few fractures/unweathered), the ERT section would show a continuing increase in resistivity with depth (Roth et al. 1999: 299). Several resistive zones in the shallow subsurface ( $<10 \text{ m}$ ) with resistivity values between 240 and  $960 \Omega\text{m}$  could be delineated from the surrounding and were interpreted as moderately fractured and/or medium weathered limestone bedrock, respectively; 5 destructive drillings subsequently served as a confirmation. The resistivity data suggested the general absence of intact limestone bedrock and air-filled voids (which would have been indicated by resistivity values of typically more than 1000 and  $2000 \Omega\text{m}$ ), which was in accordance with the borehole logs. The depth to intact, largely unweathered limestone bedrock could thus not be derived from the resistivity results.

As illustrated above, the 2D ERT data generally agreed with the results gathered from the direct probing investigations. Only directly adjoining borings (less than 2.5 m for exploration and core drillings/less than 1 m for destructive

drillings) and crossing trial pits were superimposed on the ERT section and used for interpretation. In a highly heterogeneous karstic environment, however, drilling only a few decimeters apart can easily result in a completely different borehole record. On a few locations, the drilling and resistivity data disagreed, which might at least partly be caused by the distance between a drilling location and the ERT profile, respectively.

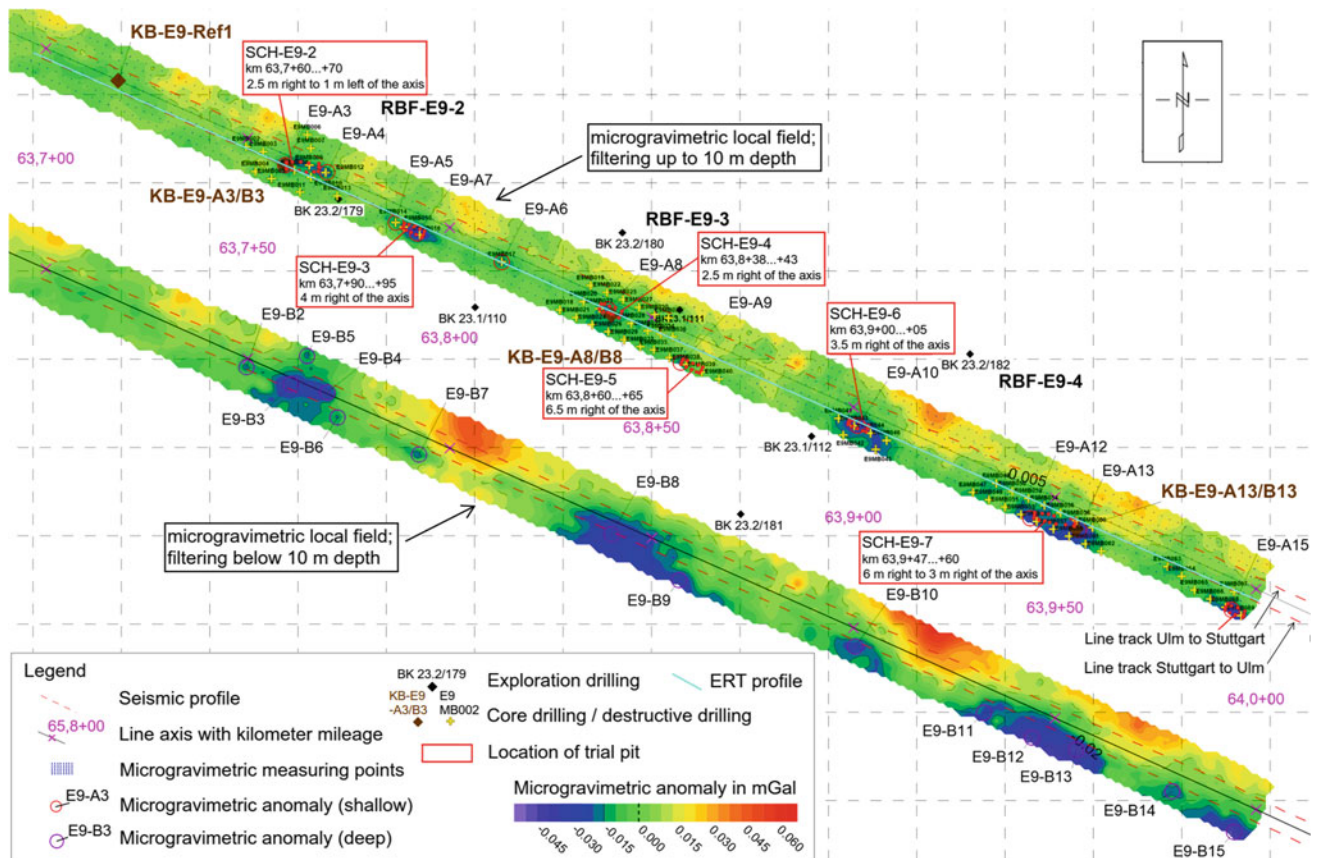
- (i) Between line km 63 + 740 and 63 + 765, the 2D ERT survey was not able to reveal an intensely fractured and/or highly weathered limestone bedrock (rock class 6, DIN 18300), which was subsequently exposed by 1 core drilling and 4 destructive drillings below a depth of approximately 15 m. This divergence was most probably caused by frequently recurring clayey/loamy (and thus conductive) fracture and void infillings with increasing depth, reducing the apparent resistivity values significantly (Prins et al. 2017: 376).
- (ii) Occasionally occurring, very gravely to very cobbly layers/limestone fragments within the conductive clayey/loamy deposits were detected in 4 of 4 core drillings. They may explain the partly increased resistivity values of the clayey/loamy deposits of up to  $160 \Omega\text{m}$  and thus the deviation between the drilling and resistivity data on a few drilling locations; these observations coincide with the remarks given by Roth et al. (2000: 362).
- (iii) At line km 63 + 958, 1 core drilling encountered an air-filled void between a depth of approximately 696.5 and 697 m a.s.l. ( $\sim 10 \text{ m}$  below the excavation bottom level), which was not shown in the 2D ERT profile; an air-filled void on a scale too fine to be resolved with the used inter-electrode spacing of 2.0 m.
- (iv) Between line km 63 + 937 and 63 + 944, 3 destructive drillings disagreed with the resistivity data at a depth of approximately 4–8 m below the excavation



bottom level. While the destructive drilling results suggested the presence of clayey/loamy deposits by drilling feeds of less than 20 bar, the 2D ERT profile indicated the existence of a moderately fractured and/or medium weathered limestone bedrock by resistivity values between 240 and 960  $\Omega\text{m}$ . It is believed that the destructive drillings entered narrow soil-filled fractures within the limestone bedrock, which did not show up in the 2D ERT profile. Local small-scale irregularities are often obscured by the volume-averaging method inherent in the ERT technique and boring data, in general, are spatially much more localized than the apparent resistivity data (Roth and Nyquist 2003: 6; Zhou et al. 2002: 926ff.). However, borings located in a fracture are often misleadingly be used to infer bedrock depths much greater than the average bedrock surface, whereas rock ledges/lenses might be interpreted as areas of shallow bedrock if they caused refusal of the drilling pipe (Ismail and Anderson 2012: 292; Roth et al. 2000: 362). In this context, it is also worth mentioning that the human operation of a drilling rig exerts a

considerable influence on the resulting boring data; a circumstance, which should not be neglected when interpreting (especially destructive) drilling records.

The microgravimetric results of the previously conducted standard investigation program coincides with the 2D ERT data to a great extent. The microgravimetry (Scintrex CG-5 Autograv Microgravity Meter, resolution: 0.005 mGal, nominal grid: 2 m, residual Bouguer gravity, error: 0.008 mGal) indicated the location, size and planar extent of five gravity lows (from  $-0.035$  to  $-0.015$  mGal) and two gravity highs ( $<+0.025$  mGal) (Fig. 3, ARGE NBS Wendlingen–Ulm 2017: 7ff.). While the gravity lows correlate with the conductive zones, interpreted as clayey/loamy deposits, the gravity highs correspond to the more resistive zones, interpreted as moderately fractured and/or medium weathered limestone bedrock, by means of 2D ERT, respectively. However, the exact spatial distribution with depth as well as the internal structure of these anomalies could only be obtained from the 2D ERT data. In addition, the microgravimetric survey alone was not able to clearly delineate compact rock from loosened zones (ARGE NBS



**Fig. 3** Microgravimetric results of the previously conducted standard investigation program (modified after ARGE NBS Wendlingen–Ulm 2017). The location of the 2D ERT profile, the seismic lines, the individual drillings and the trial pits can also be gathered from the figure

Wendlingen–Ulm 2017: 12). While the microgravimetric data suggested the presence of air-filled voids with dimensions of  $2.5 \text{ m} \times 2.5 \text{ m} \times 2.5 \text{ m}$  up to a depth of 5 m and air-filled voids with dimensions of  $5 \text{ m} \times 5 \text{ m} \times 5 \text{ m}$  up to a depth of 15 m (ARGE NBS Wendlingen–Ulm 2017: 13), the 2D ERT data, in contrast, suggested the general absence of air-filled voids, which was, as mentioned before, in accordance with the borehole investigations. This major difference might be caused by the fact that microgravimetry alone is often incapable of discriminating between an air-filled void and local bedrock loosening, both possibly producing very similar gravity anomalies (depending on the depth); microgravimetry is thus always interpreted with complementary geophysical (e.g. seismic) and/or boring data (ARGE NBS Wendlingen–Ulm 2017: 13; Goldscheider and Drew 2007: 182).

The seismic results of the previously conducted standard investigation program also coincides with the 2D ERT data to a high degree. The seismic profile along the southwestern line track (direction Stuttgart to Ulm) with combined high-resolution refraction/reflection seismics (Geometrics Geode 72-channel system, 4.5 Hz geophones, 2 m geophone spacing, 2 m shot spacing, source: 5 kg sledgehammer stroke with at least 3 individual hammer blows per shot location, vertical stacking used to enhance signal-to-noise ratio) divided the subsurface in an overlying, approximately 2–5 m thick, low velocity zone ( $v_p = 300\text{--}1000 \text{ m/s}$ ), an approximately 5–12 m thick, medium velocity transition zone ( $v_p = 1000\text{--}1700 \text{ m/s}$ ) and an underlying higher velocity zone ( $v_p = 1700\text{--}2600 \text{ m/s}$ ) (Fig. 4, ARGE NBS Wendlingen–Ulm 2017: 7f., 10ff.; Kielbassa et al. 2015b: 133). The overlying low velocity zone was interpreted as quaternary, highly cohesive loam deposit and/or completely weathered limestone bedrock (soil class 4/5, DIN 18300) (ARGE NBS Wendlingen–Ulm 2017: 11f., 26). In contrast to the 2D ERT profiling, the seismic data were thus not able to distinguish between highly cohesive loamy deposits and completely weathered limestone bedrock within the shallow subsurface (<5 m). This major difference might be caused by the fact that seismic refraction tomography exhibits only a moderate precision for subtle substrate changes and thus is limited in determining the internal stratification of overlying layers and in delineating smaller karst features from comparatively solid bedrock (Siart et al. 2011: 319, 331, 2013: 1141). The medium velocity transition zone was interpreted as medium to highly weathered limestone bedrock (rock class 6, DIN 18300), whereas the underlying higher velocity zone was interpreted as lowly weathered to intact limestone bedrock (rock class 7, DIN 18300) (ARGE NBS Wendlingen–Ulm 2017: 11f., 26). The  $v_p = 1000 \text{ m/s}$ -seismic line constituted the boundary between soil class 4/5 and rock class 6, even if in zones with a high degree of fracturing and/or void occurrences with mostly clayey/loamy infillings,

respectively, the rock class 6 could often only be found in depths with seismic velocities between  $v_p = 1350$  and  $1700 \text{ m/s}$  (ARGE NBS Wendlingen–Ulm 2017: 11f., 26). The  $v_p = 1700 \text{ m/s}$ -seismic line constituted the boundary between rock class 6 and 7 (ARGE NBS Wendlingen–Ulm 2017: 11f., 26), which was not in absolute accordance with the borehole logs. As was the case with the 2D ERT profiling, also the seismic survey had difficulties in showing the bedrock surface precisely. This inefficiency was also most probably caused by the frequently recurring clayey/loamy fracture and void infillings with increasing depth, reducing the seismic velocities significantly.

While the vertical seismic velocity gradient was weakly developed between line km 63 + 700 and 63 + 780 and between line km 63 + 830 and 63 + 860, it was moderately pronounced between line km 63 + 780 and 63 + 830 and between line km 63 + 880 and 64.0 + 20 (ARGE NBS Wendlingen–Ulm 2017: 11). While the lower seismic velocity gradients correspond to the conductive zones, interpreted as clayey/loamy deposits, the higher seismic velocity gradients correlate with the more resistive environment and the resistive zones, interpreted as moderately to intensely fractured and/or medium to highly weathered limestone bedrock, by means of 2D ERT, respectively. However, the exact spatial distribution with depth as well as the internal structure of these anomalies (clayey/loamy deposits, moderately fractured and/or medium weathered limestone bedrock) could again only be obtained from the 2D ERT data.

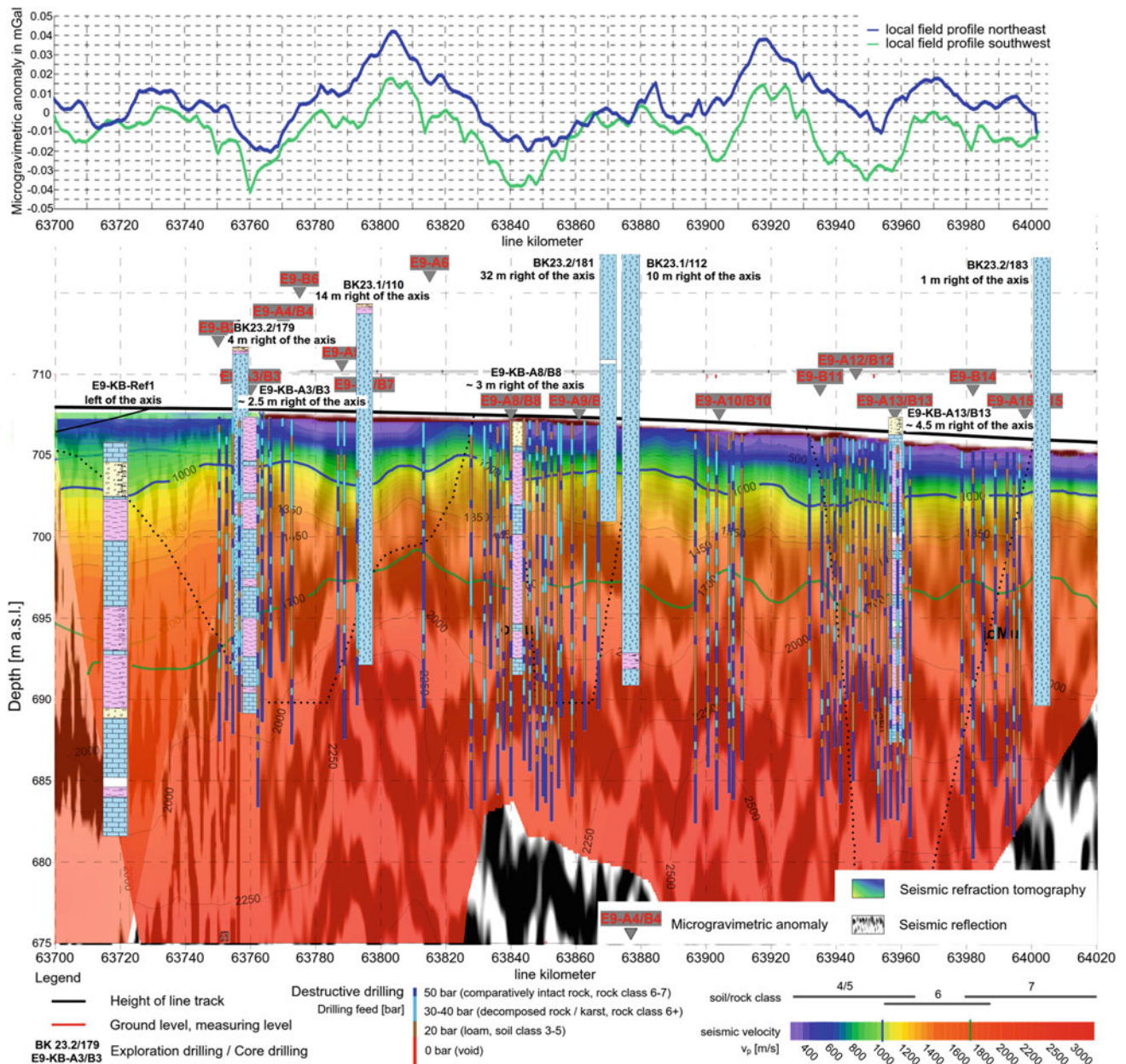
The seismic survey provided a heterogeneous subsurface image with frequently occurring, shallow karstic zones and only limited weathered bedrock occurrences, reaching near-surface areas (ARGE NBS Wendlingen–Ulm 2017: 15). While the microgravimetric data suggested the potential presence of air-filled voids by five gravity lows, the seismic as well as the 2D ERT survey, in contrast, suggested the general absence of air-filled voids (ARGE NBS Wendlingen–Ulm 2017: 17); only the latter was in accordance with extensive direct probing investigations (ARGE NBS Wendlingen–Ulm 2017: 21).

---

## 4 Conclusion

The 2D ERT survey conducted with an inverse Wenner-Schlumberger array provided a high-resolution, consistent and reliable image of the subsurface and revealed (i) numerous near-surface and a few deep-reaching, spatially limited conductive zones (<60  $\Omega\text{m}$ , interpreted as clayey/loamy deposits, existence confirmed by visual inspection of the excavation bottom level/3 core drillings/13 destructive drillings), (ii) a more resistive surrounding (60–240  $\Omega\text{m}$ , assigned to an intensely fractured and/or highly weathered





**Fig. 4** Seismic and microgravimetric results of the previously conducted standard investigation program (modified after ARGE NBS Wendlingen–Ulm 2017). Directly adjoining exploration drillings, core drillings and destructive drillings (indicating the drilling feed) are

incorporated onto the seismic section. Furthermore, a correlation between the drilling feed/seismic P-wave velocity and the associated soil/rock class is shown in the legend, respectively

limestone bedrock, in conjunction with borehole and trial pit investigations) and (iii) several resistive zones (240–960  $\Omega$ m, interpreted as moderately fractured and/or medium weathered limestone bedrock, existence confirmed by 5 destructive drillings). The 2D ERT data generally agreed with the results gathered from direct probing investigations. On the few locations, where the drilling and resistivity data disagreed, the divergences were explained and possible causes discussed. Moreover, the 2D ERT results largely

coincided with the microgravimetric and seismic results of the previously conducted standard investigation program. As was the case with the 2D ERT profiling, also the seismic survey had difficulties in showing the bedrock surface precisely. The exact spatial distribution with depth as well as the internal structure of the detected anomalies (clayey/loamy deposits, moderately fractured and/or medium weathered limestone bedrock) could only be obtained from the 2D ERT data. In contrast to the microgravimetric data,

which suggested the potential presence of air-filled voids, the seismic as well as the 2D ERT survey suggested the general absence of air-filled voids, whereby only the latter was in accordance with the direct probing investigations. In direct comparison, the resistivity method was thus superior in detecting zones with low ground bearing capacity and in delineating them from zones, generally capable of bearing weight. The bottom line of this proceedings paper: 2D ERT measurements conducted with an inverse Wenner-Schlumberger array can provide a decisive contribution to karst reconnaissance and building ground evaluations in a highly heterogeneous karstic environment like the Swabian Alb high plain, on the new line Wendlingen–Ulm.

**Acknowledgements** This paper was published with permission of the DB Projekt Stuttgart–Ulm GmbH.

## References

- ARGE NBS Wendlingen–Ulm: Dokumentation der Ergebnisse der geophysikalischen Erkundung Karst, der Nacherkundung sowie Gründungsempfehlungen, Einschnitt E9—Teil 1: km 63,6 + 66–64,0 + 41,5, Großprojekt Stuttgart–Ulm, NBS Wendlingen–Ulm, PFA 2.3 Albhochfläche, 2. Streckenabschnitt km 61,4 + 45–68,0 + 43, p. 28, Juli 2017 (in German, unpublished report) (2017)
- Degroot-Hedlin, C., Constable, S.: Occam's inversion to generate smooth, two-dimensional models from magnetotelluric data. *Geophysics* **55**(12), 1613–1624 (1990). <https://doi.org/10.1190/1.1442813>
- Farquharson, C.G., Oldenburg, D.W.: Nonlinear inversion using general measures of data misfit and model structure. *Geophys. J. Int.* **134**(1), 213–227 (1998). <https://doi.org/10.1046/j.1365-246x.1998.00555.x>
- Goldscheider, N., Drew, D.: *Methods in Karst Hydrogeology*, p. 264. Taylor & Francis, London (2007)
- Ismail, A., Anderson, N.: 2-D and 3-D resistivity imaging of karst sites in Missouri, USA. *Environ. Eng. Geosci.* **18**(3), 281–293 (2012). <https://doi.org/10.2113/gseegeosci.18.3.281>
- Kidanu, S.T., Torgashov, E.V., Varnavina, A.V., Anderson, N.L.: ERT-based investigation of a sinkhole in Greene County, Missouri. *AIMS Geosci.* **2**(2), 99–115 (2016). <https://doi.org/10.3934/geosci.2016.2.99>
- Kielbassa, S., Reinhardt, A., Gering, A., DB Projekt Stuttgart–Ulm GmbH: Albstieg tunnel: karst probing and treatment measures. *Tunnel* **4**, 26–37 (2015a)
- Kielbassa, S., Prischmann, F., Beer, N.: Karst investigation and treatment measures for the high-speed track on the Swabian Jura. *Geomech. Tunn.* **8**(2), 129–145 (2015b). <https://doi.org/10.1002/geot.201510011>
- Loke, M.H., Barker, R.D.: Rapid least-squares inversion of apparent resistivity pseudosections using a quasi-Newton method. *Geophys. Prospect.* **44**(1), 131–152 (1996). <https://doi.org/10.1111/j.1365-2478.1996.tb00142.x>
- Loke, M.H.: RES2DINV Version 3.54. Rapid 2-D Resistivity & IP Inversion Using the Least-Squares Method. Computer Disk and Manual. Geotomo Software, Penang, Malaysia (2004)
- Loke, M.H., Acworth, I., Dahlin, T.: A comparison of smooth and blocky inversion methods in 2D electrical imaging surveys. *Explor. Geophys.* **34**(3), 182–187 (2003). <https://doi.org/10.1071/EG03182>
- Prins, C., Thuro, K., Krautblatter, M.: Geoelectrical karst reconnaissance on the Swabian Alb high plain, new line Wendlingen–Ulm, southwestern Germany. In: Thuro, K. (ed.) *Tagungsband der 20. Tagung für Ingenieurgeologie mit Forum für junge Ingenieurgeologen*, Congress Centrum Würzburg, Fachsektion Ingenieurgeologie, pp. 374–397, Deutsche Gesellschaft für Geotechnik, Würzburg, Germany, 6–8 Sept (2017)
- Roth, M.J.S., Mackey, J.R., Nyquist, J.E.: A case study of the use of earth resistivity in thinly mantled karst. In: Powers, M.H., Ibrahim, A.-B., Cramer, L. (eds.) *Proceedings of the 12th Symposium on the Application of Geophysics to Environmental and Engineering Problems (SAGEEP 1999)*, pp. 293–302, Oakland, California, USA (1999)
- Roth, M.J.S., Nyquist, J.E., Guzas, B.: Locating subsurface voids in karst: a comparison of multi-electrode earth resistivity testing and gravity testing. In: Powers, M.H., Ibrahim, A.-B., Cramer, L. (eds.) *Proceedings of the 13th Symposium on the Application of Geophysics to Environmental and Engineering Problems (SAGEEP 2000)*, pp. 359–365, Arlington, Virginia, USA, 20–24 Feb (2000)
- Roth, M.J.S., Nyquist, J.E.: Evaluation of multi-electrode earth resistivity testing in karst. *Geotech. Test. J.* **26**(2), 1–12 (2003). <https://doi.org/10.1520/GTJ11322J>
- Siart, C., Hecht, S., Brilmayer Bakti, B., Holzhauer, I.: Analysis and 3D visualization of Mediterranean subsurface karst features based on tomographic mapping (Zominthos, Central Crete). *Z. Geomorphol.* **55**(3), 315–335 (2011). <https://doi.org/10.1127/0372-8854/2011/0055S3-0064>
- Siart, C., Forbriger, M., Nowaczinski, E., Hecht, S., Höfle, B.: Fusion of multi-resolution surface (terrestrial laser scanning) and subsurface geodata (ERT, SRT) for karst landform investigation and geomorphometric quantification. *Earth Surf. Process. Landf.* **38**, 1135–1147 (2013). <https://doi.org/10.1002/esp.3394>
- Telford, W.M., Geldart, L.P., Sheriff, R.E.: *Applied Geophysics*, 2nd edn, p. 770, Cambridge University Press, Cambridge (1990)
- Yassin, R.R., Muhammad, R.F., Taib, S.H., Al-Kouri, O.: Application of ERT and aerial photographs techniques to identify the consequences of sinkholes hazards in constructing housing complexes sites over karstic carbonate bedrock in Perak, Peninsular Malaysia. *J. Geogr. Geol.* **6**(3), 55–89 (2014). <https://doi.org/10.5539/jgg.v6n3p55>
- Zhou, W., Beck, B.F., Stephenson, J.B.: Reliability of dipole-dipole electrical resistivity tomography for defining depth to bedrock in covered karst terranes. *Environ. Geol.* **39**(7), 760–766 (2000). <https://doi.org/10.1007/s002540050491>
- Zhou, W., Beck, B.F., Adams, A.L.: Effective electrode array in mapping karst hazards in electrical resistivity tomography. *Environ. Geol.* **42**, 922–928 (2002). <https://doi.org/10.1007/s00254-002-0594-z>



# Experimental Study on Coupled Stress-Dissolution of Carbonate Rocks in Rocky Desertification Area of Karst Plateau, Guizhou, China

Qi Liu, You'en Bai, Yaoru Lu, and Zhuping Sheng

## Abstract

The karst rocky desertification is one of the major bottlenecks for the eco-environmental safety and economical sustainable development in karst areas of China. The formation of rocky desertification is influenced by many factors, and the lithology of carbonate rocks has the most profound influence on it as internal factors. The lithological difference of carbonate rocks determines its weathering process and the way of the accumulation and loss of surface soil, which makes the origin, temporal and spatial evolution rule and governance difficulty of rocky desertification different. In this paper, the limestone and dolomite in the moderate and severe rocky desertification region in the Guizhou plateau are selected as the research objects. Stress-dissolution experiments of carbonate rocks are carried out by the simulating open system of the water environment of epikarst zone. The differences in deformation and dissolution characteristics of limestone and dolomite under different stress conditions are analyzed. In addition, the characteristics of surface and internal pore structure of the rocks are analyzed from the microscopic view. The results further explain why the degree of rocky desertification in the dolomite area is lighter than the limestone area, but it is more difficult to control than the limestone area. These results provide a theoretical reference for the controlling of rocky desertification.

## Keywords

Karst rocky desertification • Carbonate rocks • Dissolution • Deformation

## 1 Introduction

China's Yunnan-Guizhou Plateau is one of the largest Karst distribution regions in the world. The topography in this humid area is unusually complex and diverse, and karst development is wide spread (Lu 1986; Jiang et al. 2011). Zhenfeng-Guanling-Huajiang region is a typical karst plateau canyon area. It is located on both sides of the Beipanjiang-Huajiang canyon that is in the southwest of Guizhou, a total area of 51.62 km<sup>2</sup>, and 87.92% of the total area. The intense soil erosion and the phenomenon of rock desertification mainly result from the typical dualistic structure of karst hydrogeology and the long-term inharmonious relationship between human and land. Large area of bedrock is exposed and rocks are rugged (Cao et al. 2008). In this environment, ecological degradation restricts the economic development seriously. The ecological condition needs to be restored quickly (Li et al. 2004; Xiong et al. 2012). Through a large number of investigations for many years, the results show that the lithology of carbonate rocks is one of the main internal causes that affect the evolution of soil loss and rocky desertification. The distribution area and degree of rocky desertification in the pure limestone area are wider and more obvious than the pure dolomite area (He et al. 1984; Nie 1994; Liu et al. 2013, 2015; Bai et al. 2017). Therefore, it is especially important for the control of rocky desertification to study the basic features of carbonate rocks.

The limestone and dolomite are the source of red clay, and the karst causes accumulation of acid insoluble matter in the rock. In the humid and warm climate, the weathered residue gradually forms the red soil (Li et al. 1991, 2005). Under the action of chemical dissolution and physical weathering, the internal defects of carbonate rock structure

Q. Liu (✉) · Y. Bai · Y. Lu  
Department of Geotechnical Engineering, College of Civil Engineering, Tongji University, Shanghai, 200092, China  
e-mail: liuqi472@163.com

Q. Liu · Y. Bai · Y. Lu  
Key Laboratory of Geotechnical and Underground Engineering, Tongji University, Ministry of Education, Shanghai, 200092, China

Z. Sheng  
Texas A&M AgriLife Research Center at El Paso, El Paso, TX 79927, USA



increase gradually. This leads to deformation and failure of carbonate rock in the case of low temperature and low external load, and finally forms limestone soil (Zeng 2007). During the weathering process, the difference of lithology and microstructure of carbonate rocks results in different accumulation and loss patterns of weathering residue. Different regions show different processes of formation and evolution of rocky desertification. The distribution area and degree of rocky desertification in pure limestone area are more extensive and obvious than that in pure dolomite area (Li 2006; Wang et al. 2009). In this paper, the limestone and dolomite in the demonstration area of rocky desertification control are selected as the research object to carry out a stress-chemical dissolution experiment of carbonate rock. The deformation and dissolution characteristics of carbonate rocks under the effect of mechanical-chemical coupling are studied, and the influence of these characteristics on the genesis and development of rocky desertification are analyzed, which can provide theoretical reference for rocky desertification prevention and control according to local conditions.

---

## 2 The Background of Research Area

The research area is Zhenfeng-Guanling and Huajiang demonstration area of rocky desertification control, located in the southwest of Guizhou. The total area is 51.62 km<sup>2</sup>, and karst area accounted for 87.92%. This region is a typical karst plateau canyon area with an elevation of 500–1200 m (Fig. 1). The whole drainage area is located in the slope of the plateau that dips towards Beipanjiang River, and has complicated karst landforms. In this area, the exposed strata are mainly the pure carbonate rock accounting for more than 95% in the Upper and Middle Triassic strata, with the Yangliu group and Longtou group. It is warm and arid in the winter and spring, hot and humid in the summer and fall, with an average annual temperature of 18.4 °C, the maximum temperature of 32.4 °C, and minimum temperature of 6.6 °C. The average annual rainfall is 1100 mm with uneven spatial and temporal distribution. Rain storms occur more often in the summer and fall, and the precipitation from May to October accounts for 83% of total annual precipitation. In some valleys, there are seasonal or perennial surface water flows. Due to human activity, the forest coverage in the research area is very low, the soil erosion is widespread, and the bedrock is exposed.

## 3 Stress-Dissolution Experiments

### 3.1 Experimental Sample

Four carbonate rock samples were collected respectively from potential, strong, medium and slight degree of rocky desertification areas in the demonstration area (Fig. 1). The rock samples were numbered, and the unweathered samples R3, R6, R8, R10 were selected to form a test block for dissolution-deformation experiment. Samples R3 and R10 were collected from light rocky desertification areas. Samples R6 and R8 were collected from moderate to severe rocky desertification areas. Their lithology and chemical composition were shown in Table 1.

### 3.2 Experimental Process

The selected rock samples were respectively processed into a cylindrical test block and placed in an open plexiglass dissolution dish. The load was applied to the test block using the rock rheological machine, and two strain gauges were used to collect the deformation. The computer connected with the strain gauge and the rheological machine collected the experimental data automatically every 30 s. At the same time, through a peristaltic pump, the hydrochloric acid solution of pH = 3 was continuously pumped into the dissolution dish at the constant flow rate of 3 ml/min. The dissolved solution released from the corrosion dish was collected, and the chemical composition of the collected liquid was analyzed. The laboratory temperature was 20 °C, the load path was 1.0–2.0–3.0–4.0 kN, the load duration of each stage is 72 h, and each sample was continuously loaded for 288 h (Fig. 2).

---

## 4 The Result of This Experiment

### 4.1 Dissolution Characteristics of Carbonate Rock Under Stress-Dissolution Coupling

In this experiment, the concentrations of Ca and Mg ions in the continuous collected dissolution liquid were tested at each fixed time interval. By measuring the ion concentrations at different deformation stages, the total surface dissolution amount (Table 2) and the average dissolution rate of carbonate rocks in the different deformation stages were



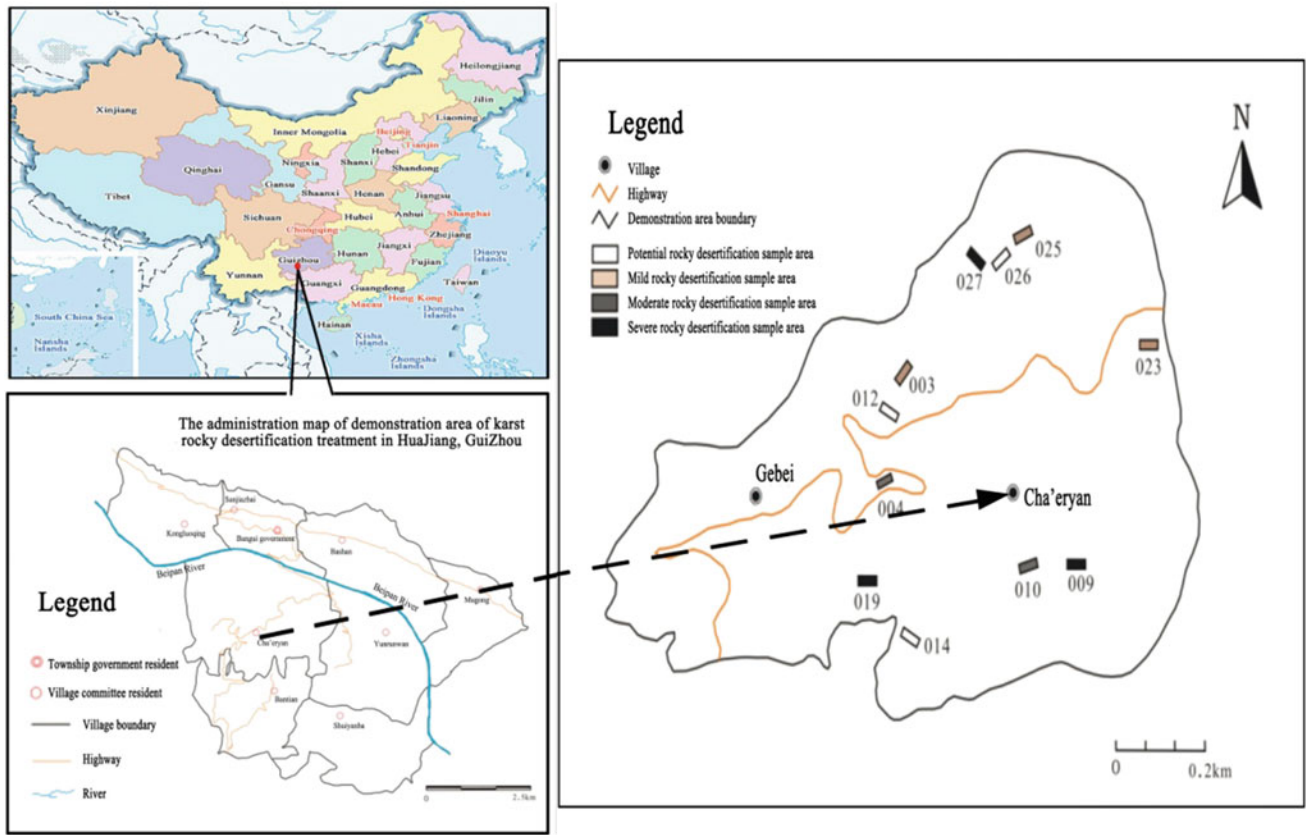


Fig. 1 The distribution of rock samples in demonstration area

Table 1 Chemical composition and lithology of unweathered rock specimens

Sample	Lithology	Content of chemical composition (%)					Compressive strength (MPa)
		CaO	MgO	CO <sub>2</sub>	SiO <sub>2</sub>	Insoluble substance	
R3	Aplite dolomite	32.38	18.69	44.58	1.31	2.59	99.366
R6	Microcrystalline limestone	53.42	1.69	43.04	0.49	0.74	95.207
R8	Microcrystalline limestone	52.79	1.02	42.53	1.39	2.03	42.96
R10	Microcrystalline dolomite	36.00	15.80	44.00	2.20	3.36	87.997

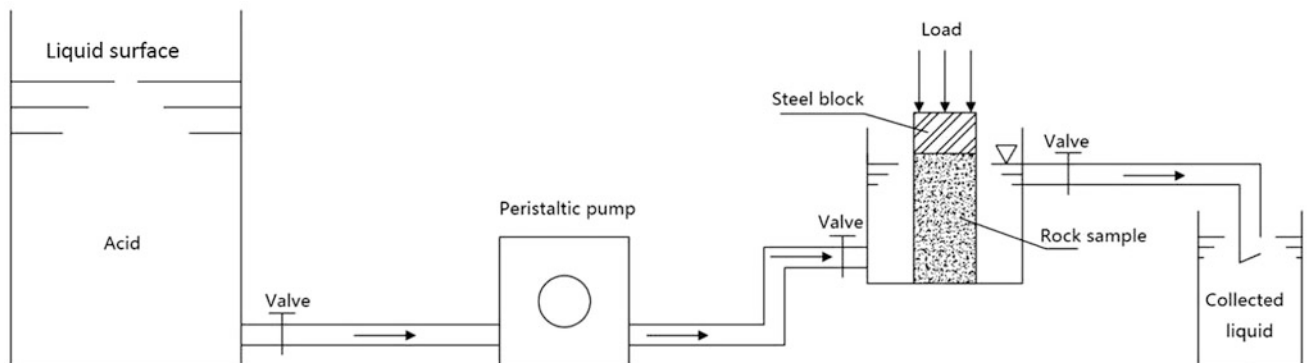


Fig. 2 Sketch of experimental equipment

**Table 2** Results of dissolution experiment under stress-dissolution coupling

Sample	Lithology	Diameter (cm)	High (cm)	Surface area (cm <sup>2</sup> )	Weight (g)	Dry density (g/cm <sup>3</sup> )	Surface dissolution amount (mg/cm <sup>2</sup> )
R3	Aplite dolomite	5.037	10.058	198.23	565.36	2.822	9.65
R6	Microcrystalline limestone	5.056	10.078	200.11	543.86	2.690	11.61
R8	Microcrystalline limestone	5.095	9.971	200.26	544.36	2.680	10.33
R10	Microcrystalline dolomite	5.072	10.075	200.83	572.12	2.812	9.45

**Table 3** Average dissolution rate under different stresses (Unit: mg/h)

Sample	Lithology	Stress (MPa)				Average dissolution rate (mg/h)
		0.5	1	1.5	2	
R3	Aplite dolomite	5.079	5.141	5.301	5.807	5.332
R6	Microcrystalline limestone	7.757	5.761	5.459	6.896	6.468
R8	Microcrystalline limestone	5.167	5.528	5.856	6.465	5.754
R10	Microcrystalline dolomite	4.238	5.173	5.795	5.864	5.268

**Table 4** The results of dissolution experiment in static pressureless condition

Sample	Lithology	Surface area (cm <sup>2</sup> )	Volume (cm <sup>3</sup> )	Weight (g)	Dry density (g/cm <sup>3</sup> )	Surface dissolution amount (mg/cm <sup>2</sup> )
R3	Aplite dolomite	7.442	1.075	3.001	2.792	7.93
R6	Microcrystalline limestone	7.364	1.059	2.845	2.686	8.96
R8	Microcrystalline limestone	7.327	1.044	2.807	2.689	8.69
R10	Microcrystalline dolomite	7.245	1.058	2.827	2.672	7.97

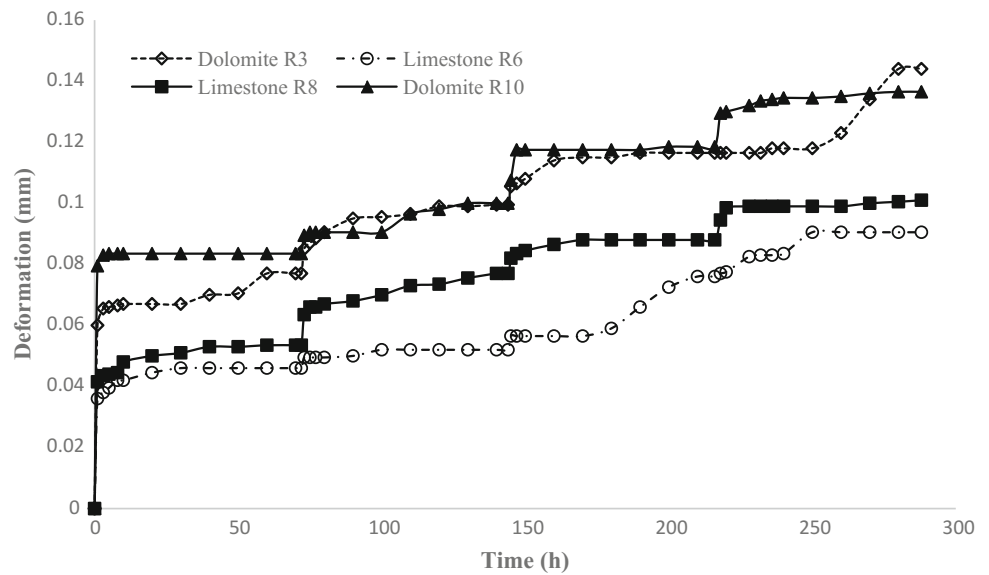
obtained (Table 3). In the whole deformation period, the total amount of dissolution of limestone was greater than that of dolomite, and the average dissolution rate of limestone was also greater than that of dolomite. All samples except R6 have a positive correlation between dissolution and stress. The initial dissolution rate of R6 is obviously larger, which is due to its special rock joint.

In order to further explore the difference of dissolution rate of carbonate rocks under different conditions. A dissolution experiment under the same environment was carried out with no applied load, and the results are shown in Table 4. In contrast to the loading case, the average surface dissolution amount of the non-loaded samples is lower.

## 4.2 Deformation Characteristics of Carbonate Rock Under Stress-Dissolution Coupling

The experimental results show that the carbonate deformation occurs at the moment of loading, and then the deformation convergence as the extension of time, and the total deformation tends to level out. According to Fig. 3, the deformation of each rock sample under different load levels is shown (Table 5). It shows that under different loads, the initial deformation of dolomite is greater than that of limestone, and dolomite is easier to deform than limestone under load. Through the deformation curve, the average deformation rate from beginning to stabilization of deformation was

**Fig. 3** Deformation curve of carbonate rocks under mechanics-chemistry coupling



**Table 5** Deformation under different loads (Unit: mm)

Sample	Lithology	Load (kN)			
		1	2	3	4
R3	Aplite dolomite	0.057	0.014	0.010	0.006
R6	Microcrystalline limestone	0.038	0.005	0.006	0.004
R8	Microcrystalline limestone	0.042	0.010	0.005	0.003
R10	Microcrystalline dolomite	0.077	0.017	0.010	0.011

calculated (Table 6). It shows that the average deformation rate under high stress level is higher, and the average deformation rate of limestone is larger than dolomite, but its deformation duration is short, and the deformation stabilized quickly. Dolomite will continue to deform at a low deformation rate, which indicates that dolomite under external force is prone to sustained internal damage. The main reason is that limestone is composed of dense calcite. These calcite grains are fine grained with homogeneous texture and good structural stability, and the limestone does not easily deformation. The structure of dolomite has the larger dolomite particles embedded in the calcite matrix, that does not have good stability, and under the action of stress, the dolomite is subjected to sustained failure, which shows a continuous deformation.

### 4.3 Changes of Microscopic Characteristics of Rock Surface Before and After Stress-Dissolution Test

In order to obtain the change of microscopic characteristics of rocks surface before and after dissolution, the original rock samples and the corroded rock samples were analyzed by SEM. Results are presented in Table 7. SEM images

show that the microscopic characteristics of rock samples have changed greatly before and after corrosion. The surface of the original rock is dense, and the secondary pores are not obvious. The surface of the rock sample is corroded after dissolution, the cementation between minerals decreases, the secondary pores increases, and the grains become irregular.

### 4.4 Pore Characteristics of Carbonate Rock Under Stress-Dissolution Condition

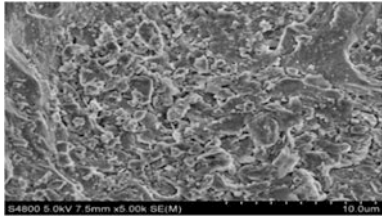
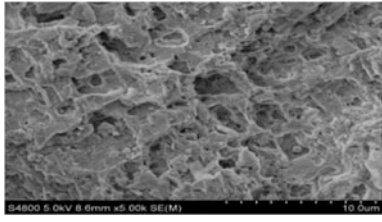
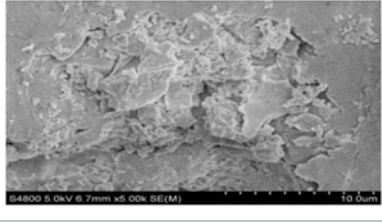
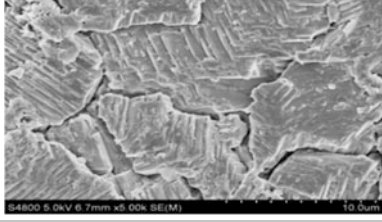
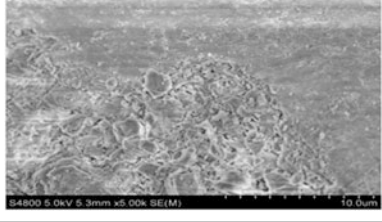
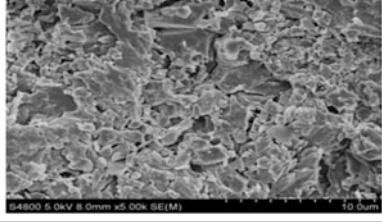
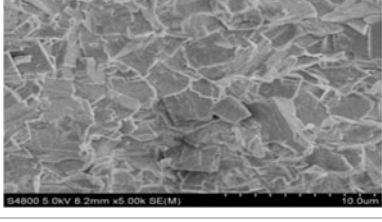
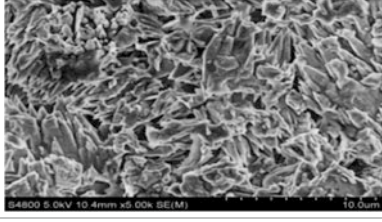
The dissolution of carbonate rocks is affected not only by chemical composition, but also by pore structure (Wang et al. 2009). In order to analyze the internal pore structure characteristics of rock samples before and after the stress-dissolution test, a mercury intrusion test was carried out, and the experimental data were analyzed by referring to the theory of Han (1998). The experimental results are shown in Table 8. The experimental results show that the average pore size and porosity increase after the dissolution, which indicates that the number and diameter of pores increase, and dissolution also occurs inside the rock. After dissolution, the bulk density is higher than that before dissolution, which indicates that the connectivity of pores is improved after dissolution.

**Table 6** Average deformation rate at different stress stages (Unit:  $10^{-4}$  mm/h)

Sample	Lithology	Stress (MPa)			
		0.5	1	1.5	2
R3	Aplite dolomite	2.88	3.158	4.250	11.250
R6	Microcrystalline limestone	8.710	2.080	10.833	40.000
R8	Microcrystalline limestone	5.162	2.955	10.000	22.857
R10	Microcrystalline dolomite	3.750	4.130	–	–

– Deformation occurs instantaneously

**Table 7** SEM photos comparison of rock samples before and after stress-dissolution test

Sample	Lithology	Before dissolution	After dissolution
R3	Aplite dolomite		
R6	Microcrystalline limestone		
R8	Microcrystalline limestone		
R10	Microcrystalline dolomite		

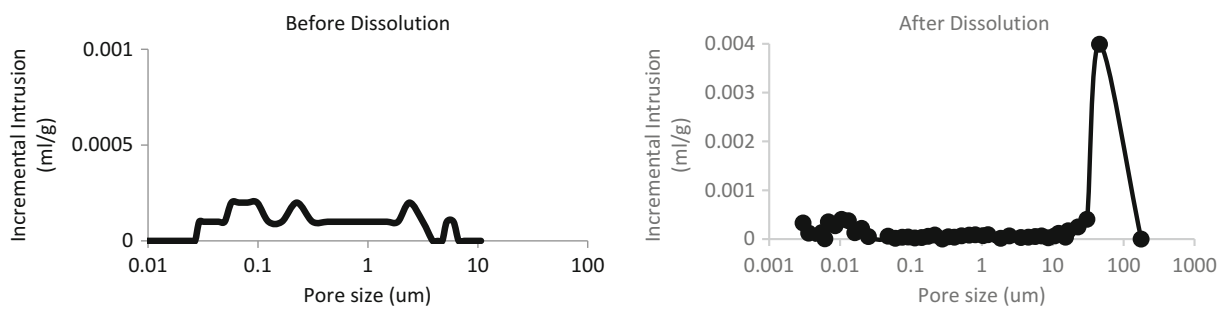
Depending on the curve of pore diameter and stage mercury incremental intrusion (Figs. 4, 5, 6 and 7), the dolomite before experiment belongs to the type of the dolomite is super micro-pores, micro-pores or small pores, multi-pass throats dissolved rock, and the limestone belongs to the type of macro-pore and solution fissure dissolved rock. After the experiment, the intrusion volume in the large pore part of all rock samples increases, and the porosity and

average pore radius increase. It indicates that secondary pores are generated, resulting in an increase of intrusion volume. Especially dolomite R3, the increase of its porosity is obviously larger than limestone, and form large pores. It indicates that dolomite is obviously affected by mechanical damage. Dolomite R3 does not produce some small pores and the dissolution is even. For sample R6, R8 and R10 after dissolution, the incremental intrusion volume increases not

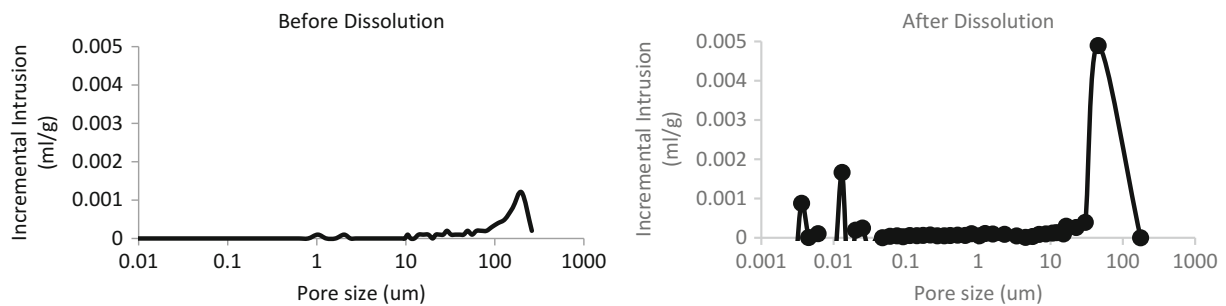


**Table 8** Comparison of mercury intrusion data before and after stress-dissolution

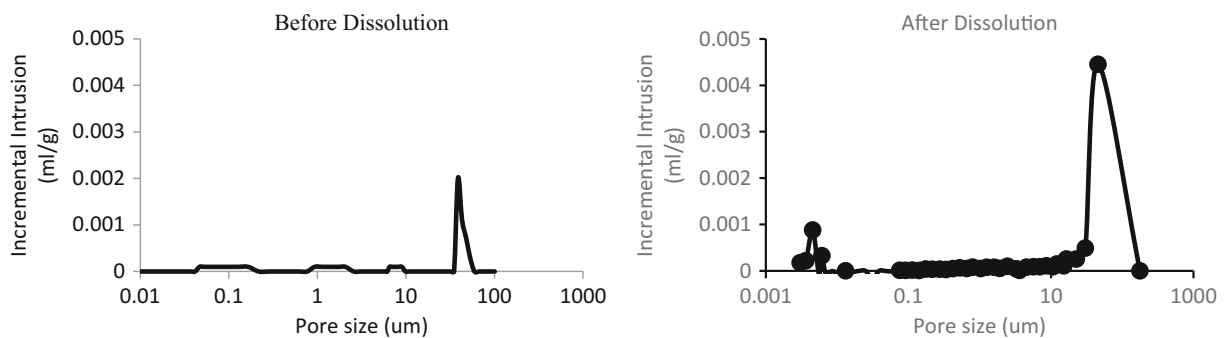
Sample No.	Lithology	Dissolution state	Total intrusion volume (ml/g)	Average pore radius (nm)	Bulk density (g/ml)	Porosity (%)	Breakthrough pressure (psia)	Skewness
R3	Aplite dolomite	Before	0.0033	75.71	2.3527	0.9039	25.16	2.2198
		After	0.0084	275.00	2.588	2.1843	6.87	12.8758
R6	Microcrystalline limestone	Before	0.0059	139.53	2.4795	1.9507	0.9652	2.2080
		After	0.0105	175.00	2.7262	2.8628	4.66	9.2338
R8	Microcrystalline limestone	Before	0.0041	98.17	2.5120	1.0393	2.9790	2.2183
		After	0.0082	270.00	2.6149	2.1395	5.10	10.3084
R10	Microcrystalline dolomite	Before	0.0073	198.32	2.5316	2.2993	1.0102	2.2040
		After	0.0074	257.00	2.6787	2.9564	4.43	9.2811



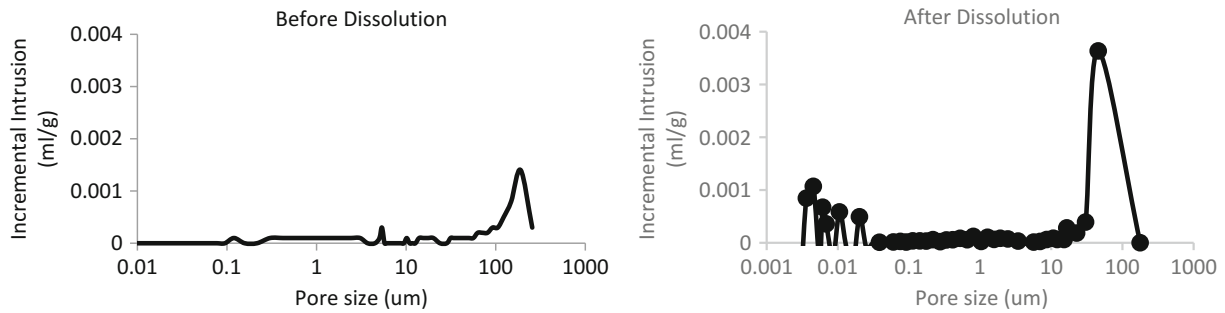
**Fig. 4** The relationship between pore diameter and incremental intrusion of R3



**Fig. 5** The relationship between pore diameter and incremental intrusion of R6



**Fig. 6** The relationship between pore diameter and incremental intrusion of R8



**Fig. 7** The relationship between pore diameter and incremental intrusion of R10

only in the macro-pore parts, but also in the small pore parts. They have the characteristic of differential dissolution.

## 5 Dissolution-Deformation Characteristics of Carbonate Rock and Rock Desertification

There is a significant correlation between rocky desertification and the distribution of carbonate rocks in the study area. The regions of limestone and dolomite exhibit different karst morphology, karst development degree, soil layer thickness and weathering crust features. During the weathering process, the difference of lithology and microstructure of carbonate rocks results in different accumulation and loss patterns of weathering residue. This study shows that:

1. The internal structure of dolomite is easily damaged by stress, which is conducive to the development of fractures, physical and chemical weathering and the formation of dolomite clastic gravel or soil. Dolomite minerals are coarse, and intergranular pores are well-developed. The joints and fissures formed in dolomite are dense and homogeneous, which encourages water retention within near-surface dolomite. All of this is conducive to the overall weathering of dolomite rocks. The bedrock surface fluctuation of dolomite weathering crust is relatively small, and the distribution of soil formed by weathering residue is relatively homogeneous. The dolomite is generally not easy to have obvious uneven dissolution, which makes it difficult to form some Karst caves that cause soil loss. The surface of the dolomite after dissolution is rough, and the rough surface can not only retain water to promote weathering, but also retain the soil. Therefore, the degree of rocky desertification in dolomite area is weaker than that in limestone area (Jiang et al. 2011).
2. Limestone has a lot of fine calcite minerals, compact structure and small intergranular porosity. Under the action of various tectonic stresses, limestone is easy to

produce tensional joints and fissures that will accelerate dissolution. Therefore, limestone is easier to be dissolved than dolomite under the action of acid. Limestone is more likely to occur intense uneven dissolution in surface and internal, and some primitive joints are rapidly dissolved to form fissures and holes, resulting in rapid loss of the soil. The soil will aggregate in the fissure and underground void system. This makes the limestone area more prone to form rocky desertification with discontinuous soil layer.

In summary, although the degree of rocky desertification in dolomite area is less than that in the limestone area, the soil in dolomite area is thinner and contains a lot of gravel and silt. Therefore, ecological remediation of rocky desertification in dolomite area is more difficult.

## 6 Conclusion

1. Under the effect of stress-dissolution coupling, the deformation of dolomite is greater than that of limestone, and the deformation of dolomite increases continuously with the loading time. The deformation of limestone mainly occurs in the initial stage of loading, and then tends to stabilize quickly. The total deformation of dolomite is greater than that of limestone, and dolomite is more susceptible to deformation and failure due to an external force.
2. The dissolution rate of carbonate in acid solution with constant concentration is positively related to the stress level. The greater the load, the faster the dissolution rate, and the dissolution rate under the stress-dissolution condition is faster than that under the static non-loading condition.
3. The dissolution of carbonate occurs not only on the rock surface, but also in the pore space. The corrosion results show the increase of pore diameter and porosity.

The dissolution of limestone is stronger than dolomite, and has differential corrosion. The dissolution of dolomite is more even, but it is obviously affected by stress damage.

4. Different lithology carbonate rocks have different dissolution-deformation properties, which make them have different weathering and soil loss patterns. The degree of rocky desertification in dolomite area is less than that in the limestone area. But ecological remediation of rocky desertification in dolomite area is more difficult.

**Acknowledgements** This work was supported by research of the National Key Research and Development Program of China (2016YFC0502603) and Grant 41772292 from the National Natural Science Foundation of China, and US Department of Agriculture-National Institute of Food and Agriculture Hatch Project (TEX0-1-9448) via Texas AgriLife Research.

## References

- Bai, Y.E., Liu, Q., et al.: The dissolution mechanism and karst development of carbonate rocks in karst rocky desertification area of ZhenFeng-GuanLing-HuaJiang County, GuiZhou, China [J]. *Carbonates Evaporites* 1–7 (2017)
- Cao, J.H., Yuan, D.X., Tong, L.Q.: Features of karst ecosystem and integrating measure for rock desertification in Southwest China. *Pratacult. Sci.* **25**(9), 40–50 (2008)
- Han, B.P.: *The Study on the Mechanism of Micro Karst* [M], pp. 37–156. Geological Publishing House, Beijing (1998)
- He, Y.B., Jin, Y.Z., Li, K.: An experimental study of carbonate rock corrosion mechanism [J]. *Carsol. Sin.* 12–16 (1984)
- Jiang, Z.C., Li, X.K., Hu, B.Q., et al.: *Research and Control of Rocky Desertification in Karst Mountain Area of GuangXi* [M]. Science Press, Beijing (2011)
- Li, H.X.: Preliminary Study of Soil Profile Features in Karst Fracture and its Evolution Characteristic [D]. Xi'an University of Science and Technology, Xi'an (2006)
- Li, J.Y., Wang, C.F., et al.: Weathering crust of carbonate rocks and process of karst earth formation [J]. *Carsol. Sin.* **10**(1), 29–38 (1991)
- Li, Y.B., Wang, S.J., Xiong, K.N.: Preliminary Study on karst rocky desertification genesis in Huajiang gorge district. *Hydrogeol. Eng. Geol.* **37**(6), 37–42 (2004)
- Li, M.Q., Zhang, Z.R., Wang, Z.Y., et al.: Tracing the pedogenic process to carbonate rocks in light of maceral and microfabric characteristics of clay and carbonate rocks [J]. *Earth Environ.* **12**(4), 77–82 (2005)
- Liu, Q., Lu, Y.R., Zhang, F.E.: Design and experimental analysis of pressure dissolution test equipment of rocks [J]. *Res. Explor. Lab.* **32**(9), 34–37 (2013)
- Liu, Q., Gu, Z.F., Lu, Y.R.: The experimental study of dolomite dissolution and pore characteristics in Shibing, Guizhou [J]. *Acta Geosci. Sin.* **36**(4), 413–418 (2015)
- Lu, Y.R.: Evolution model of karst landform in China [J]. *Geogr. Res.* 25–34 (1986)
- Nie, Y.P.: Karst development characteristics under the lithologic control of carbonate rocks—a case study in south-central GuiZhou [J]. *Carsol. Sin.* **13**(1), 31–36 (1994)
- Wang, S.Z., Kuang, S.D., Dai, C.G., et al.: Analyses on the reason of rocky desertification speed difference of dolomite and limestone in mountain area [J]. *Guizhou Geol.* **1**, 49–51 (2009)
- Xiong, K.N., Li, J., Long, M.Z.: Features of soil and water loss and key issues in demonstration areas for combating karst rocky desertification. *ACTA Geogr. Sin.* **67**(4), 878–888 (2012)
- Zeng, C.L.: Study on Mechanical Behavior of Soft Rock in Coupled Effect of High Temperature, High Pressure and Seepage [D]. Qingdao University of Science and Technology, Qingdao (2007)

---

## Author Index

### A

Ammirati, Lorenzo, [51](#)  
Avci, Erdi, [79](#)

### B

Bai, You'en, [123](#)  
Bednarczyk, Zbigniew, [3](#)  
Bilen, Candan Alptekin, [79](#)  
Boni, Maria, [51](#)

### C

Cai, Guangtao, [43](#)  
Calcaterra, Domenico, [51](#)  
Chan, Kitty, [73](#)  
Cho, Yong-Chan, [59](#)  
Czinder, Balázs, [95](#)

### D

del Pilar Durante Ingunza, Maria, [67](#)  
de Medeiros, Ana Beatriz Azevedo, [67](#)  
Di Martire, Diego, [51](#)

### E

Elokhina, S. N., [109](#)  
Eremina, Olga, [13](#)

### F

Fedotova, Ksenia, [13](#)  
Fernandes, Isabel, [91](#)

### G

Galindo, Antonio Carlos, [67](#)  
Gorbova, S. V., [109](#)

### H

Hingston, Egerton Daniel Christian, [19](#)

### K

Kasemodel, Mariana Consiglio, [35](#)  
Kazeev, Andrey, [13](#)

Khurchik, Vadim, [103](#)

Khumalo, Cebolenkosi, [19](#)  
Krautblatter, Michael, [115](#)

### L

Lima, Jacqueline Zanin, [27](#)  
Liu, Jiawei, [43](#)  
Liu, Qi, [123](#)  
Lu, Yaoru, [123](#)

### M

Maksimovich, Nikolay, [103](#)  
Mamaev, Yuri, [13](#)  
Meshcheriakova, Olga, [103](#)  
Millis, Stuart, [73](#)  
Mondillo, Nicola, [51](#)  
Mtshali, Sihle, [19](#)

### N

Nankua, Quinton, [19](#)

### O

Osipov, Victor, [13](#)

### P

Prins, Constantin, [115](#)

### R

Raimondi, Isabela Monici, [27](#)  
Ribeiro, Maria dos Anjos, [91](#)  
Rodrigues, Valéria Guimarães Silvestre, [27](#), [35](#)

### S

Selman Er, [79](#)  
Sheng, Zhuping, [123](#)  
Song, Young-Suk, [59](#)  
Sui, Wanghua, [43](#)

### T

Tessitore, Serena, [51](#)



Thuro, Kurosch, [115](#)  
Török, Ákos, [91](#), [95](#)  
Tugrul, Atiye, [79](#), [85](#)

**Y**  
Yastrebov, Alexey, [13](#)  
Yılmaz, Murat, [79](#), [85](#)